An Investigation of Conformable Antennas for the Astronaut Backpack Communication System

Stuart A. Long

David R. Jackson

Jeffery T. Williams

Donald R. Wilton

A final report submitted to

NASA-Johnson Space Center

Houston, Texas 77058

Technical Report Number 88-18

A final report submitted for grant NAG 9-219 from NASA-JSC, June 1, 1988

Applied Electromagnetics Laboratory

Department of Electrical Engineering

University of Houston

An Investigation of Conformable Antennas for the Astronaut Backpack Communication System

Stuart A. Long
David R. Jackson
Jeffery T. Williams
Donald R. Wilton

A final report submitted to
NASA-Johnson Space Center
Houston, Texas 77058

Technical Report Number 88-18

A final report submitted for grant NAG 9-219
from NASA-JSC, June 1, 1988

Applied Electromagnetics Laboratory
Department of Electrical Engineering
University of Houston

AN INVESTIGATION OF CONFORMABLE ANTENNAS FOR THE ASTRONAUT BACKPACK COMMUNICATION SYSTEM

1. INTRODUCTION

During periods of extravehicular activity it is obviously important that communication and telemetry systems continue to function independent of the orientation of the astronaut. A system of antennas must therefore be designed that will provide the necessary isotropic coverage using circular polarization over both the transmit and receive frequency bands. To avoid the inherent physical limitations to motion that would be incurred with any sort of protruding antenna, it is necessary that the radiator be essentially flush-mounted or conformable to the structure on which it is attached.

Several individual antenna elements are needed for the desired coverage. Both the particular elements chosen and their location determine the ultimate radiation pattern of the overall system. For these reasons a two-fold research plan was undertaken. First, individual elements were investigated and designed. Then various mounting locations were considered and the radiation patterns were predicted taking into account the effects of the astronaut's backpack.

2. ANTENNA ELEMENT

The required antenna element (as distinguished from the array in the complex scattering environment in which it is to be placed) is discussed in this section. The general requirements for the element are that it produce a circularly polarized (CP) pattern over as wide a beam as possible and have *two distinct bands* each having a bandwidth of 2-2.5% with a separation between the band centers of 8-10%. The element is to be unobtrusive in the sense that it has a low profile exterior to the backpack and does not require any space within the backpack except that required by a feeding coaxial transmission line.

Several designs are presented. Two of them involve reactive loading to provide distinct dual band behavior. As an alternative, a thick-substrate element is also considered, in which the bandwidth is sufficient to cover both the transmit and receive frequencies.

2.1 Previous Work

Earlier work [1,2] has presented a method of designing dual-band microstrip elements with band separations that are adjustable by using reactively-loaded microstrip elements. The reactive load, which can be realized as a lumped element, or as a distributed element such as an open or short-circuited transmission line or resonator, splits the mode of interest in the original microstrip element into two distinct modes with radiation patterns essentially indentical to those of the original, parent mode. This technique has been successfully applied to rectangular microstrip elements with linear polarization, and is equally applicable to a *square* microstrip element driven by a pair of lines feeding two adjacent edges in phase quadrature. Such an element can theoretically produce perfect CP broadside (the direction normal to the plane of the element) and good CP over an angular region centered about broadside.

Almost square, rectangular patches are also investigated and are shown to provide circular polarization without the use of hybrids. The details of each of the designs are given in Section 3 and have been recently reported [3].

2.2 Element Design

In order to obtain dual-frequency operation from a microstrip patch element, two different approaches are possible. One approach is to design the element to be resonant at the two different frequencies. The other approach is to make the element sufficiently broad band so that both frequencies are within the bandwidth of the element, which may imply a thick substrate. If the two specified frequencies of operation are sufficiently close together so that the broad band element is feasible, this is the simplest method. The advantage of the dual frequency approach is that the element is usually more conformal.

Figs. 2.1-2.3 show three representative ways in which a dual band CP microstrip element may be constructed. Fig. 2.1 shows a broad band element which simply consists of a single patch antenna on an electrically thick substrate. Fig. 2.2 shows a dual frequency element obtained by reactively loading a single patch. Fig. 2.3 shows a different dual frequency design in which two stacked patches are used, each resonant at a different frequency. In this study the elements of Figs. 2.1 and 2.2 were experimentally investigated to explore the feasibility for use in the NASA program application. These two elements are discussed further in the subsections that follow. The third element design has been investigated by others in the past [4], and was not studied during this investigation. Other elements such as printed spiral antennas hold great promise for obtaining large bandwidth CP operation, but were also not investigated in this study.

Although the actual design requirements specify transmit and receive frequency bands near 14 GHz, a lower scaled frequency of approximately 3 GHz was used for each of the elements investigated. This was done simply for ease in fabrication. In principle, both impedance and pattern data should remain vaild for the higher design frequency if all dimensions are scaled down accordingly. The higher operating frequency will result in microstrip elements which are much more conformal. This would be particularly advantageous for the thick-substrate patch discussed in section 2.4.

2.3 Reactively Loaded Patch Antenna

Earlier work has established the utility of using a nearly square, diagonally fed microstrip patch for circularly polarized applications. Previous work has also demonstrated the feasibility of obtaining dual-band operation from a linearly polarized patch by using a single reactive load. The addition of two reactive loads to the nearly square patch gives rise to the possibility of providing circular polarization over two distinct frequency bands. The geometry of such a patch is shown in Fig. 2.2. For the purposes of this experimental study, the reactive loads were obtained by using sliding shorts on the back side of the ground plane, shown in Fig. 2.2a. In the final design, the loads could be implemented monolithically as microstrip stubs, as shown in Fig. 2.2b. An empirical study was undertaken to determine the radiation and circuit properties of the antenna shown in Fig. 2.2a. For this study two special cases were investigated: the nearly square patch and the exactly square patch.

2.4 Broadband Microstrip Antenna on Electrically Thick Substrate

It is well known [5] that the bandwidth of a microstrip patch increases with substrate thickness. Hence the bandwidth can be increased directly with no additional effort by simply using a thicker substrate. There is of course a limit to which the bandwidth can be increased. This limit usually occurs when the patch element is approximately 0.25 dielectric wavelengths from the ground plane. At this thickness, depending on the patch dimensions, bandwidths on the order of 25% - 50% may be obtained. There are normally a couple of disadvantages with having a very thick substrate, however. One is that the antenna element is simply no longer as conformal. The severity of this disadvantage depends on the application, and the frequency range of operation. For an operating center frequency of 14 GHz, the dielectric wavelength in a teflon- fiberglass material having a permittivity of 2.33 is 1.404 cm. In order to have a bandwidth of about 15%, the substrate thickness should be approximately 0.15 dielectric wavelengths. This gives a substrate thickness of 0.21 cm, which is physically still relatively thin.

Another disadvantage often associated with antennas on thick substrates is the strong excitation of surface waves. This produces two undesirable effects. First, it reduces the efficiency of the antenna, efficiency being defined as the radiated power relative to the total

(radiated plus surface-wave) power. Secondly, the excited surface waves may propagate to considerable distances and diffract off of the substrate edges, which may cause a serious interference effect in the radiation pattern. Both of these disadvantages may be eliminated, however, by simply truncating the dielectric directly around the perimeter of the patch. The patch in essence then becomes a modified dielectric resonator, having a conductive top surface. Such a patch antenna may be square in shape, and fed at the centers of two adjacent edges with a 90° phase shift. The phase shifter should be broad-band, such as a 3 dB hybrid. Fig. 2.1 shows such an element, along with a possible monolithic feeding arrangement.

3. MEASURED RESULTS

3.1 Nearly Square, Diagonally Fed, Reactively Loaded Microstrip Antenna

To begin, an unloaded microstrip radiator was fabricated for initial testing. Its dimensions were 3.13 cm by 2.90 cm and it was etched on a Duroid 5870 substrate with a thickness of 0.3175 cm and a relative permittivity of 2.35 as shown in Fig. 3.1. When fed at the point $(x = f_{d1}, y = f_{d2}) = (0.52, 0.48$ cm) the impedance as a function of frequency was measured using an HP8510 network analyzer with the results shown in Figs. 3.2 and 3.3. Circular polarized behavior was found near 2.964 GHz, with the spinning-linear pattern shown in Fig. 3.4.

Next, reactive loads were added to the radiating structure by attaching sliding short-circuited loads on the back side of the ground plane, as shown in Fig. 3.5. As the lengths of these stubs were changed, various reactive loads could be simulated. As the stub lengths are increased different circular polarization "modes" can be obtained. The first patch investigated had its loads inset a distance $d = 0.70$ cm in from each edge. When stub lengths of $s_1 = 3.95$ cm and $s_2 = 4.43$ cm are chosen, the impedance plots shown in Figs. 3.6 and 3.7 are obtained. Two pairs of peaks are clearly visible. When the radiation pattern is measured, it is found that linear polarization in the x-direction is obtained near the right-most peak of each of the pairs, while linear polarization in the y-direction is found at the left-most peak of each pair. In between each pair (near 2.487 GHz and 3.382 GHz) circular polarization is obtained (as shown in Figs. 3.8 and 3.9).

As the length of the stubs are increased a second mode can be found. When $s_1 = 8.6$ cm and $s_2 = 9.38$ cm the impedances shown in Figs. 3.10 and 3.11 are obtained. The major change in characteristics is the shifting of the circular polarization frequencies closer together in frequency (2.699 GHz and 3.312 GHz). The resulting patterns are shown in Figs. 3.12 and 3.13. Similar data for a third mode are shown in Figs. 3.14-3.17 and for a fourth mode in Figs. 3.18-3.21.

Additional sets of data were taken for several other stub lengths and feed points with the goal of learning how the various parameters affected the separation of the two res-

onant frequencies. To illustrate this behavior more clearly, summary graphs have been prepared to show the behavior of the circular polarized resonant frequencies as a function of the stub lengths. Fig. 3.22 shows this data for the case of a feed location of (0.15, 0.15 cm) and a load inset of $d = 0.35$ cm. This information is also shown in Fig 3.23 where only the separation between the upper and lower resonant frequencies is shown. Here the modal behavior is more clearly seen. In each case the best circular polarization (smallest axial ratio at broadside) occurs very near the minimum of each of the modal curves. Similar data is shown in Figs. 3.24 and 3.25 for the case of a feed at (0.09, 0.09 cm) and load insets of $d = 0.50$ cm, and in Figs. 3.26 and 3.27 for a feed at (.29, .33 cm)and load insets of $d = .70$ cm. The data for four different inset positions are then plotted in the graph of Fig. 3.28. The three curves represent the different modes with the higher order modes giving the smaller band separations. Thus, the band separation is seen to decrease both for higher mode number and for increasing load inset distances.

3.2 Square, Reactively Loaded Microstrip Antenna

During the investigation of the nearly square patch, it was discovered that dual band circular polarization could also be obtained from a square patch by using different reactive loads for the two spatially orthogonal modes. This geometry is depicted in Fig. 3.29. Measurements were then taken for different feed and load inset positions to investigate the possibilities of providing the required dual band, circularly polarized characteristics. In each instance, a square patch 2.96 cm on a side was etched on Duroid 5870 of thickness 0.157 cm and relative permittivity 2.35.

In the first case the patch was fed along the diagonal at $f_{d1} = f_{d2} = 0.25$ cm. The impedance of the unloaded version was measured and found to be resonant at 3.196 GHz as shown in Figs. 3.30 and 3.31, with the linearly polarized pattern (along the plane of the diagonal) given in Fig. 3.32. Reactive loads were then added at inset positions of $d = 0.11$ cm. The first circularly polarized (CP) mode was found for stub lengths of $s_1 = 4.3$ cm and $s_2 = 4.48$ cm, with the resulting impedance behavior shown in Figs. 3.33 and 3.34. Similar data are shown in Figs. 3.35 and 3.36 for the second mode with $s_1 = 8.85$ cm and $s_2 = 9.03$ cm; Figs. 3.37 and 3.38 for mode three with $s_1 = 13.5$ cm and $s_2 = 13.73$ cm; and Figs. 3.39 and 3.40 for mode four with $s_1 = 18.4$ cm and $s_2 = 18.53$ cm.

This information is summarized in Figs. 3.41-3.44 which show the resonant frequencies of the x and y polarized modes and their separations versus the corresponding stub lengths. The center frequency of the CP band is shown as a function of each stub length in Figs. 3.45 and 3.46, and the CP band separation in Figs. 3.47 and 3.48.

For the next case the same 2.96 cm square patch was used with loads still at $d = 0.11$ cm and the y-coordinate of the feed remaining at $f_{d1} = 0.25$ cm. The x-coordinate of the feed was then allowed to vary and the impedance and patterns were measured. This was done in an attempt to excite the lower frequency mode of each pair more strongly. The case of $f_{d2} = 0.475$ cm, $s_1 = 18.1$ cm, and $s_2 = 18.48$ cm is shown in Fig. 3.49; that for $f_{d2} = 0.775$ cm, $s_1 = 18.2$ cm, and $s_2 = 18.53$ cm in Figs. 3.50-3.52, and that for $f_{d2} = 1.15$ cm, $s_1 = 18.3$ cm, and $s_2 = 18.43$ cm in Fig. 3.53.

Next the feed was allowed to move in both directions with the data taken for the first five modes for $f_{d1} = 0.45$ cm and $f_{d2} = 1.05$ cm. This is shown in Figs. 3.54-3.56 for $s_1 = 4.5$ cm and $s_2 = 4.48$ cm; Fig. 3.57-3.59 for $s_1 = 9.1$ cm and $s_2 = 8.98$ cm; Fig. 3.60-3.62 for $s_1 = 13.7$ cm and $s_2 = 13.78$ cm; Figs. 3.63-3.65 for $s_1 = 18.4$ cm and $s_2 = 18.73$ cm; and Figs. 3.66-3.68 for $s_1 = 24.8$ cm and $s_2 = 25.03$ cm.

Summary graphs of this data for the resonant frequencies of the x and y-polarized modes are shown in Fig 3.69-3.76. Similar data with parameters identified in individual figure captions are shown in Figs. 3.77-3.99 for the case of $f_{d1} = 1.05$ cm, $f_{d2} = 0.45$ cm, and $d = 0.35$ cm, and in Figs. 3.100-3.123 for the case of $f_{d1} = 0.85$ cm, $f_{d2} = 0.45$ cm, and $d = 0.60$ cm.

3.3 Single Broadband Microstrip Antenna

An experimental patch resonator was built on a 0.9525 cm thick Duroid material having a permittivity of 2.33. The patch dimensions were 3.0 x 3.0 cm, which gave a resonant frequency near 3.13 GHz. In the experimental study a commercially available 90° hybrid was used instead of a monolithic hybrid. The feeds were along the centerlines of the patch, inset a distance .65 cm from the edges. At this feed location the input impedance at either

port is approximately 100 ohms at resonance. In order to obtain a 50 ohm match the feeds would have to be inset further toward the center of the patch. Fig. 3.124 shows the measured impedance at one of the antenna ports, with a 50 ohm load on the other port. Fig. 3.125 shows part of the impedance locus plotted on a 100 ohm Smith chart. The two frequencies f_1 and f_2 correspond to the 2.0 SWR bandwidth limits. The bandwidth is approximately 15%. Fig. 3.126 shows the real and imaginary parts of the input impedance, with the band limits indicated by the arrows at the bottom. Fig. 3.127 shows S_{11} looking into the 50 ohm hybrid when connected to the patch. The performance is shown for an open circuit on the isolated port of the hybrid and for a 50 ohm load on the isolated port. For a wide band match, the hybrid should be matched on the isolated port. The match looking into the hybrid should be considerably improved if the patch impedance were 50 ohms. Figs. 3.128-3.130 show the measured spinning-linear pattern of the patch at three frequencies, corresponding to near resonance and approximately 6% on either side of the resonant frequency. These patterns would probably also improve if the patch impedance was 50 ohms, due to a better match in the feeding circuit.

4. ANALYSIS OF THE ANTENNA ARRAY ENVIRONMENT

In order to determine whether adequate antenna performance and coverage is achieved, it is necessary to compute radiation patterns of the proposed microstrip antenna elements in their operating environment. Since it is not possible to model the entire astronaut/backpack in detail, approximate modeling techniques can be used to to assess element designs and antenna placement.

Since the antenna elements are electrically small and the field distributions on the patch antennas are relatively independent of the operating environment, it is possible to replace them with equivalent magnetic dipoles for far field computations. Due to the large electrical size of the backpack assembly and the suited astronaut, general full wave analysis techniques are not possible. Therefore, we must use approximate high frequency techniques to predict the field behavior. For such an analysis it is necessary to simplify the backpack geometry. Several simplified models can be used. For our problem, it is known that in many instances electrically large circular cylindrical structures can be approximated by rectangular structures [6]. Therefore, our approach will be to model the astronaut backpack as a rectangular block structure, approximately accounting for its effect by computing the geometrical optics and edge diffraction contributions from the edges near the source. In a similar fashion, the effects of the astronaut's head, body, arms, and legs, as well as the MMU, can be modeled by rectangular blocks and analyzed by geometrical diffraction procedures.

The modeling effort can be divided into three stages: First, a simplified block model for the backpack is developed. This model is used to determine the position and number of antennas necessary to give complete coverage, without the astronaut present. Next, we will demonstrate the effect the astronaut has on the radiation pattern of the backpack antennas. In the final stage of the coverage analysis, we will discuss the effects of arm and leg positions on the radiation patterns.

4.1 Discussion of Analysis

As mentioned previously, we will use high frequency electromagnetic techniques to approximate the fields radiated by antennas on the astronaut backpack. More specifically, we will use the Geometrical Theory of Diffraction (GTD). A detailed discussion of this method is given by Kouyoumjian and Pathak [7]. To model the backpack and astronaut geometries, we will use finite flat plates. These plates are very useful for modeling general shapes and are ideal for GTD analyses. Each plate is specified by its corners, in an arbitrary coordinate system, and is not limited to a particular number of vertices as long as all the edges lie in the same plane. These plates can be joined to form wedges and the appropriate field diffraction can be determined. The algorithm developed for this study is sufficiently general to handle any geometry that can be modeled with plates, and it only requires the locations of all the corners and sources. Techniques have been developed such that all geometrical factors are computed automatically. The dominant first order diffraction events are calculated, along with dominant specular reflections and blockage effects. The present code does not include higher order diffraction events, such as slope diffraction or corner diffraction. In addition, it does not account for multiple reflections or diffractions. However, these contributions are usually much less than the first order effects, particularly for objects which have dimensions greater than a few wavelengths (as is the case for this problem). The results given by this algorithm compared very favorably with the results from more accurate/exact solutions for several test cases.

4.2 Backpack investigation

To begin, we studied the radiation of antennas mounted on the backpack without the astronaut present. In this way we were able to determine the optimal positions for the antennas to achieve near complete coverage. Figures 4-1 to 4-4 show the model used for the backpack. Note that it consists of 11 flat plates of different sizes and shapes. Also note that several of the tested antenna positions are marked on these diagrams. To represent a circularly polarized antenna we used two orthogonal magnetic dipoles, with a quadrature phase shift. To present the field pattern results we have isolated each antenna, and in general only show the fields radiated by one antenna in each plot. This greatly simplifies the interpretation of the results. Also note that all the patterns presented show a curve

representing the maximum electric field component received at the observation point and the minimum electric field received at the observation point. Therefore, the difference between the two curves is the axial ratio for the radiated field (spinning dipole pattern).

One of our initial concerns was that it would be very difficult to obtain adequate coverage in the back of the pack since the presence of the MMU prohibited the mounting of an antenna on the back face. To cover the back area an antenna was mounted at location 1 shown in the previous figures. Its far field patterns are shown in Figures 4-5 to 4-7. From these results we note that an antenna at position 1 does a very good job of covering a broad region above and behind the backpack. The slope of the back tends to steer the pattern upward. The circular polarization (CP) is well maintained in this region. The pattern starts to drop off near vertical and beyond the horizontal in the back. To compensate for this decrease in the lower region an antenna is mounted on the bottom of the pack, position 3. The corresponding patterns are shown in Figures 4-8 to 4-10. Note that this antenna covers the lower region well and overlaps nicely with the position 1 antenna. Note in all these patterns there is significant diffraction from the edges near the antenna. This diffraction appears as the *spill over* around the edges and the *scalloping* in the main beam.

To obtain coverage in the front an antenna is mounted at position 2, just above the head of the astronaut. The patterns corresponding to this antenna are shown in Figures 4-11 to 4-13. As expected, this antenna does a good job of covering the front area and does a moderate job of covering the bottom forward region. Notice that in combination with the antenna at position 1 (Figures 4-5 to 4-7), these two antennas adequately cover the region directly above the pack. A better job of covering the vertical region is done by an antenna at location 8 (Figures 4-14 to 4-16), however, this antenna does a poor job of covering both the forward and rear regions. Therefore, it is probably a better decision to choose the antennas at positions 1 and 2.

With the choice of the antennas in positions 1, 2, and 3 the front, rear, bottom, and top regions are covered adequately. It remains to choose a location of an antenna that will cover the sides. Four positions where considered, 4, 5, 6, and 7. The corresponding far field patterns are shown in Figures 4-17 to 4-19, 4-20 to 4-22, 4-23 to 4-25, and 4-26 to

4-28, respectively. Notice that the axial ratio for first three antennas is poor in the x-z plane, as one would expect, whereas, the axial ratio for the antenna mounted on the slope (position 7) is good in that plane. This antenna, however, does a poor job of covering the side region. The plots show that there is very little difference between the other three antennas, all seem to radiate the same. Position 4 is probably the best choice since it is further away from the arms of the astronaut, thus reducing the effects of blockage. To cover both side an antenna should be mounted at position 4 on both the left and right faces of the pack.

In summary, we have found that for the backpack alone, adequate CP coverage can be obtained by using 5 CP antennas mounted at positions 1, 2, 3, and 4. However, this section did not address the problem of the astronaut blocking or scattering the fields of the antennas.

4.3 Astronaut blockage

In the previous section we found a backpack antenna combination that provided near complete coverage. However, when the backpack is mounted on an astronaut, the radiation patterns will be altered. To help quantitify this effect we have modeled the astronaut using flat plates and used our GTD analysis to solve for the far field antenna patterns. Figures 4-29 and 4-30 show the elementary model used for the astronaut. Although relatively simple, this model is sufficient to determine the magnitude of the astronaut blockage effect and to help identify problem areas. A side view of the complete model (astronaut and backpack) is shown in Figure 4-31. As we did in the previous section, we will only consider antennas individually.

The first example (Figures 4-32 to 4-34) shows the radiation patterns for an antenna mounted above the head of the astronaut, in position 2. Notice that the fields are dramatically reduced for large θ due to the blockage by the head. In addition, note that the other patterns are distorted by the field scattered from the body. Unfortunately, this effect is difficult to eliminate. Other antenna locations suffer from similar effects. From our earlier analysis, we found that the only other main contributor to the fields in this blocked out region is the antenna mounted at the bottom of the pack (position 3). Figures

4-35 to 4-37 show the patterns for this antenna in the presence of the astronaut. As one might expect by examining the geometry in Figure 4-31, the fields radiated by this bottom antenna are extremely distorted due to the blockage by the astronaut's legs. Therefore, due to blockage there is a blind spot in the pattern down below the astronaut, in front of his feet. Figures 4-38 to 4-40 show the patterns for the antenna in position 4, in the presence of the astronaut. Note that they are significantly different than the unperturbed case shown earlier.

References

[1] W.F. Richards, S.E. Davidson, and S.A. Long, "Dual-band, reactively loaded microstrip antenna," *IEEE Trans. Antennas Propagat.*, vol. AP-33, pp. 556-561, May 1985.

[2] S.E. Davidson, S.A. Long, and W.F. Richards, "Dual-band microstrip antennas with monolithic reactive loading," *Electronics Letters*, vol. 21, no. 20, pp. 936-937, Sept. 26, 1985.

[3] S.E. Slawson and S.A. Long, "The use of reactive loading for dual-band circularly polarized characteristics in microstrip antennas," *IEEE Antennas Propagat. Symposium Digest*, pp. 704-707, June 1988.

[4] S.A. Long and M.D. Walton, "A dual frequency, stacked circular disc antenna," *IEEE Trans. Antennas Propagat.*, vol. AP-27, pp. 270-273, March 1979.

[5] E. Chang, S.A. Long, and W.F. Richards, "An experimental investigation of electrically thick rectangular microstrip antennas," *IEEE Trans. Antennas Propagat.*, vol. AP-34, pp. 767-772, June 1986.

[6] C.A. Balanis, "Radiation characteristics of current elements near a finite length cylinder," *IEEE Trans. Antennas Propagat.*, vol. AP-18, pp. 352-359, May 1970.

[7] R.G. Kouyoumjian and P.H. Pathak, "A uniform geometrical theory of diffration for an edge in a perfectly conducting surface," *Proc. IEEE*, vol 62, No. 11, pp. 1448-1461, Nov. 1974.

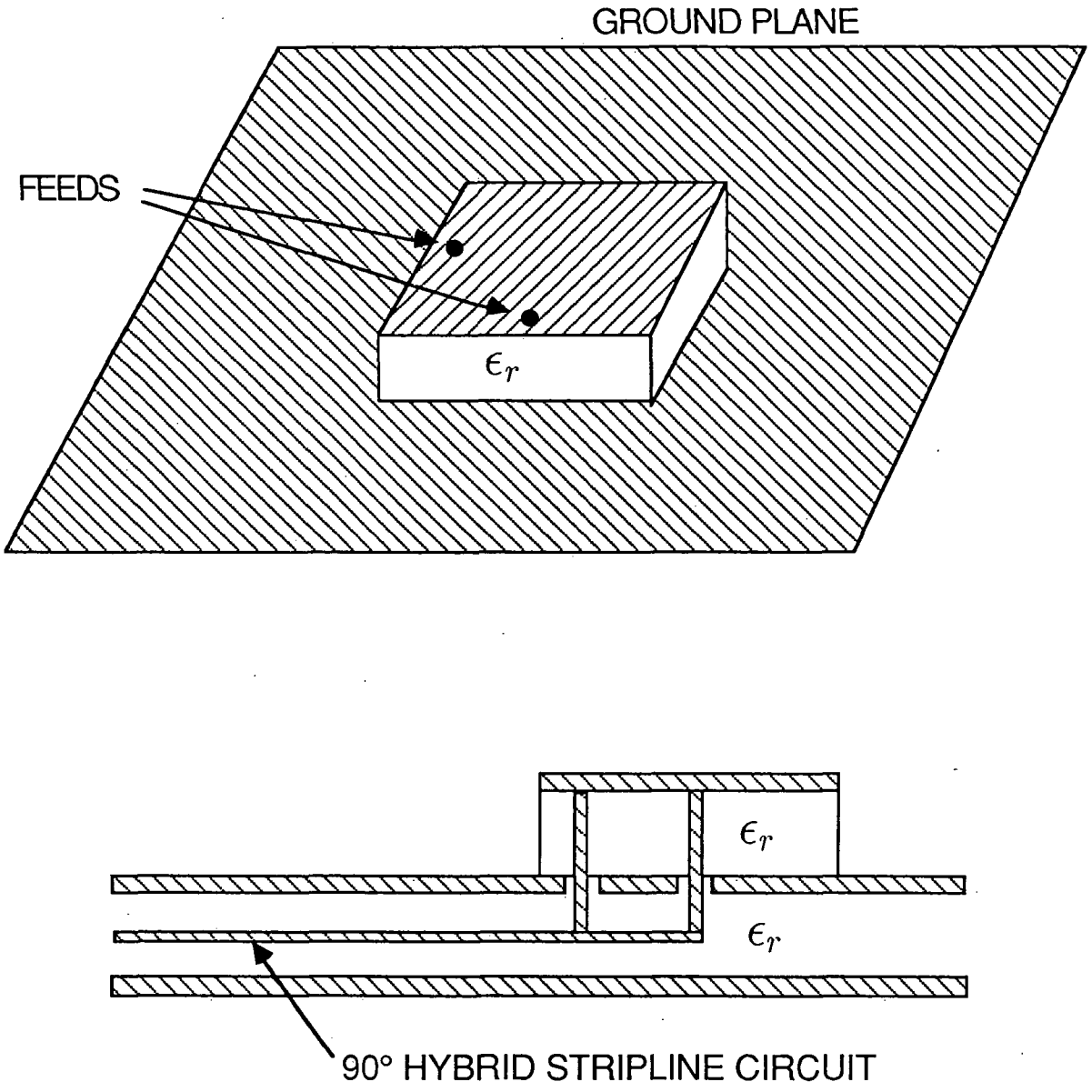

Fig. 2.1 Patch on thick substrate fed by a stripline circuit.

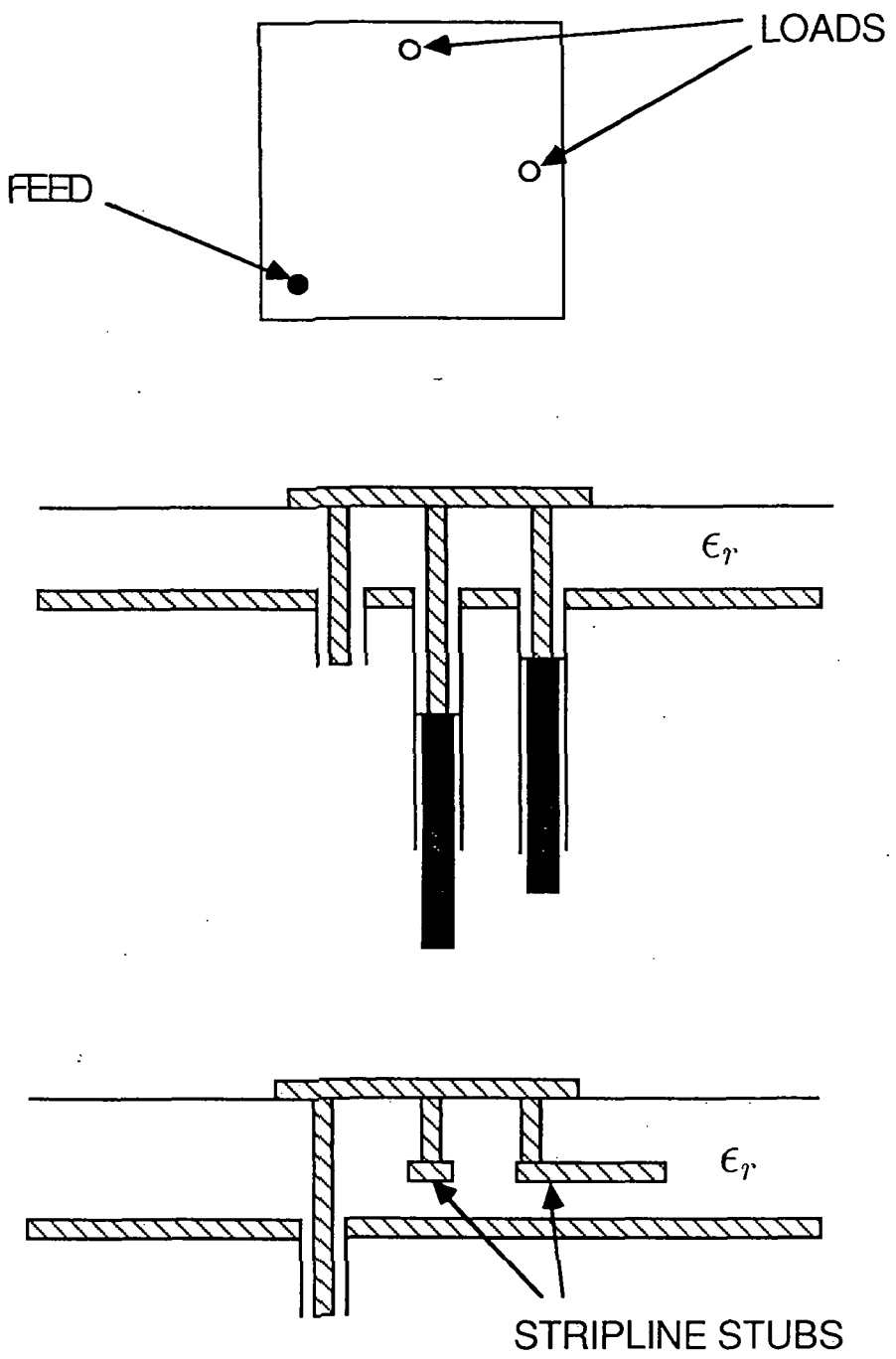

Fig. 2.2 Patch with reactive loads. (a) Sliding shorts used in measurements. (b) Mononlithic design.

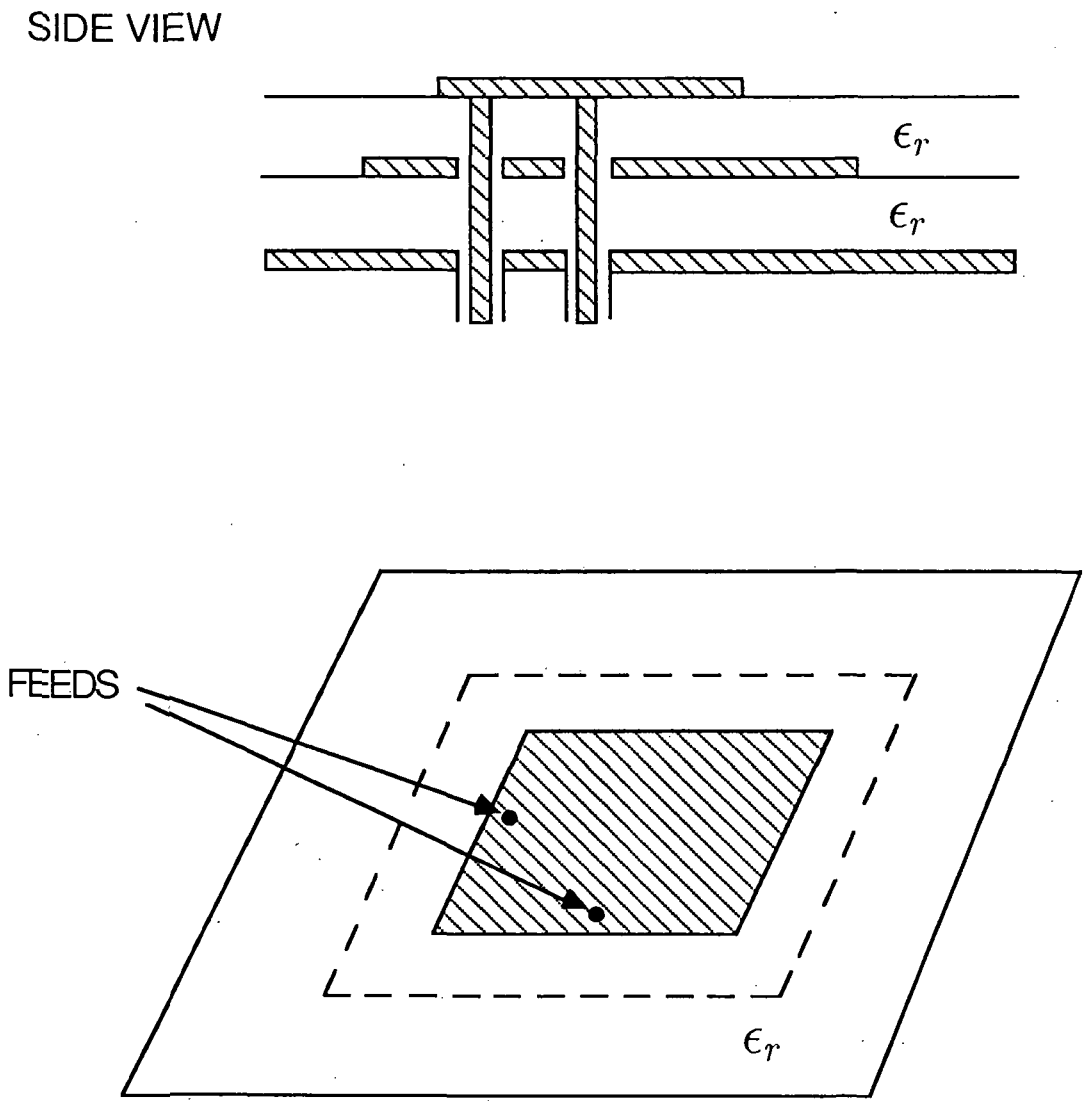

Fig. 2.3 Dual band stacked patch.

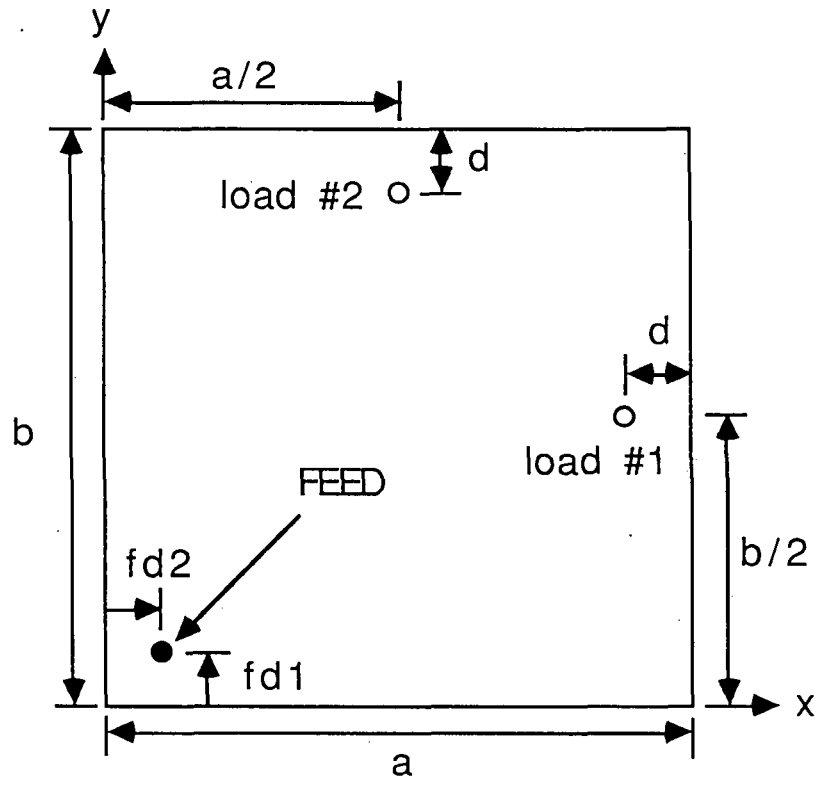

Fig. 3.1 Geometry of reactively loaded, almost square microstrip antenna.

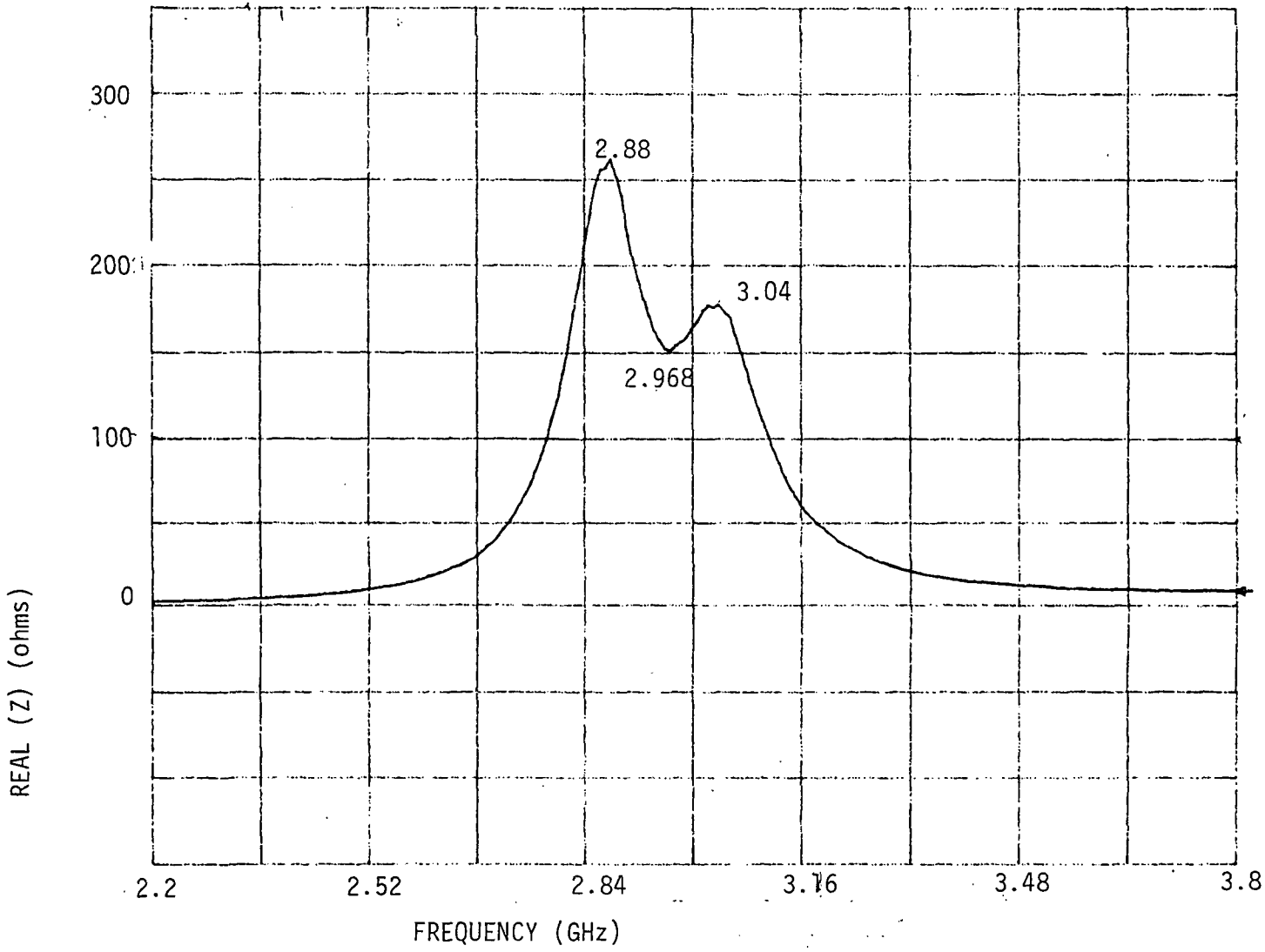

Fig. 3.2 Real part of input impedance versus frequency for an unloaded 3.13 cm by 2.90 cm rectangular patch with a feed location of (.52, .48 cm).

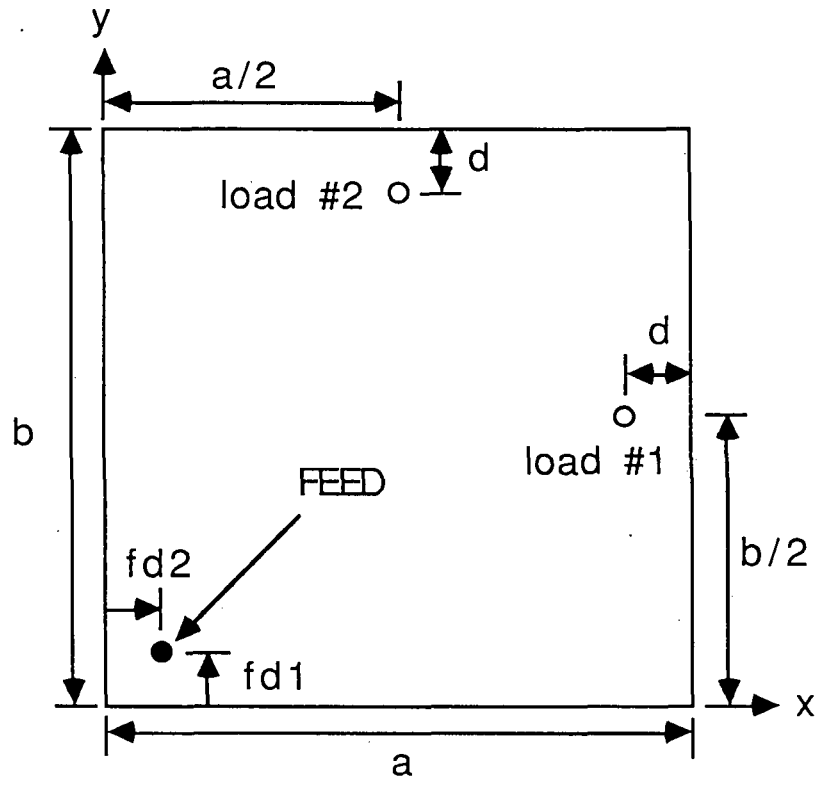

Fig. 3.1 Geometry of reactively loaded, almost square microstrip antenna.

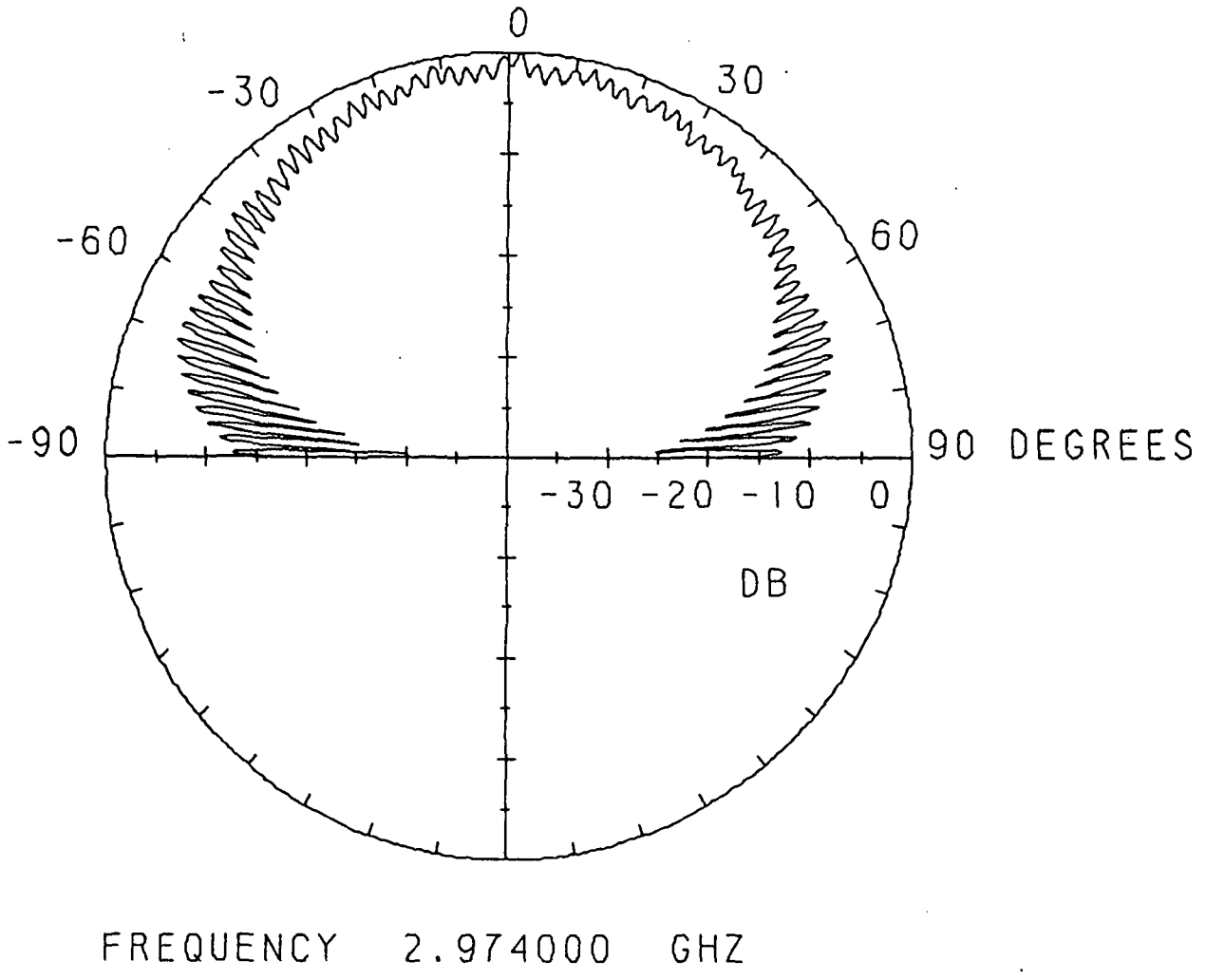

Fig. 3.4 Spinning linear pattern for an unloaded 3.13 cm by 2.90 cm rectangular patch with a feed location of (.52, .48 cm).

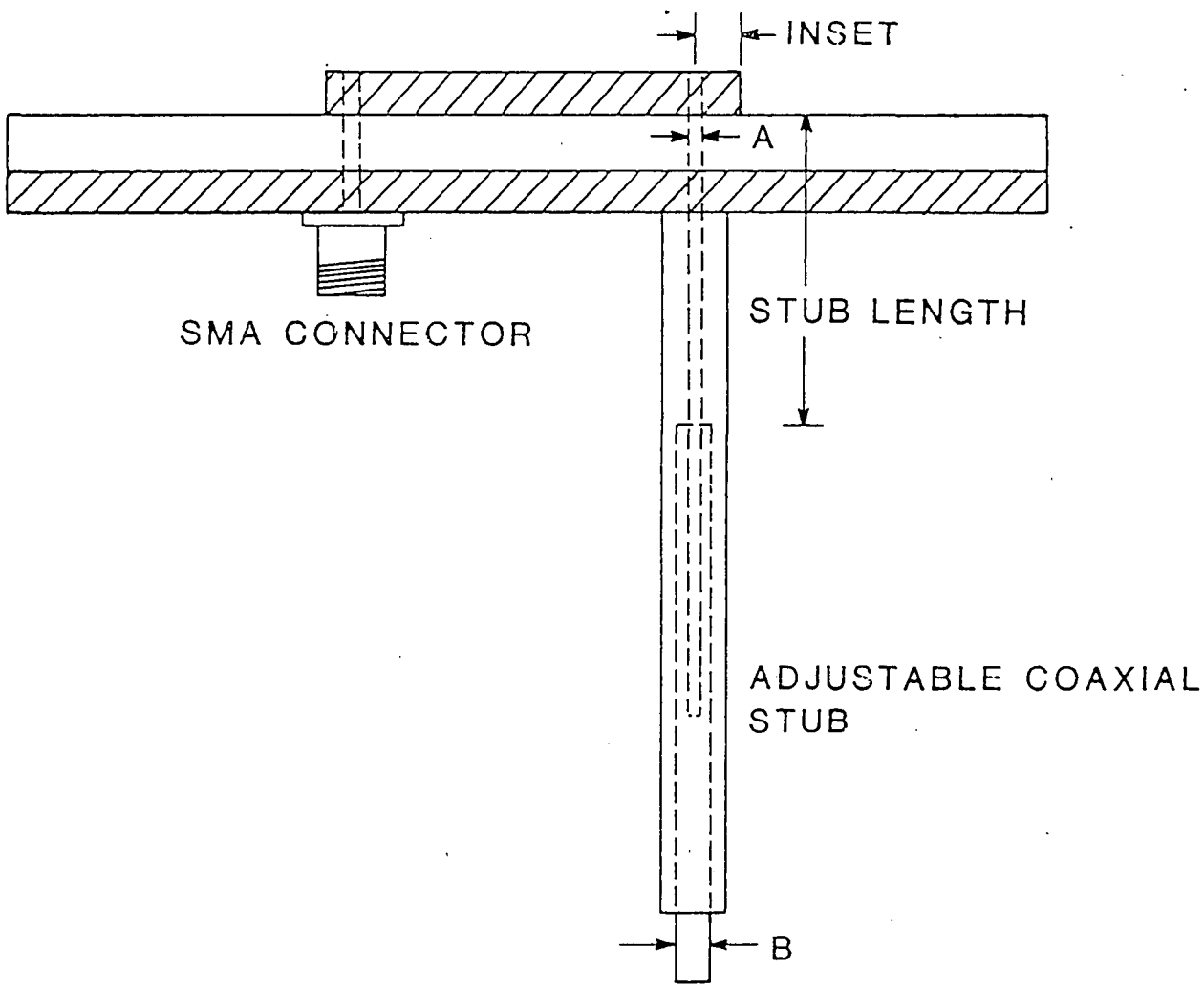

Fig. 3.5 Reactive loading using adjustable coaxial stubs.

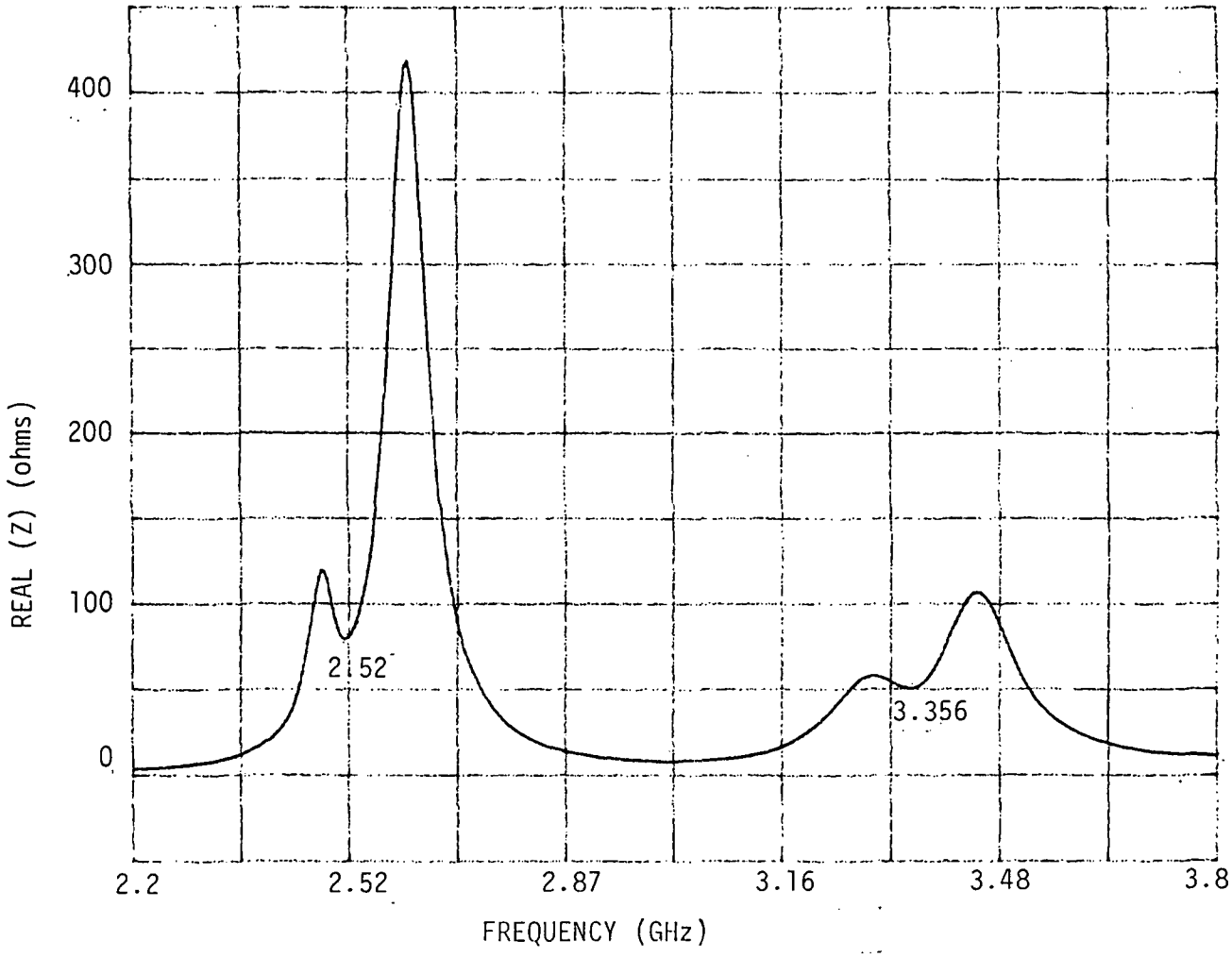

Fig. 3.6 Real part of impedance verses frequency of the first mode for a loaded 3.13 by 2.90 cm rectangular patch with a feed location of (.52, .48 cm), load insets of d = .70 cm, and stub lengths of s_1 = 3.95 cm and s_2 = 4.43 cm.

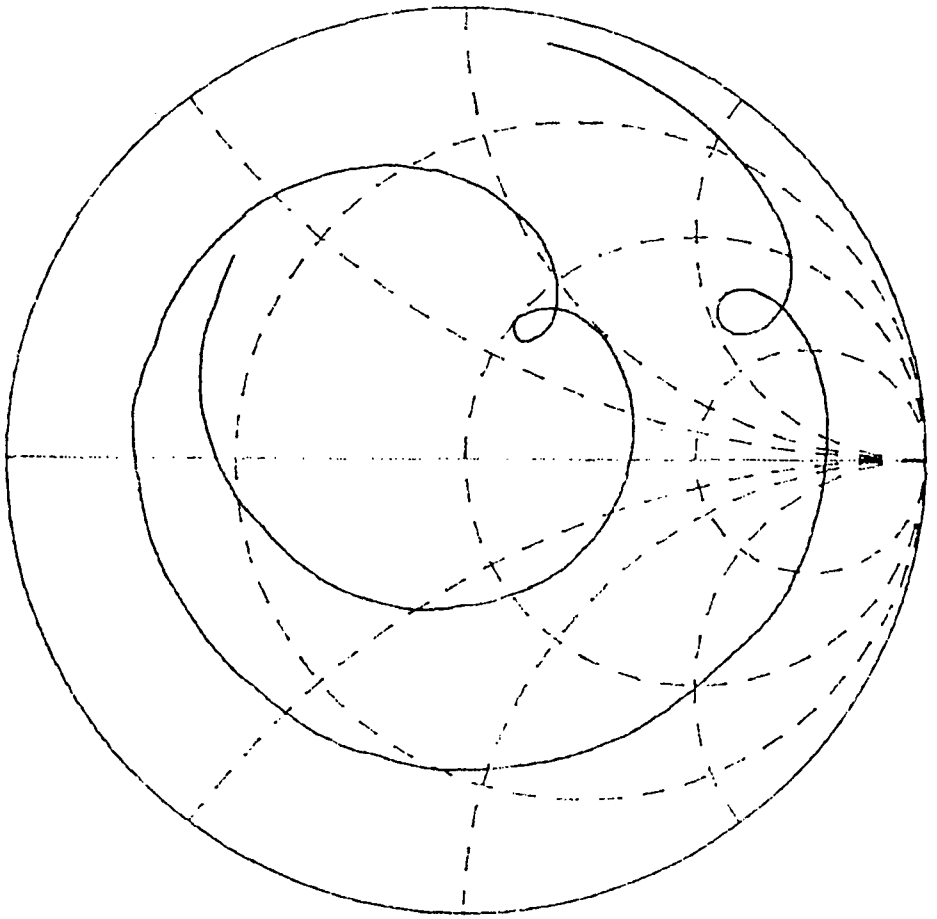

Fig. 3.7 Smith chart representation of the input impedance of the first mode for a loaded 3.13 by 2.90 cm rectangular patch with a feed location of (.52, .48 cm), load insets of d = .70 cm, and stub lengths of s_1 = 3.95 cm and s_2 = 4.43 cm.

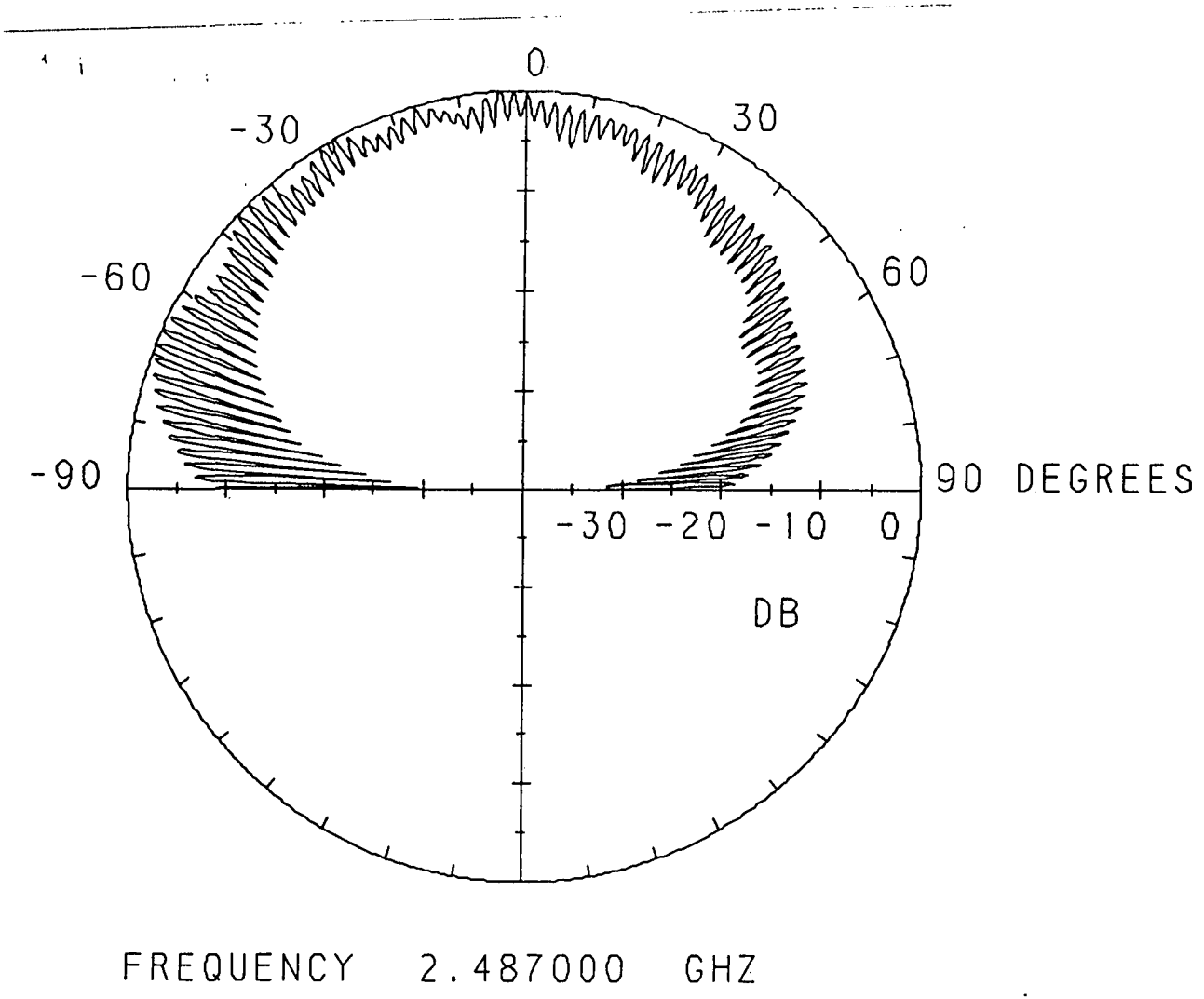

Fig. 3.8 Spinning linear pattern for the lower cp band of the first mode for a loaded 3.13 by 2.90 cm rectangular patch with a feed location of (.52, .48 cm), load insets of d = .70 cm, and stub lengths of s_1 = 3.95 cm and s_2 = 4.43 cm.

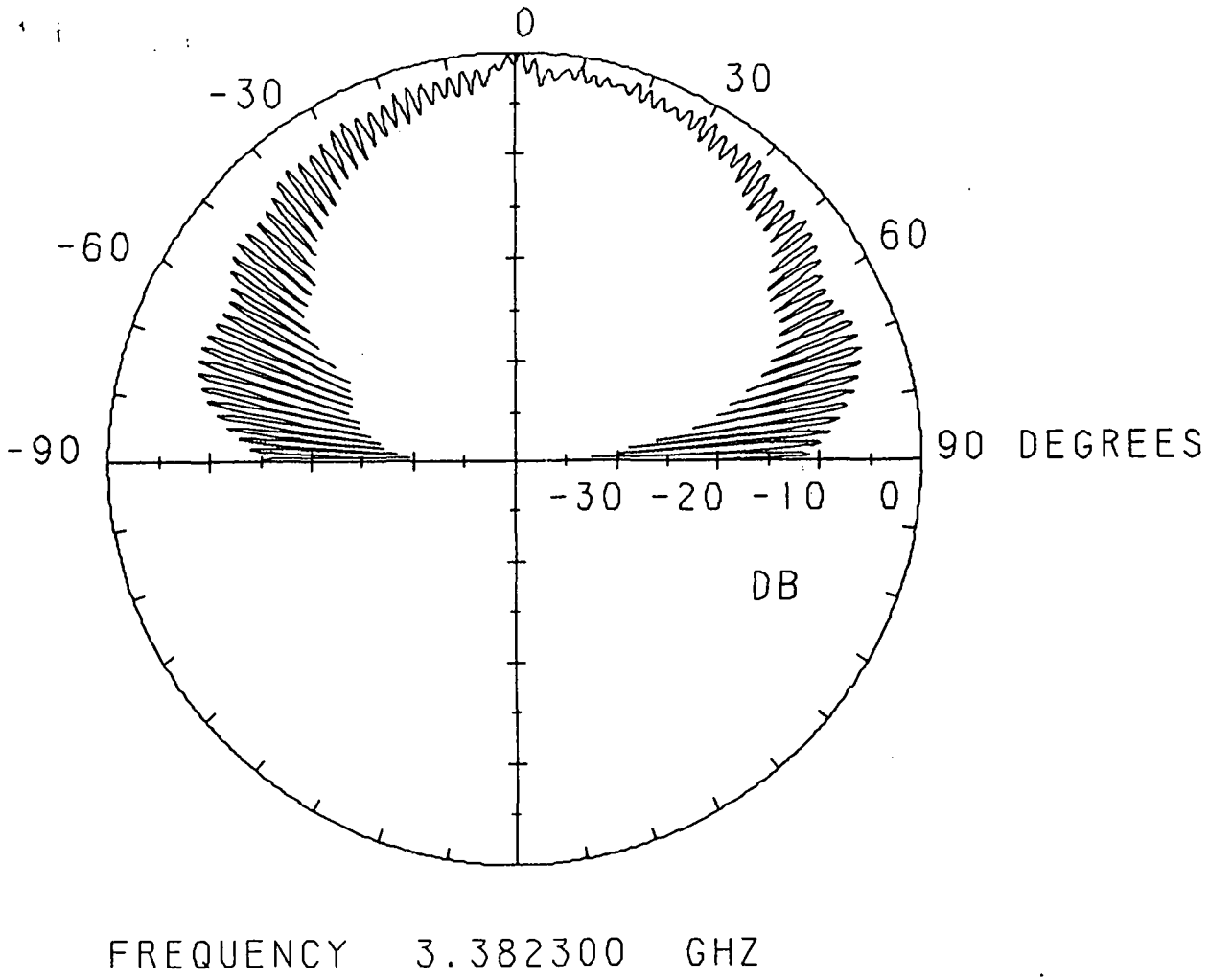

Fig. 3.9 Spinning linear pattern for the upper cp band of the first mode for a loaded 3.13 by 2.90 cm rectangular patch with a feed location of (.52, .48 cm), load insets of d = .70 cm, and stub lengths of s_1 = 3.95 cm and s_2 = 4.43 cm.

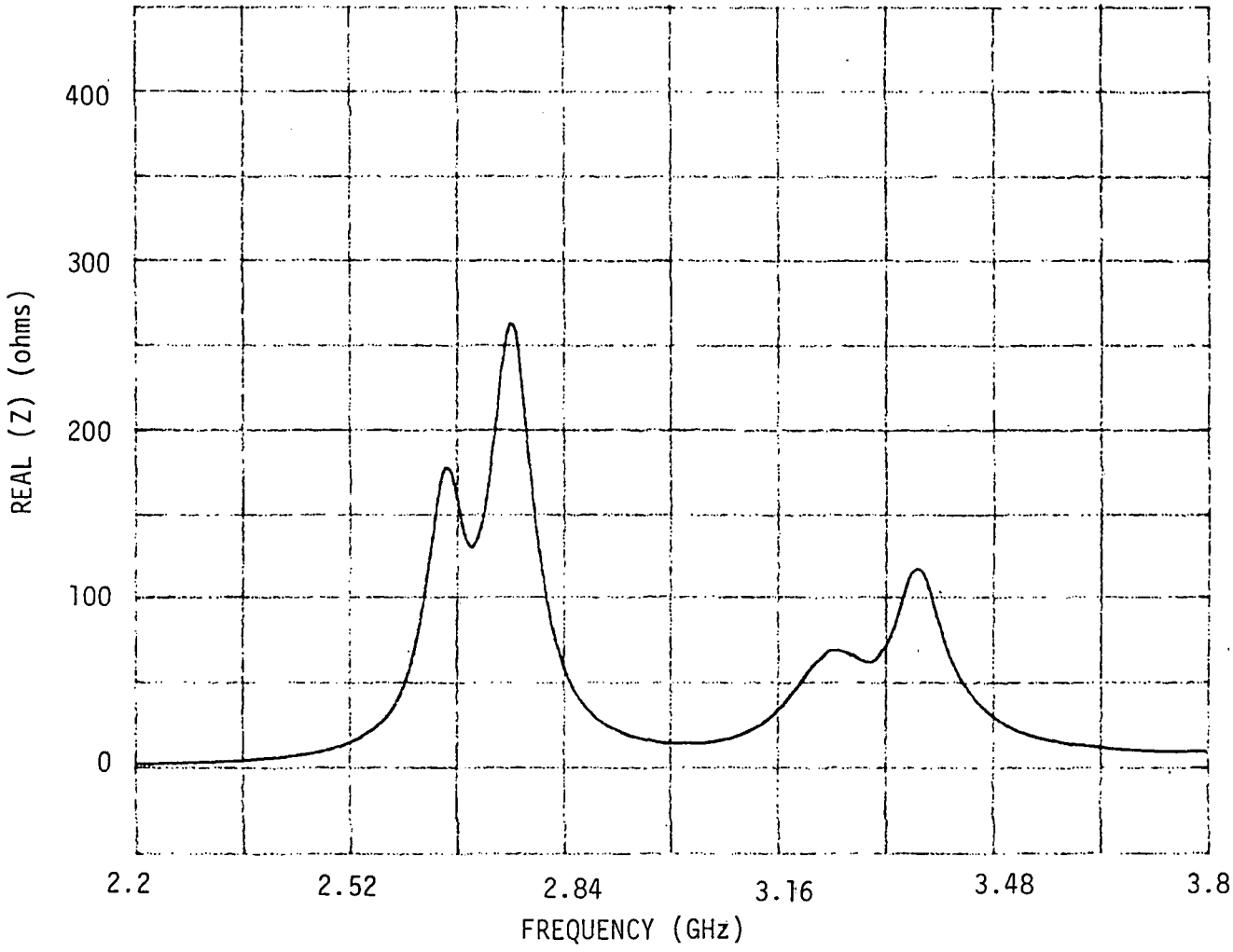

Fig. 3.10 Real part of impedance verses frequency of the second mode for a loaded 3.13 by 2.90 cm rectangular patch with a feed location of (.52, .48 cm), load insets of d = .70 cm, and stub lengths of s_1 = 8.6 cm and s_2 = 9.38 cm.

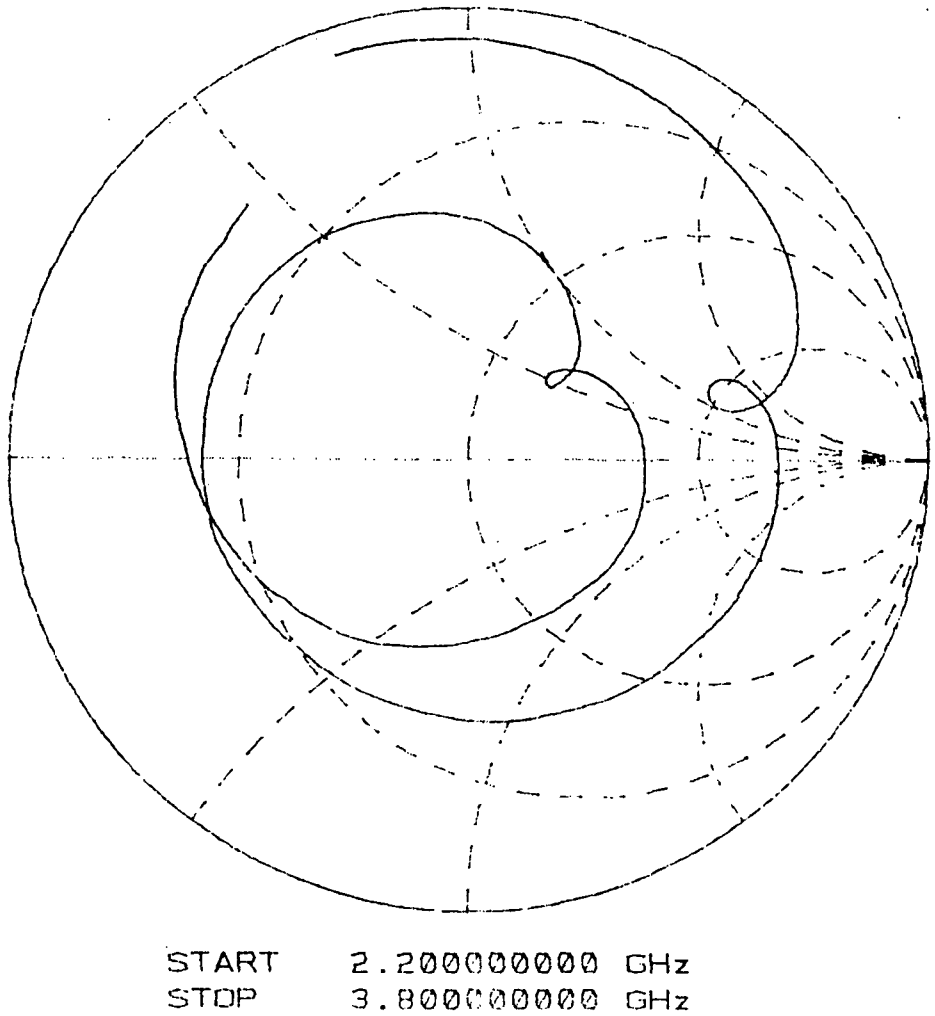

Fig. 3.11 Smith chart representation of the input impedance of the second mode for a loaded 3.13 by 2.90 cm rectangular patch with a feed location of (.52, .48 cm), load insets of d = .70 cm, and stub lengths of s_1 = 8.6 cm and s_2 = 9.38 cm.

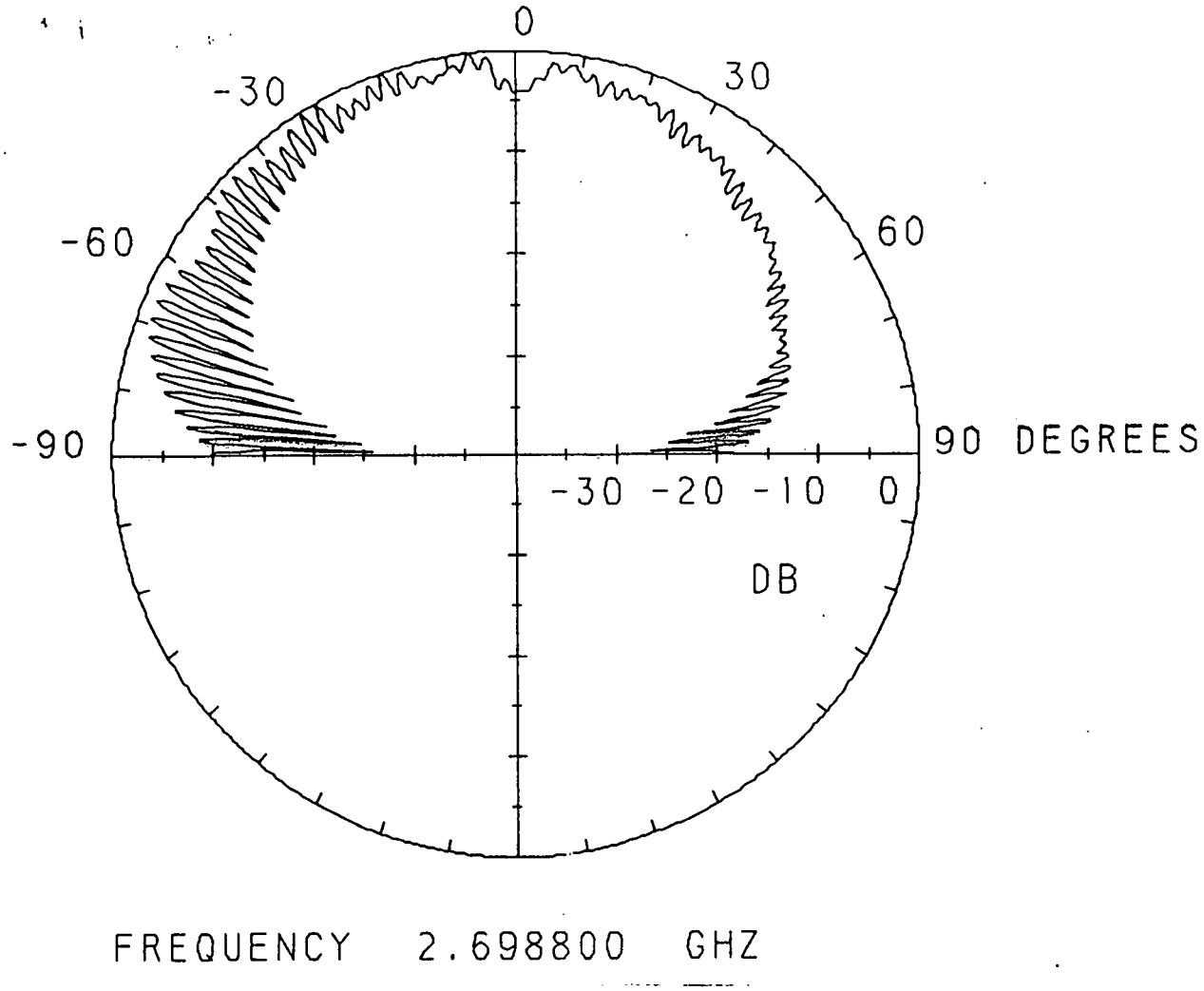

Fig. 3.12 Spinning linear pattern for the lower cp band of the second mode for a loaded 3.13 by 2.90 cm rectangular patch with a feed location of (.52, .48 cm), load insets of d = .70 cm, and stub lengths of s_1 = 8.6 cm and s_2 = 9.38 cm.

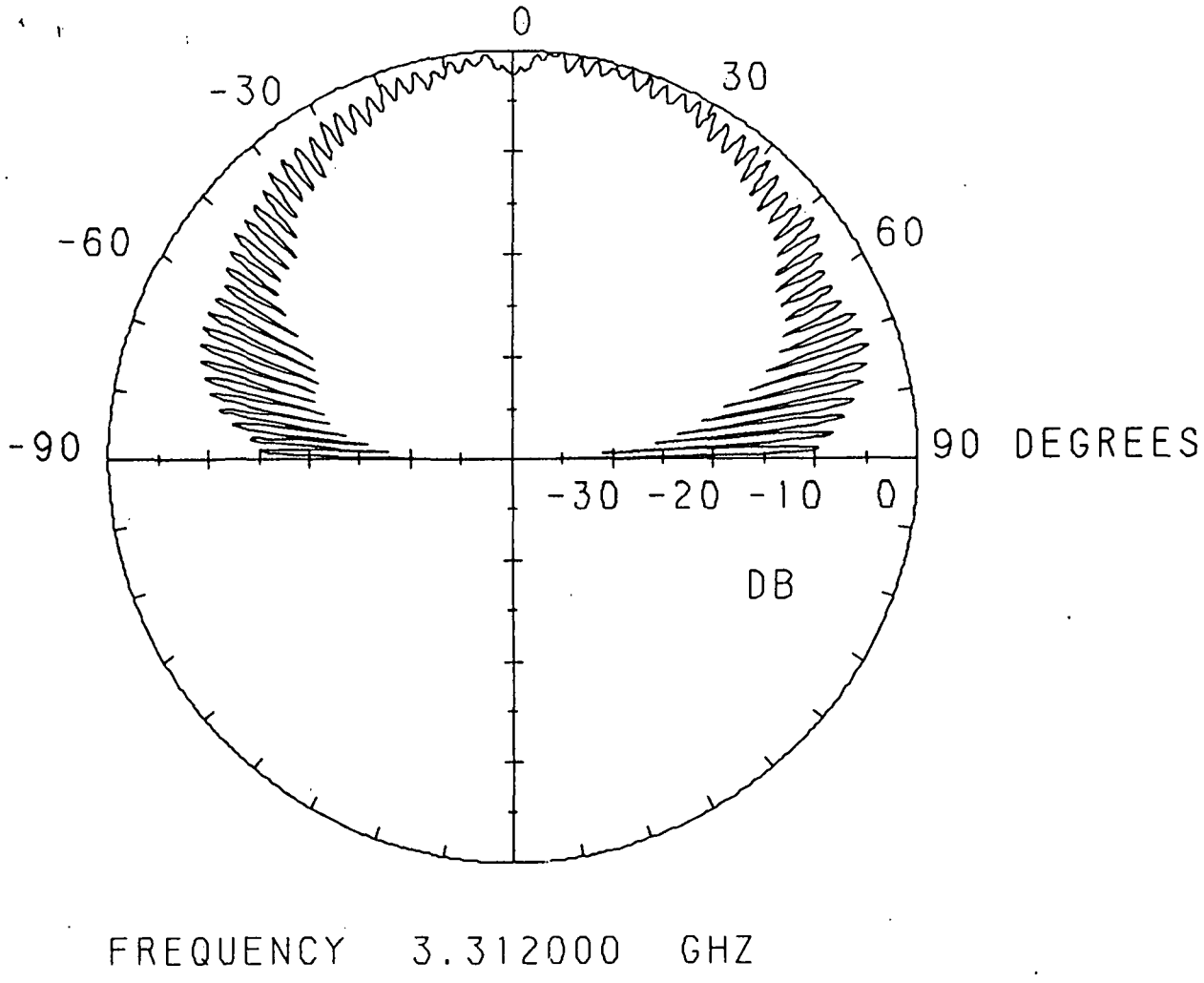

Fig. 3.13 Spinning linear pattern for the upper cp band of the second mode for a loaded 3.13 by 2.90 cm rectangular patch with a feed location of (.52, .48 cm), load insets of d = .70 cm, and stub lengths of s_1 = 8.6 cm and s_2 = 9.38 cm.

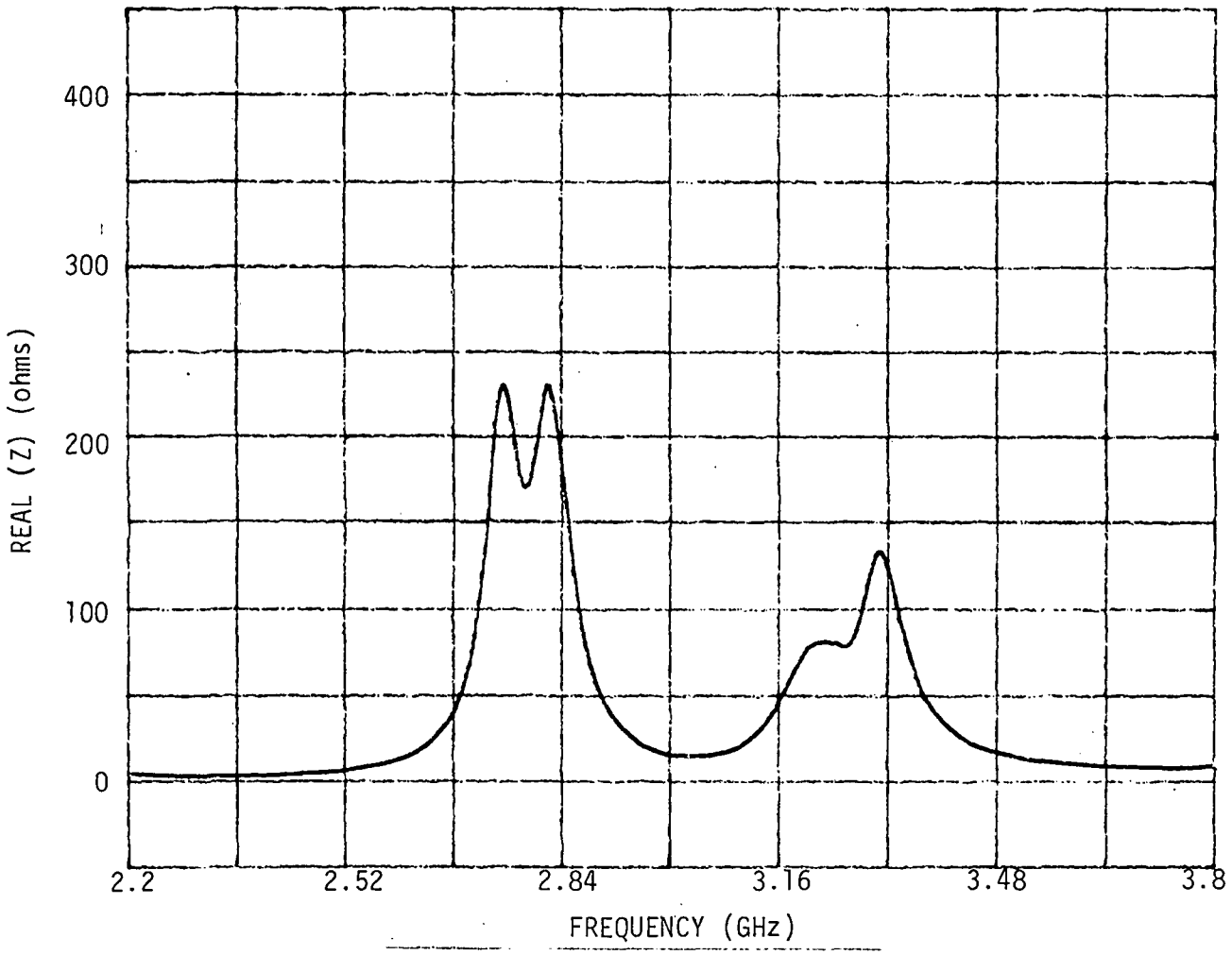

Fig. 3.14 Real part of impedance verses frequency of the third mode for a loaded 3.13 by 2.90 cm rectangular patch with a feed location of (.52, .48 cm), load insets of d = .70 cm, and stub lengths of s_1 = 13.35 cm and s_2 = 14.38 cm.

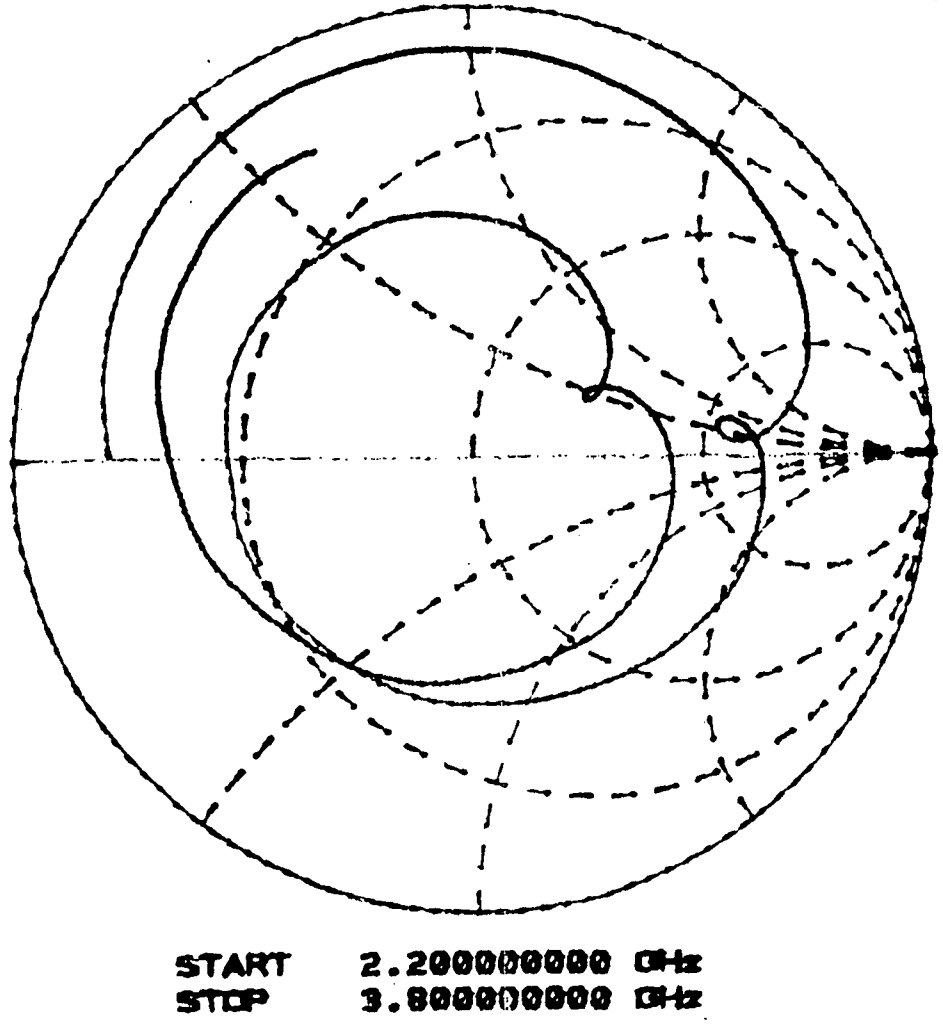

Fig. 3.15 Smith chart representation of the input impedance of the third mode for a loaded 3.13 by 2.90 cm rectangular patch with a feed location of (.52, .48 cm), load insets of d = .70 cm, and stub lengths of s_1 = 13.35 cm and s_2 = 14.38 cm.

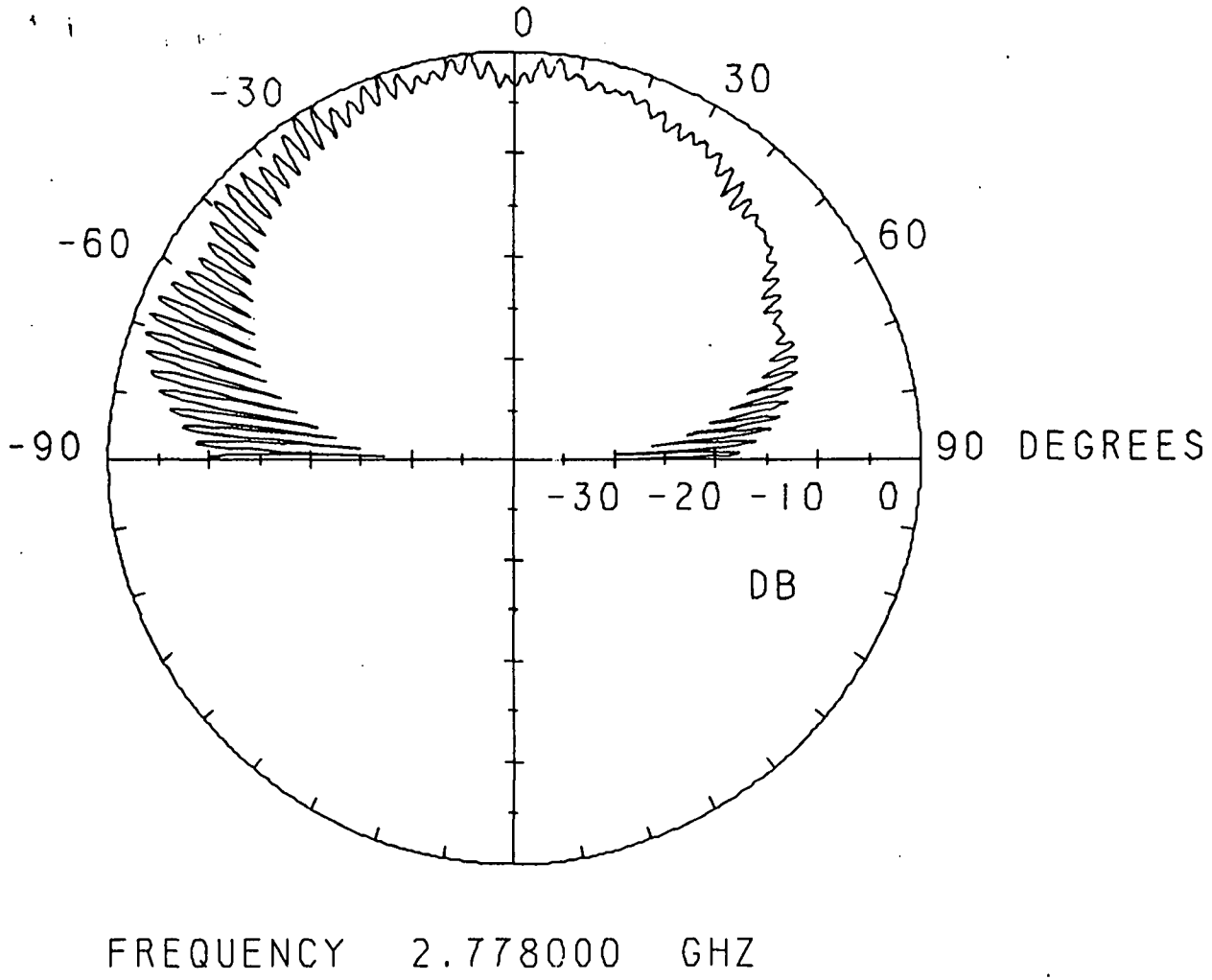

Fig. 3.16 Spinning linear pattern for the lower cp band of the third mode for a loaded 3.13 by 2.90 cm rectangular patch with a feed location of (.52, .48 cm), load insets of d = .70 cm, and stub lengths of s_1 = 13.35 cm and s_2 = 14.38 cm.

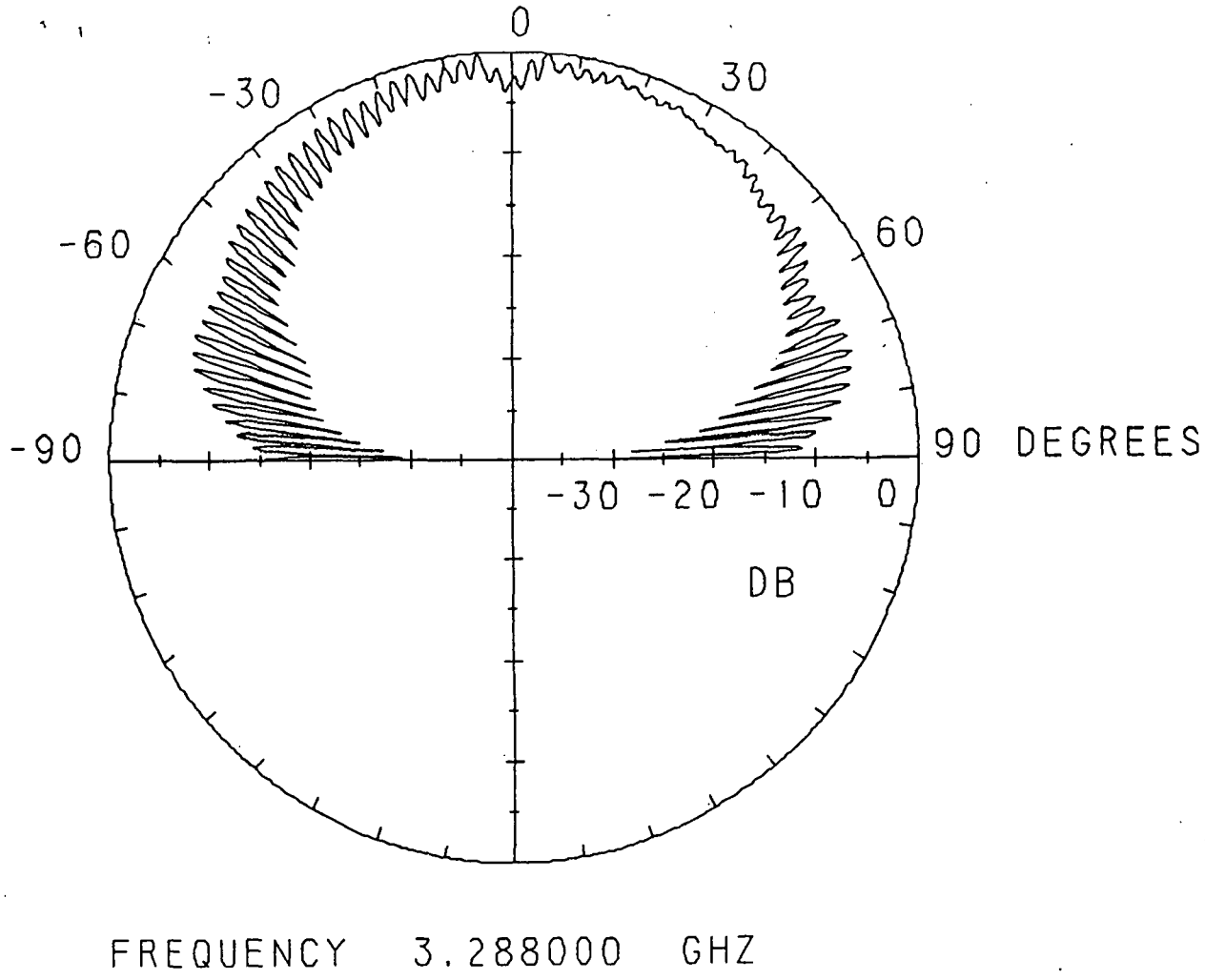

Fig. 3.17 Spinning linear pattern for the upper cp band of the third mode for a loaded 3.13 by 2.90 cm rectangular patch with a feed location of (.52, .48 cm), load insets of d = .70 cm, and stub lengths of s_1 = 8.6 cm and s_2 = 9.38 cm.

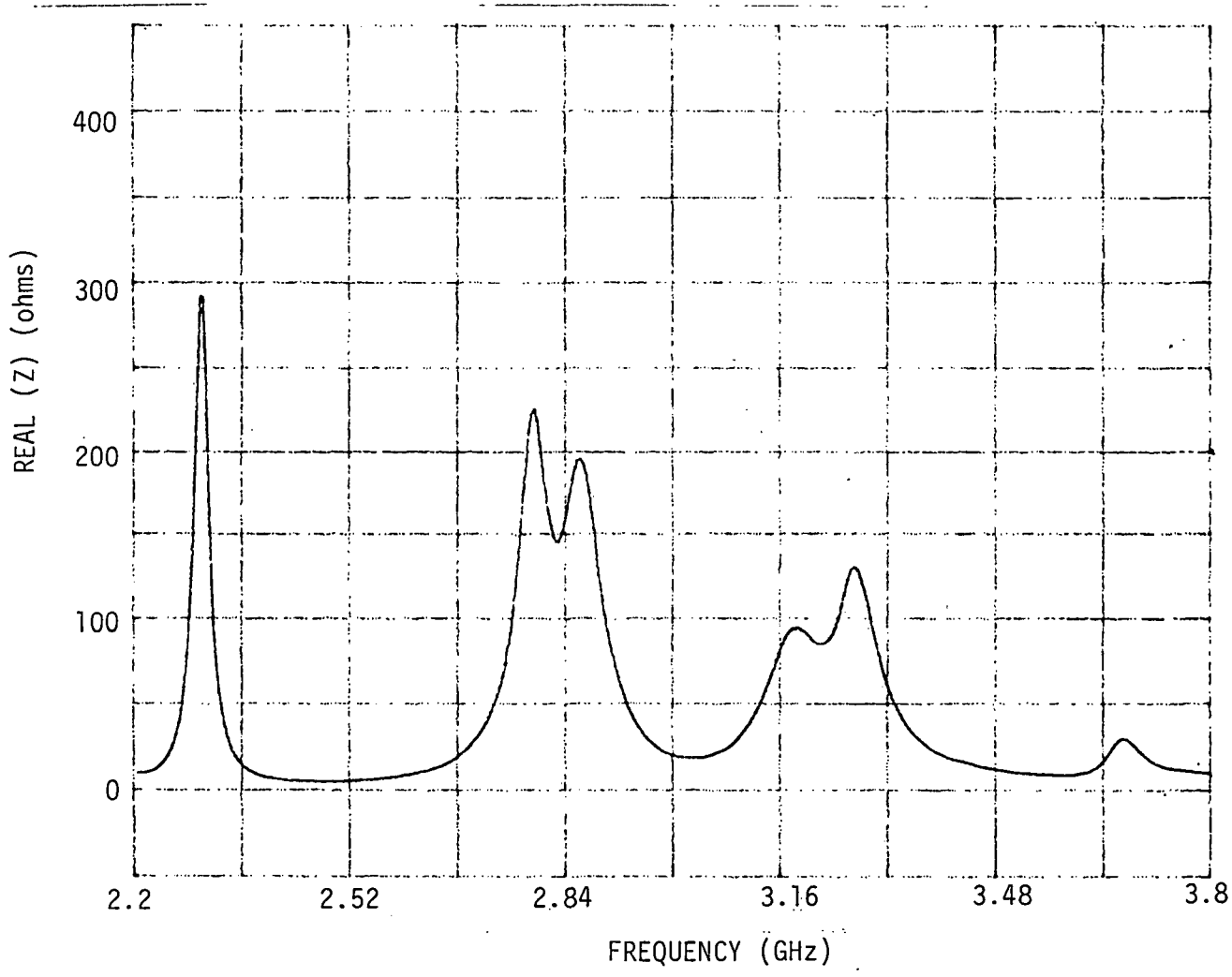

Fig. 3.18 Real part of impedance verses frequency of the fourth mode for a loaded 3.13 by 2.90 cm rectangular patch with a feed location of (.52, .48 cm), load insets of d = .70 cm, and stub lengths of s_1 = 18.1 cm and s_2 = 19.43 cm.

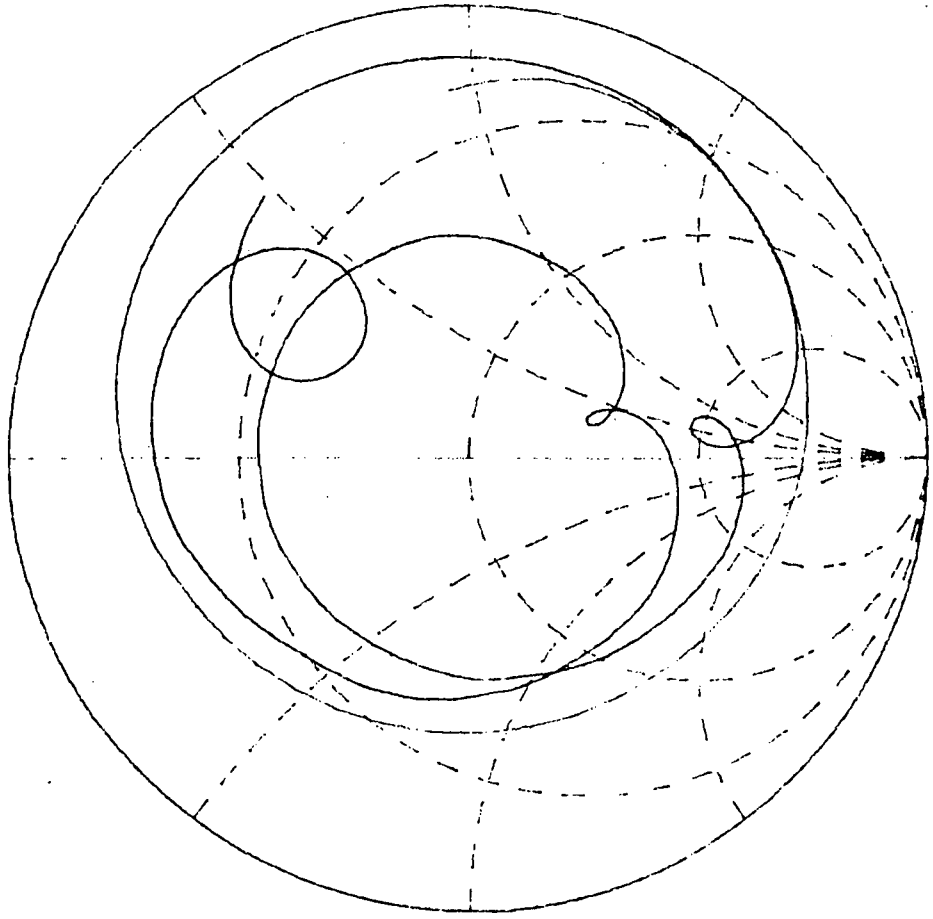

Fig. 3.19 Smith chart representation of the input impedance of the fourth mode for a loaded 3.13 by 2.90 cm rectangular patch with a feed location of (.52, .48 cm), load insets of d = .70 cm, and stub lengths of s_1 = 18.1 cm and s_2 = 19.43 cm.

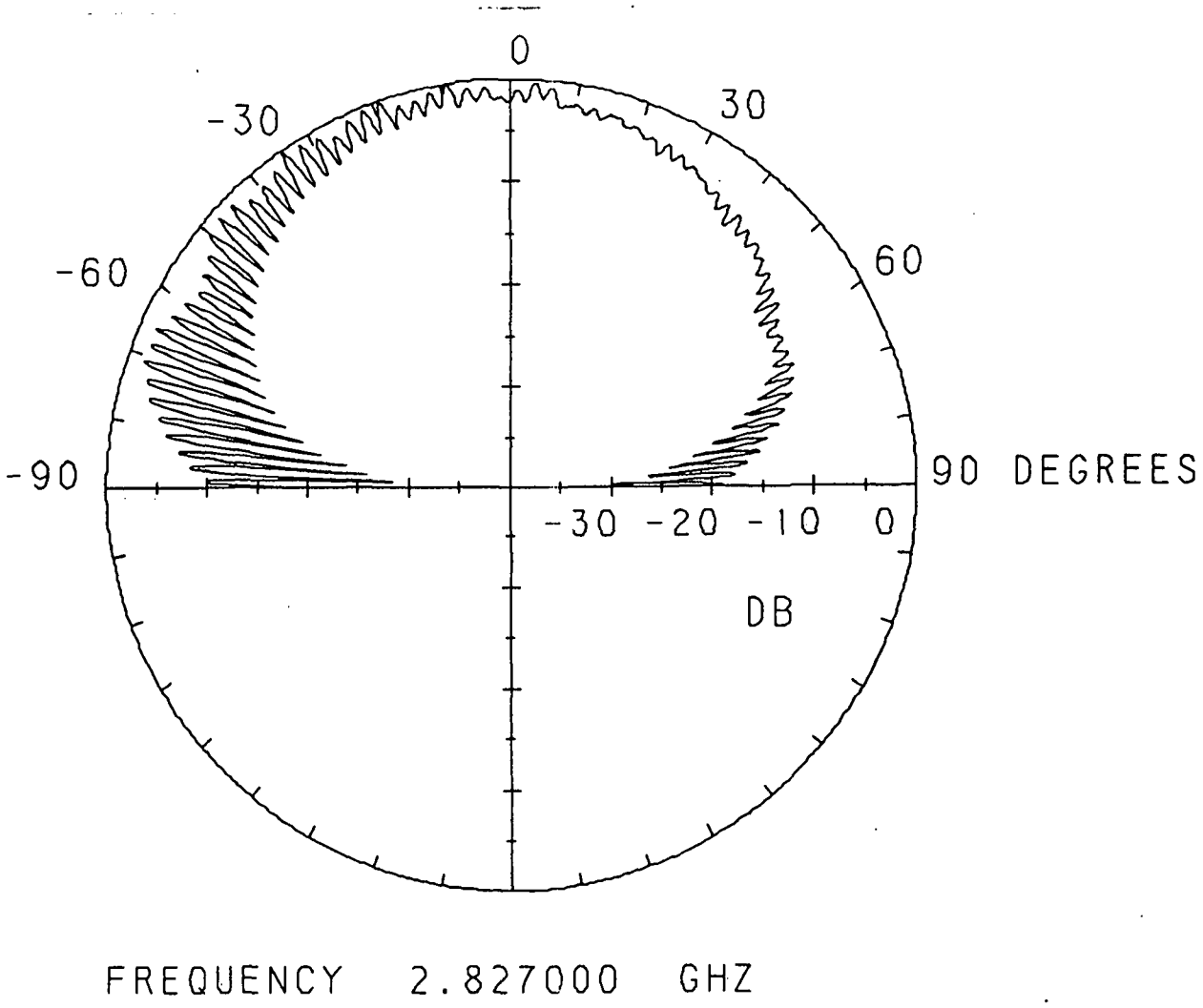

Fig. 3.20 Spinning linear pattern for the lower cp band of the fourth mode for a loaded 3.13 by 2.90 cm rectangular patch with a feed location of (.52, .48 cm), load insets of d = .70 cm, and stub lengths of s_1 = 18.1 cm and s_2 = 19.43 cm.

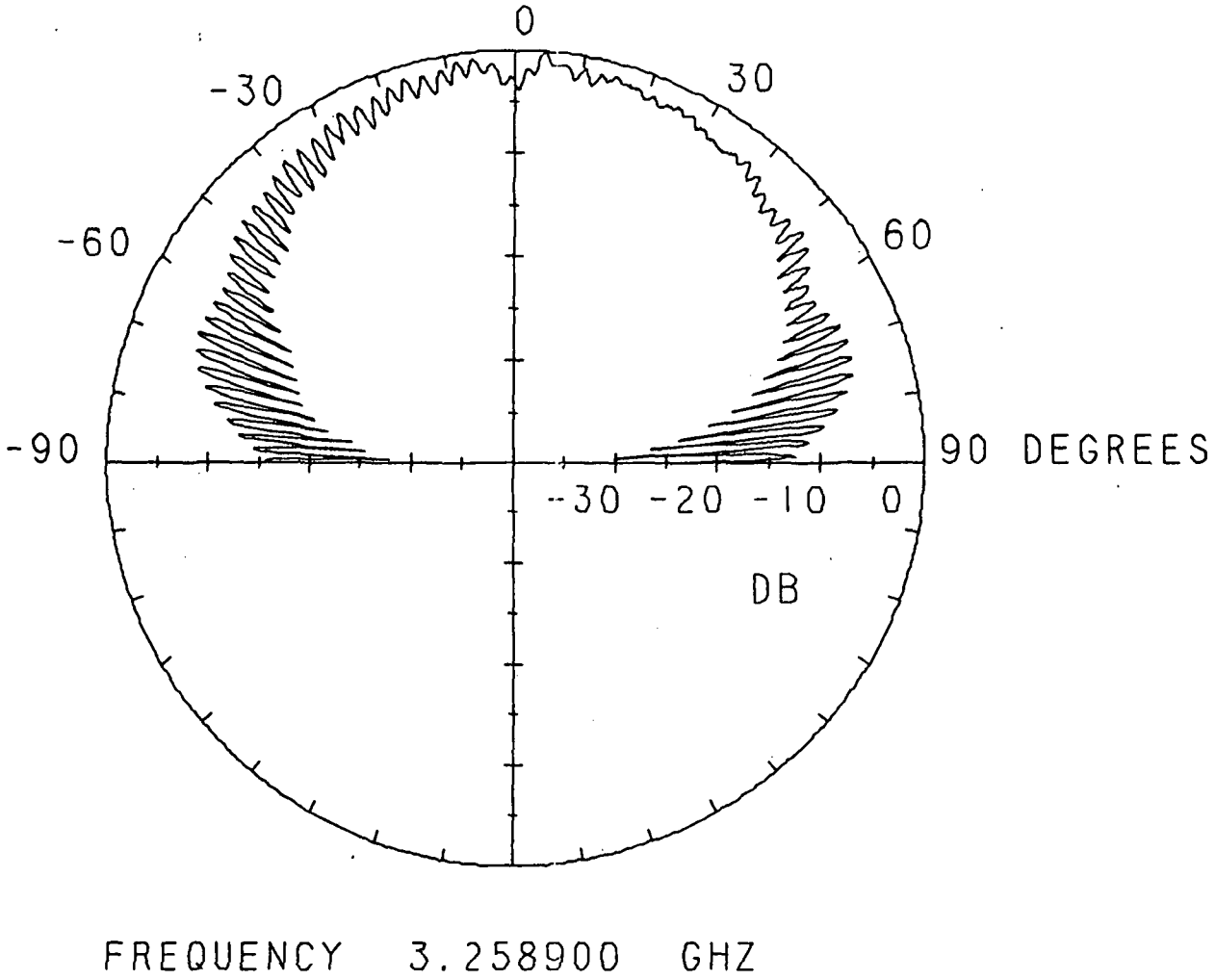

Fig. 3.21 Spinning linear pattern for the upper cp band of the fourth mode for a loaded 3.13 by 2.90 cm rectangular patch with a feed location of (.52, .48 cm), load insets of d = .70 cm, and stub lengths of s_1 = 18.1 cm and s_2 = 19.43 cm.

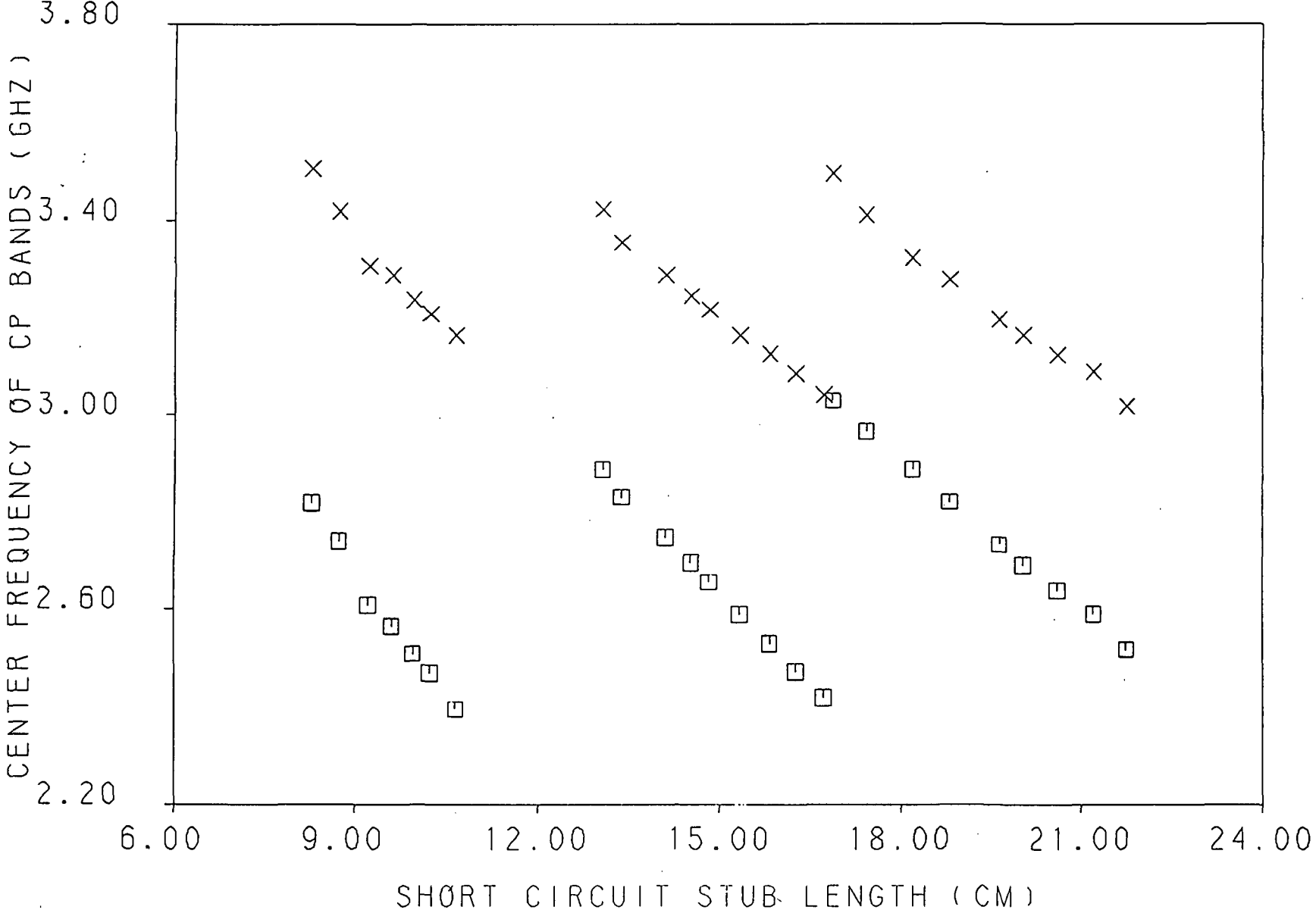

Fig. 3.22 Center frequency of cp bands verses the average short circuit stub length for a loaded 3.13 by 2.90 cm rectangular patch with a feed location of (.15, .15 cm), and load insets of d = .35 cm .

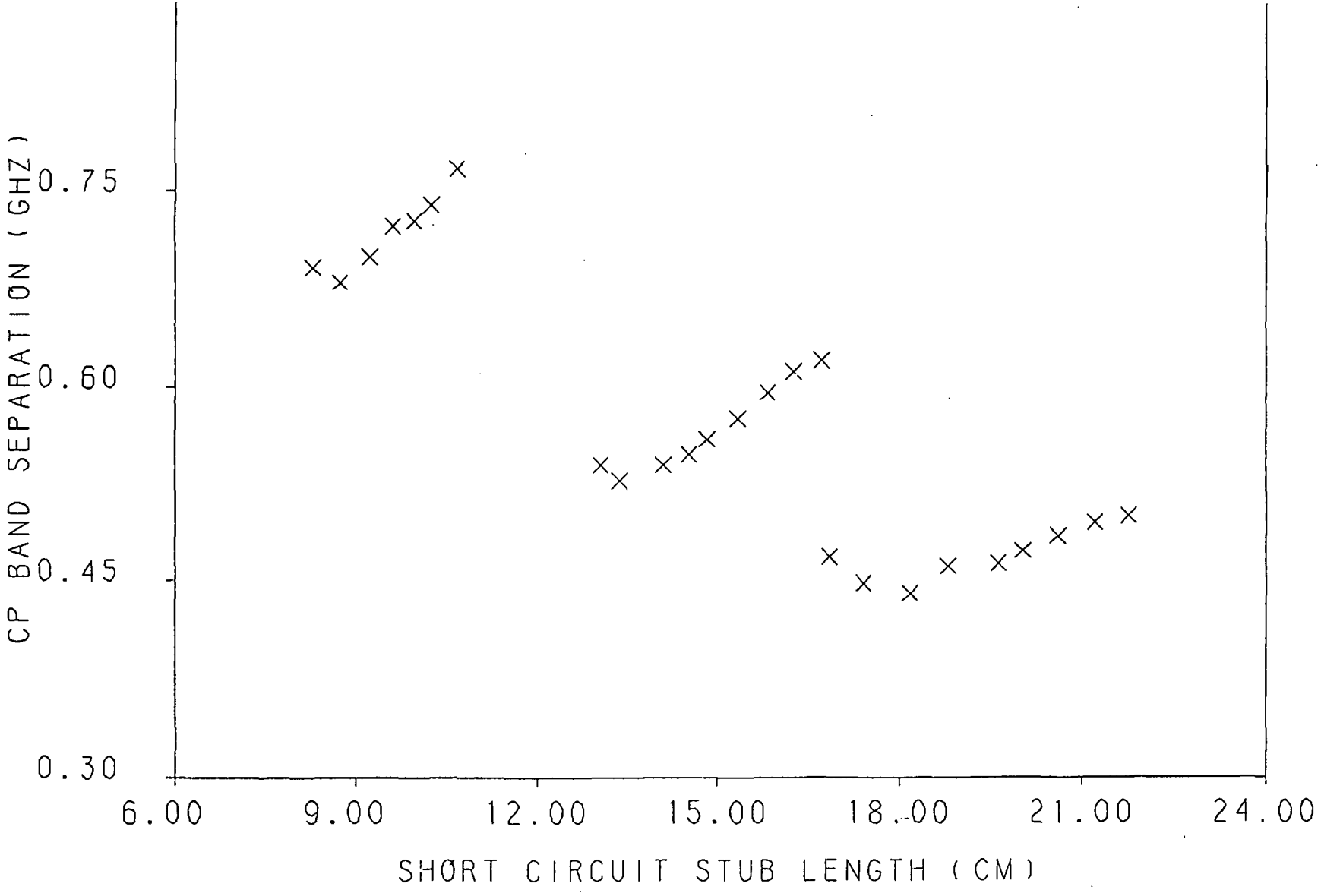

Fig. 3.23 Cp band separation verses the average short circuit stub length for a loaded 3.13 by 2.90 cm rectangular patch with a feed location of (.15, .15 cm), and load insets of d = .35 cm .

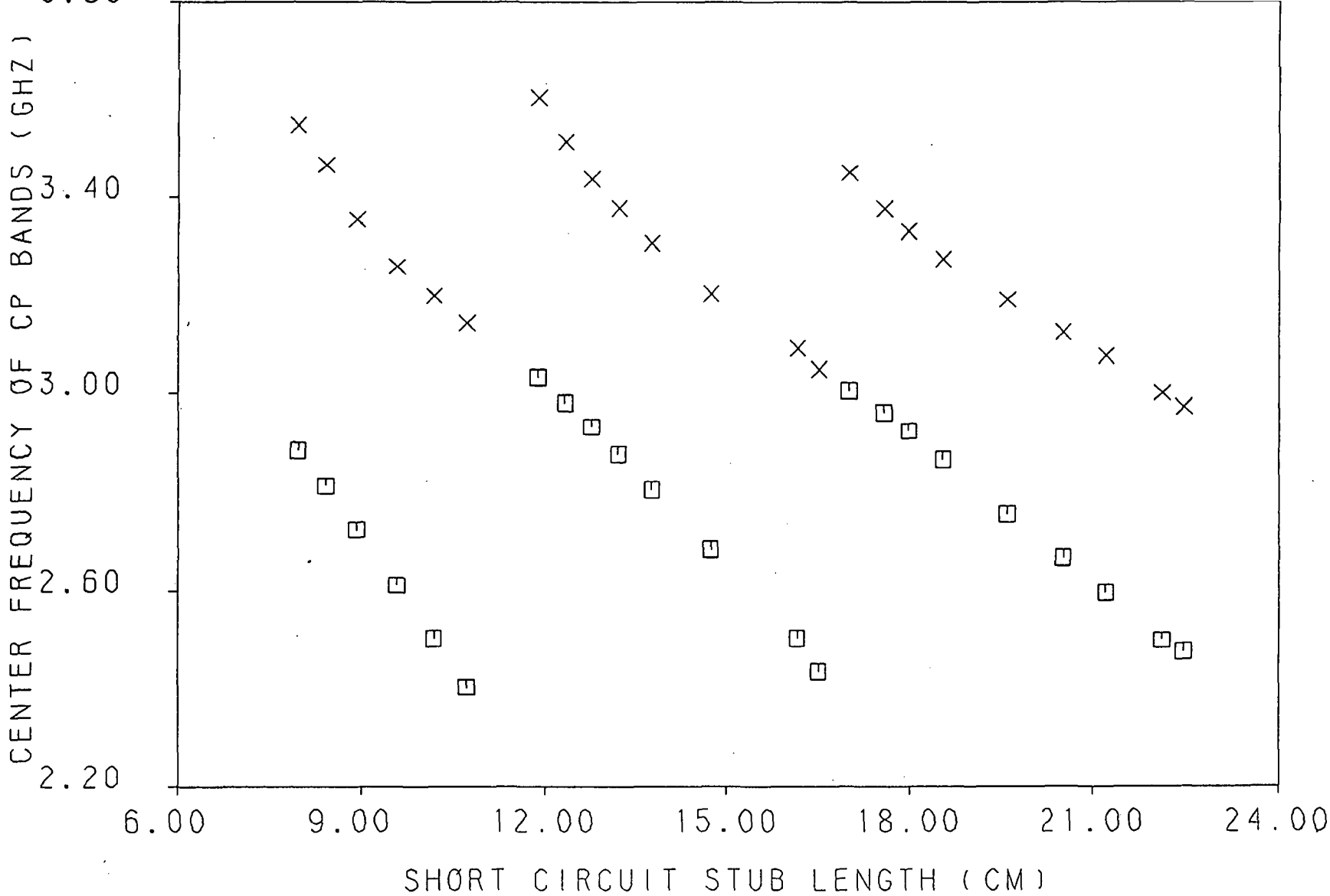

Fig. 3.24 Center frequency of cp bands verses the average short circuit stub length for a loaded 3.13 by 2.90 cm rectangular patch with a feed location of (.09, .09 cm), and load insets of d = .50 cm .

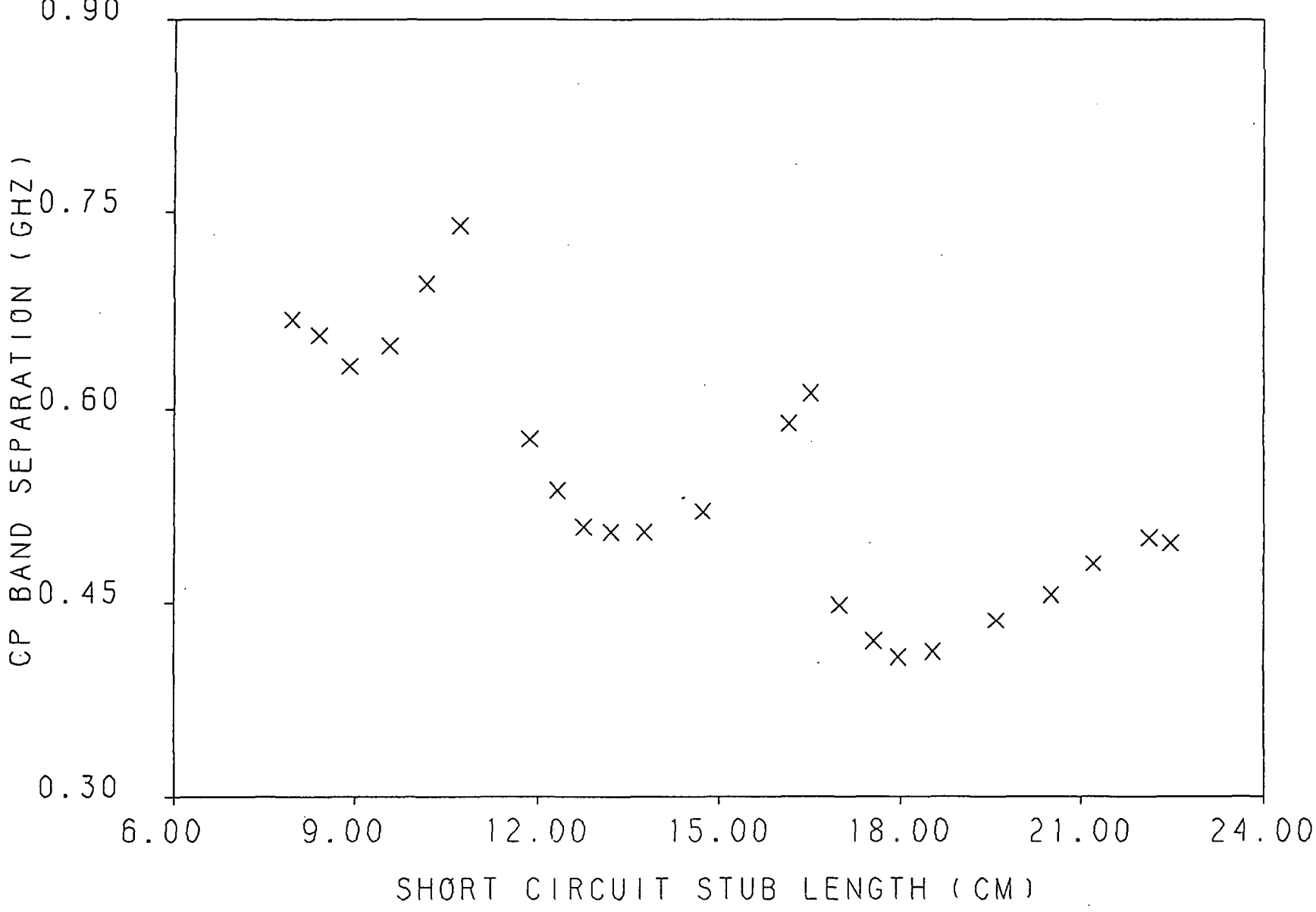

Fig. 3.25 Cp band separation verses the average short circuit stub length for a loaded 3.13 by 2.90 cm rectangular patch with a feed location of (.09, .09 cm), and load insets of d = .50 cm .

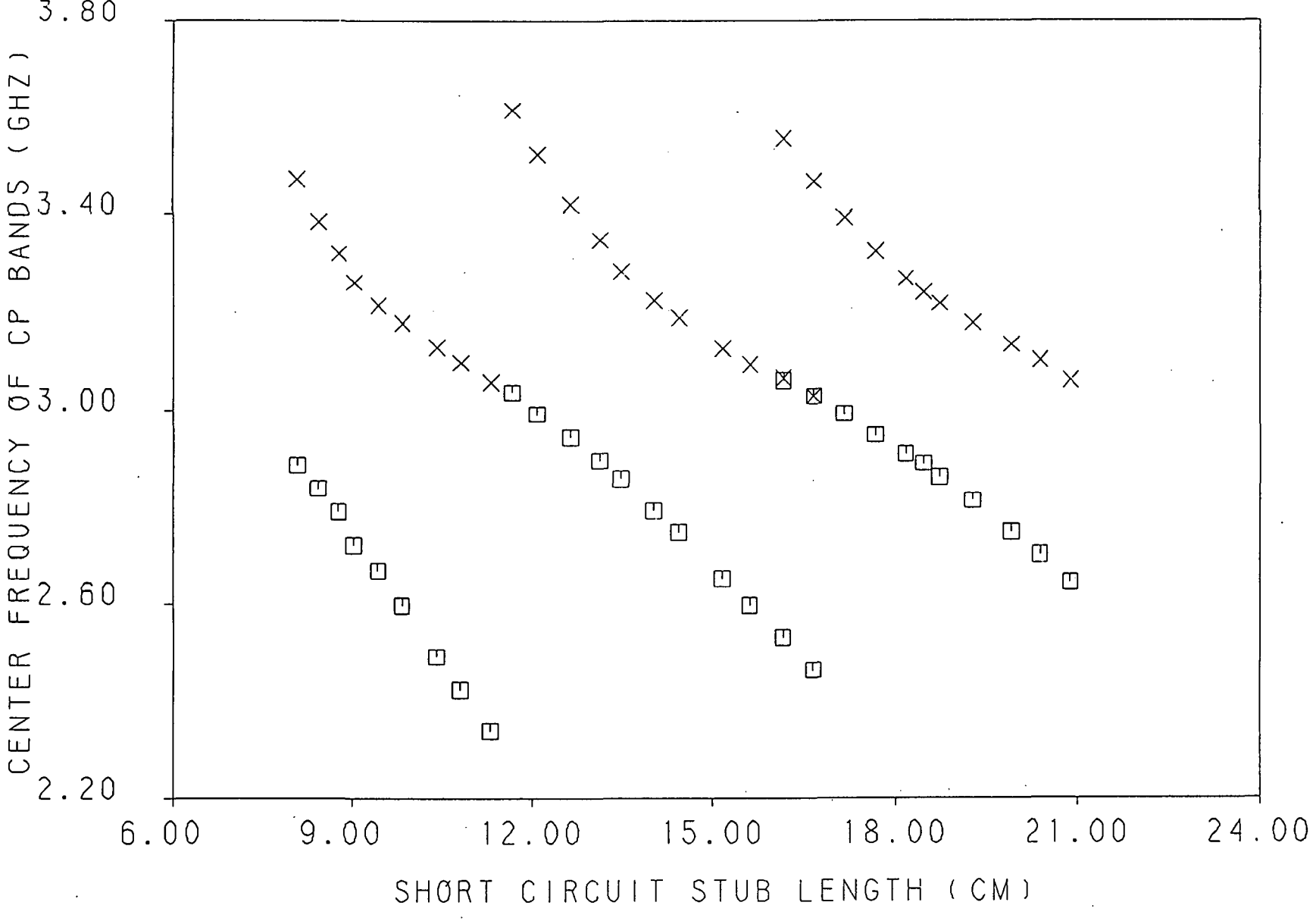

Fig. 3.26 Center frequency of cp bands verses the average short circuit stub length for a loaded 3.13 by 2.90 cm rectangular patch with a feed location of (.48, .52 cm), and load insets of d = .70 cm .

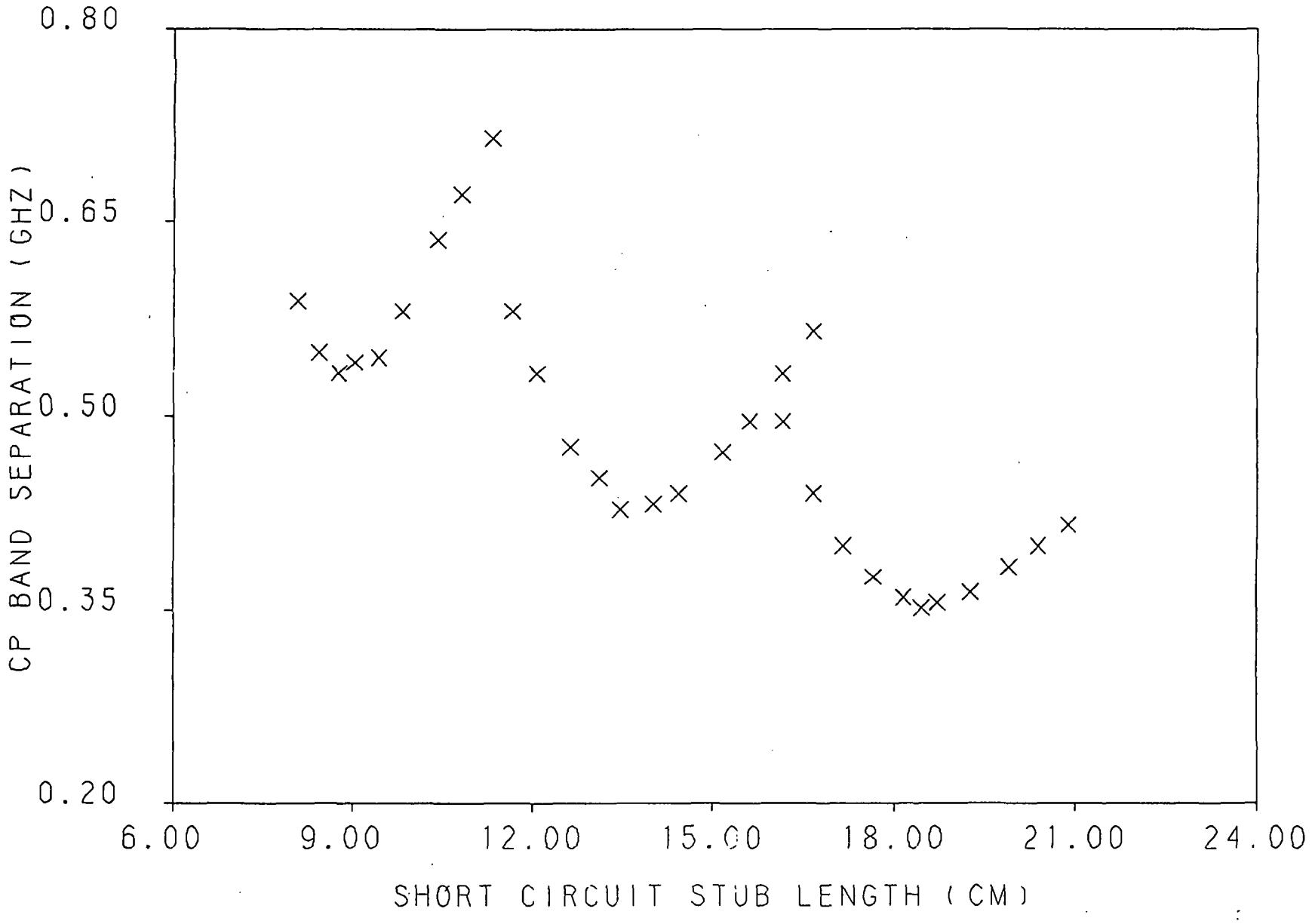

Fig. 3.27 Cp band separation verses the average short circuit stub length for a loaded 3.13 by 2.90 cm rectangular patch with a feed location of (.48, .52 cm), and load insets of d = .70 cm .

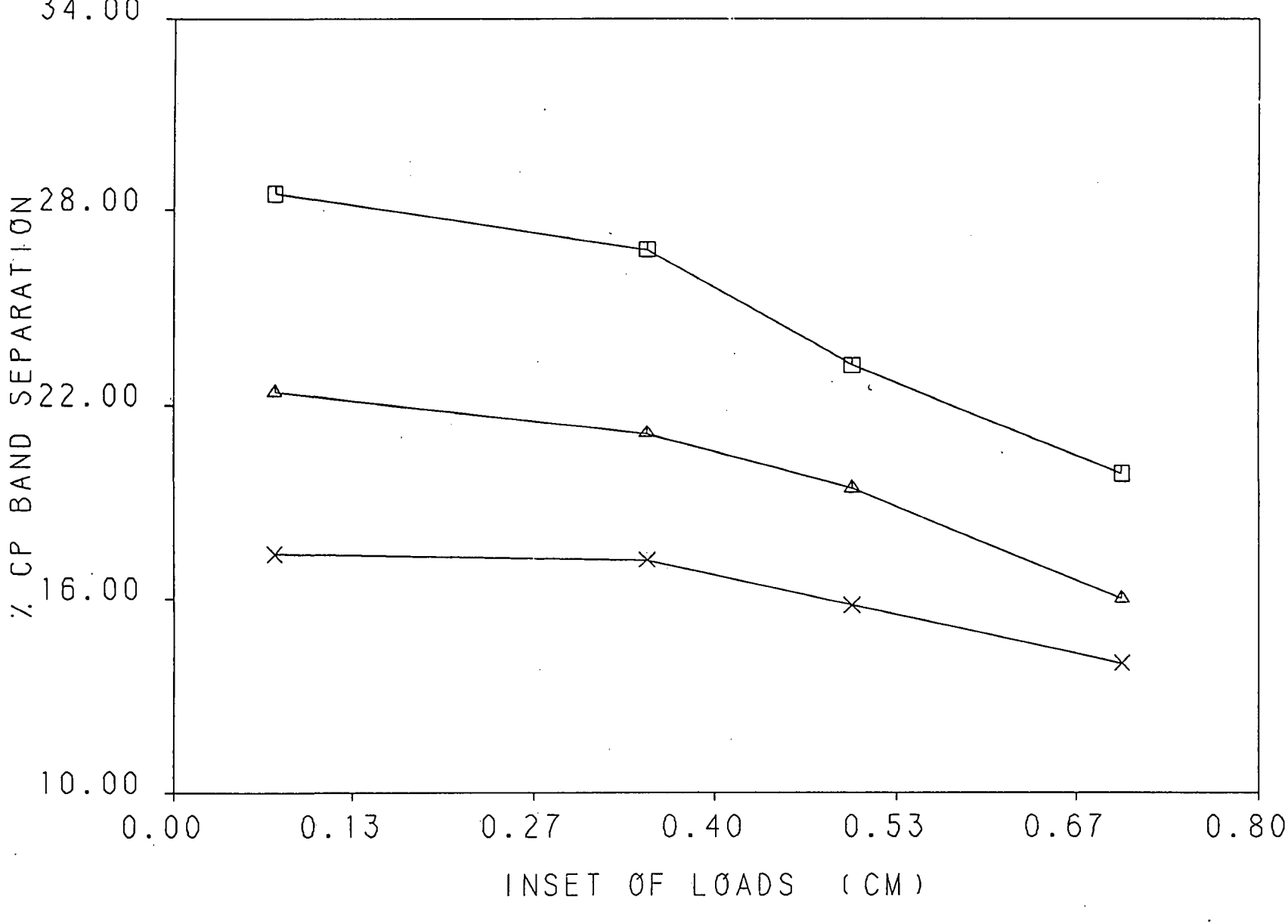

Fig. 3.28 Percentage cp band separation for modes 2, 3, and 4 verses the inset , d, of the loads for a loaded 3.13 by 2.90 cm rectangular patch.

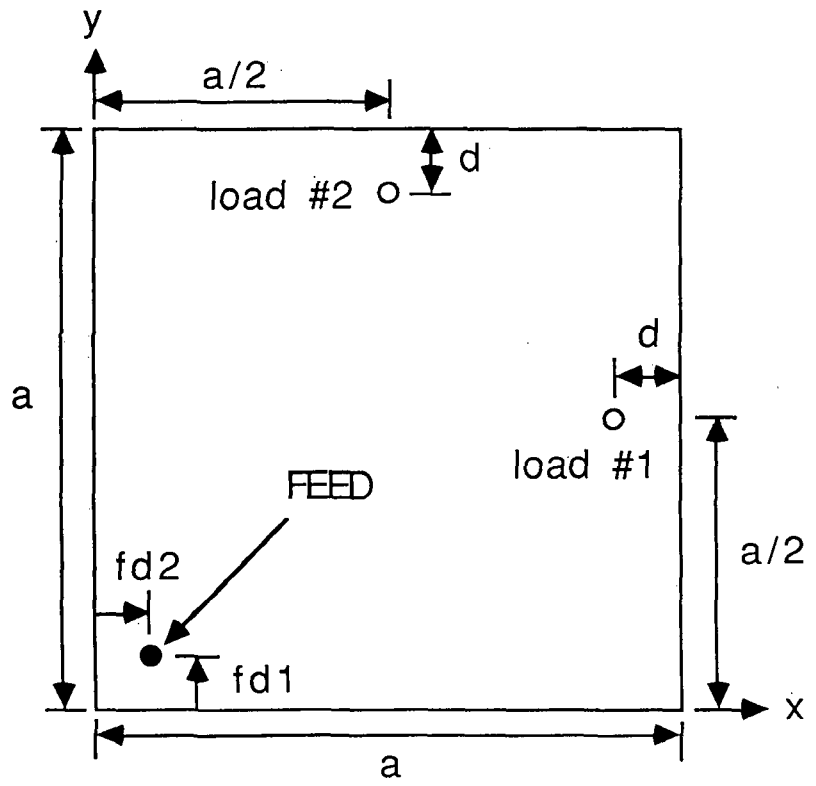

Fig. 3.29 Reactively loaded square microstrip antenna.

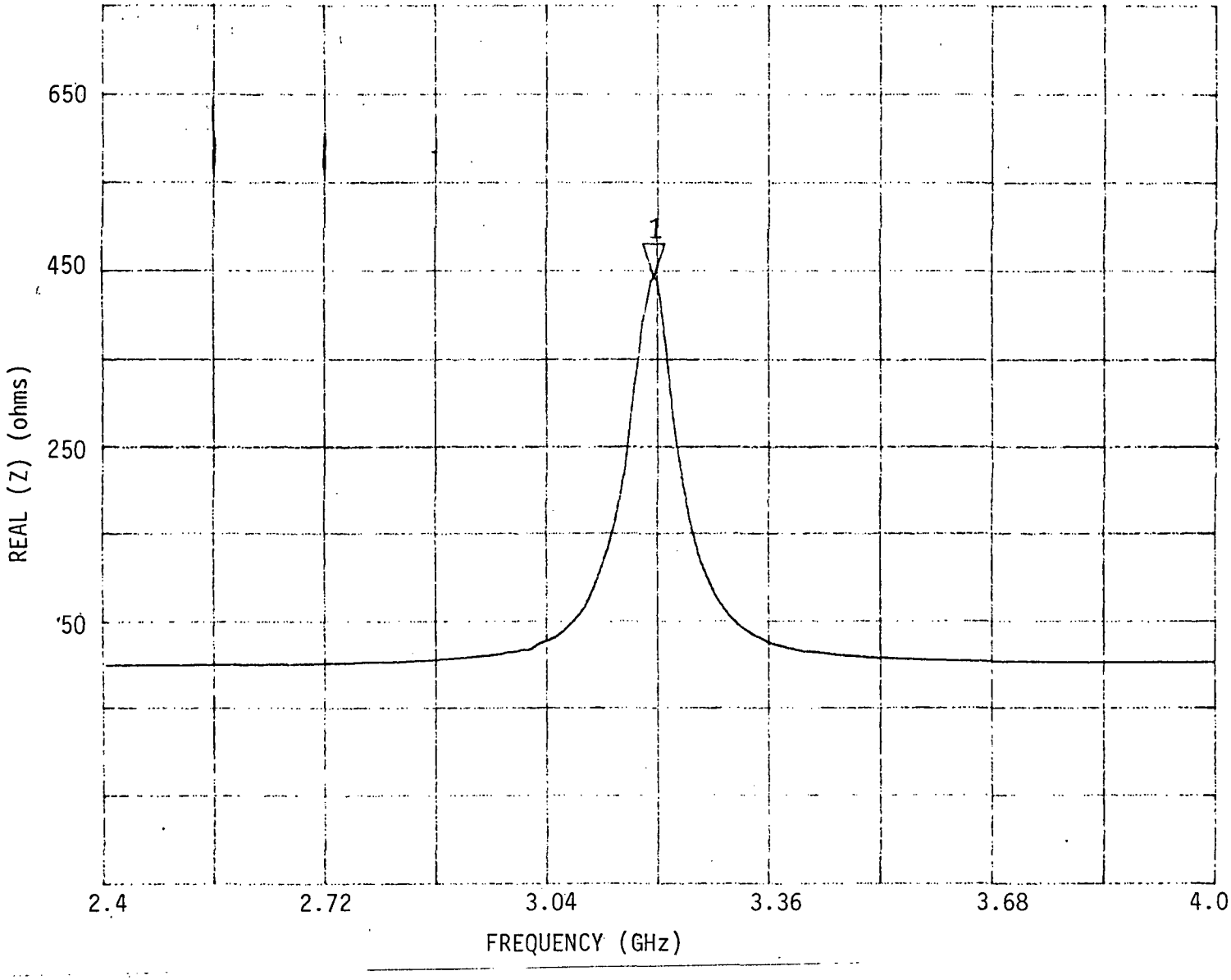

Fig. 3.30 Real part of input impedance verses frequency for a unloaded 2.96 by 2.96 cm square patch with a feed location of (.25, .25 cm) .

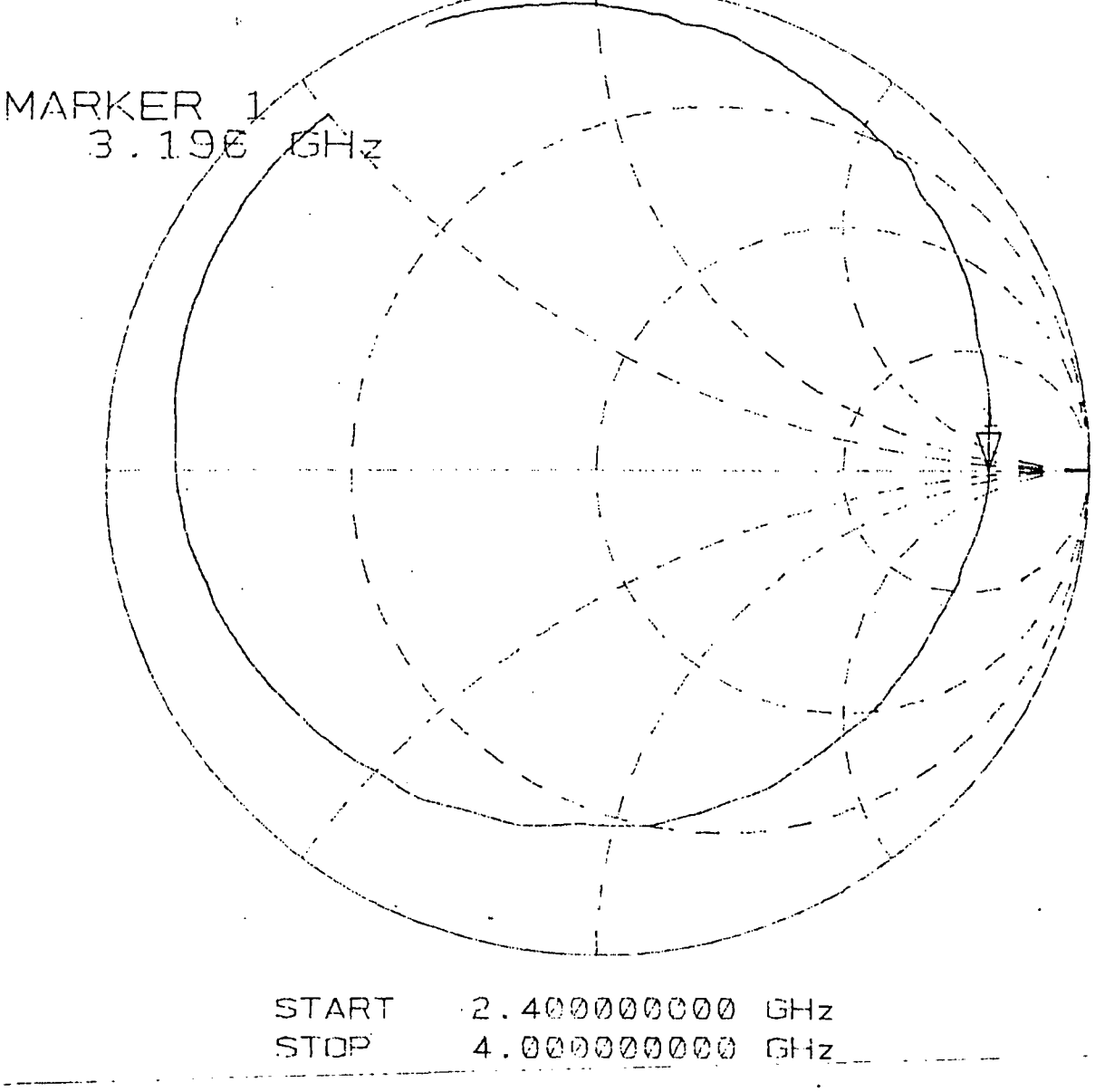

Fig. 3.31 Smith chart representation of the input impedance for a unloaded 2.96 by 2.96 cm square patch with a feed location of (.25, .25 cm) .

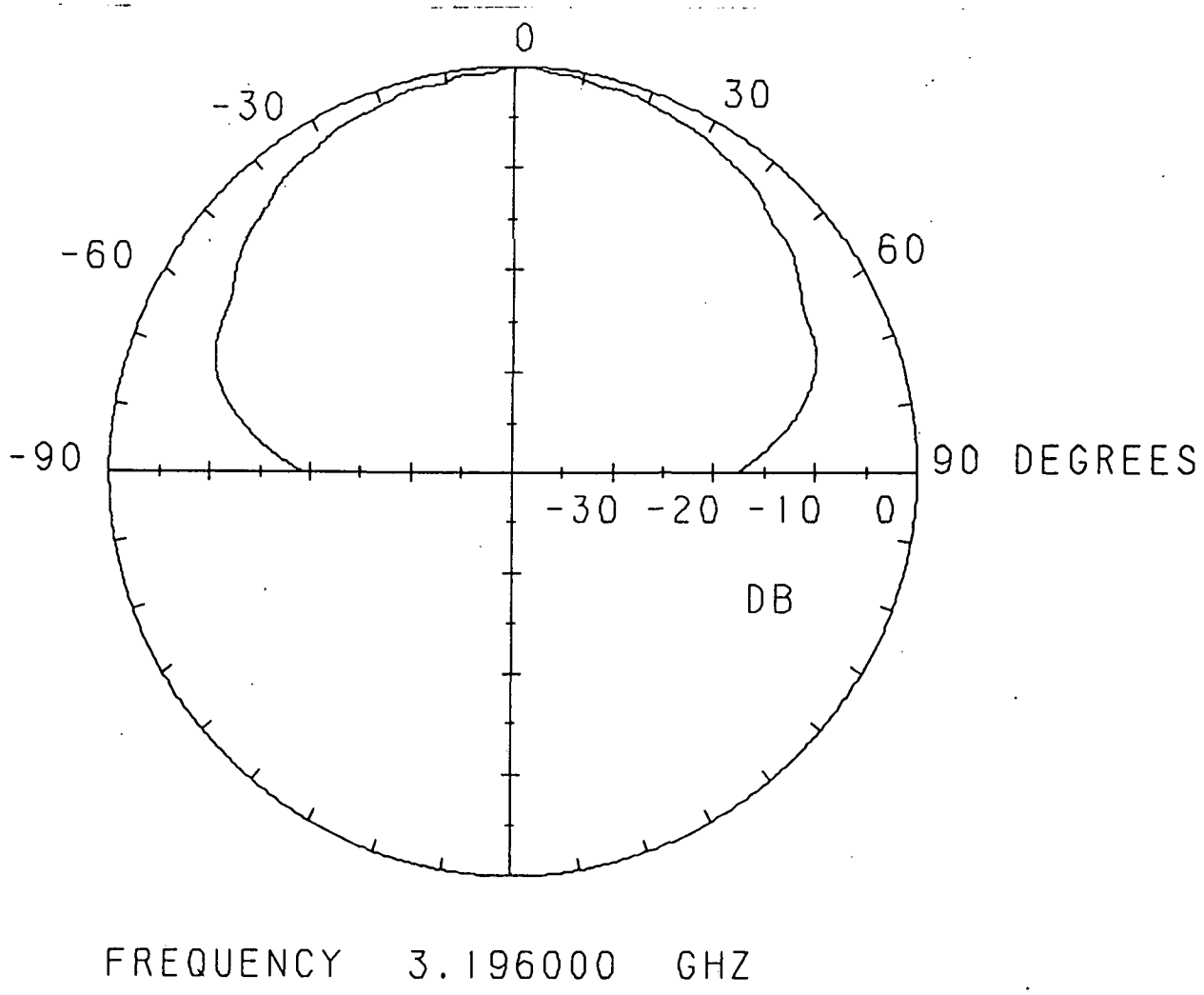

Fig. 3.32 Linearly polarized radiation pattern (along the plane of the diagonal) for an unloaded 2.96 cm by 2.96 cm square patch with a feed location of (.25, .25 cm).

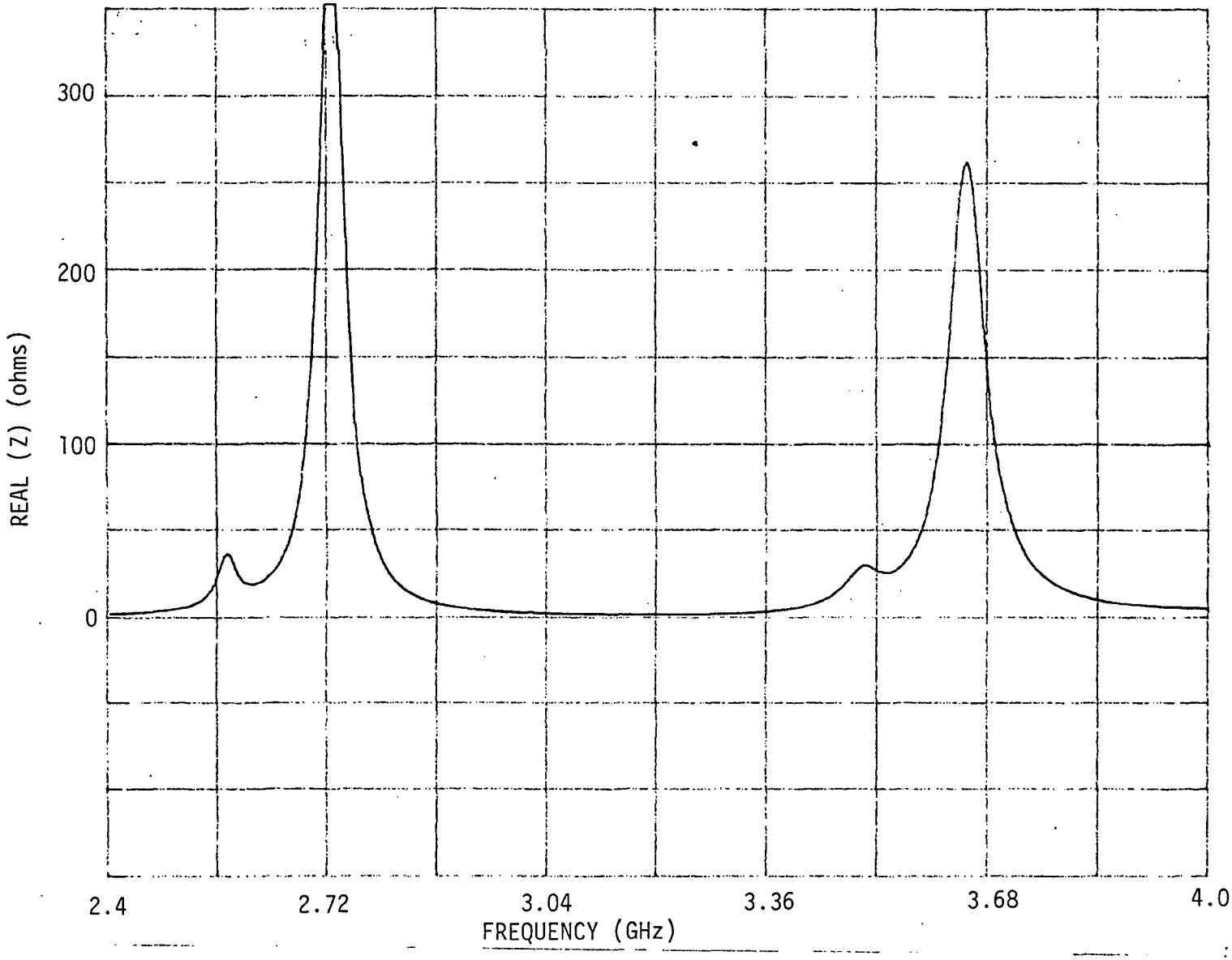

Fig. 3.33 Real part of input impedance verses frequency of the first mode for a loaded 2.96 by 2.96 cm square patch with a feed location of (.25, .25 cm), load insets of d = .11 cm, and stub lengths of s_1 = 4.3 cm and s_2 = 4.48 cm.

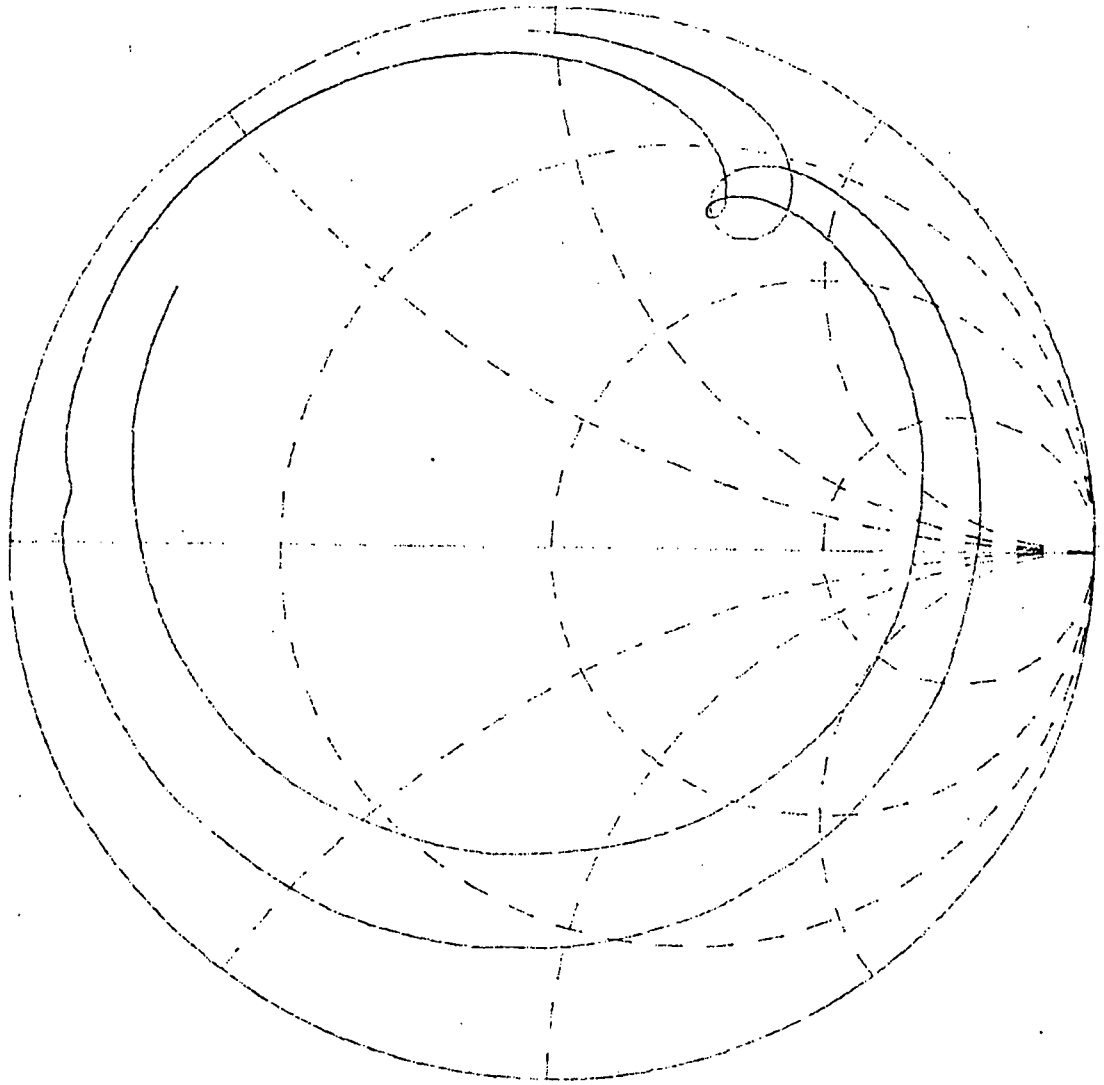

Fig. 3.34 Smith chart representation of the input impedance of the first mode for a loaded 2.96 by 2.96 cm square patch with a feed location of (.25, .25 cm), load insets of d = .11 cm, and stub lengths of s_1 = 4.3 cm and s_2 = 4.48 cm.

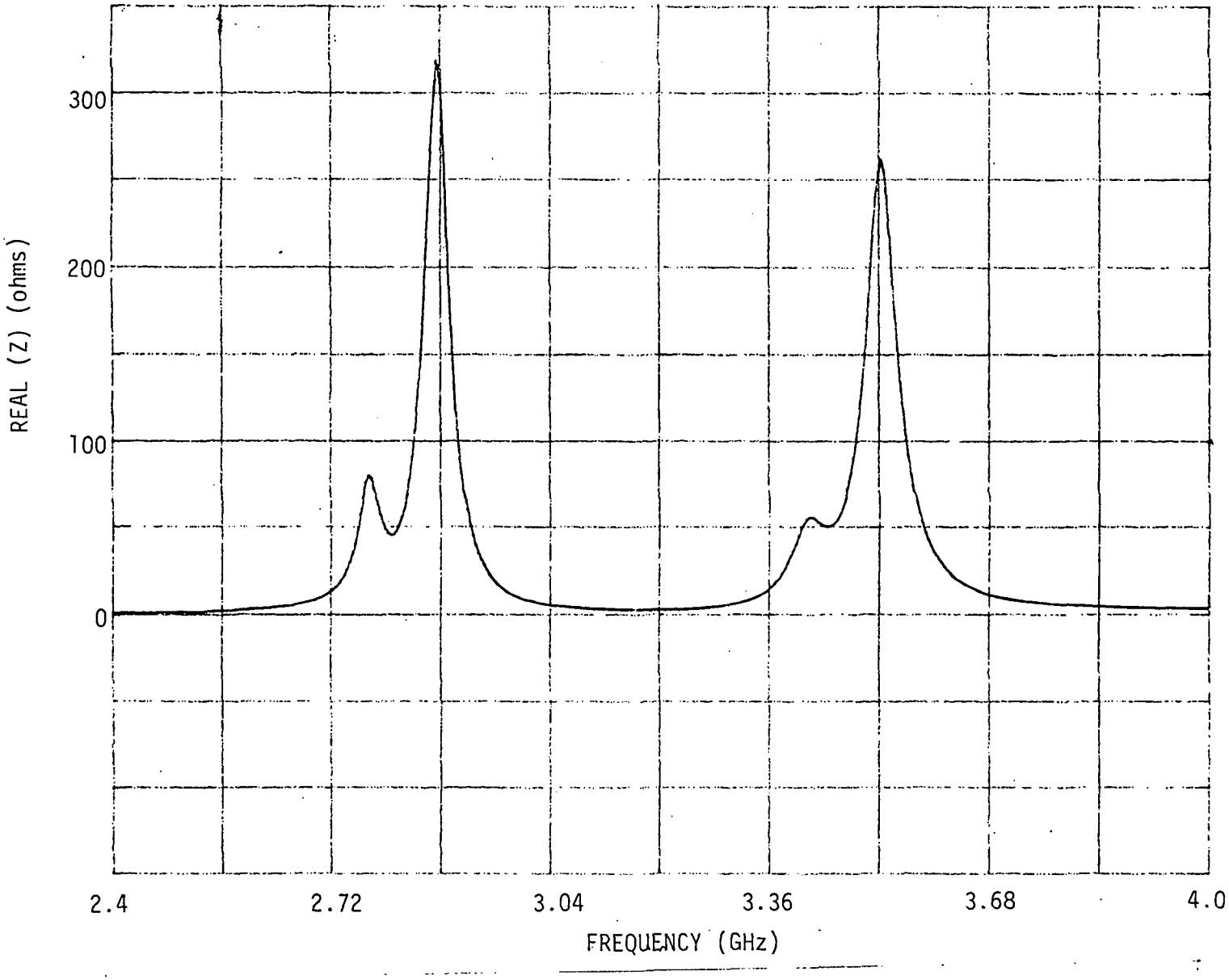

Fig. 3.35 Real part of input impedance verses frequency of the second mode for a loaded 2.96 by 2.96 cm square patch with a feed location of (.25, .25 cm), load insets of d = .11 cm, and stub lengths of s_1 = 8.85 cm and s_2 = 9.03 cm.

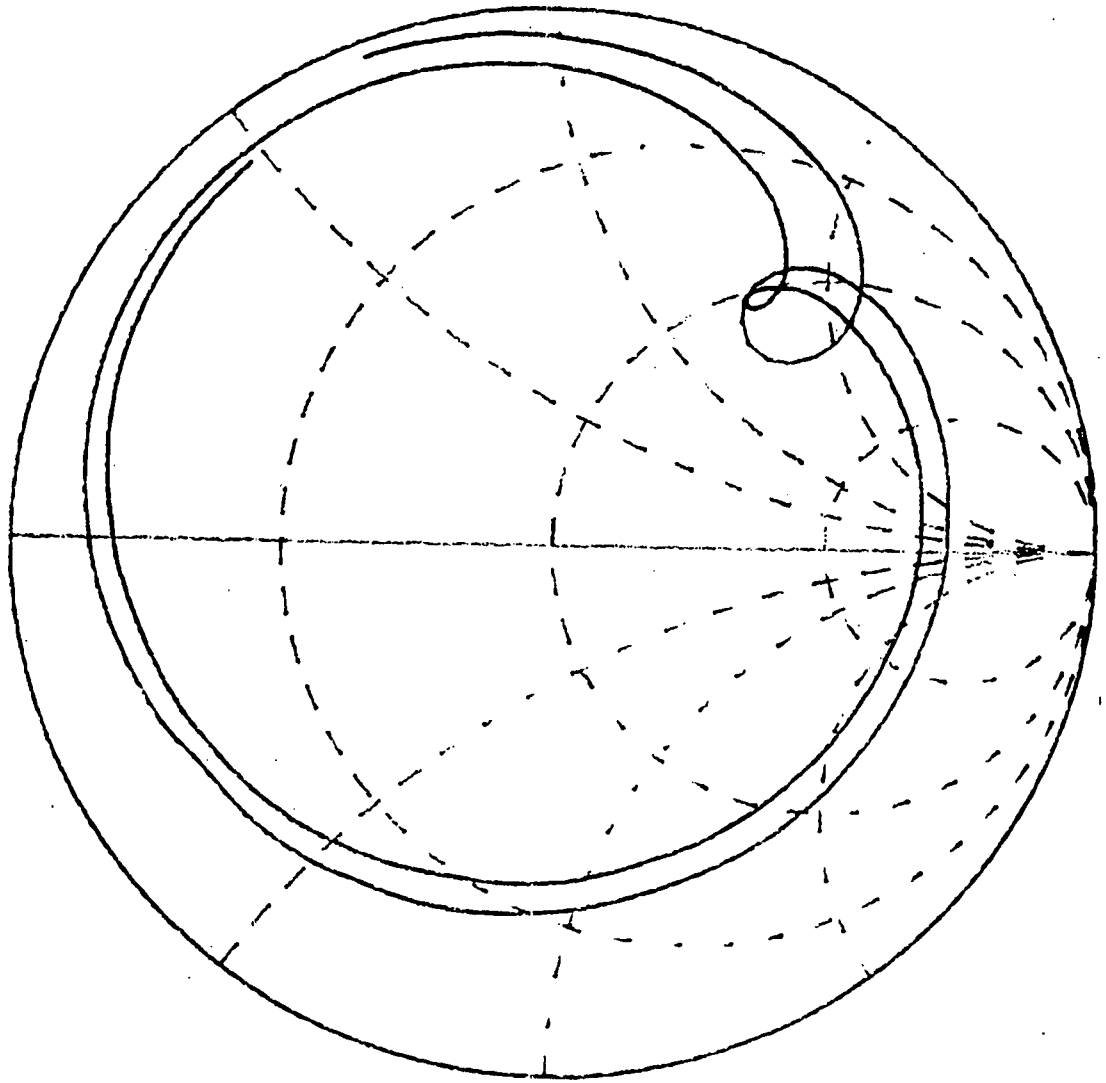

Fig. 3.36 Smith chart representation of the input impedance of the second mode for a loaded 2.96 by 2.96 cm square patch with a feed location of (.25, .25 cm), load insets of d = .11 cm, and stub lengths of s_1 = 8.85 cm and s_2 = 9.03 cm.

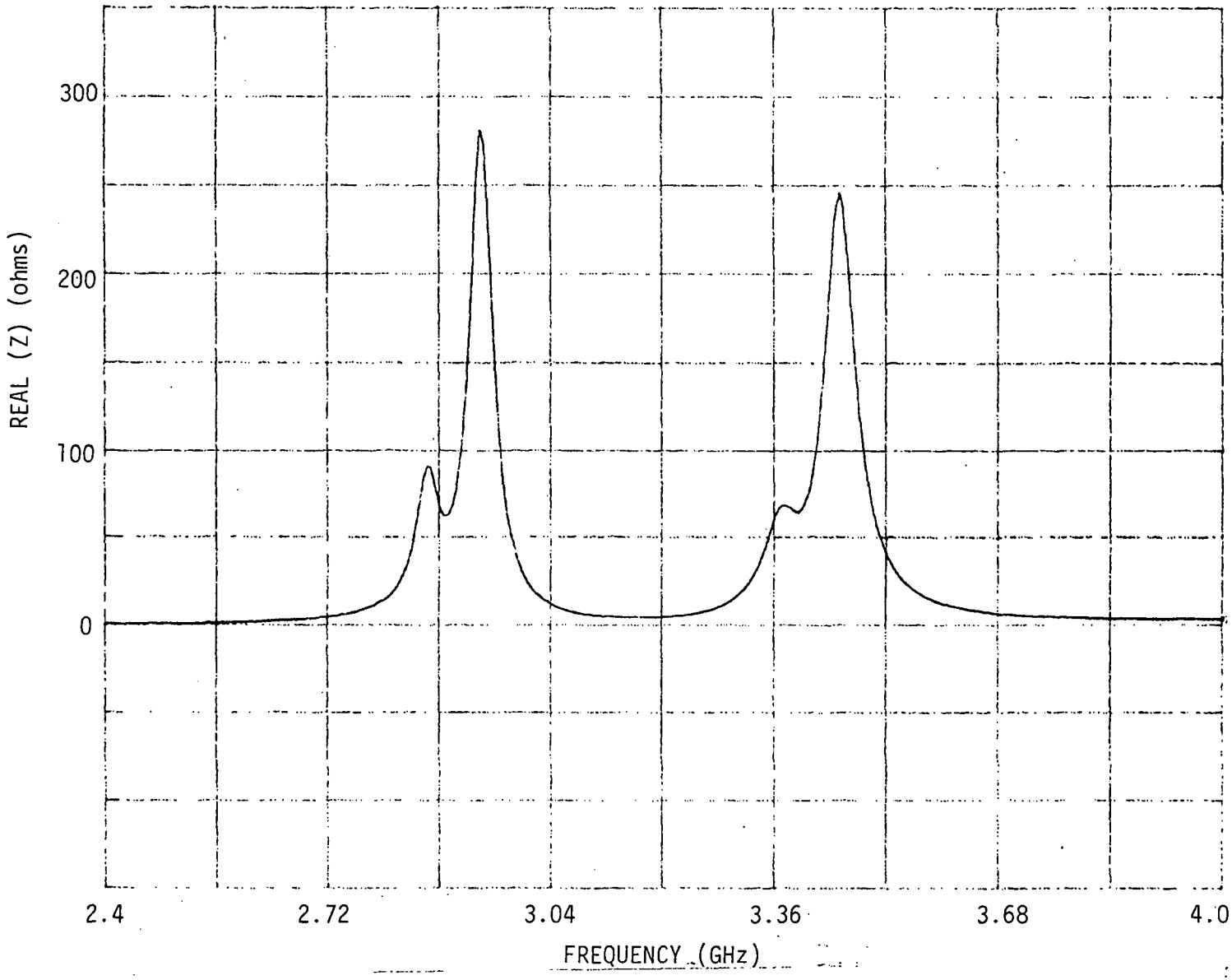

Fig. 3.37 Real part of input impedance verses frequency of the third mode for a loaded 2.96 by 2.96 cm square patch with a feed location of (.25, .25 cm), load insets of d = .11 cm, and stub lengths of s_1 = 13.5 cm and s_2 = 13.73 cm.

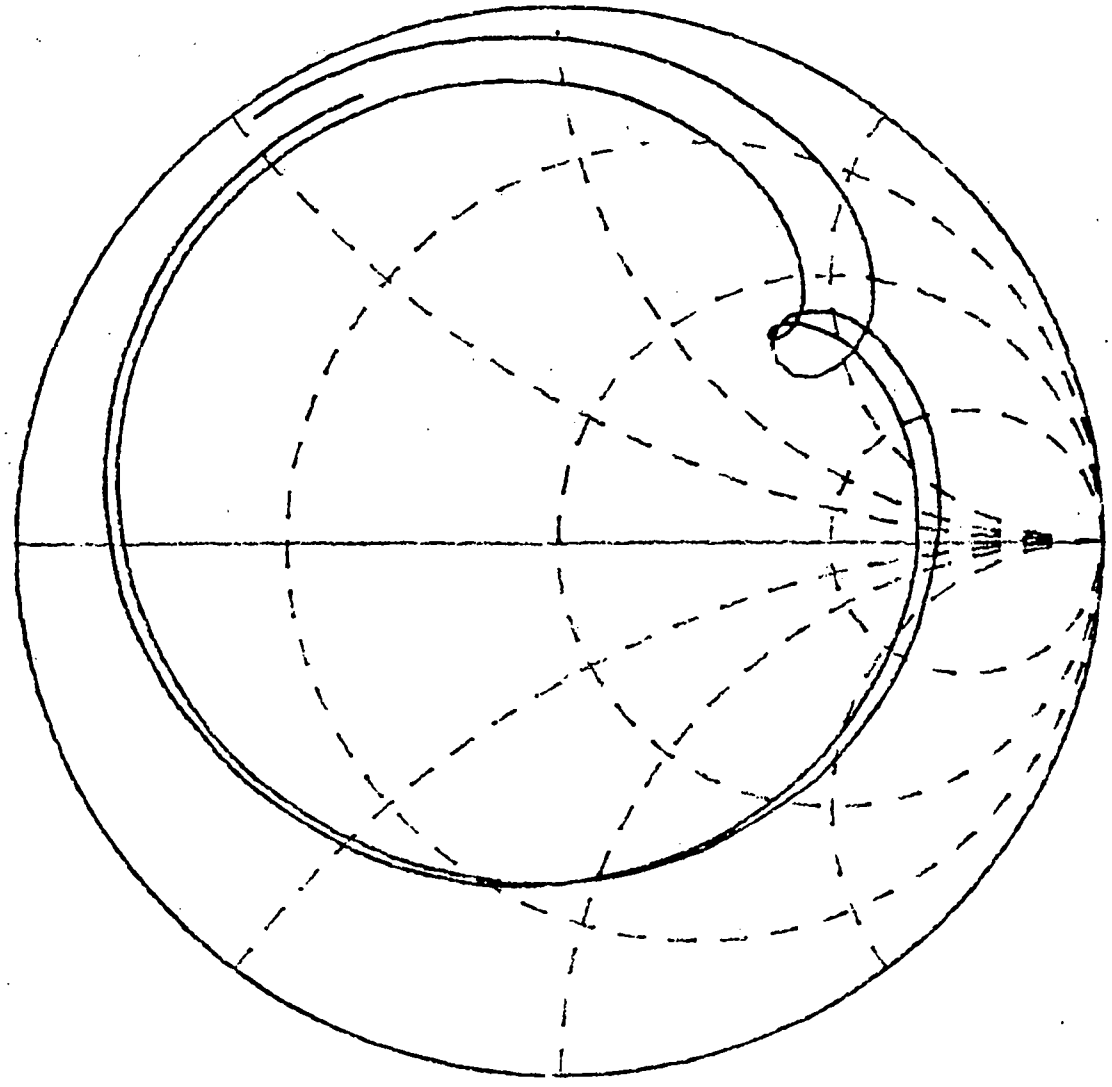

Fig. 3.38 Smith chart representation of the input impedance of the third mode for a loaded 2.96 by 2.96 cm square patch with a feed location of (.25, .25 cm), load insets of d = .11 cm, and stub lengths of s_1 = 13.5 cm and s_2 = 13.73 cm.

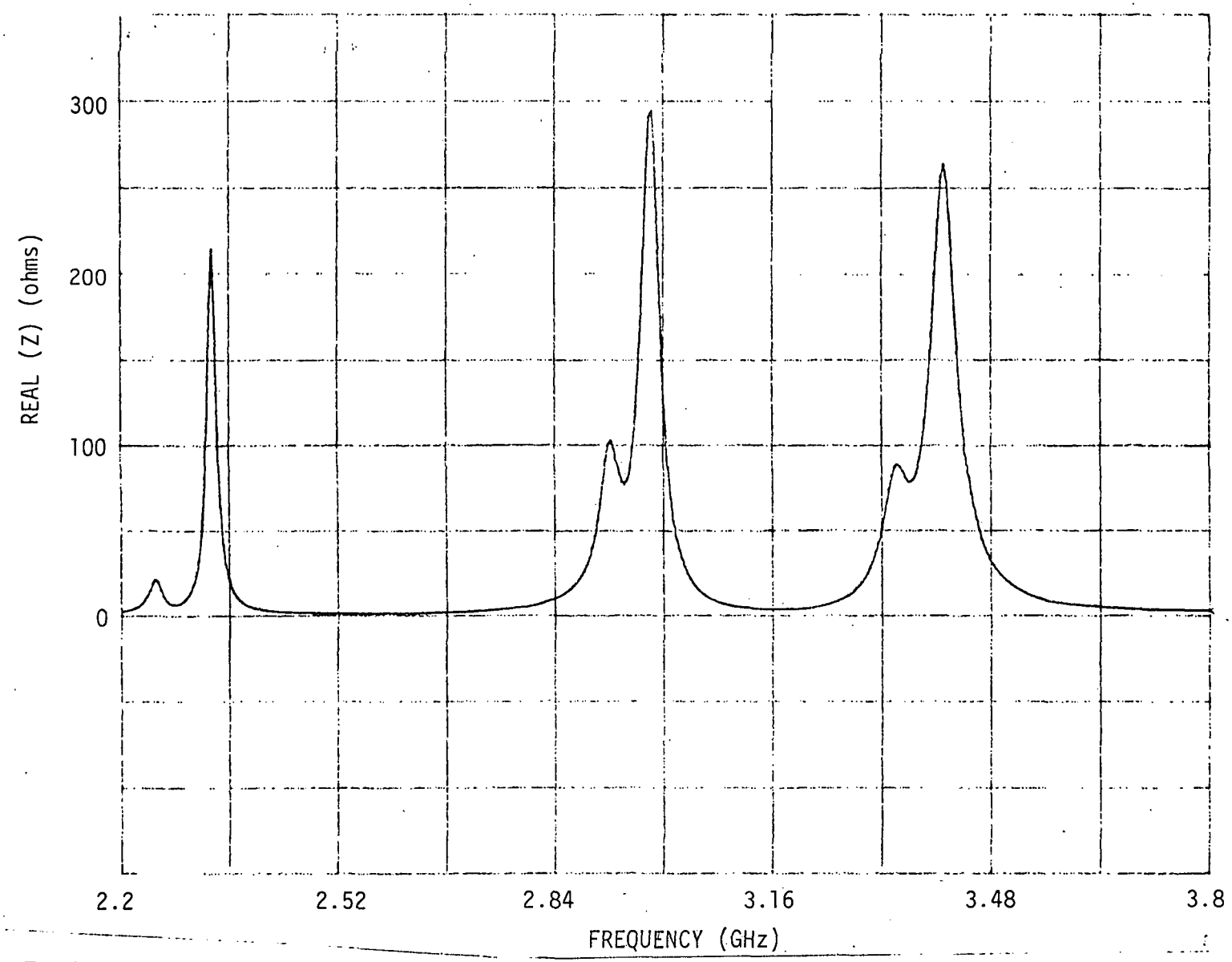

Fig. 3.39 Real part of input impedance verses frequency of the fourth mode for a loaded 2.96 by 2.96 cm square patch with a feed location of (.25, .25 cm), load insets of d = .11 cm, and stub lengths of s_1 = 18.4 cm and s_2 = 18.53 cm.

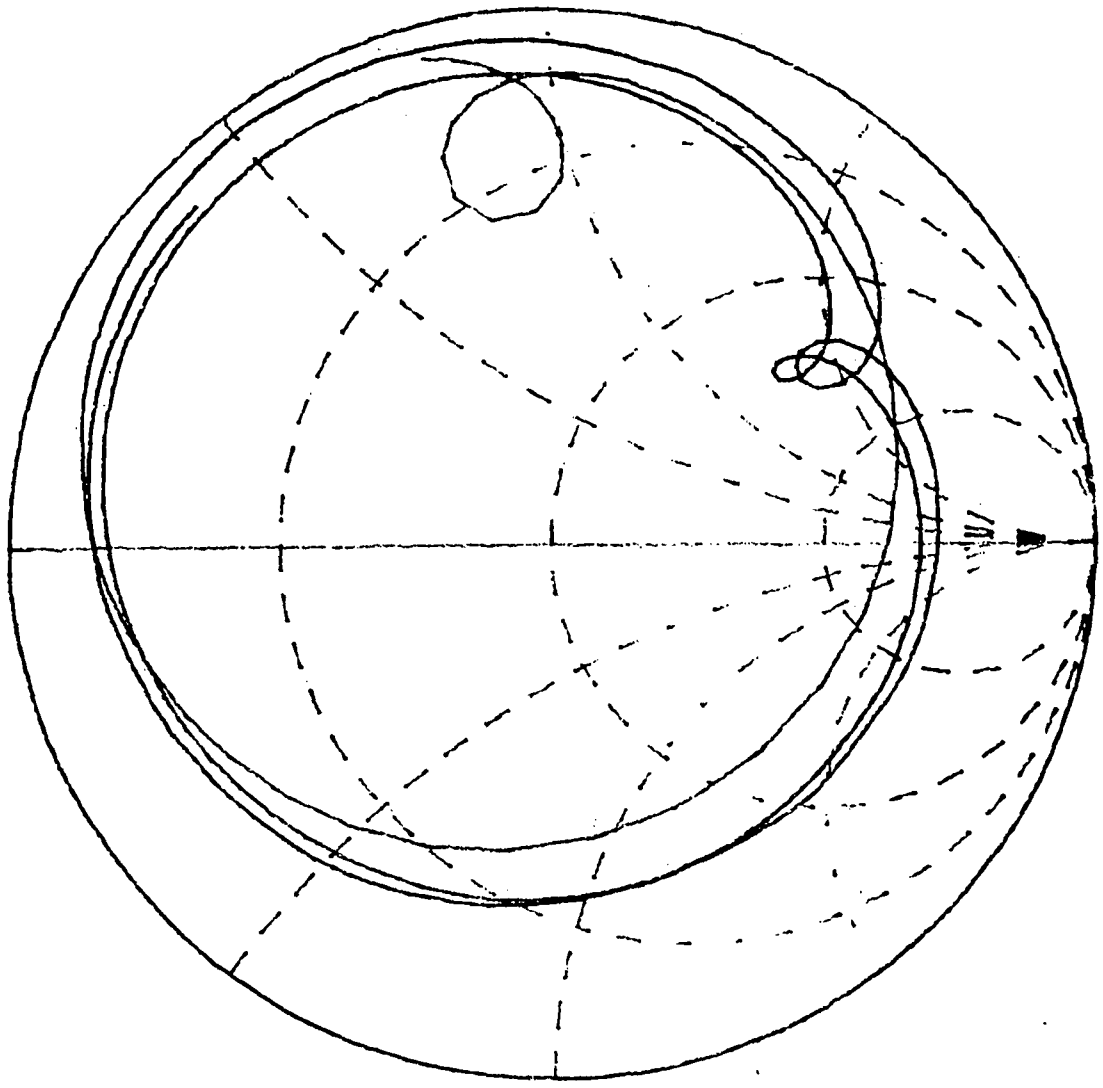

Fig. 3.40 Smith chart representation of the input impedance of the fourth mode for a loaded 2.96 by 2.96 cm square patch with a feed location of (.25, .25 cm), load insets of d = .11 cm, and stub lengths of s_1 = 18.4 cm and s_2 = 18.53 cm.

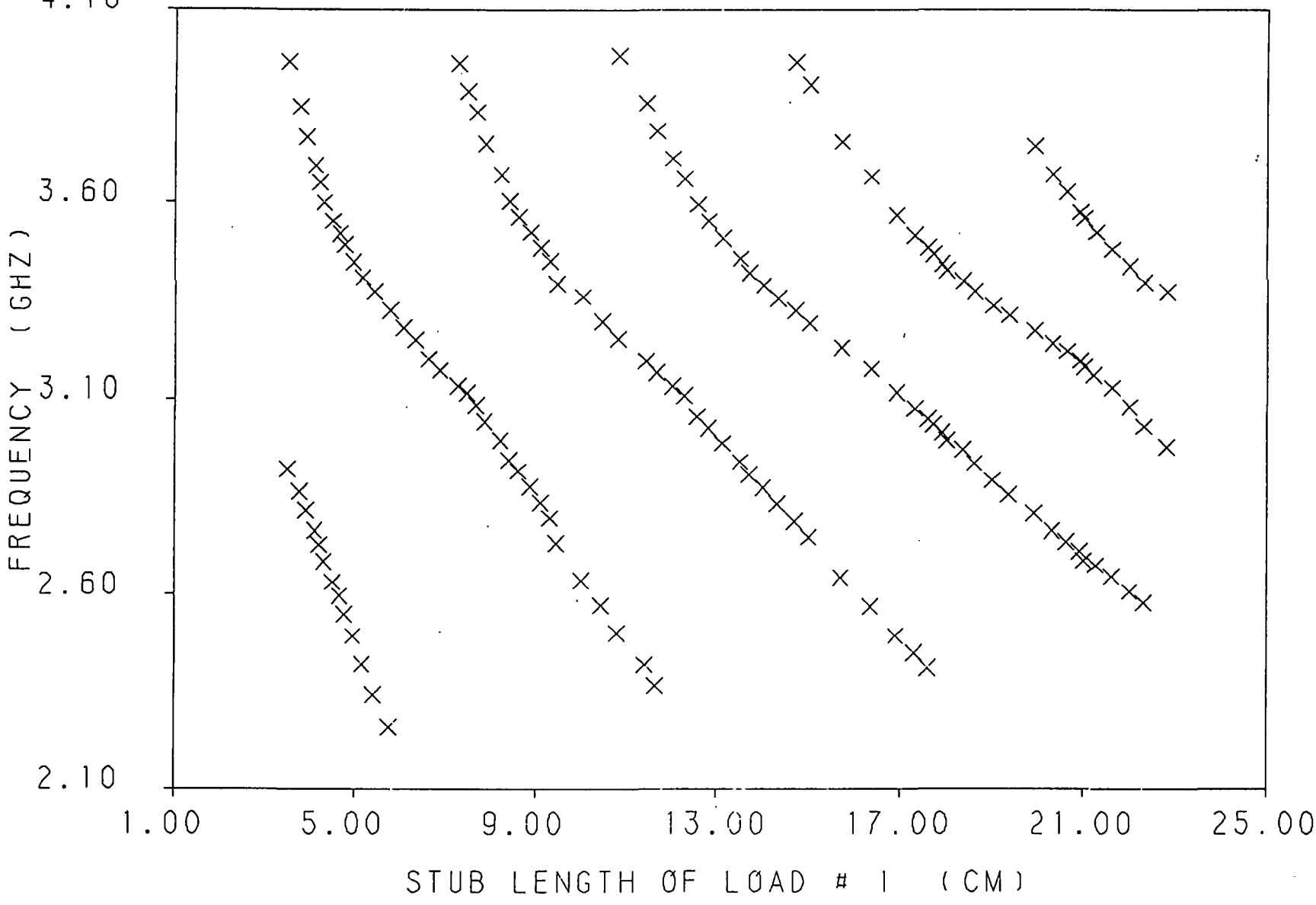

Fig. 3.41 Frequency of upper linearly polarized band (the x-polarized band) verses the short circuit stub length of load #1 for a loaded 2.96 by 2.96 cm square patch with a feed location of (.25, .25 cm), and load insets of d = .11 cm .

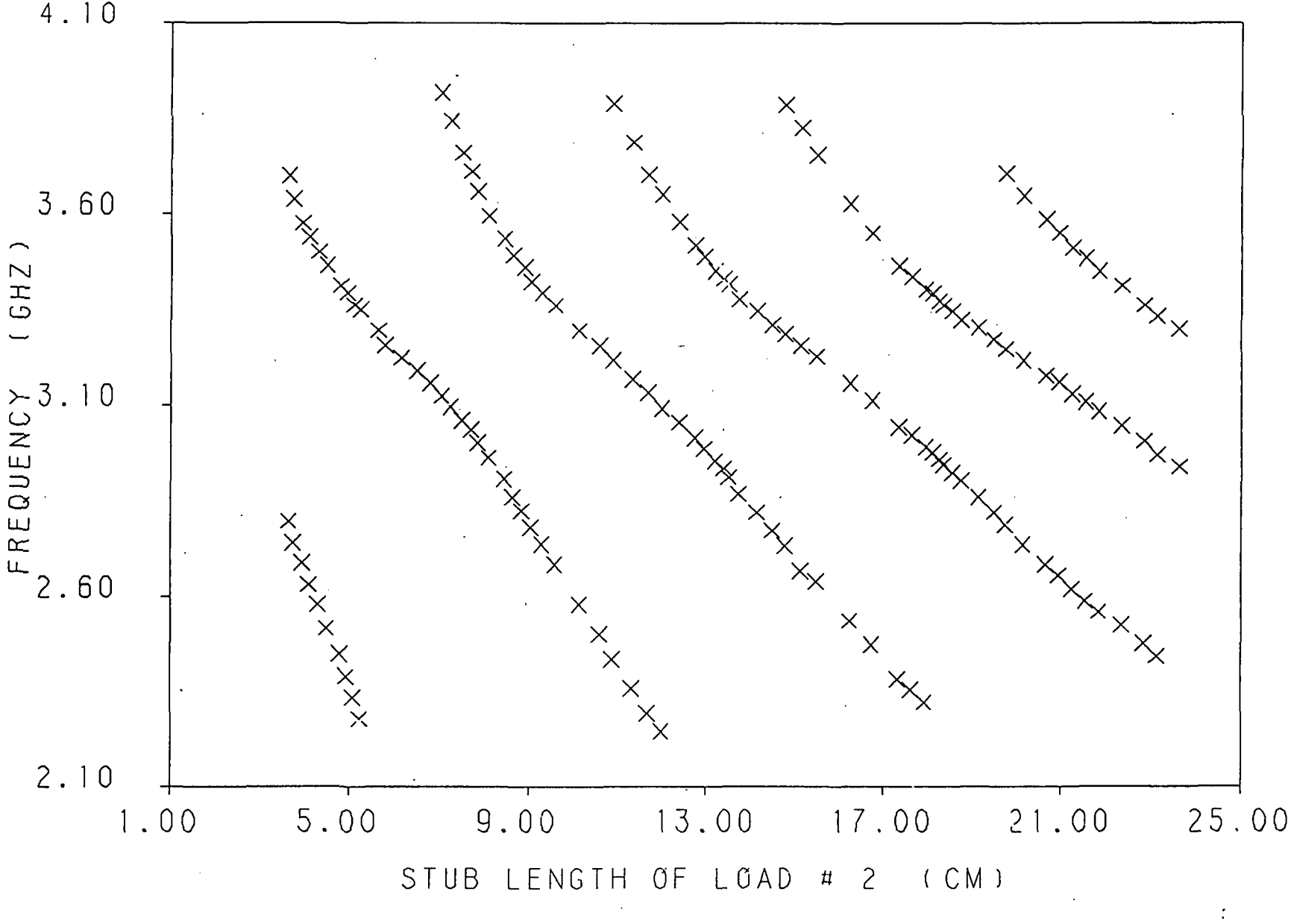

Fig. 3.42 Frequency of lower linearly polarized band (the *y*-polarized band) verses the short circuit stub length of load #2 for a loaded 2.96 by 2.96 cm square patch with a feed location of (.25, .25 cm), and load insets of d = .11 cm .

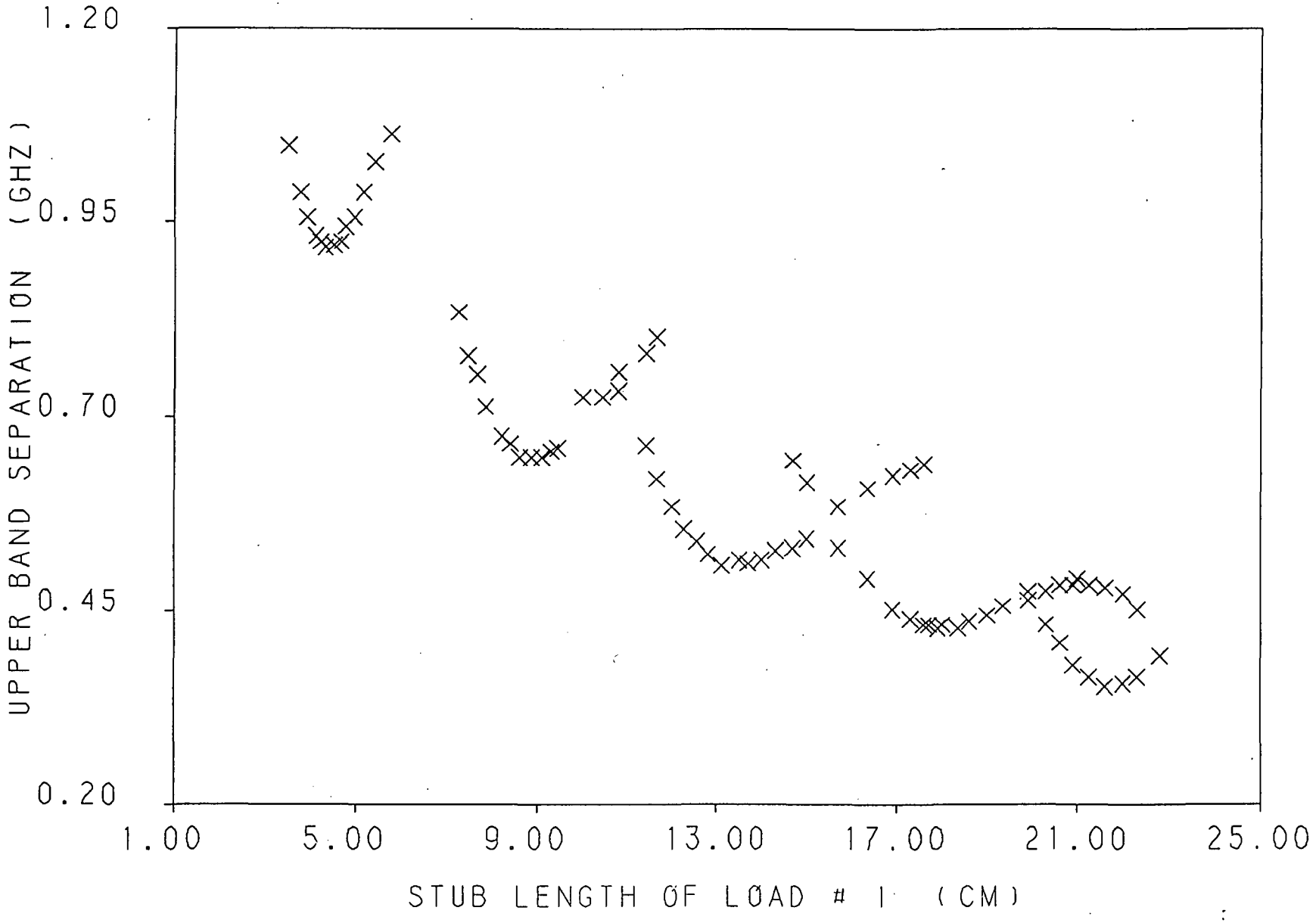

Fig. 3.43 Upper frequency band (the x-polarized band) separation verses the short circuit stub length of load #1 for a loaded 2.96 by 2.96 cm square patch with a feed location of (.25, .25 cm), and load insets of d = .11 cm .

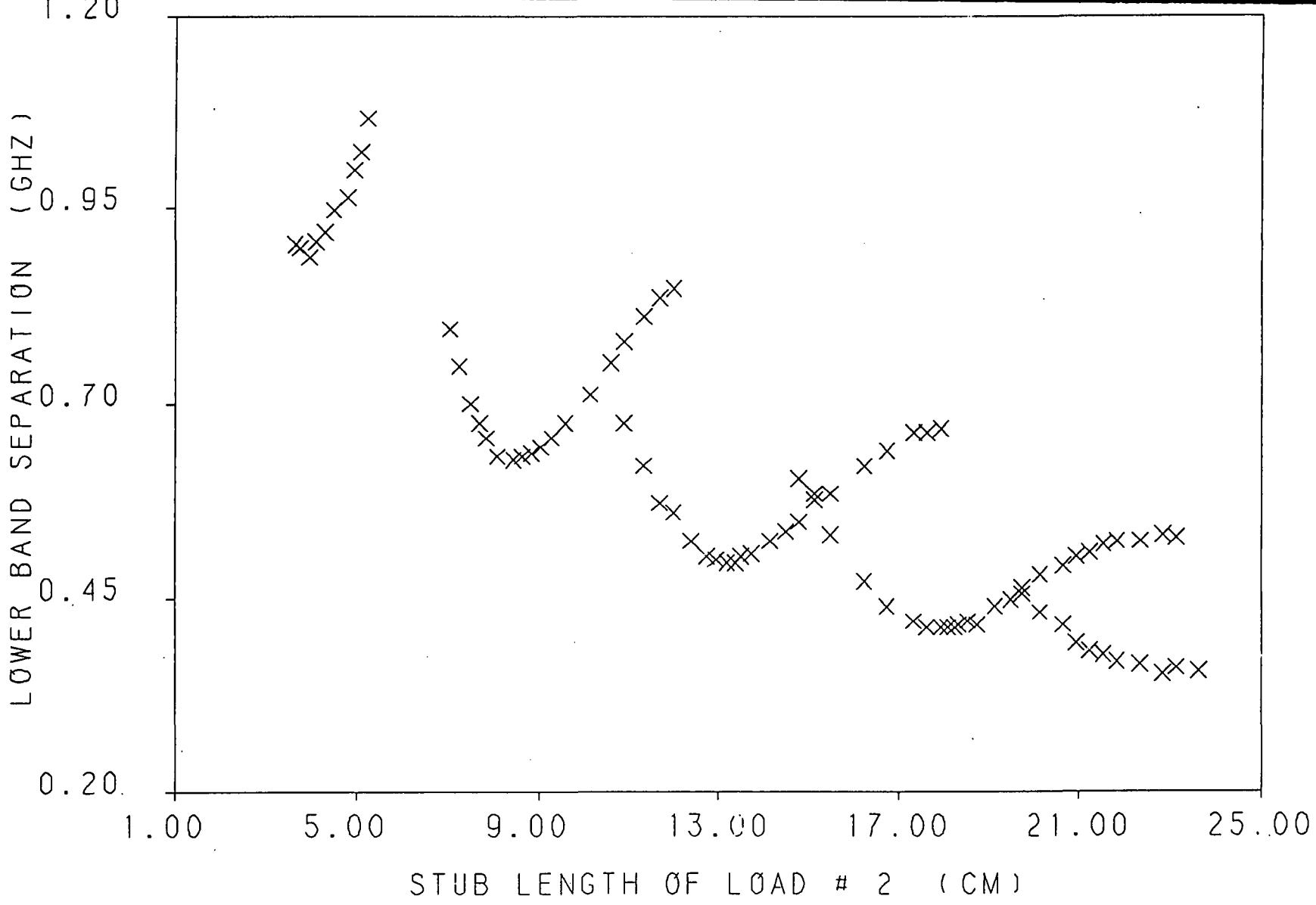

Fig. 3.44 Lower frequency band (the *y*-polarized band) separation verses the short circuit stub length of load #2 for a loaded 2.96 by 2.96 cm square patch with a feed location of (.25, .25 cm), and load insets of d = .11 cm .

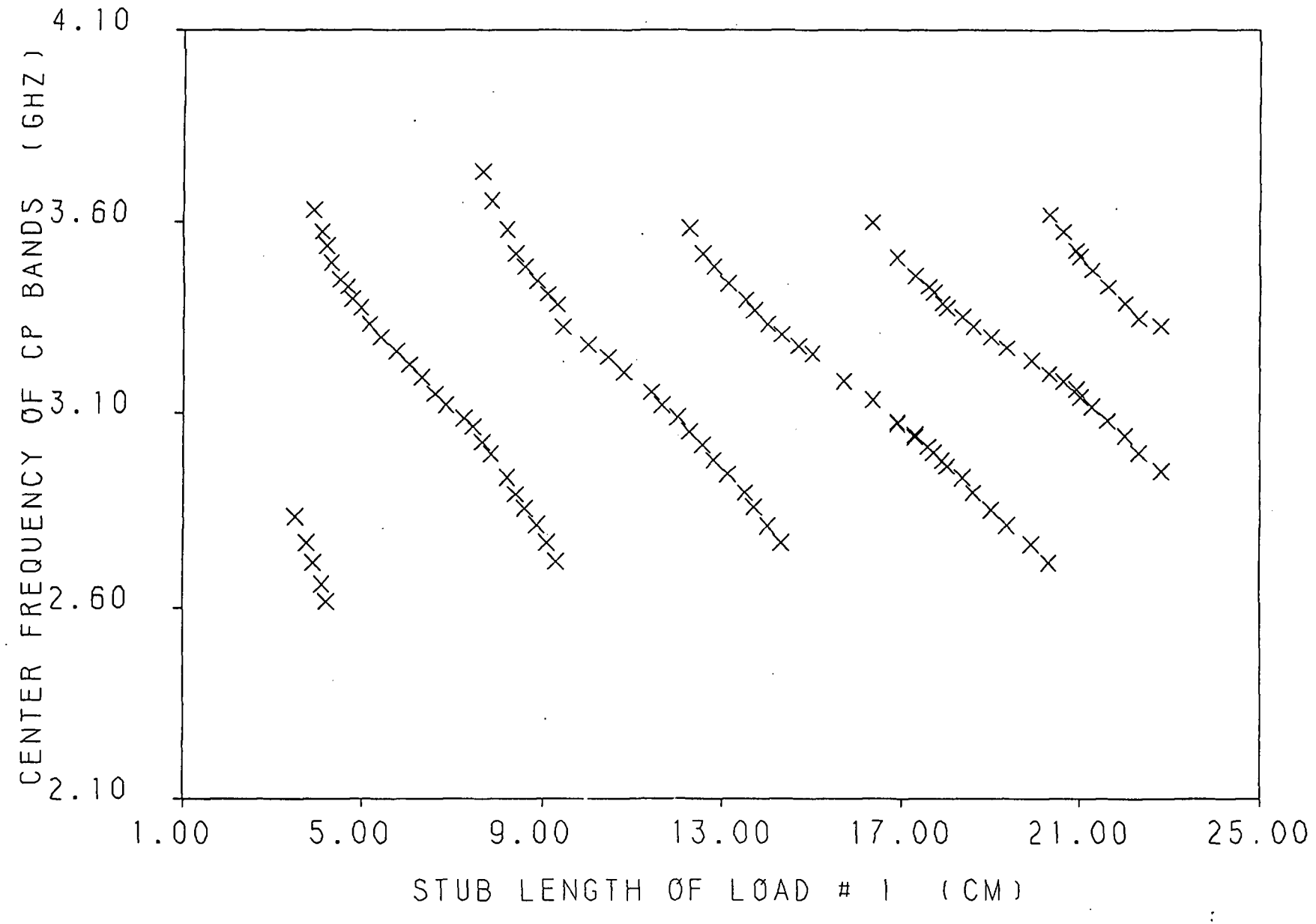

Fig. 3.45 Center frequency of cp bands verses the short circuit stub length of load # 1 for a loaded 2.96 by 2.96 cm square patch with a feed location of (.25, .25 cm), and load insets of d = .11 cm .

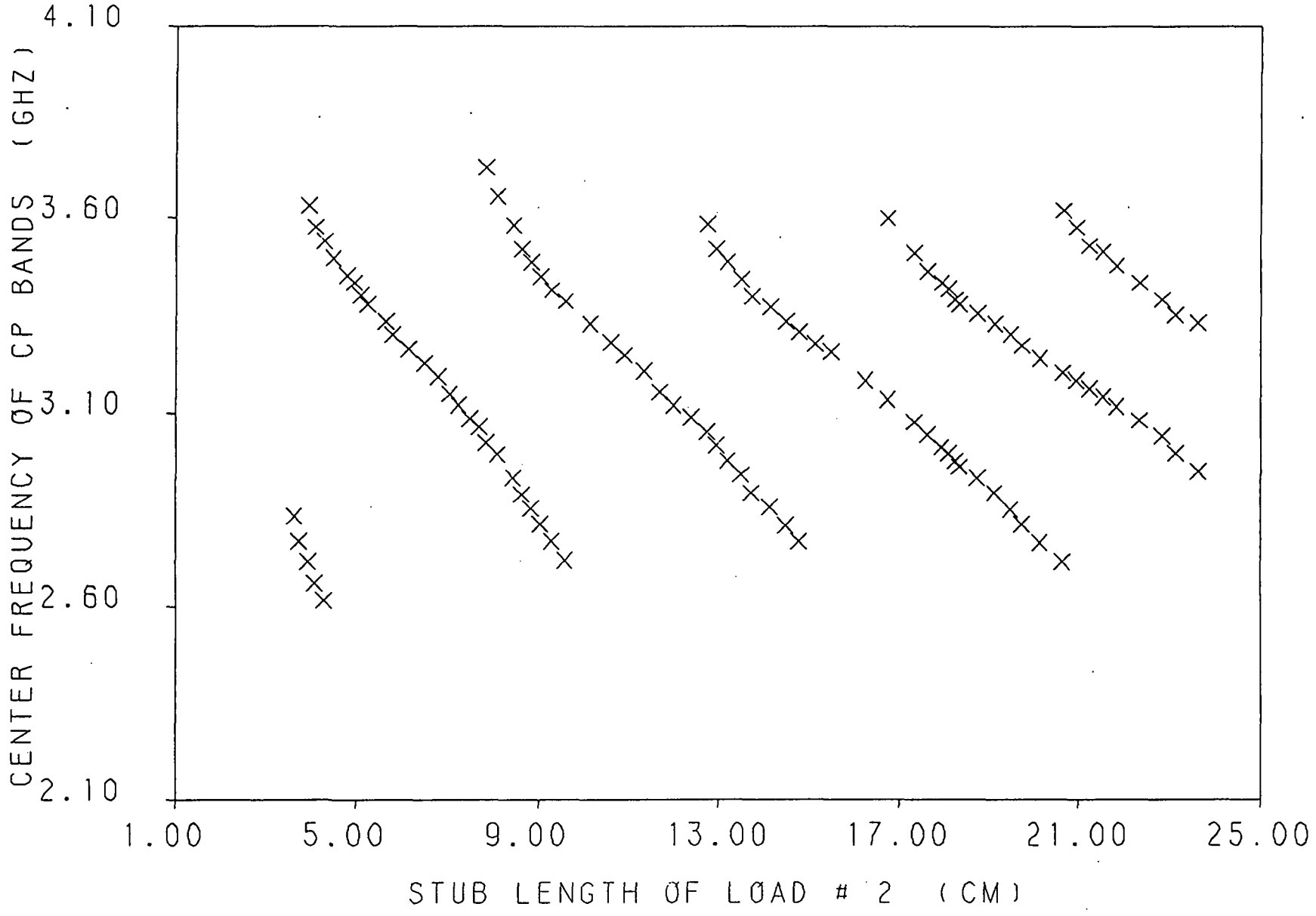

Fig. 3.46 Center frequency of cp bands verses the short circuit stub length of load # 2 for a loaded 2.96 by 2.96 cm square patch with a feed location of (.25, .25 cm), and load insets of d = .11 cm .

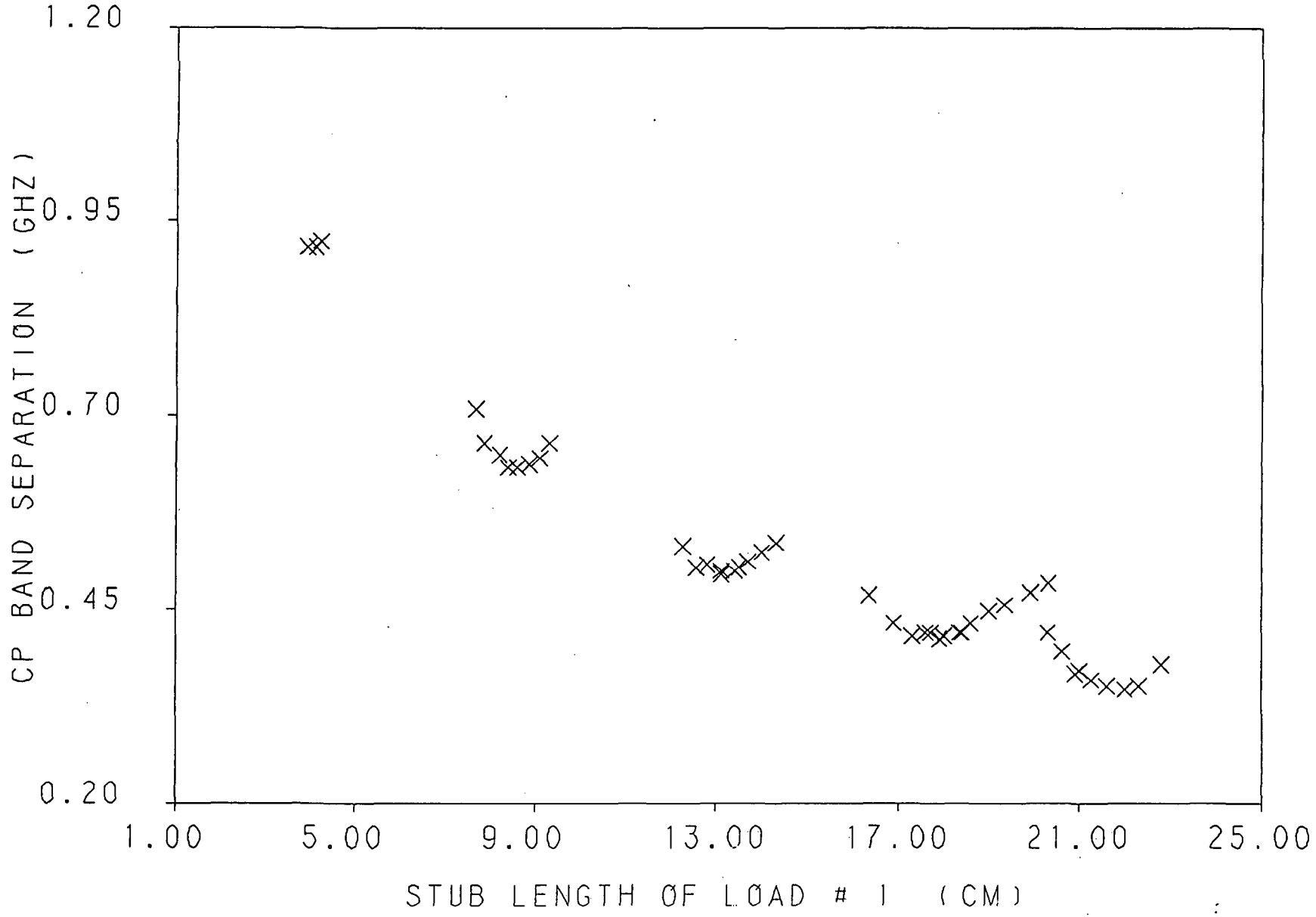

Fig. 3.47 Cp band separation verses the short circuit stub length of load # 1 for a loaded 2.96 by 2.96 cm square patch with a feed location of (.25, .25 cm), and load insets of d = .11 cm .

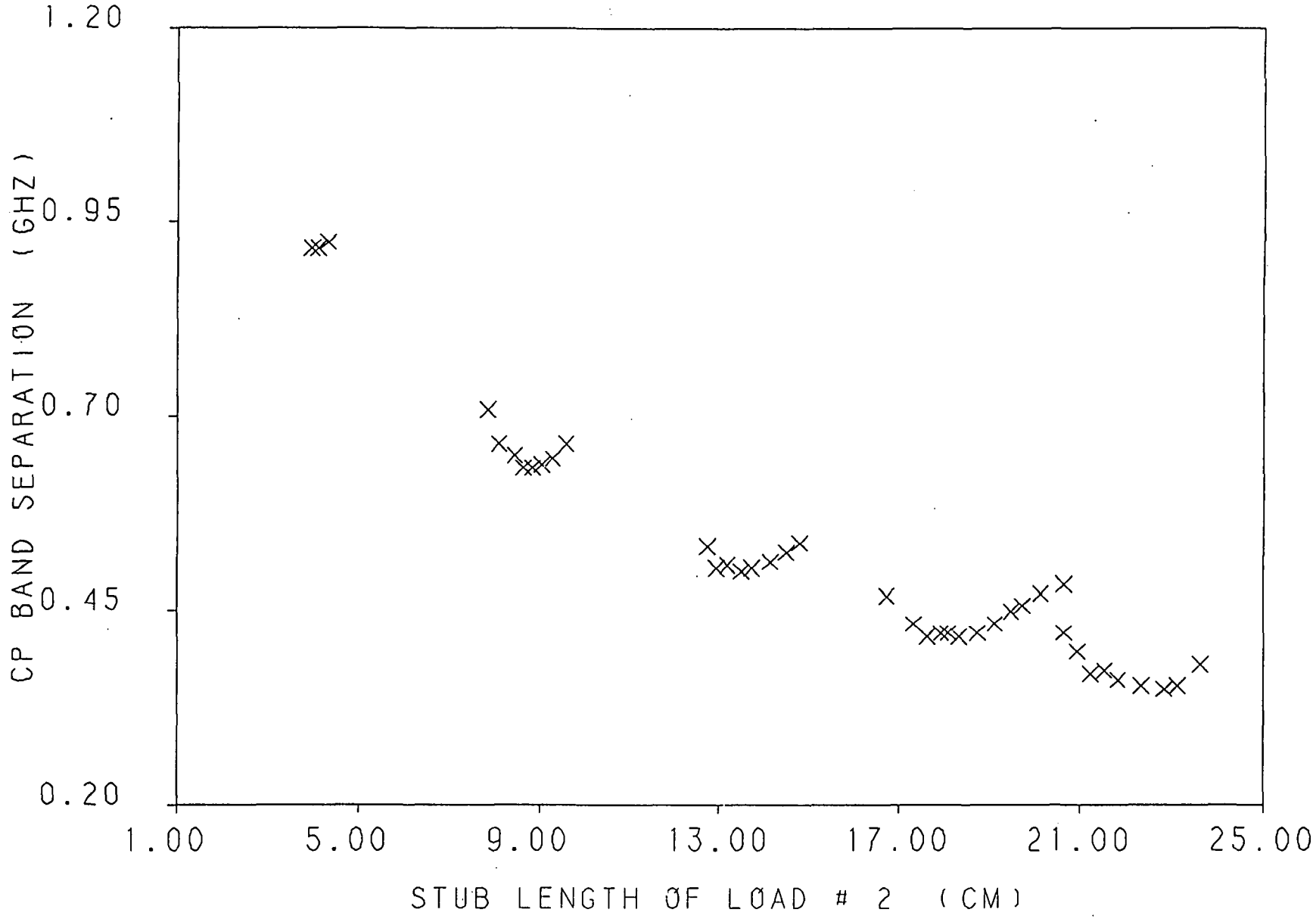

Fig. 3.48 Cp band separation verses the short circuit stub length of load # 2 for a loaded 2.96 by 2.96 cm square patch with a feed location of (.25, .25 cm), and load insets of d = .11 cm .

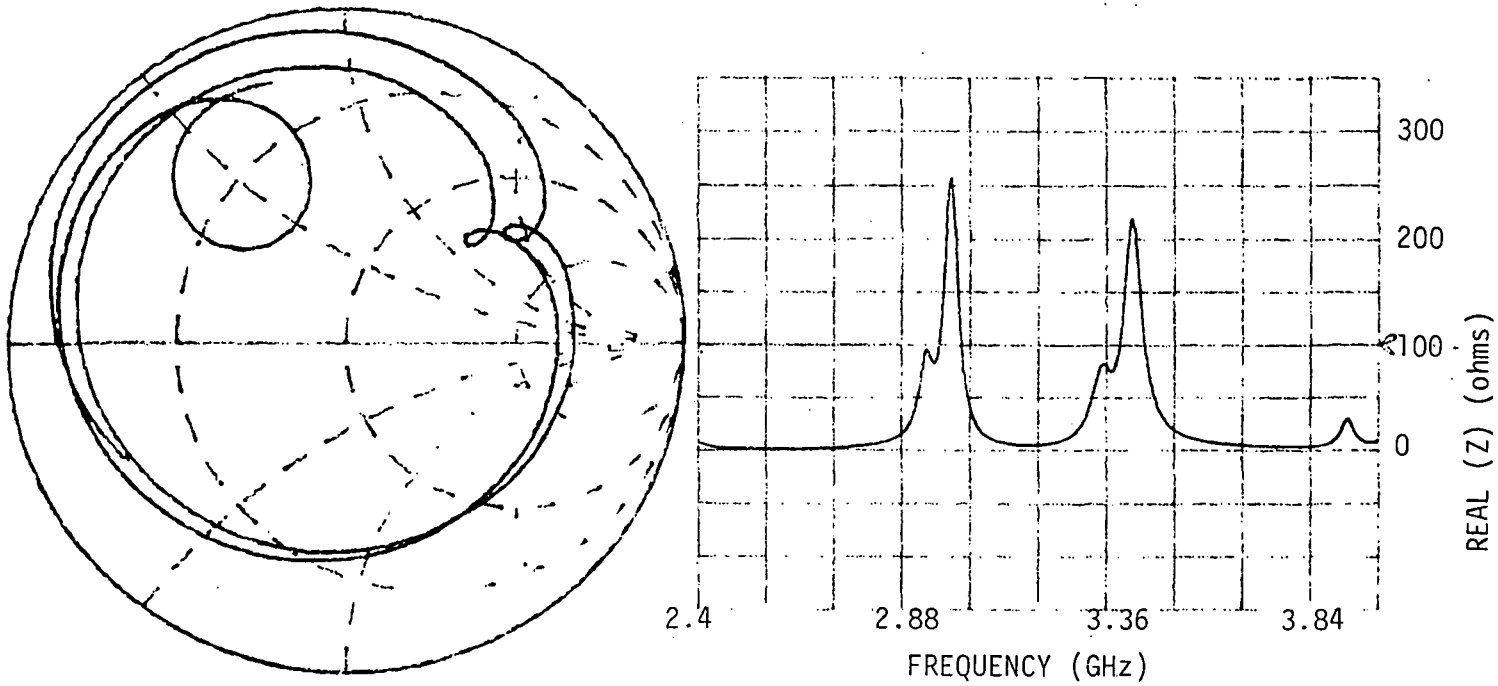

Fig. 3.49 Real part (right) and Smith Chart (left) representation of input impedance of the fourth mode for a loaded 2.96 cm by 2.96 cm square patch with a feed location of (.25, .475 cm), load insets of d = .11 cm, and stub lengths of s_1= 18.1 cm and s_2= 18.48 cm.

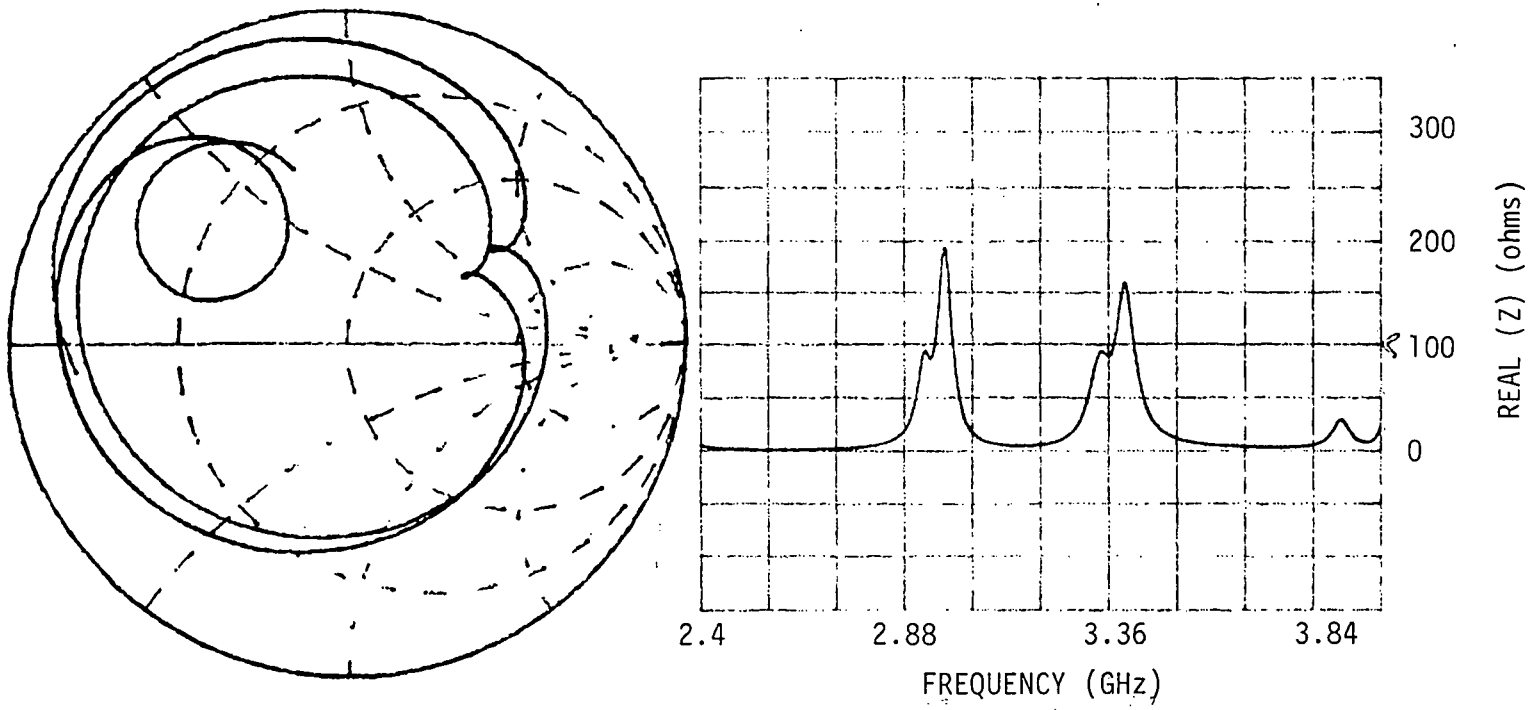

Fig. 3.50 Real part (right) and Smith Chart (left) representation of input impedance of the fourth mode for a loaded 2.96 cm by 2.96 cm square patch with a feed location of (.25, .775 cm), load insets of d = .11 cm, and stub lengths of $s1$ = 18.2 cm and $s2$ = 18.53 cm.

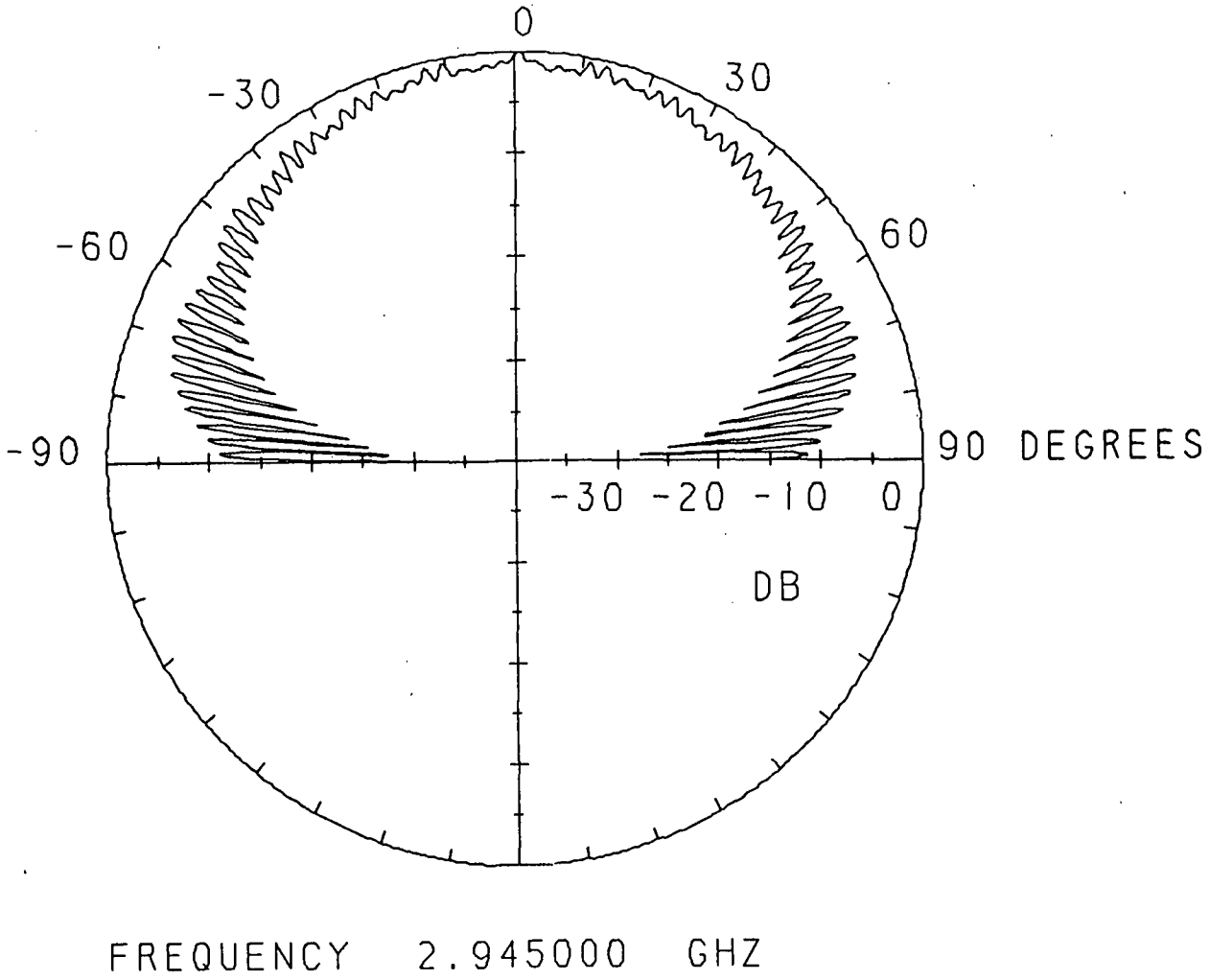

Fig. 3.51 Spinning linear pattern for the lower cp band of the fourth mode for a loaded 2.96 by 2.96 cm square patch with a feed location of (.25, .775 cm), load insets of d = .11 cm, and stub lengths of s_1 = 18.2 cm and s_2 = 18.53 cm.

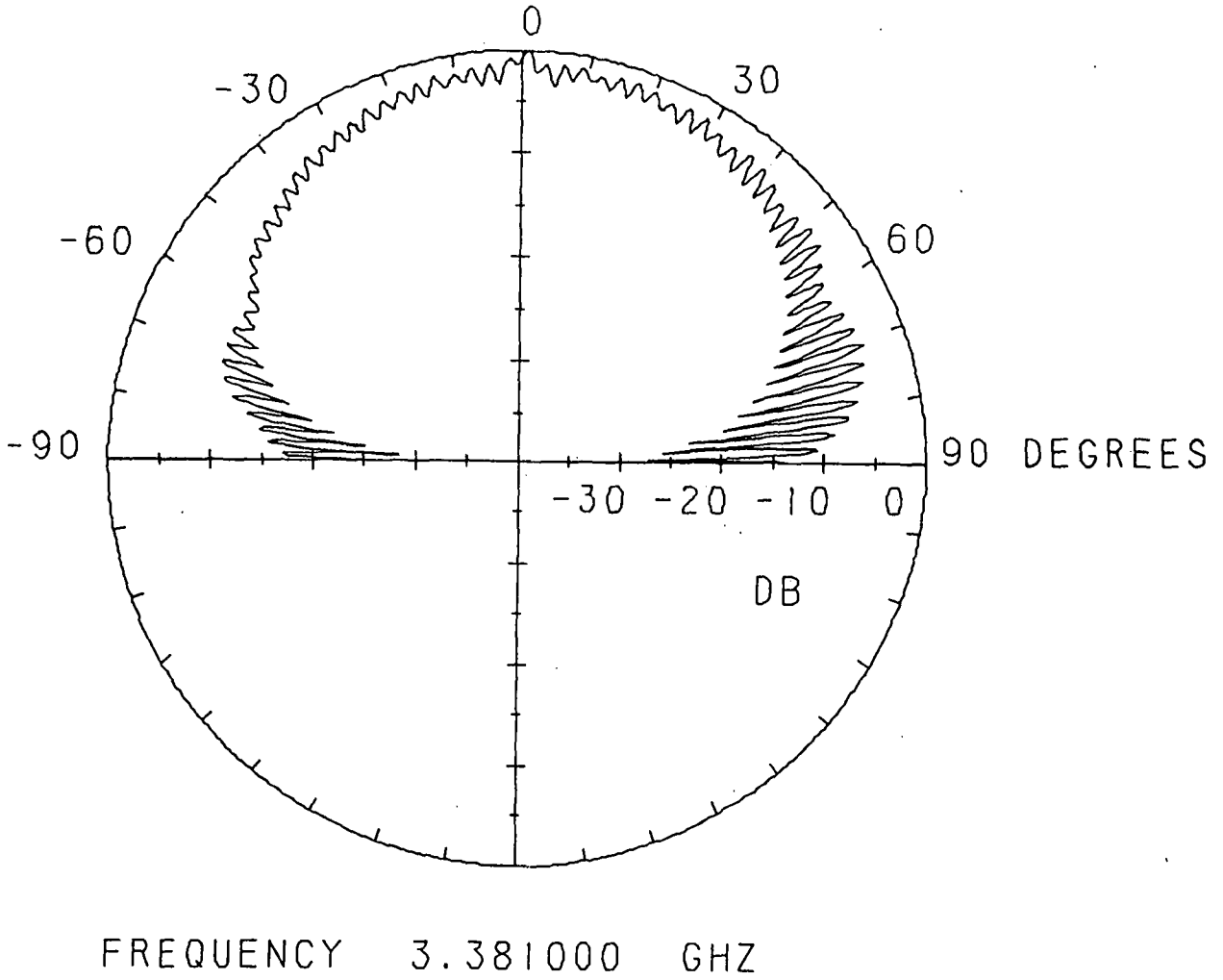

Fig. 3.52 Spinning linear pattern for the upper cp band of the fourth mode for a loaded 2.96 by 2.96 cm square patch with a feed location of (.25, .775 cm), load insets of d = .11 cm, and stub lengths of s_1 = 18.2 cm and s_2 = 18.53 cm.

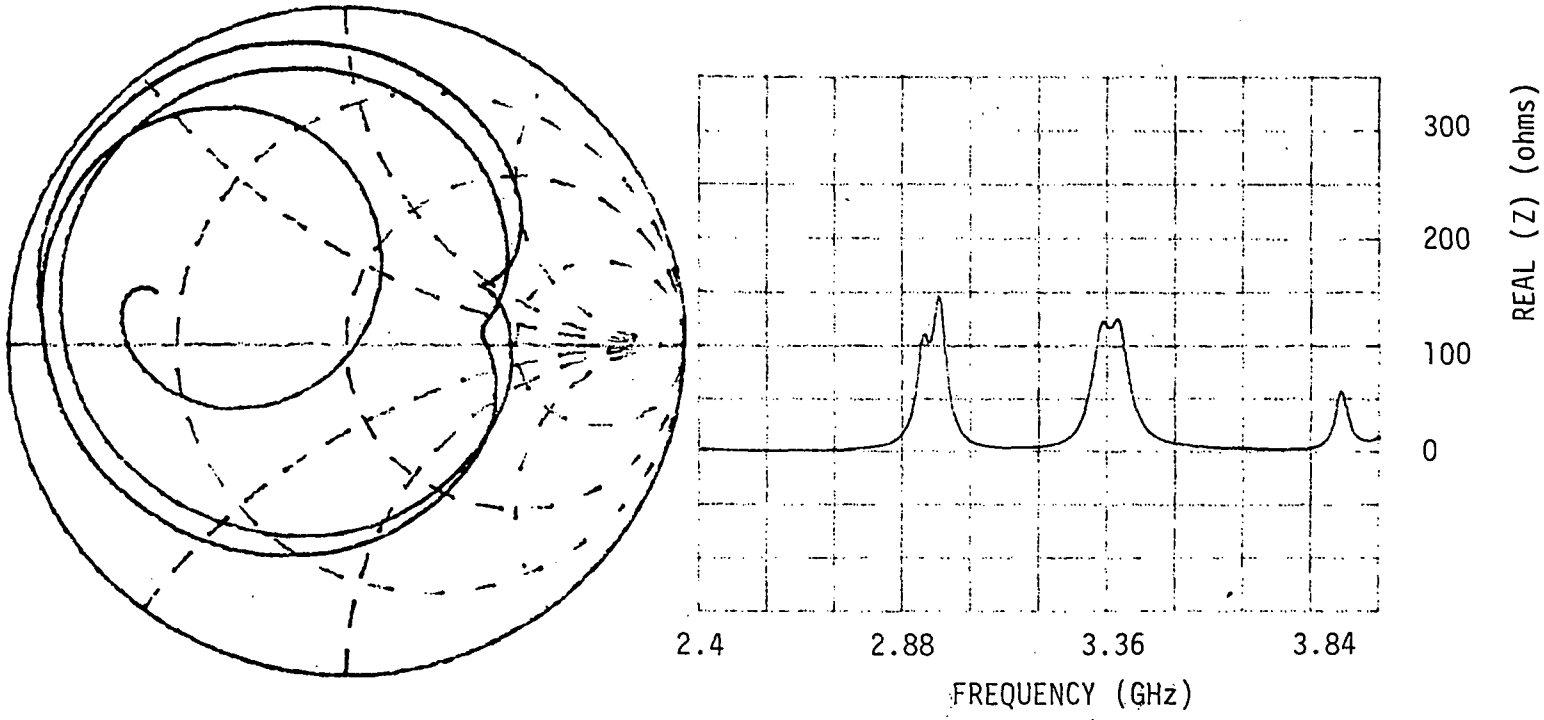

Fig. 3.53 Real part (right) and Smith Chart (left) representation of input impedance of the fourth mode for a loaded 2.96 cm by 2.96 cm square patch with a feed location of (.25, 1.15 cm), load insets of d = .11 cm, and stub lengths of $s1$ = 18.3 cm and $s2$ = 18.43 cm.

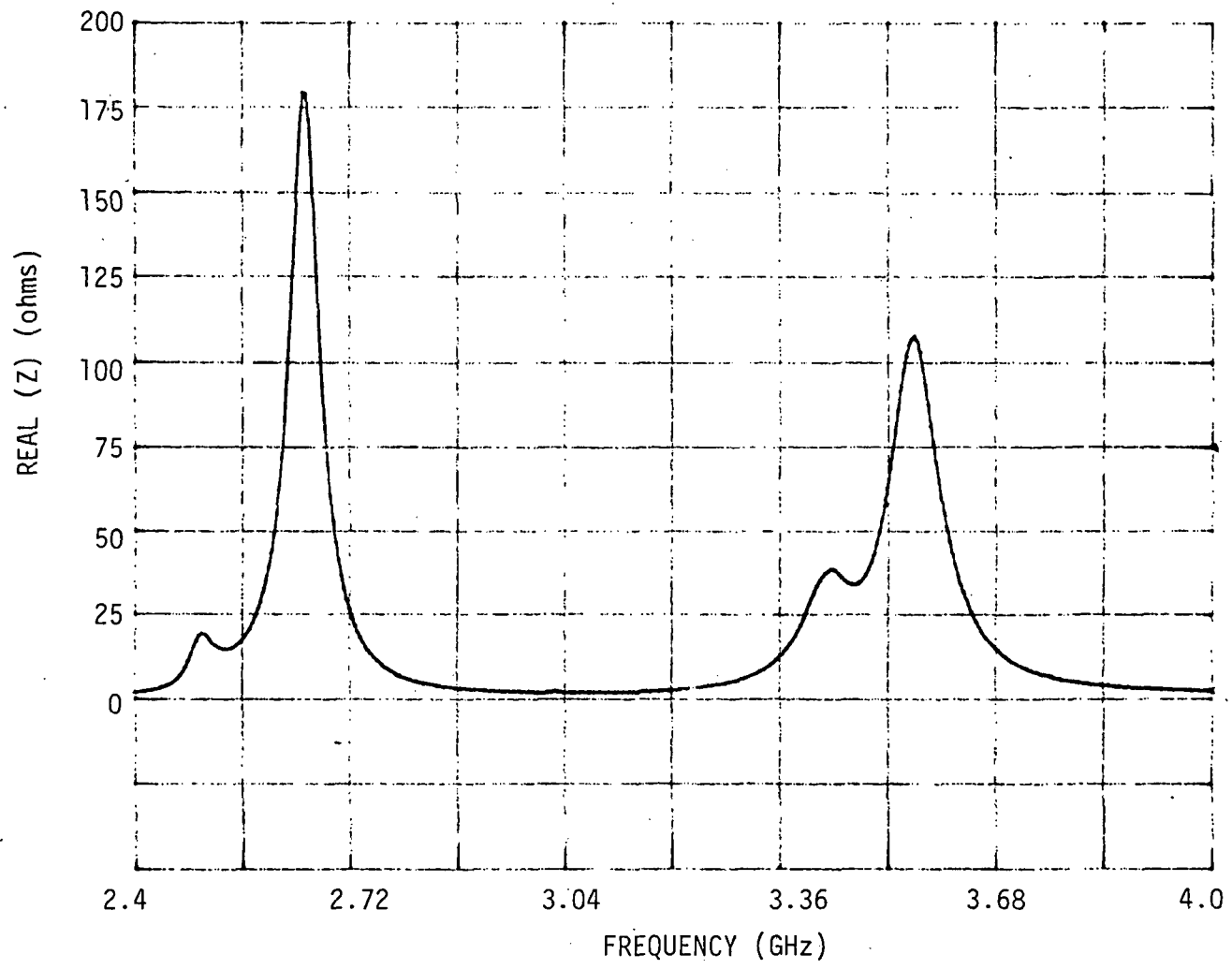

Fig. 3.54 Real part of input impedance verses frequency of the first mode for a loaded 2.96 by 2.96 cm square patch with a feed location of (.45, 1.05 cm), load insets of d = .11 cm, and stub lengths of s_1 = 4.5 cm and s_2 = 4.48 cm.

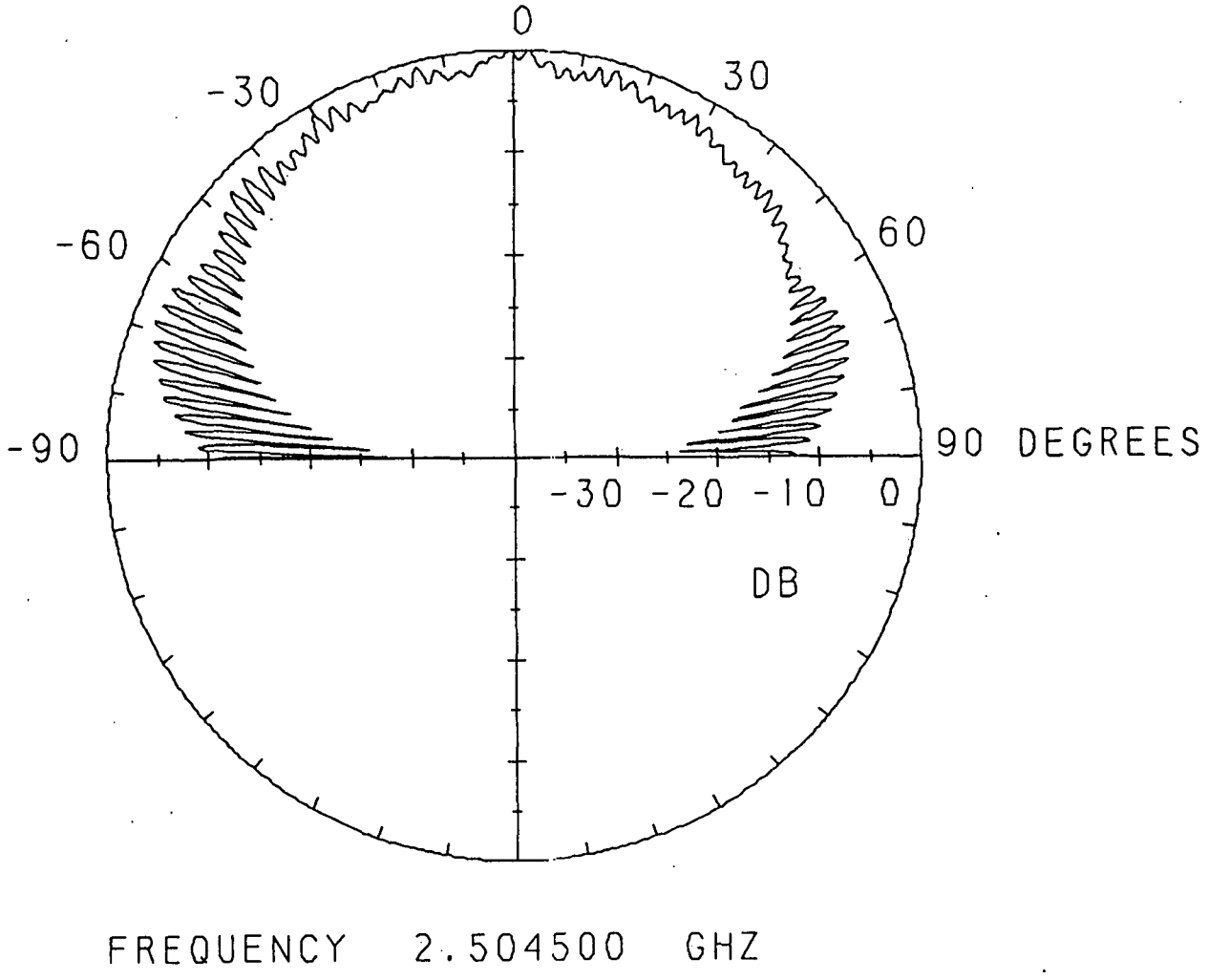

Fig. 3.55 Spinning linear pattern for the lower cp band of the first mode for a loaded 2.96 by 2.96 cm square patch with a feed location of (.45, 1.05 cm), load insets of d = .11 cm, and stub lengths of s_1 = 4.5 cm and s_2 = 4.48 cm.

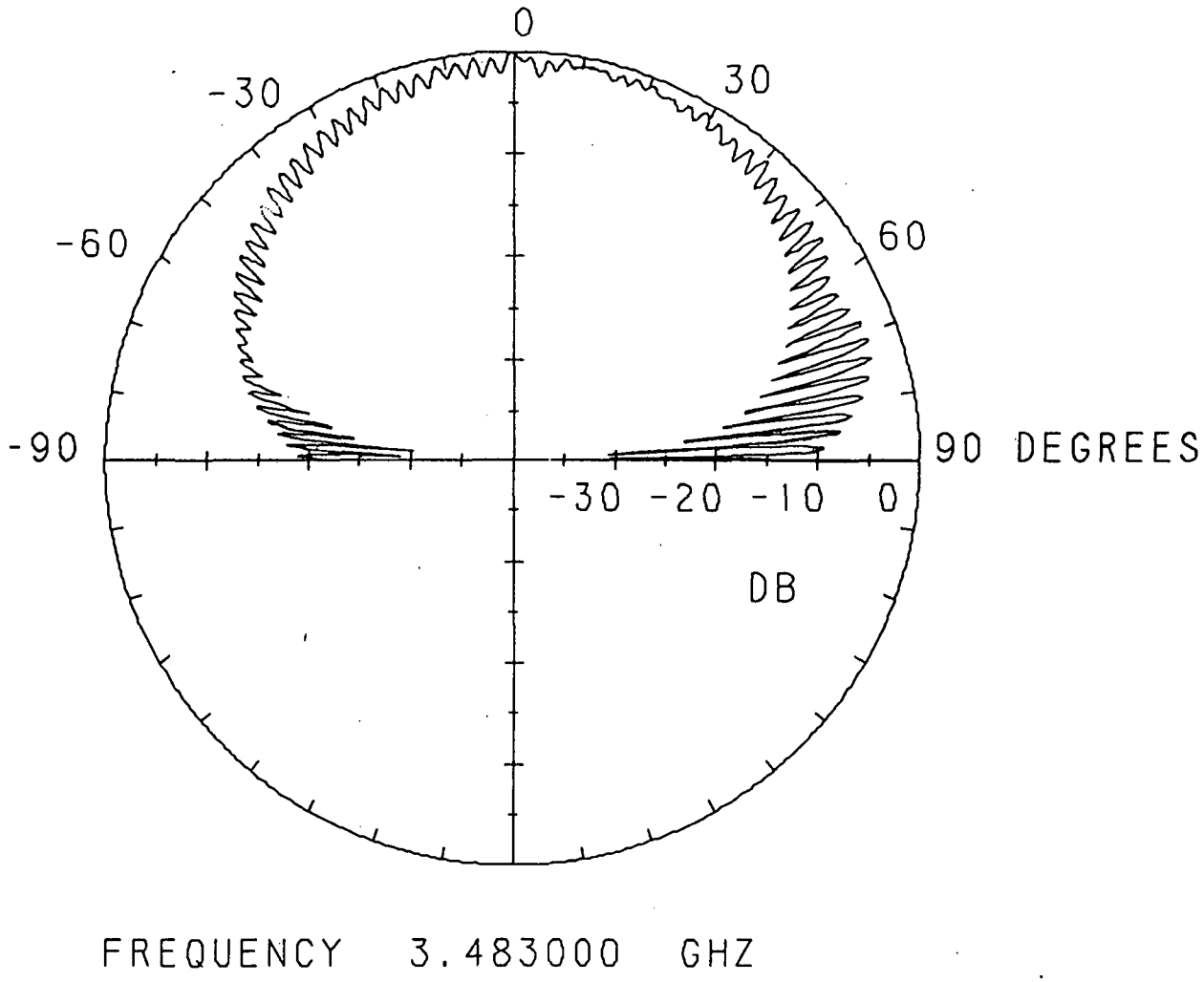

Fig. 3.56 Spinning linear pattern for the upper cp band of the first mode for a loaded 2.96 by 2.96 cm square patch with a feed location of (.45, 1.05 cm), load insets of d = .11 cm, and stub lengths of s_1 = 4.5 cm and s_2 = 4.48 cm.

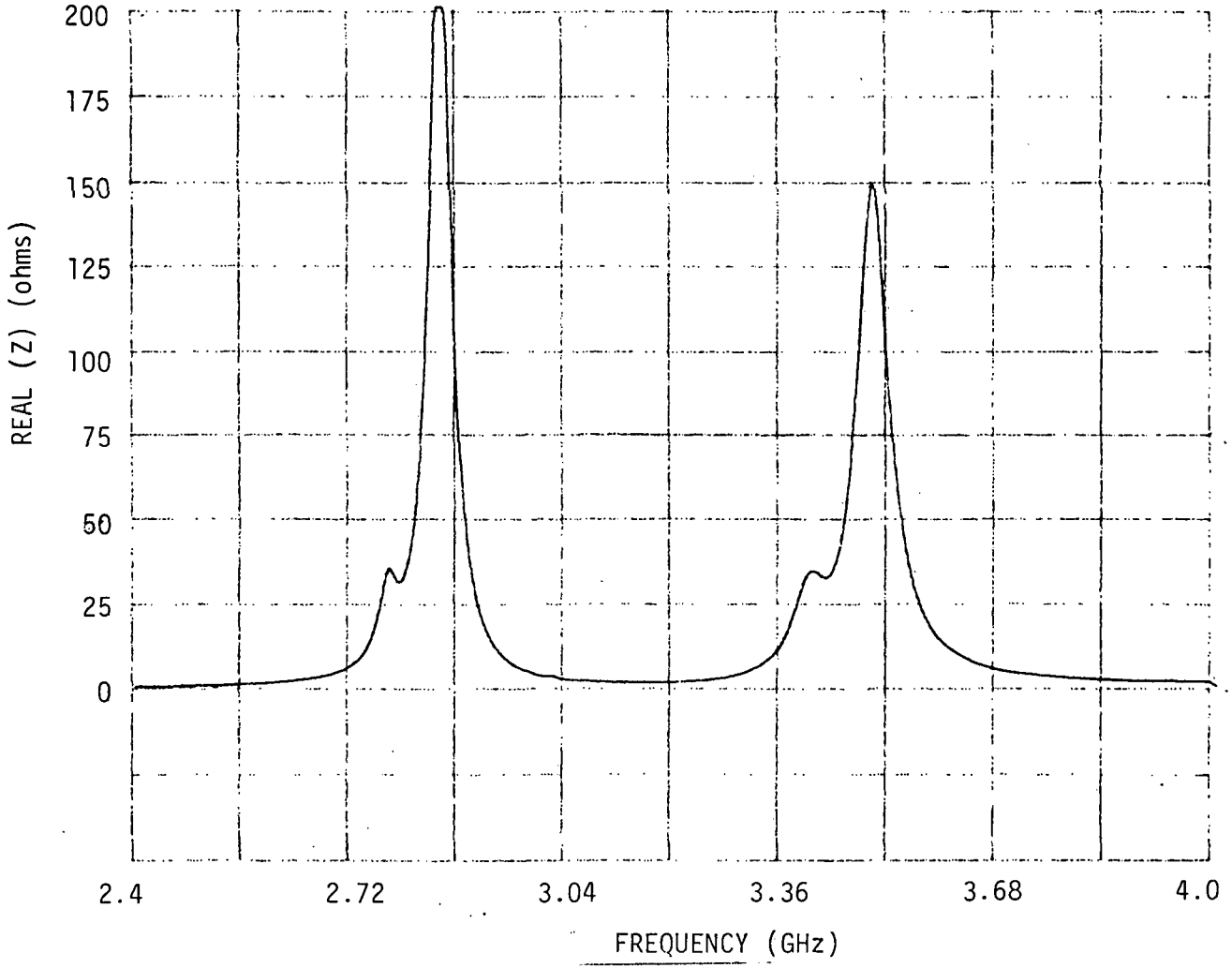

Fig. 3.57 Real part of input impedance verses frequency of the second mode for a loaded 2.96 by 2.96 cm square patch with a feed location of (.45, 1.05 cm), load insets of d = .11 cm, and stub lengths of s_1 = 9.1 cm and s_2 = 8.98 cm.

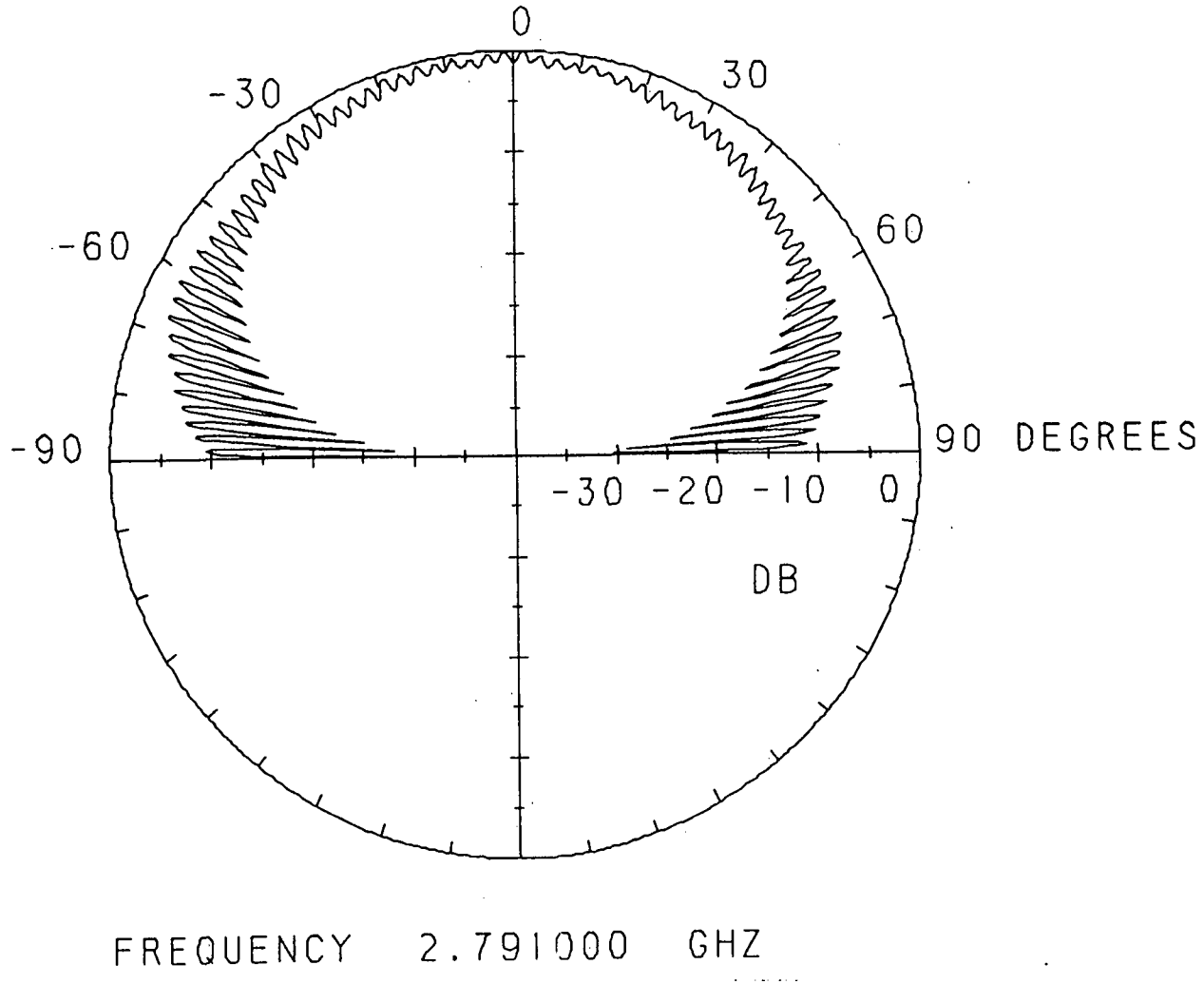

Fig. 3.58 Spinning linear pattern for the lower cp band of the second mode for a loaded 2.96 by 2.96 cm square patch with a feed location of (.45, 1.05 cm), load insets of d = .11 cm, and stub lengths of s_1 = 9.1 cm and s_2 = 8.98 cm.

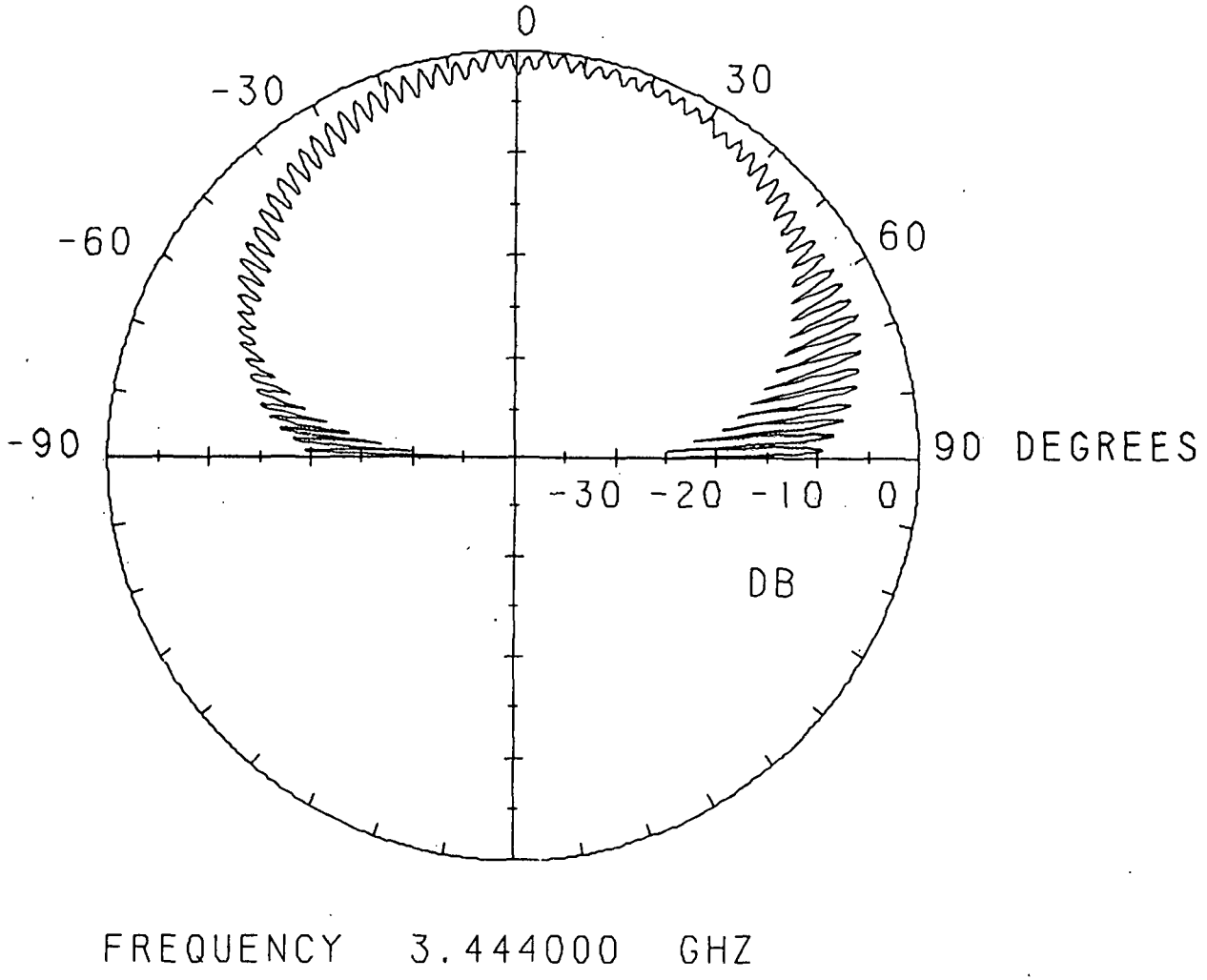

Fig. 3.59 Spinning linear pattern for the upper cp band of the second mode for a loaded 2.96 by 2.96 cm square patch with a feed location of (.45, 1.05 cm), load insets of d = .11 cm, and stub lengths of s_1 = 9.1 cm and s_2 = 8.98 cm.

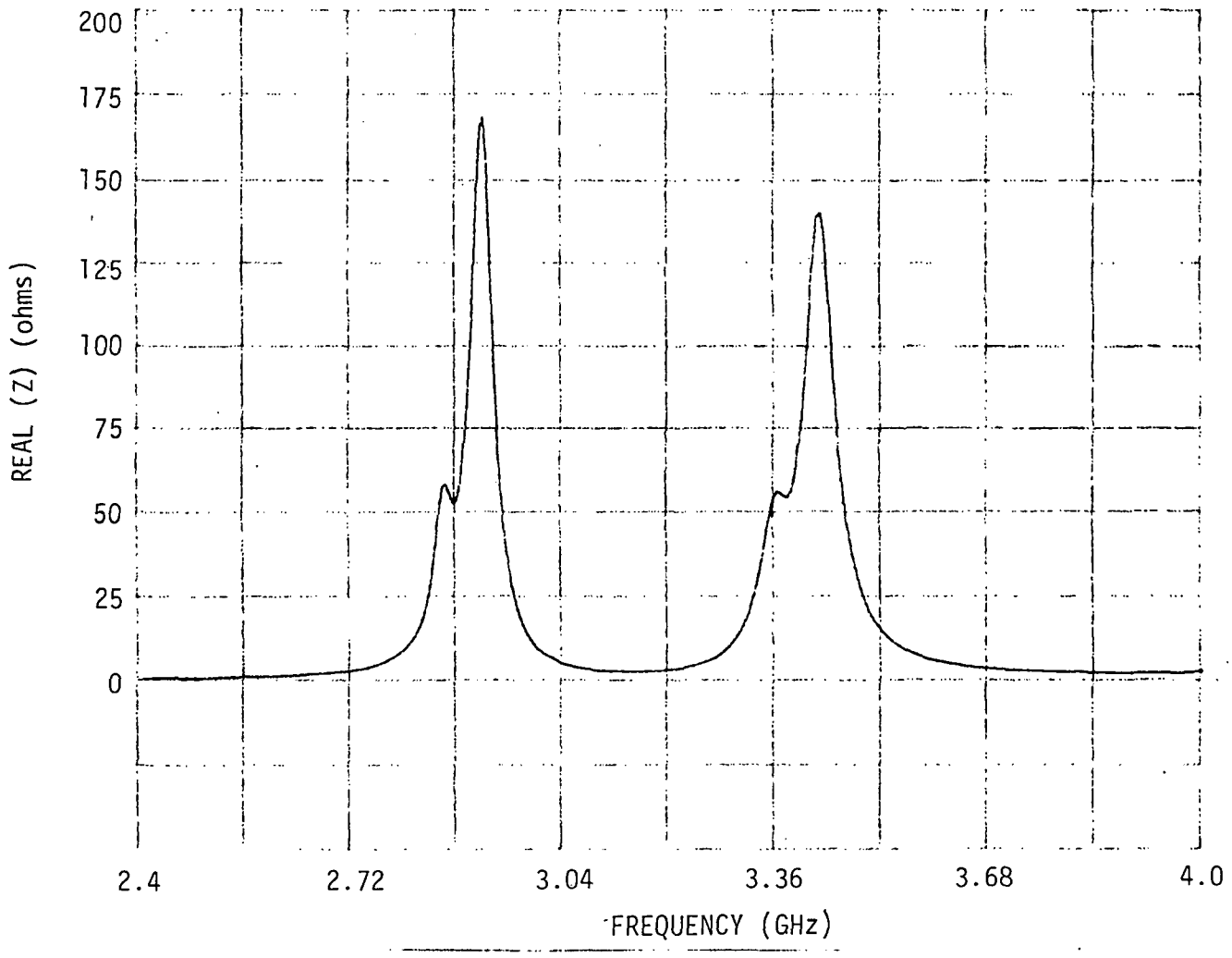

Fig. 3.60 Real part of input impedance verses frequency of the third mode for a loaded 2.96 by 2.96 cm square patch with a feed location of (.45, 1.05 cm), load insets of d = .11 cm, and stub lengths of s_1 = 13.7 cm and s_2 = 13.78 cm.

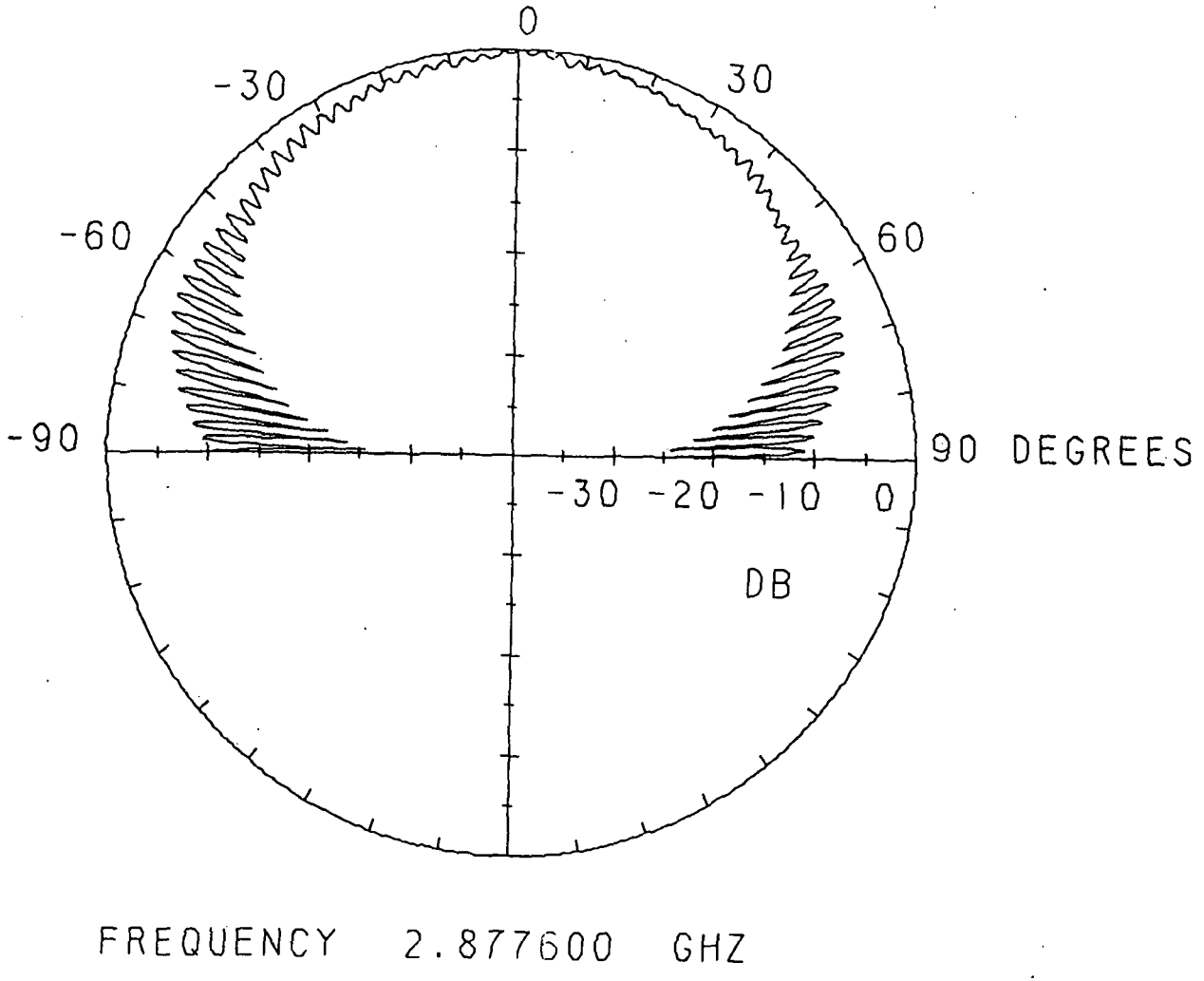

Fig. 3.61 Spinning linear pattern for the lower cp band of the third mode for a loaded 2.96 by 2.96 cm square patch with a feed location of (.45, 1.05 cm), load insets of d = .11 cm, and stub lengths of s_1 = 13.7 cm and s_2 = 13.78 cm.

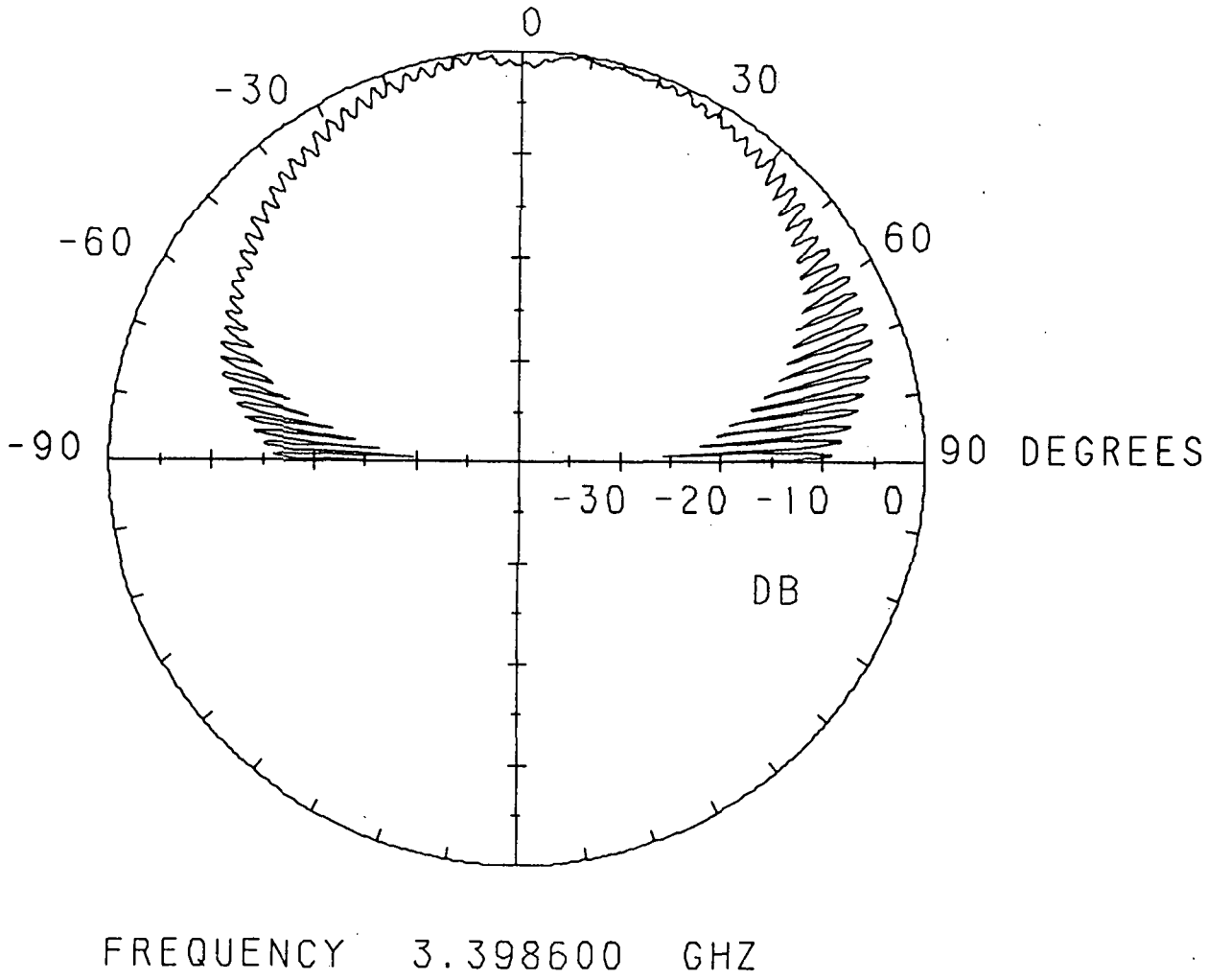

Fig. 3.62 Spinning linear pattern for the upper cp band of the third mode for a loaded 2.96 by 2.96 cm square patch with a feed location of (.45, 1.05 cm), load insets of d = .11 cm, and stub lengths of s_1 = 13.7 cm and s_2 = 13.78 cm.

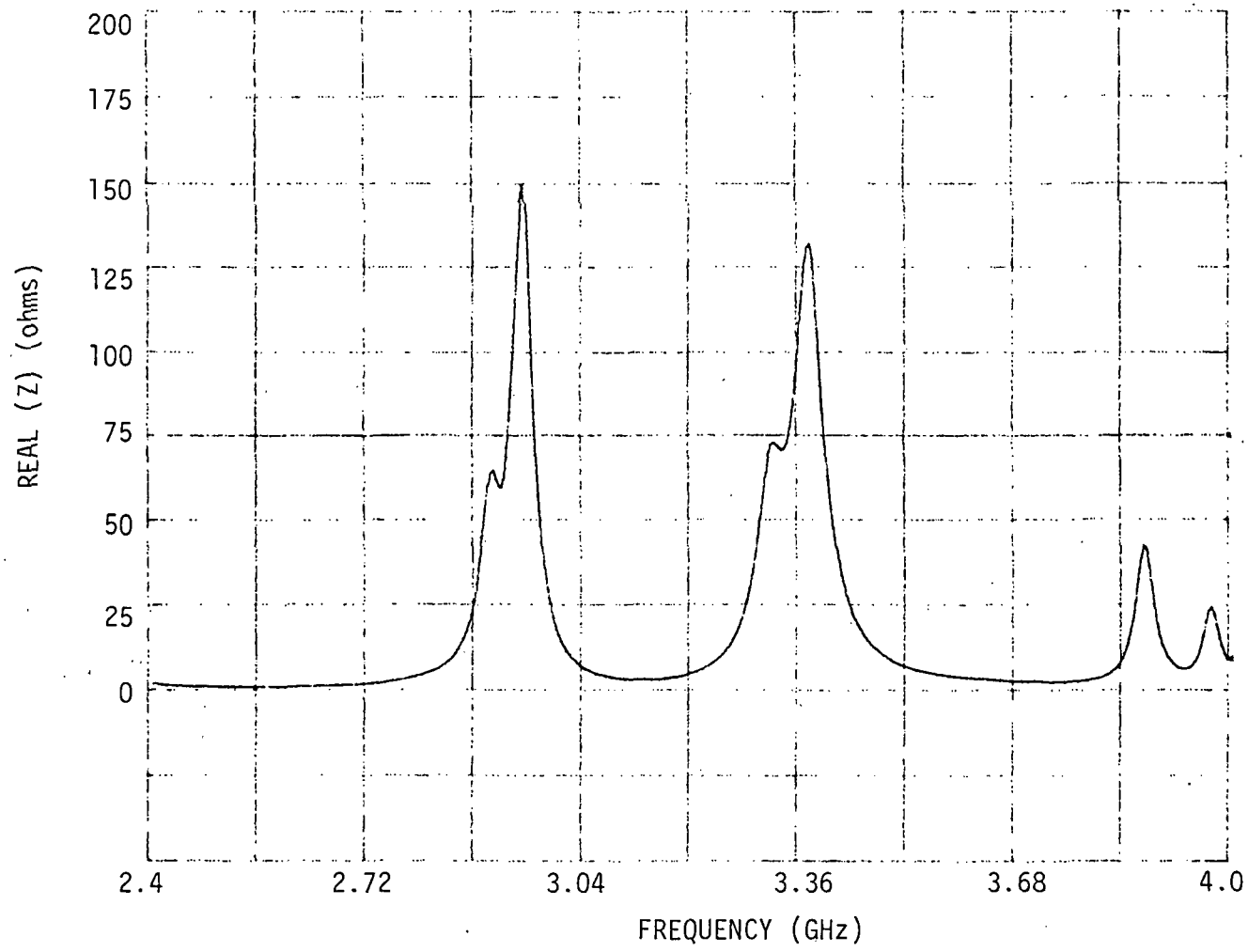

Fig. 3.63 Real part of input impedance verses frequency of the fourth mode for a loaded 2.96 by 2.96 cm square patch with a feed location of (.45, 1.05 cm), load insets of d = .11 cm, and stub lengths of s_1 = 18.4 cm and s_2 = 18.73 cm.

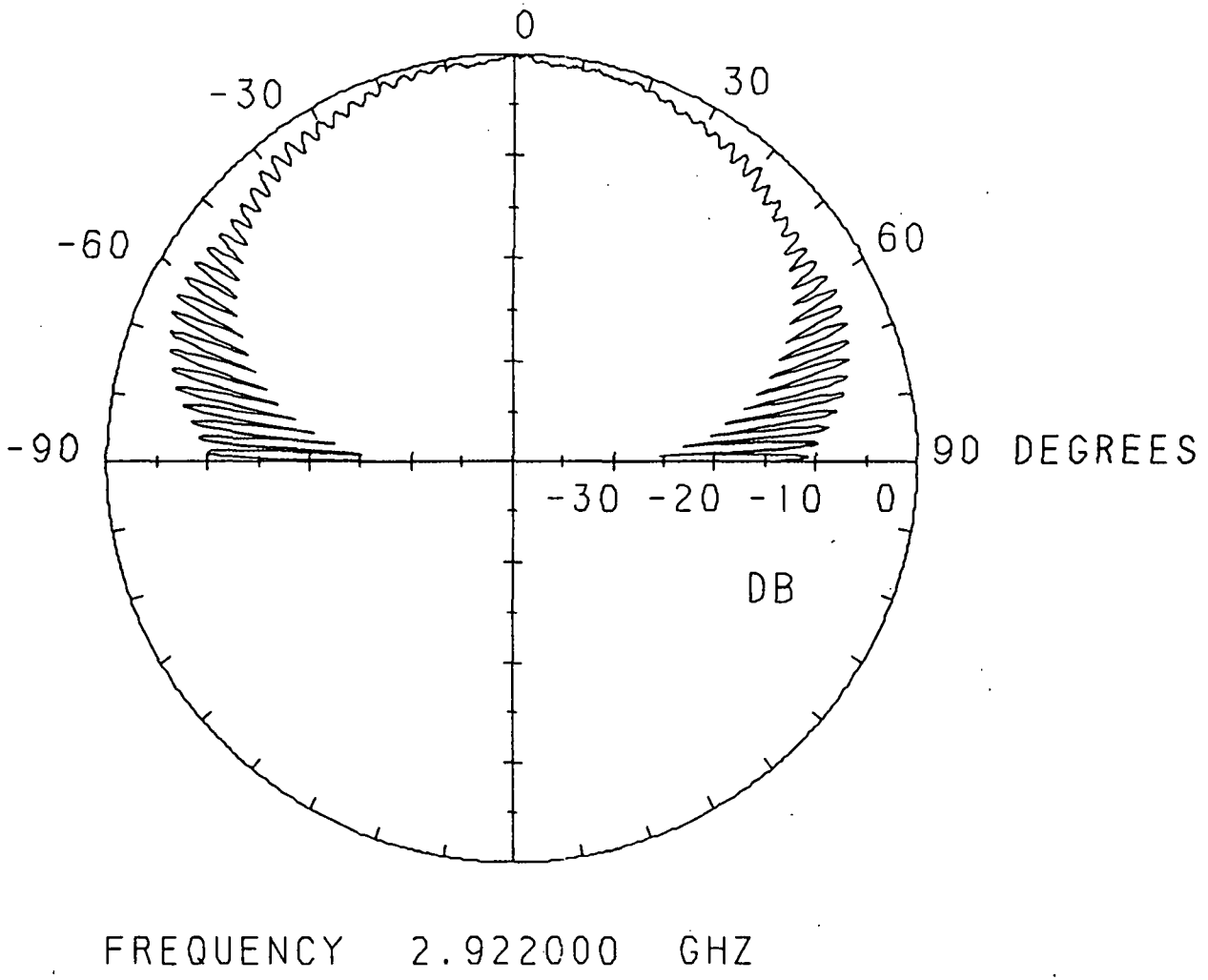

Fig. 3.64 Spinning linear pattern for the lower cp band of the fourth mode for a loaded 2.96 by 2.96 cm square patch with a feed location of (.45, 1.05 cm), load insets of d = .11 cm, and stub lengths of s_1 = 18.4 cm and s_2 = 18.73 cm.

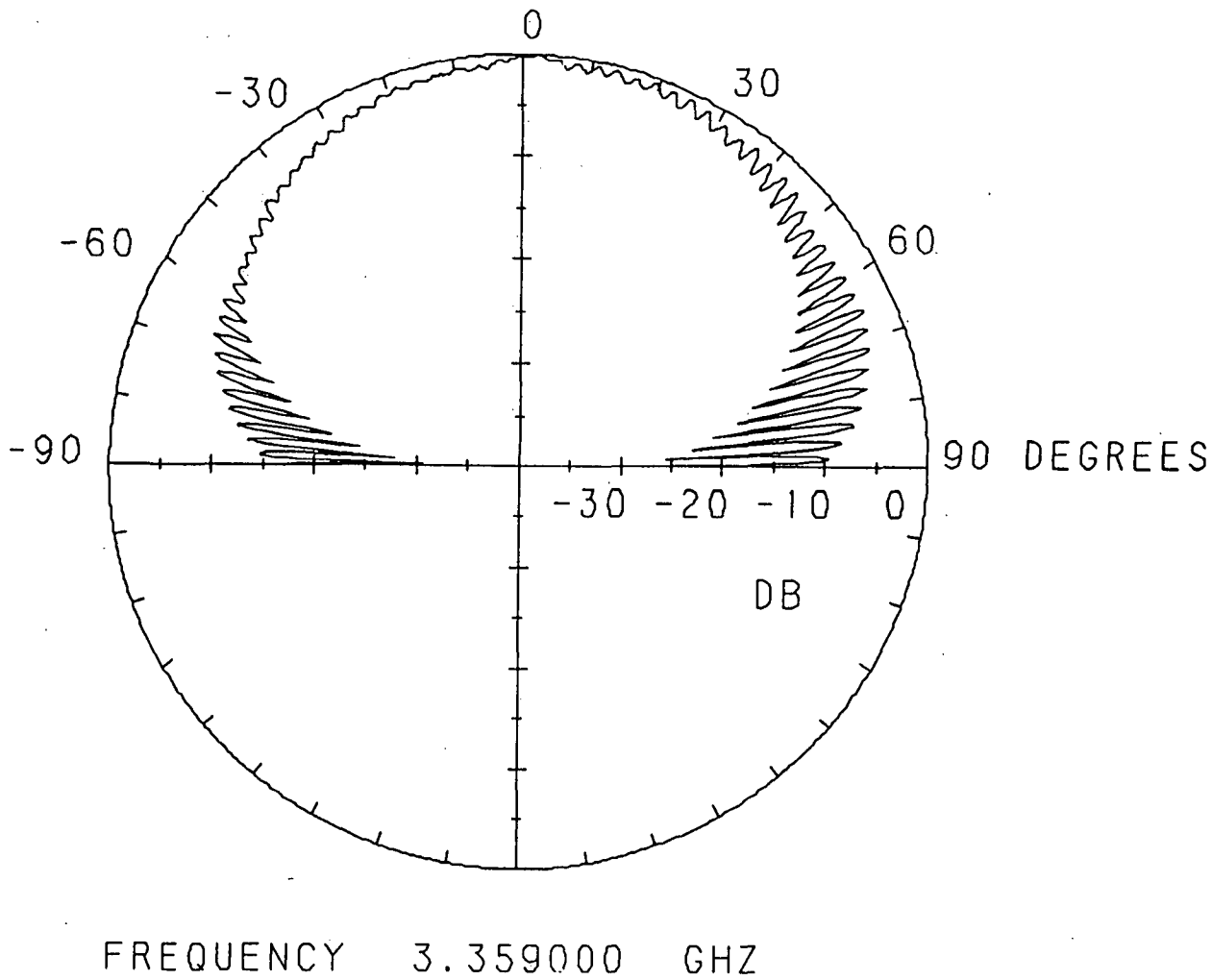

Fig. 3.65 Spinning linear pattern for the upper cp band of the fourth mode for a loaded 2.96 by 2.96 cm square patch with a feed location of (.45, 1.05 cm), load insets of d = .11 cm, and stub lengths of s_1 = 18.4 cm and s_2 = 18.73 cm.

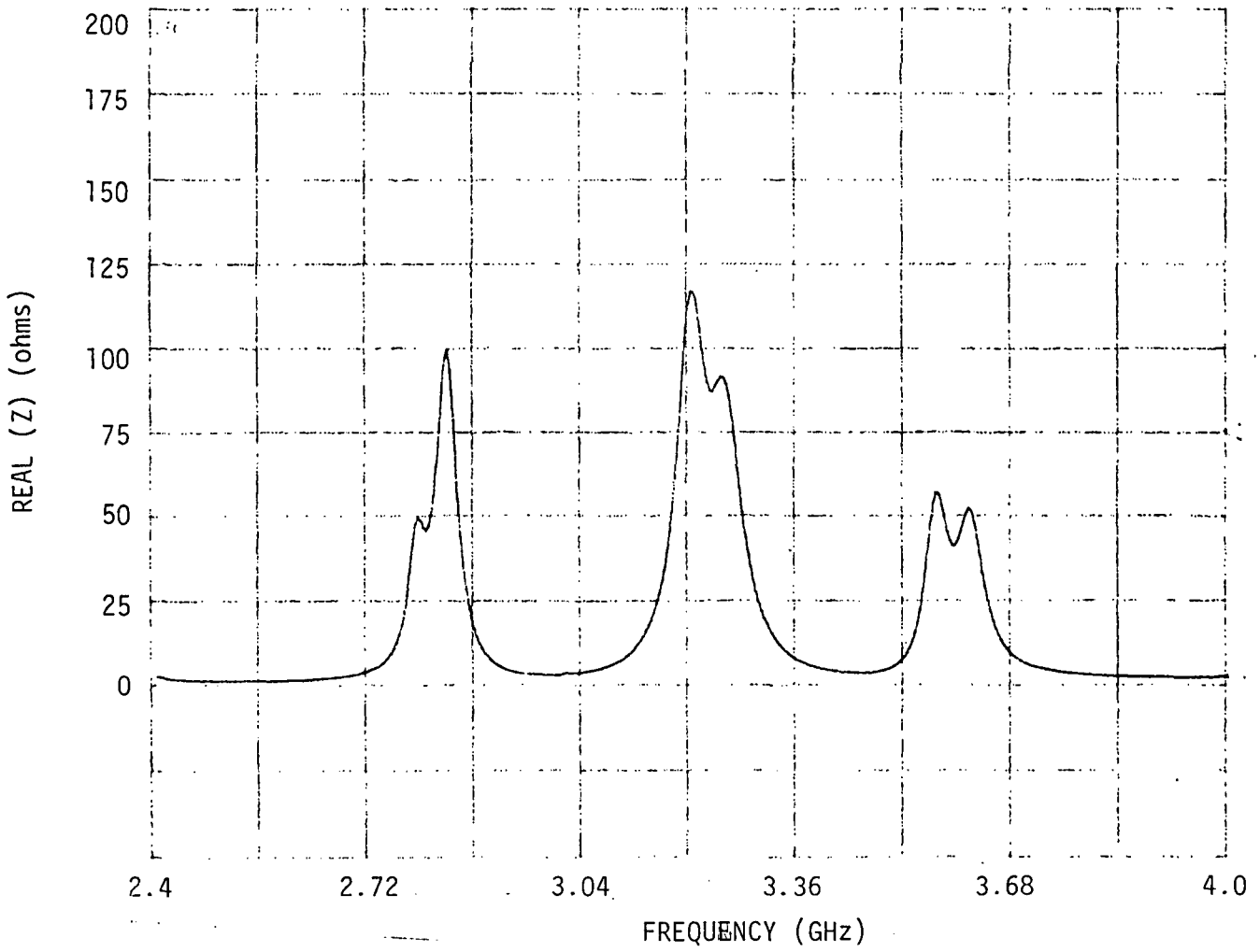

Fig. 3.66 Real part of input impedance verses frequency of the fifth mode for a loaded 2.96 by 2.96 cm square patch with a feed location of (.45, 1.05 cm), load insets of d = .11 cm, and stub lengths of s_1 = 24.8 cm and s_2 = 25.03 cm.

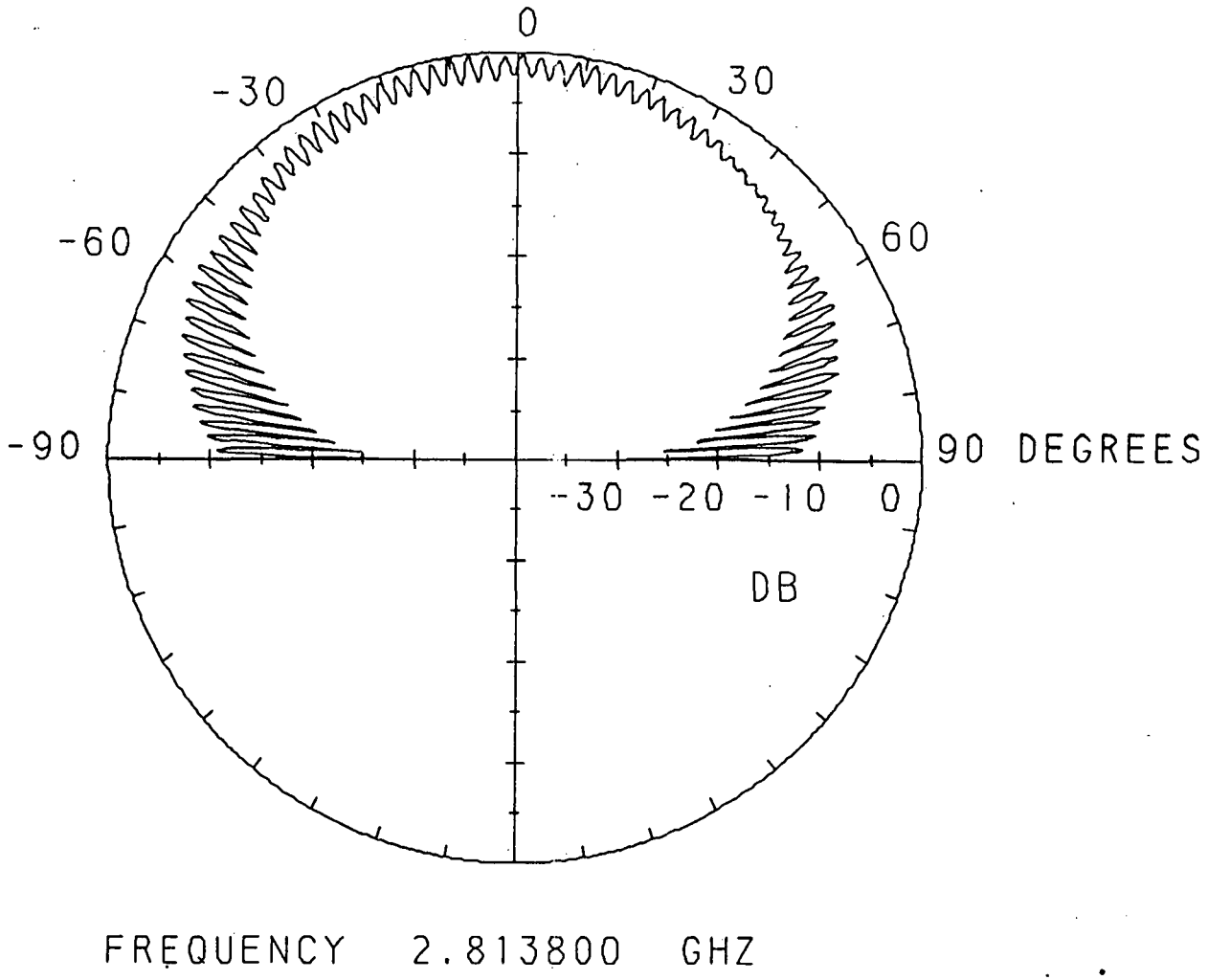

Fig. 3.67 Spinning linear pattern for the lower cp band of the fifth mode for a loaded 2.96 by 2.96 cm square patch with a feed location of (.45, 1.05 cm), load insets of d = .11 cm, and stub lengths of s_1 = 24.8 cm and s_2 = 25.03 cm.

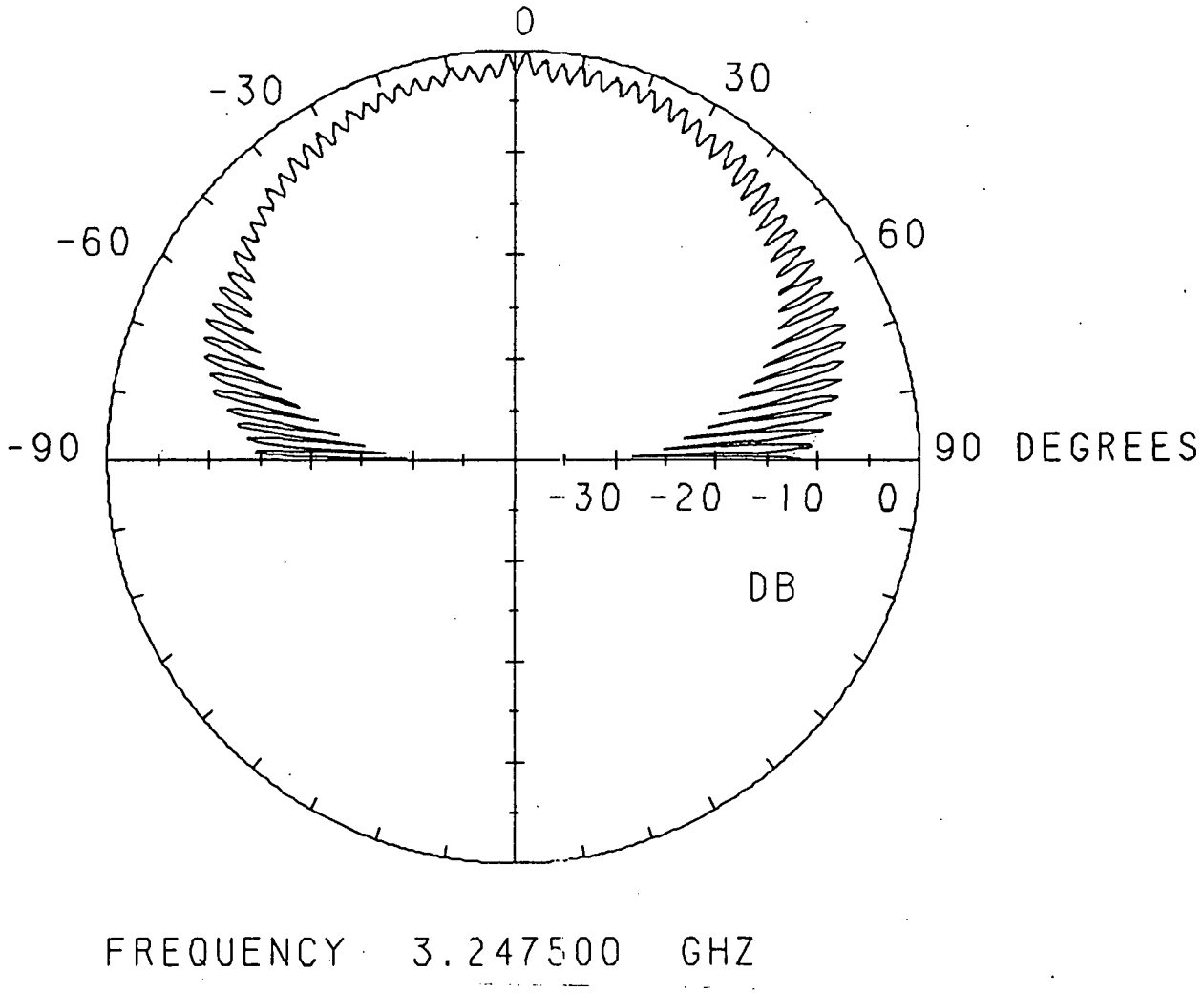

Fig. 3.68 Spinning linear pattern for the upper cp band of the fifth mode for a loaded 2.96 by 2.96 cm square patch with a feed location of (.45, 1.05 cm), load insets of d = .11 cm, and stub lengths of s_1 = 24.8 cm and s_2 = 25.03 cm.

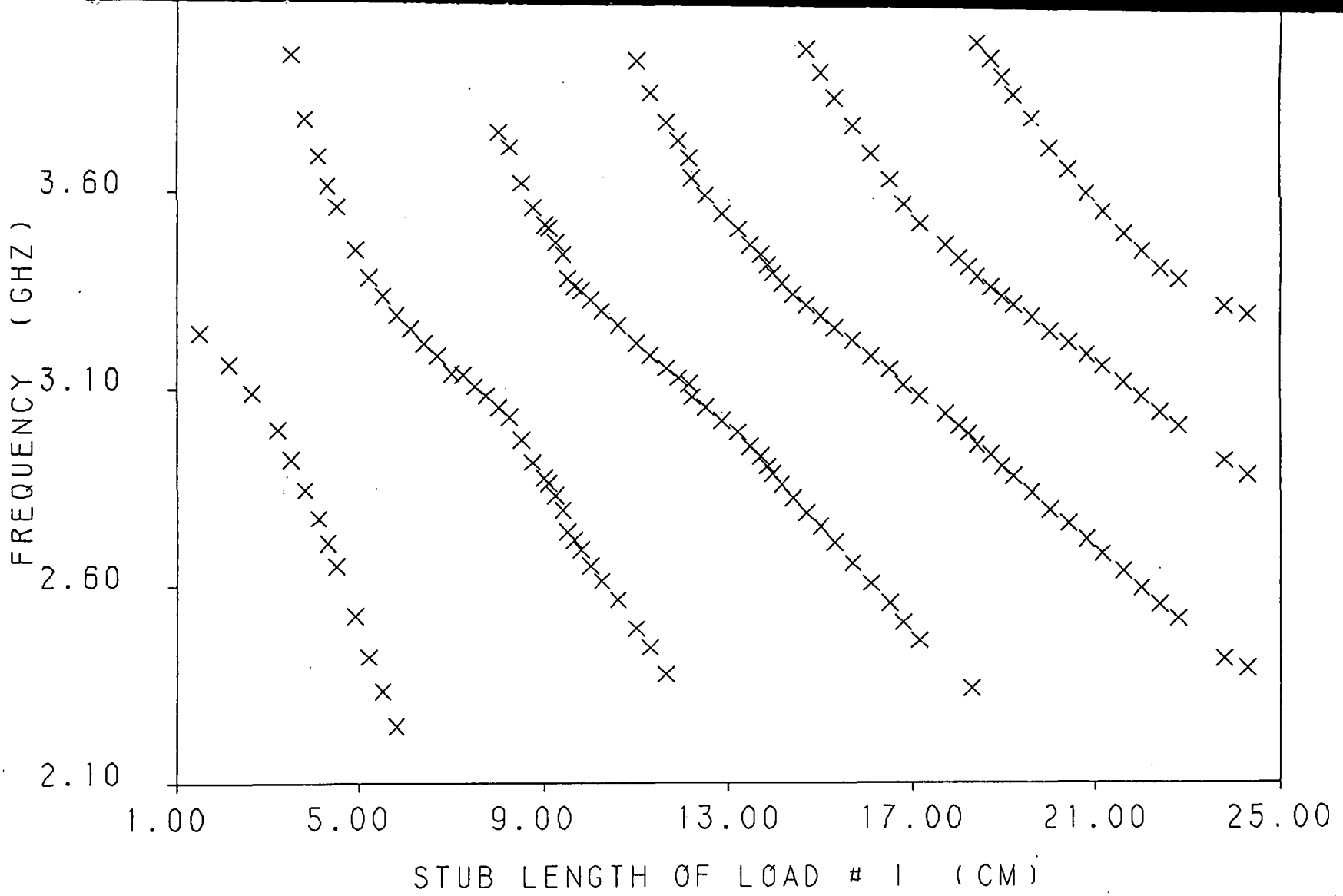

Fig. 3.69 Frequency of upper linearly polarized band (the x-polarized band) verses the short circuit stub length of load #1 for a loaded 2.96 by 2.96 cm square patch with a feed location of (1.05, .45 cm), and load insets of d = .11 cm .

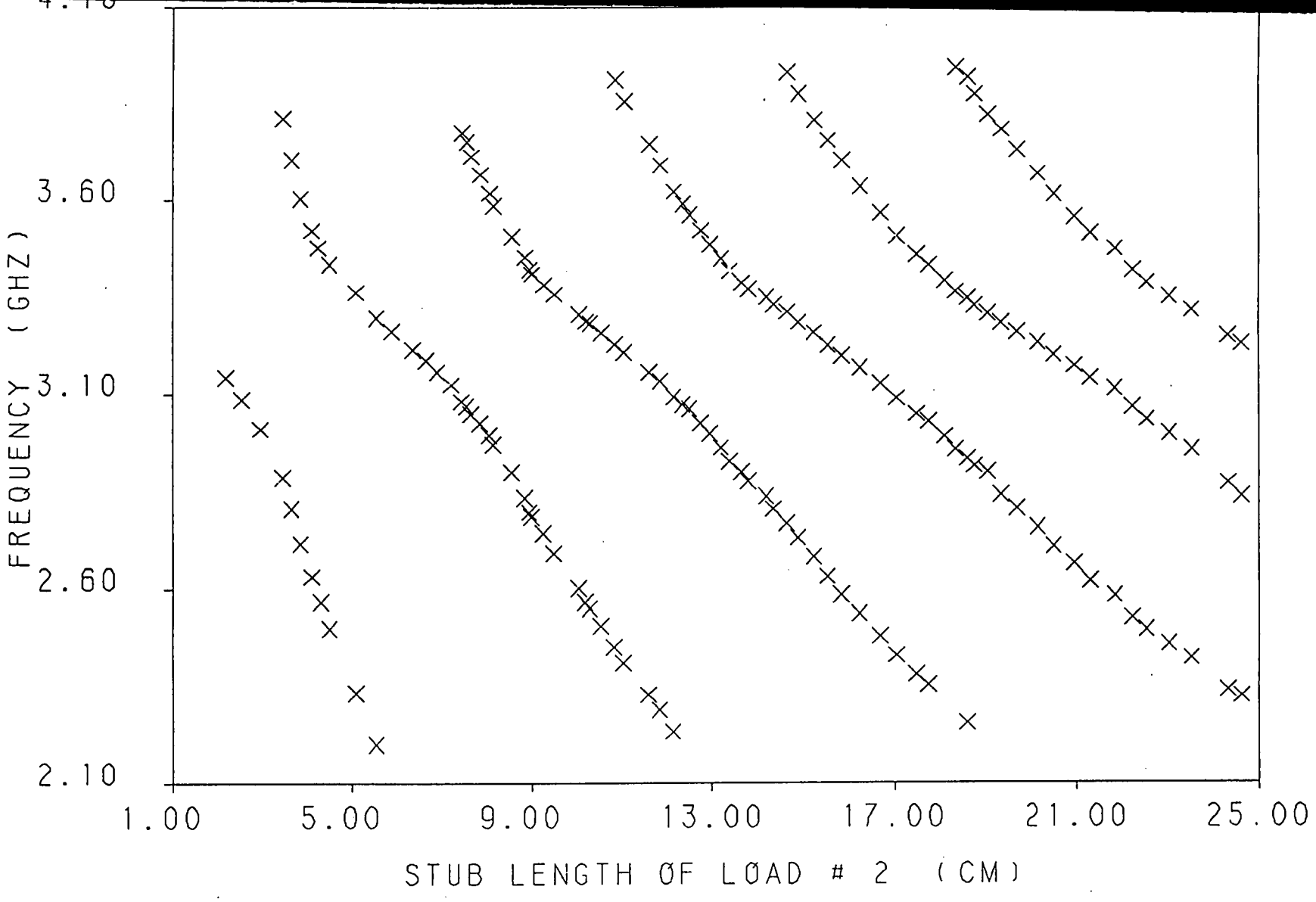

Fig. 3.70 Frequency of lower linearly polarized band (the *y*-polarized band) verses the short circuit stub length of load #2 for a loaded 2.96 by 2.96 cm square patch with a feed location of (1.05, .45 cm), and load insets of d_1 = .11 cm .

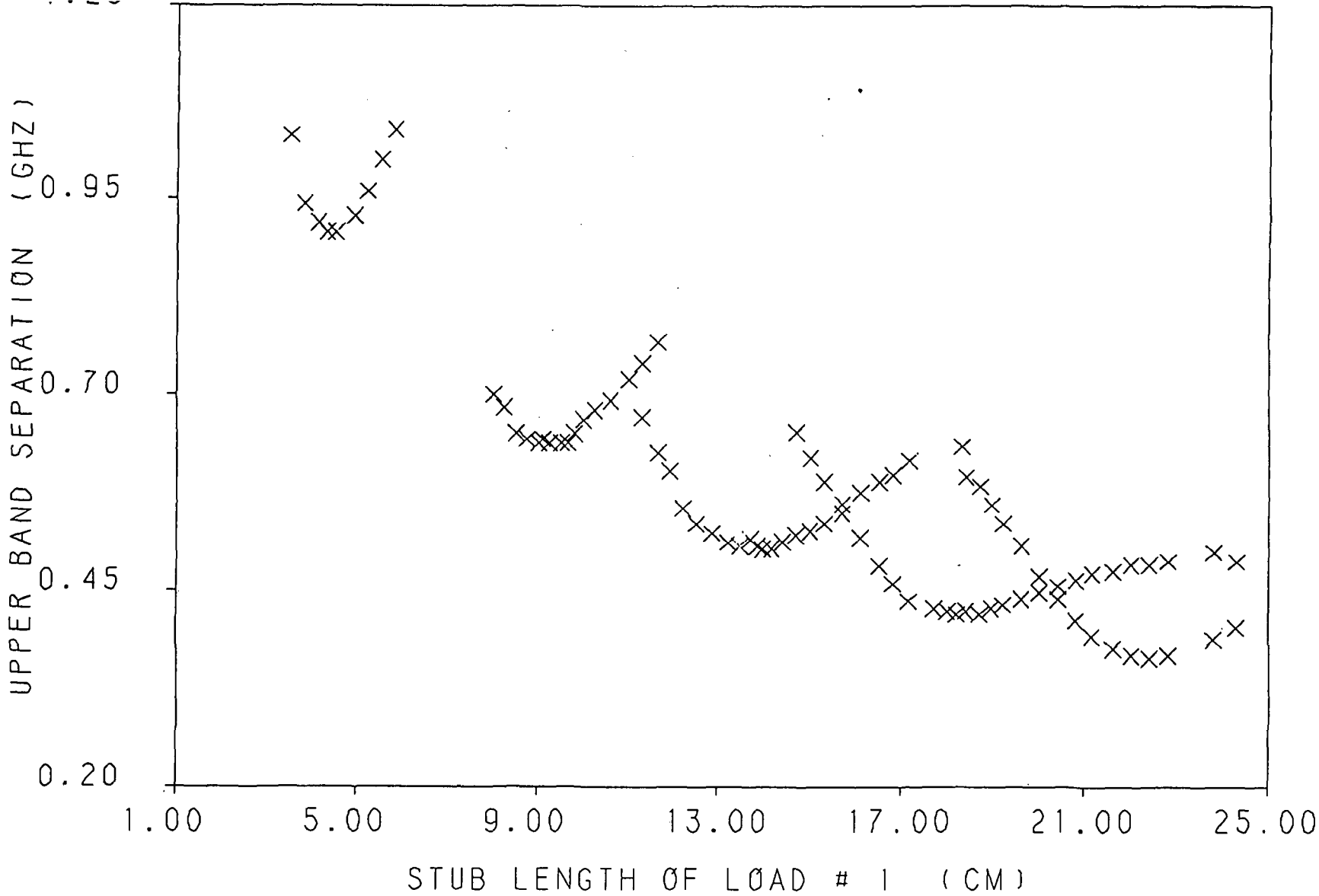

Fig. 3.71 Upper frequency band (the x-polarized band) separation verses the short circuit stub length of load #1 for a loaded 2.96 by 2.96 cm square patch with a feed location of (1.05, .45 cm), and load insets of d = .11 cm .

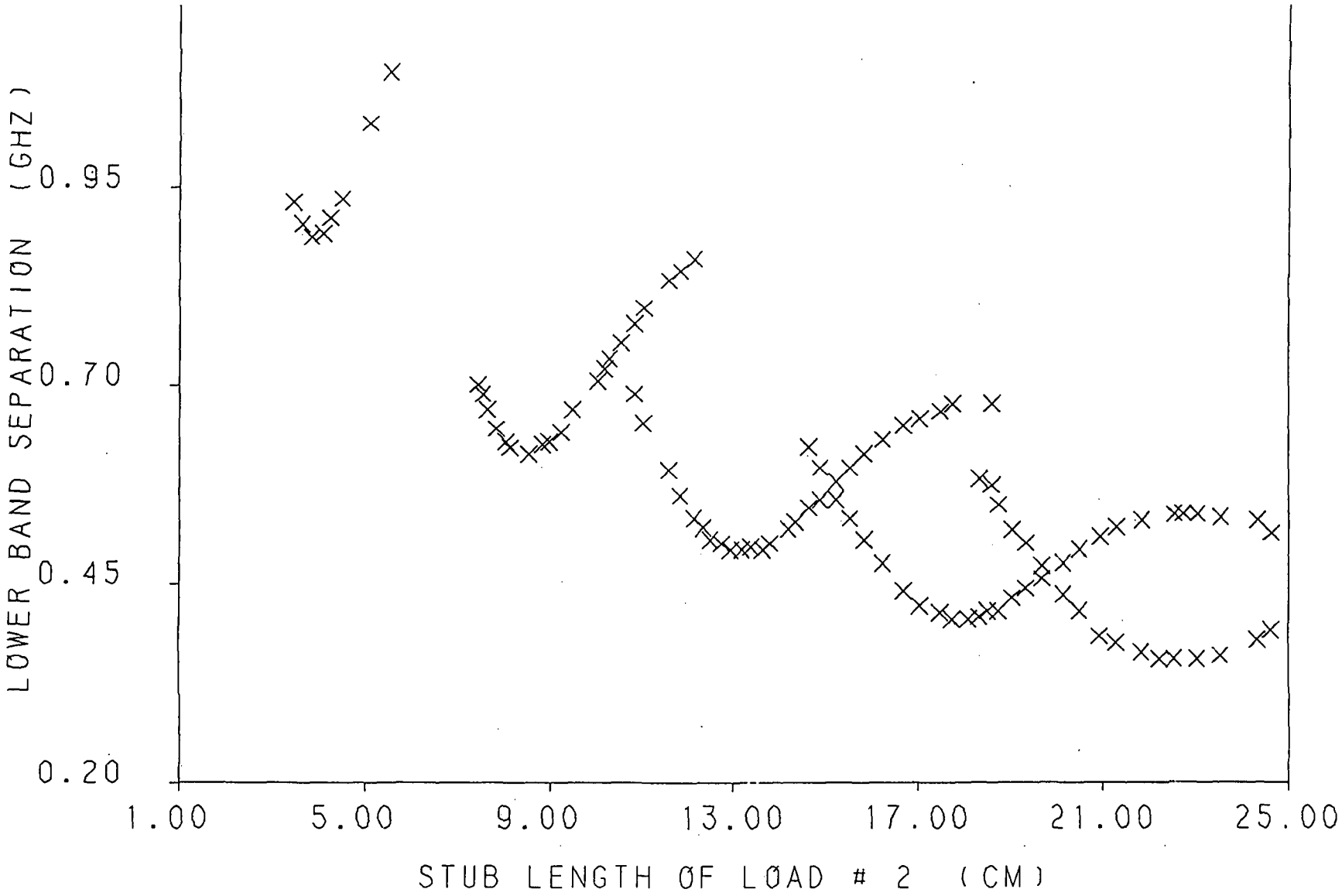

Fig. 3.72 Lower frequency band (the *y*-polarized band) separation verses the short circuit stub length of load #2 for a loaded 2.96 by 2.96 cm square patch with a feed location of (1.05, .45 cm), and load insets of d = .11 cm .

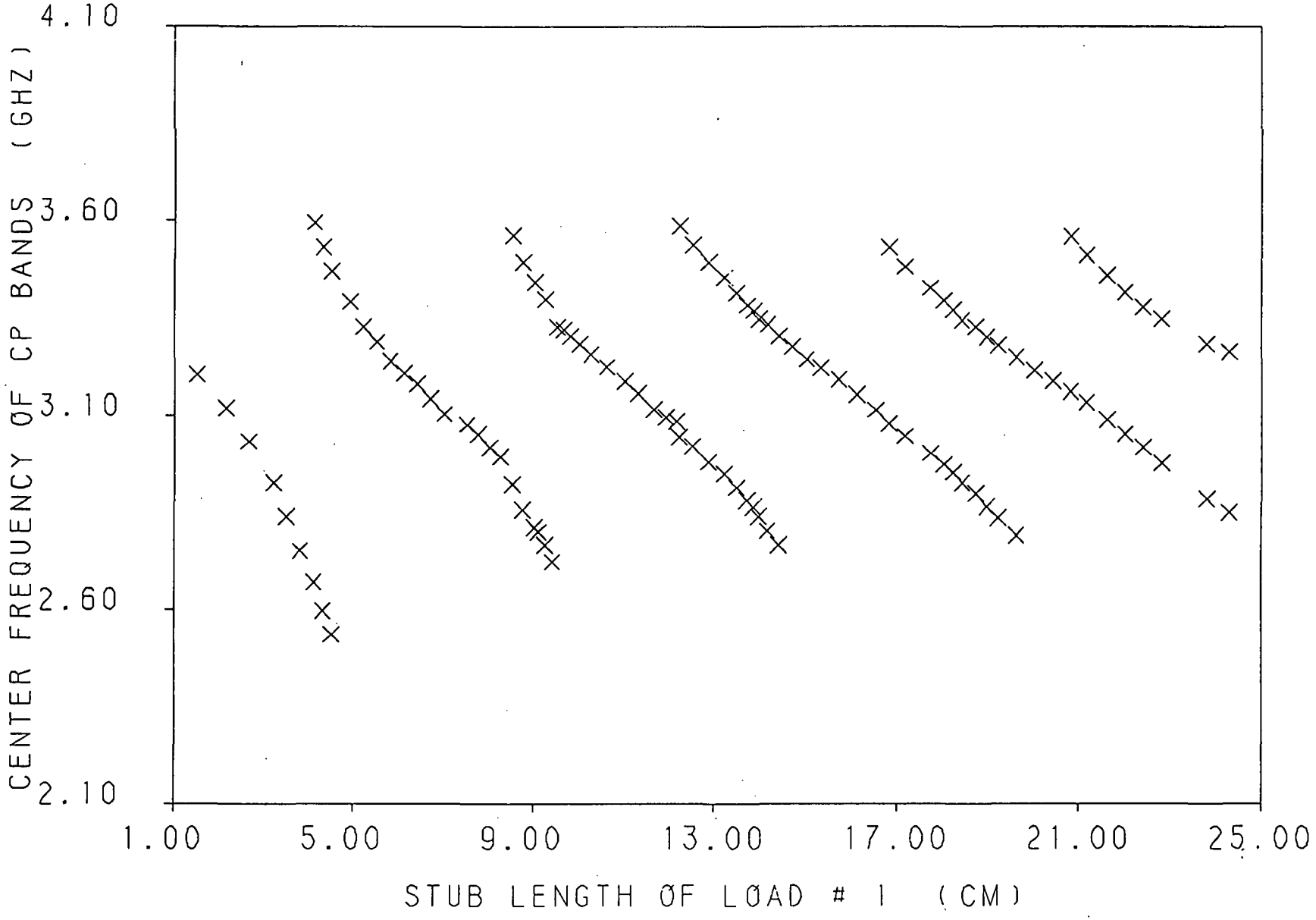

Fig. 3.73 Center frequency of cp bands verses the short circuit stub length of load # 1 for a loaded 2.96 by 2.96 cm square patch with a feed location of (1.05, .45 cm), and load insets of d = .11 cm .

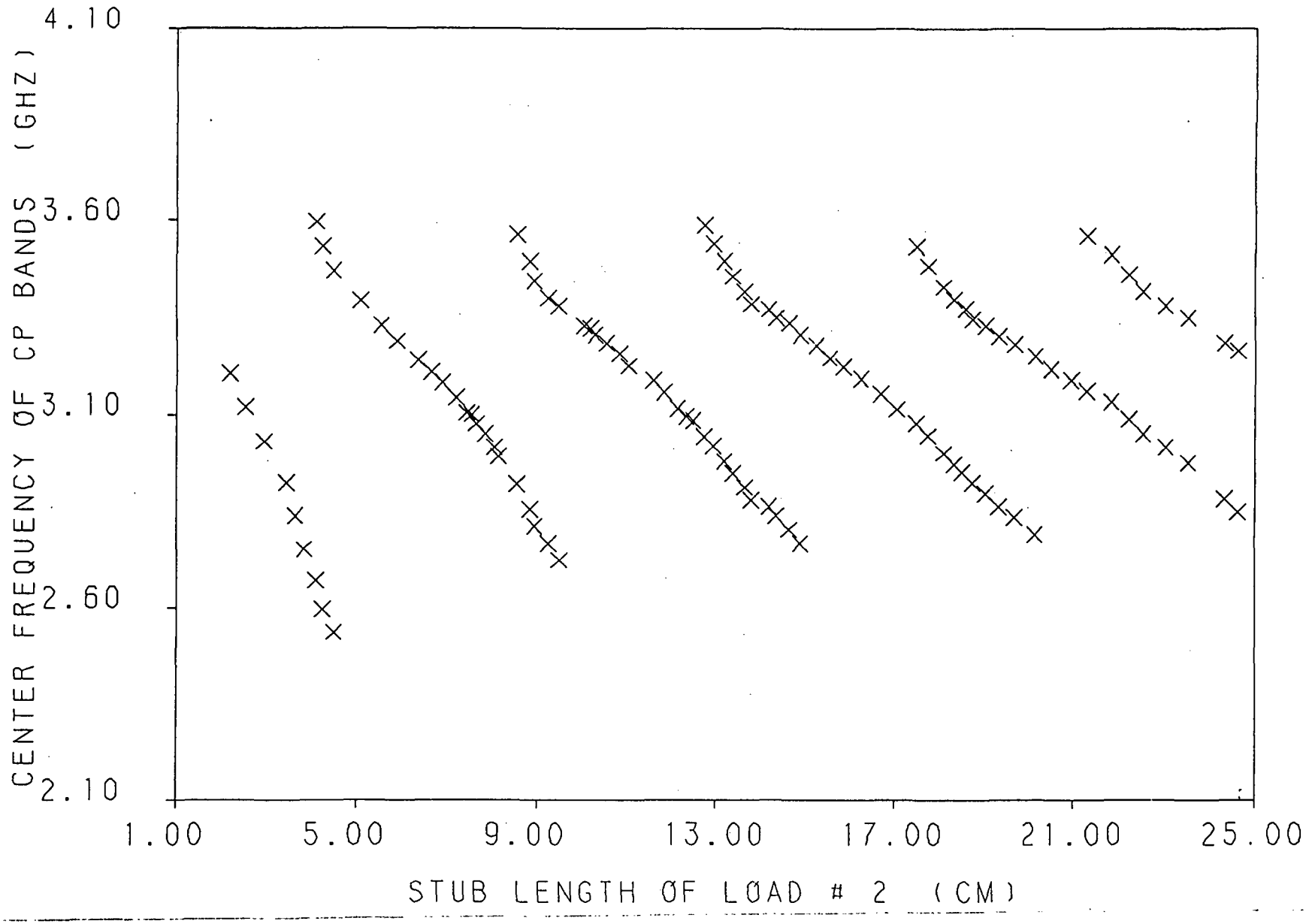

Fig. 3.74 Center frequency of cp bands verses the short circuit stub length of load # 2 for a loaded 2.96 by 2.96 cm square patch with a feed location of (1.05, .45 cm), and load insets of d = .11 cm .

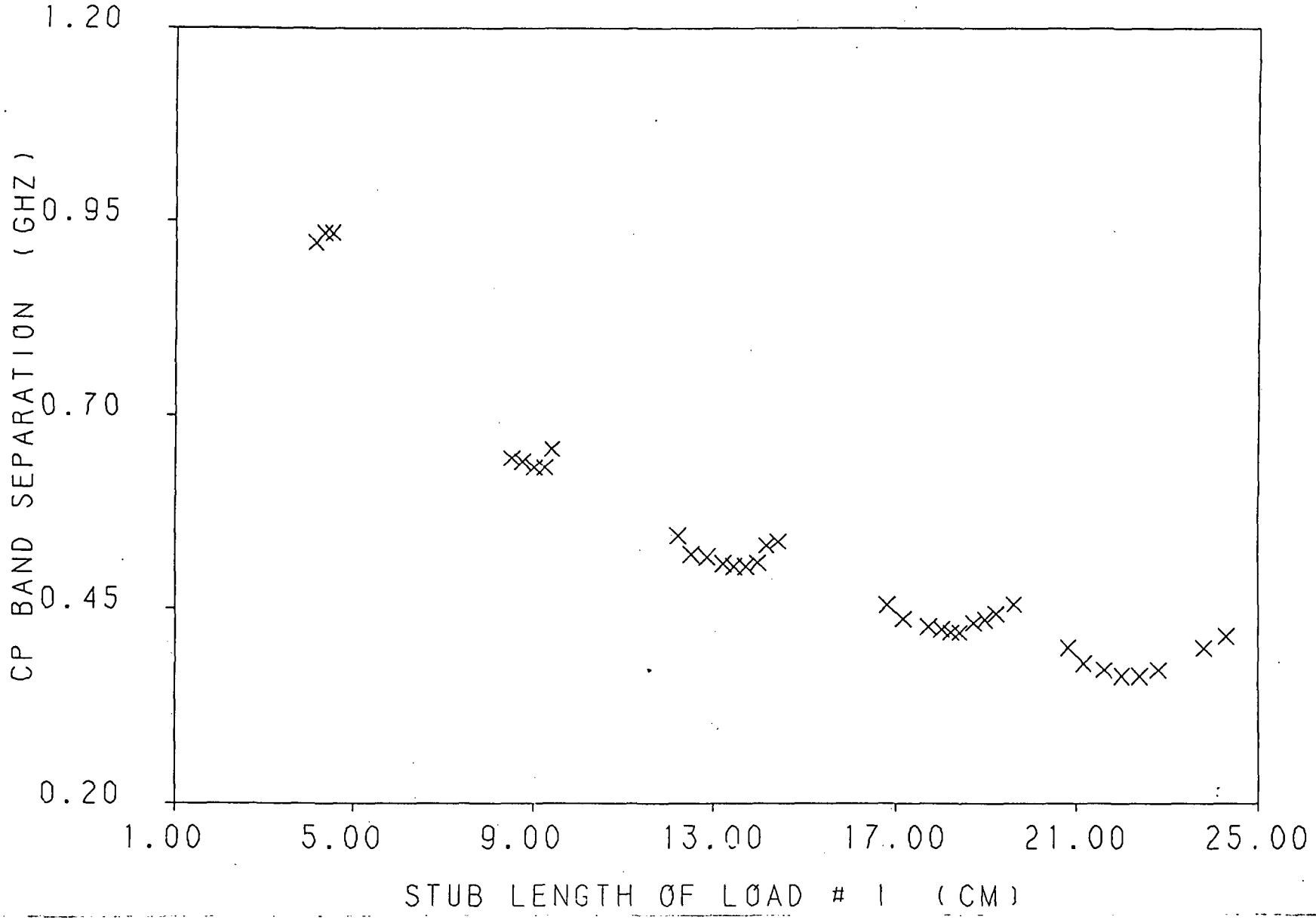

Fig. 3.75 Cp band separation verses the short circuit stub length of load # 1 for a loaded 2.96 by 2.96 cm square patch with a feed location of (1.05, .45 cm), and load insets of d = .11 cm .

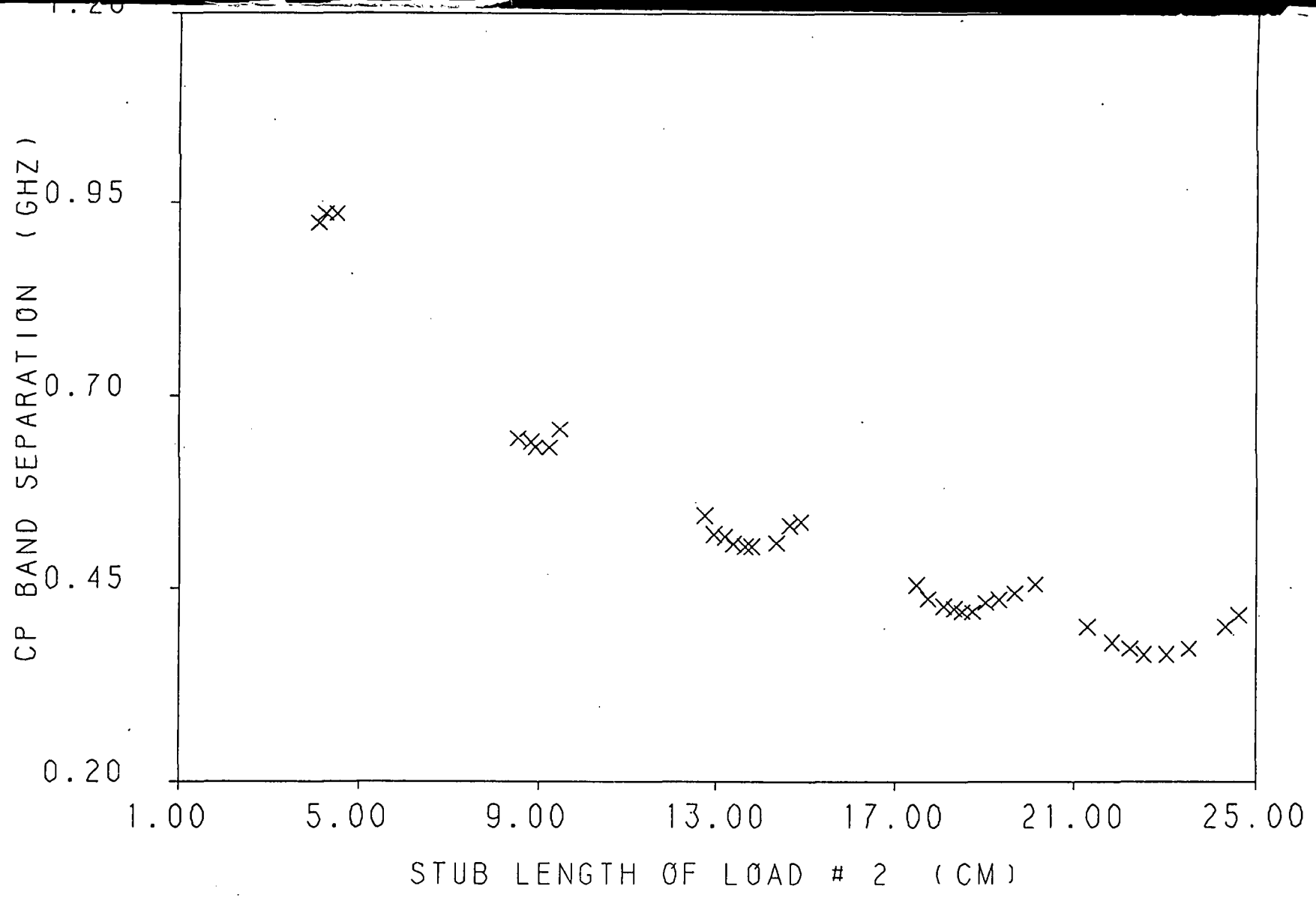

Fig. 3.76 Cp band separation verses the short circuit stub length of load # 2 for a loaded 2.96 by 2.96 cm square patch with a feed location of (1.05, .45 cm), and load insets of d = .11 cm .

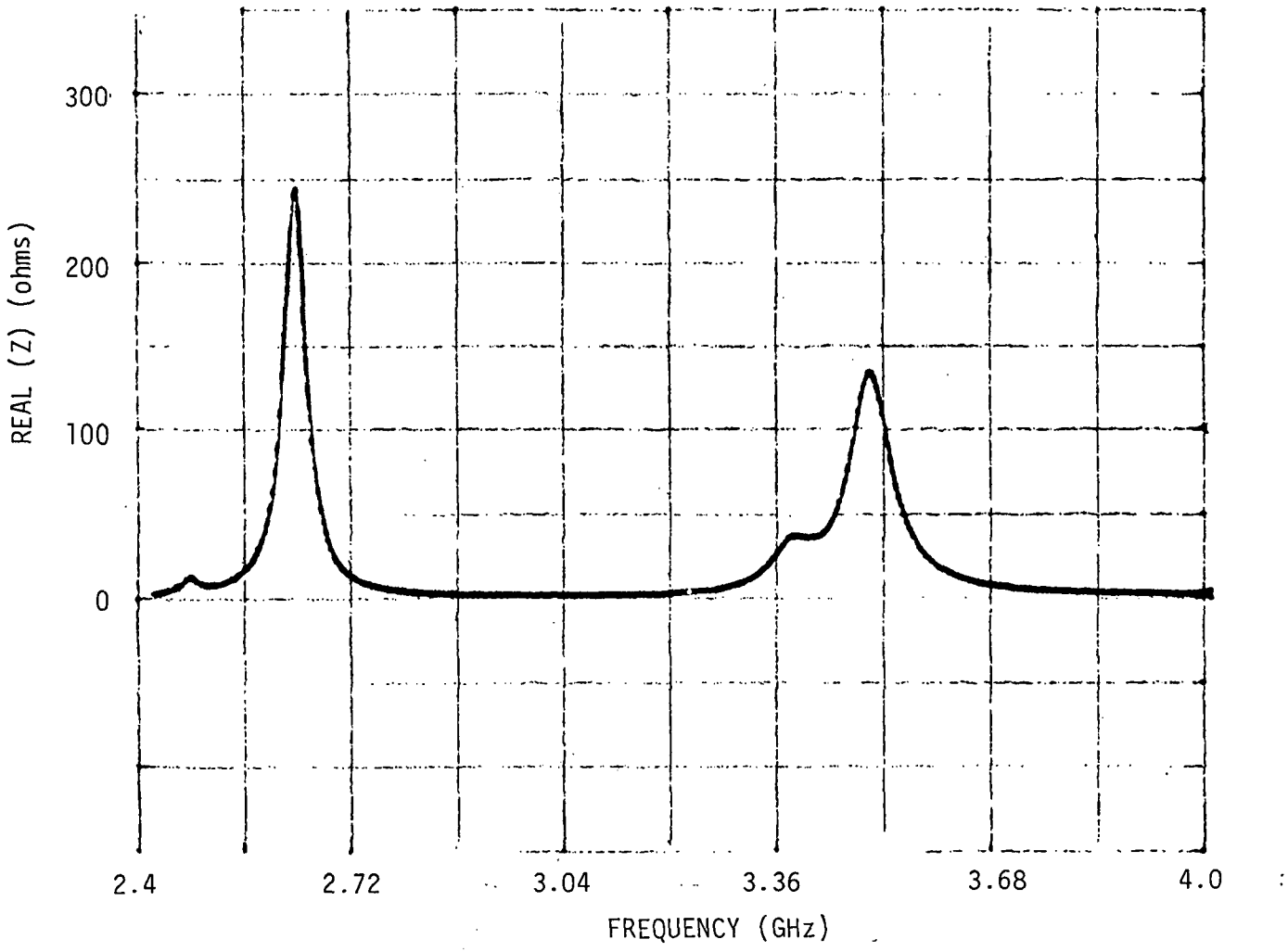

Fig. 3.77 Real part of input impedance verses frequency of the first mode for a loaded 2.96 by 2.96 cm square patch with a feed location of (.45, 1.05 cm), load insets of d = .35 cm, and stub lengths of s_1 = 4.75 cm and s_2 = 4.63 cm.

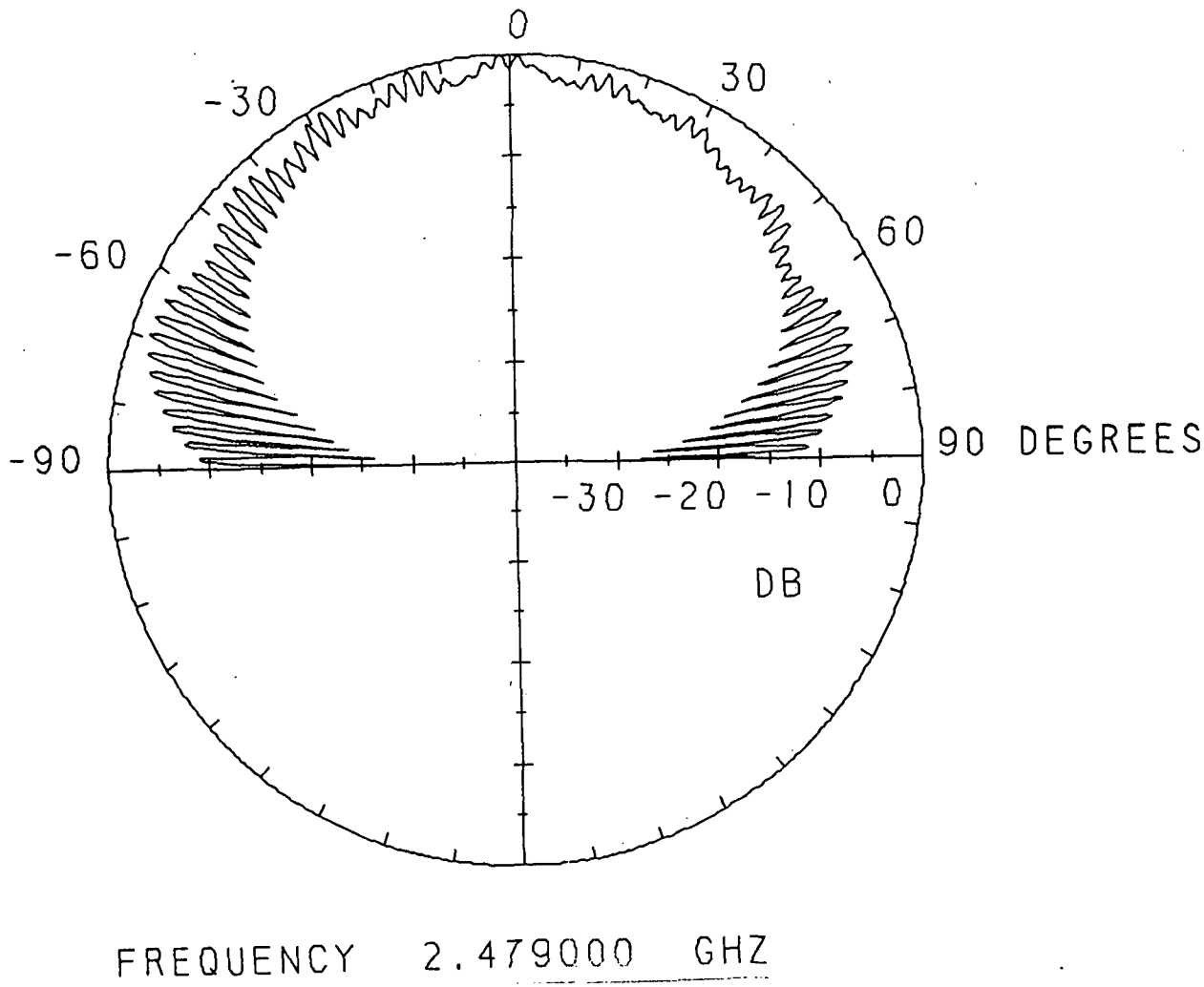

Fig. 3.78 Spinning linear pattern for the lower cp band of the first mode for a loaded 2.96 by 2.96 cm square patch with a feed location of (.45, 1.05 cm), load insets of d = .35 cm, and stub lengths of s_1 = 4.75 cm and s_2 = 4.63 cm.

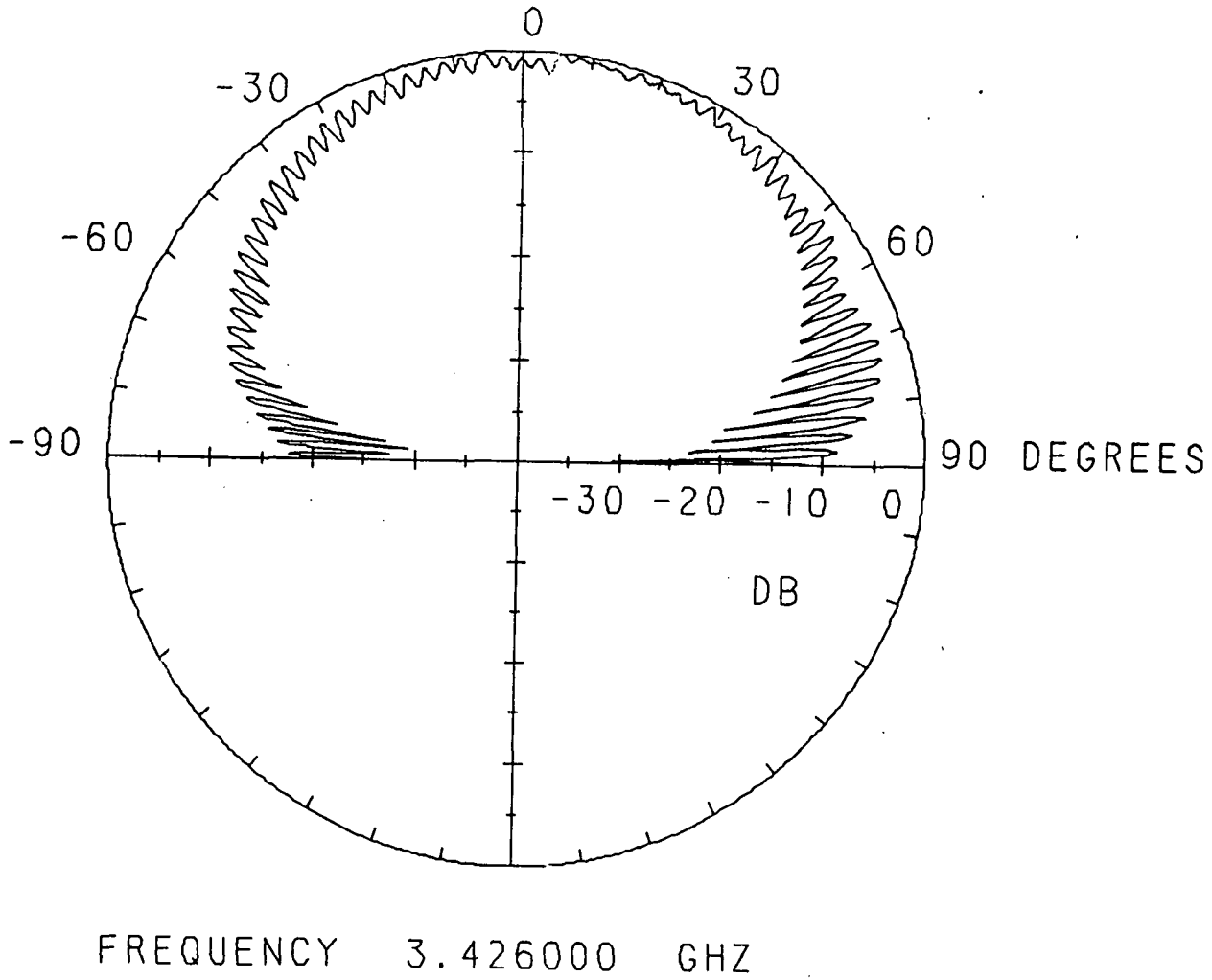

Fig. 3.79 Spinning linear pattern for the upper cp band of the first mode for a loaded 2.96 by 2.96 cm square patch with a feed location of (.45, 1.05 cm), load insets of d = .35 cm, and stub lengths of s_1 = 4.75 cm and s_2 = 4.63 cm.

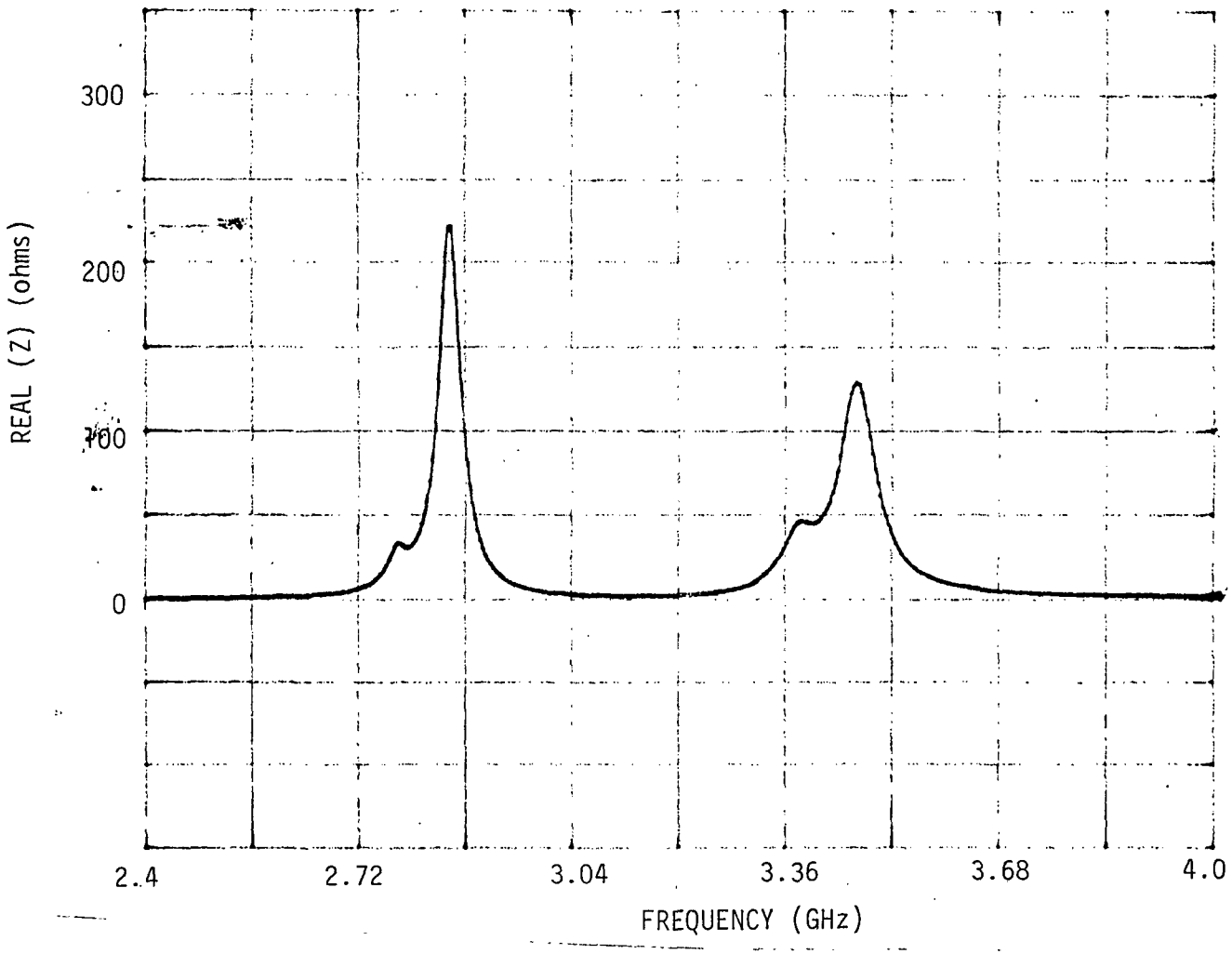

Fig. 3.80 Real part of input impedance verses frequency of the second mode for a loaded 2.96 by 2.96 cm square patch with a feed location of (.45, 1.05 cm), load insets of d = .35 cm, and stub lengths of s_1 = 9.3 cm and s_2 = 9.23 cm.

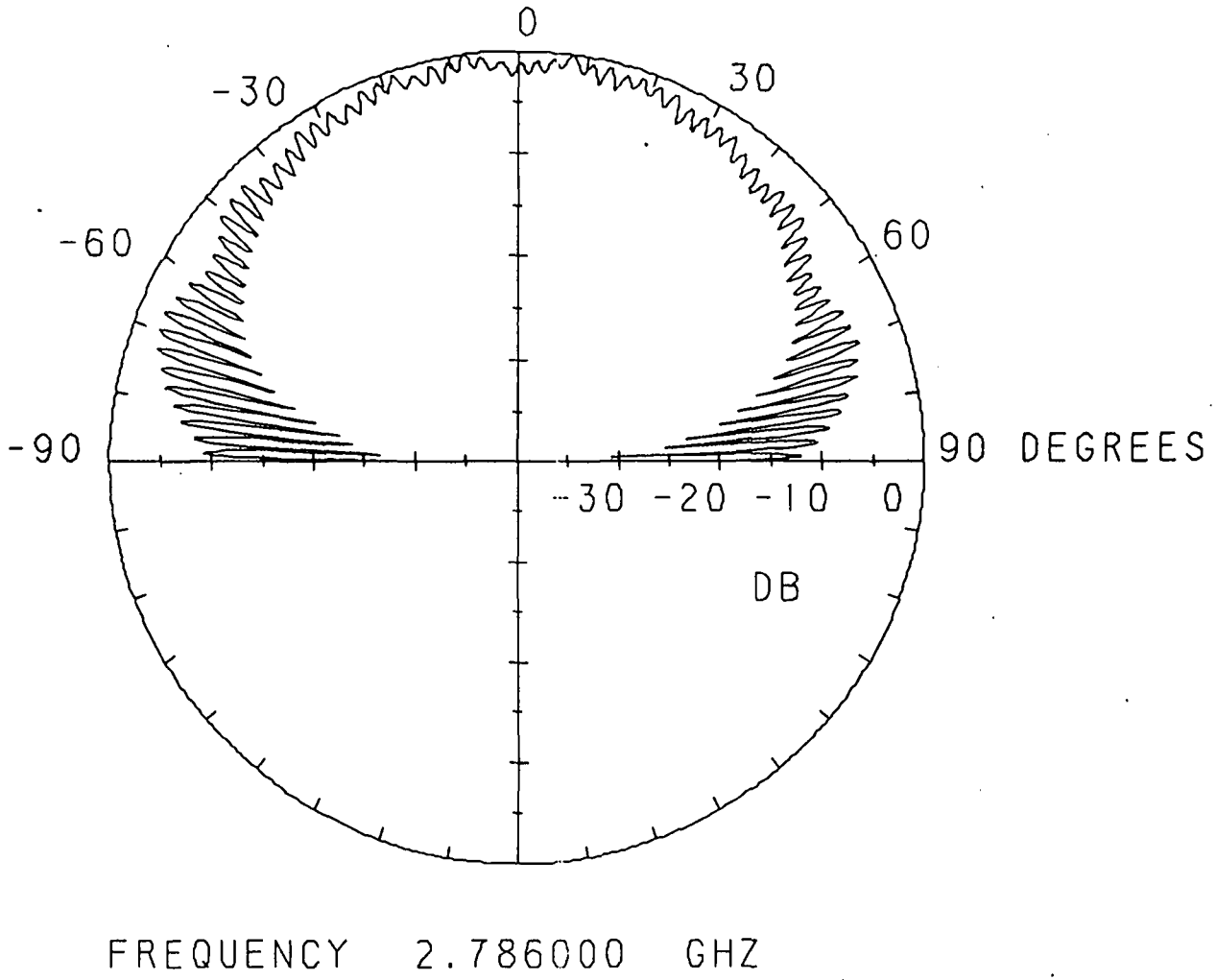

Fig. 3.81 Spinning linear pattern for the lower cp band of the second mode for a loaded 2.96 by 2.96 cm square patch with a feed location of (.45, 1.05 cm), load insets of d = .35 cm, and stub lengths of s_1 = 9.3 cm and s_2 = 9.23 cm.

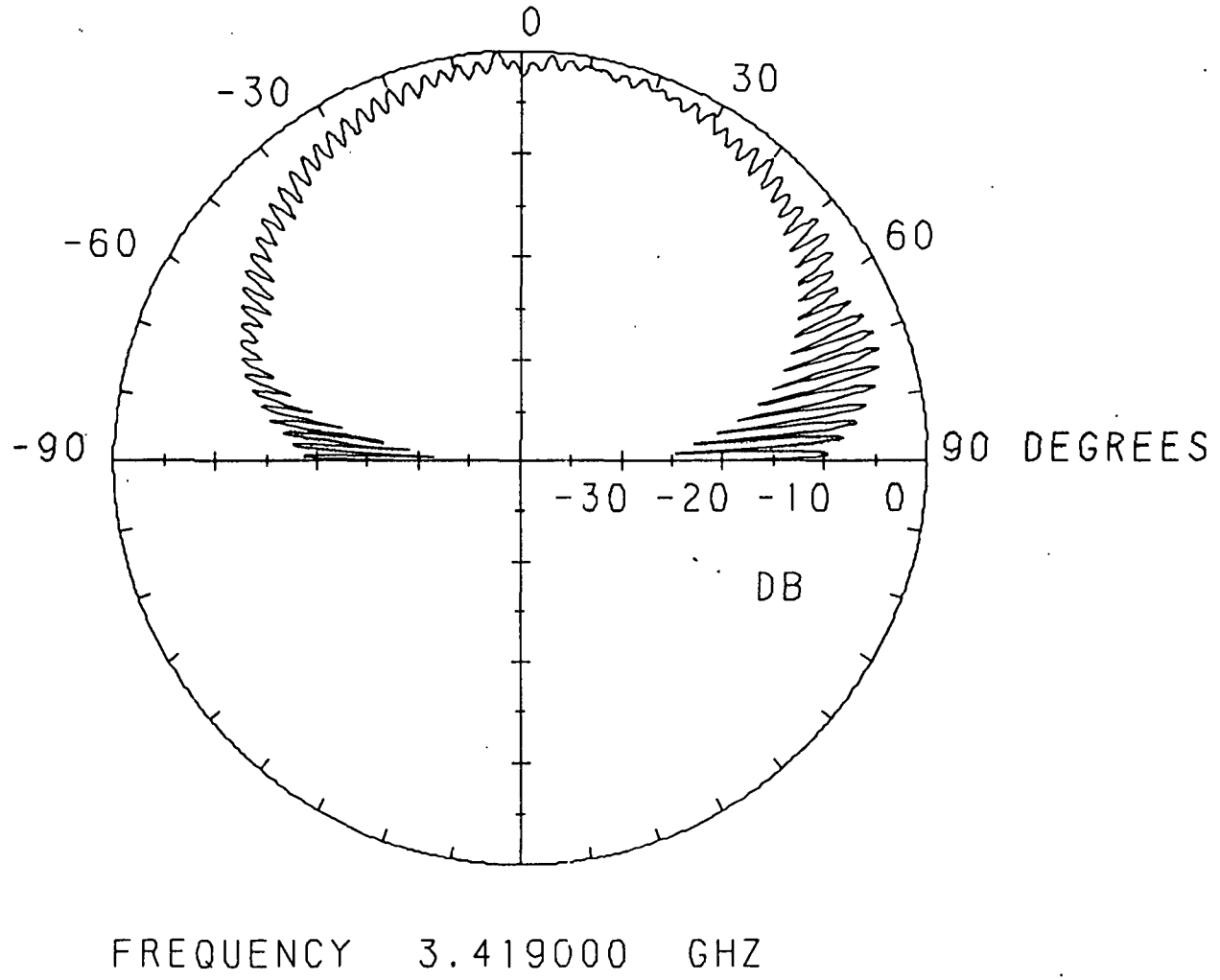

Fig. 3.82 Spinning linear pattern for the upper cp band of the second mode for a loaded 2.96 by 2.96 cm square patch with a feed location of (.45, 1.05 cm), load insets of d = .35 cm, and stub lengths of s_1 = 9.3 cm and s_2 = 9.23 cm.

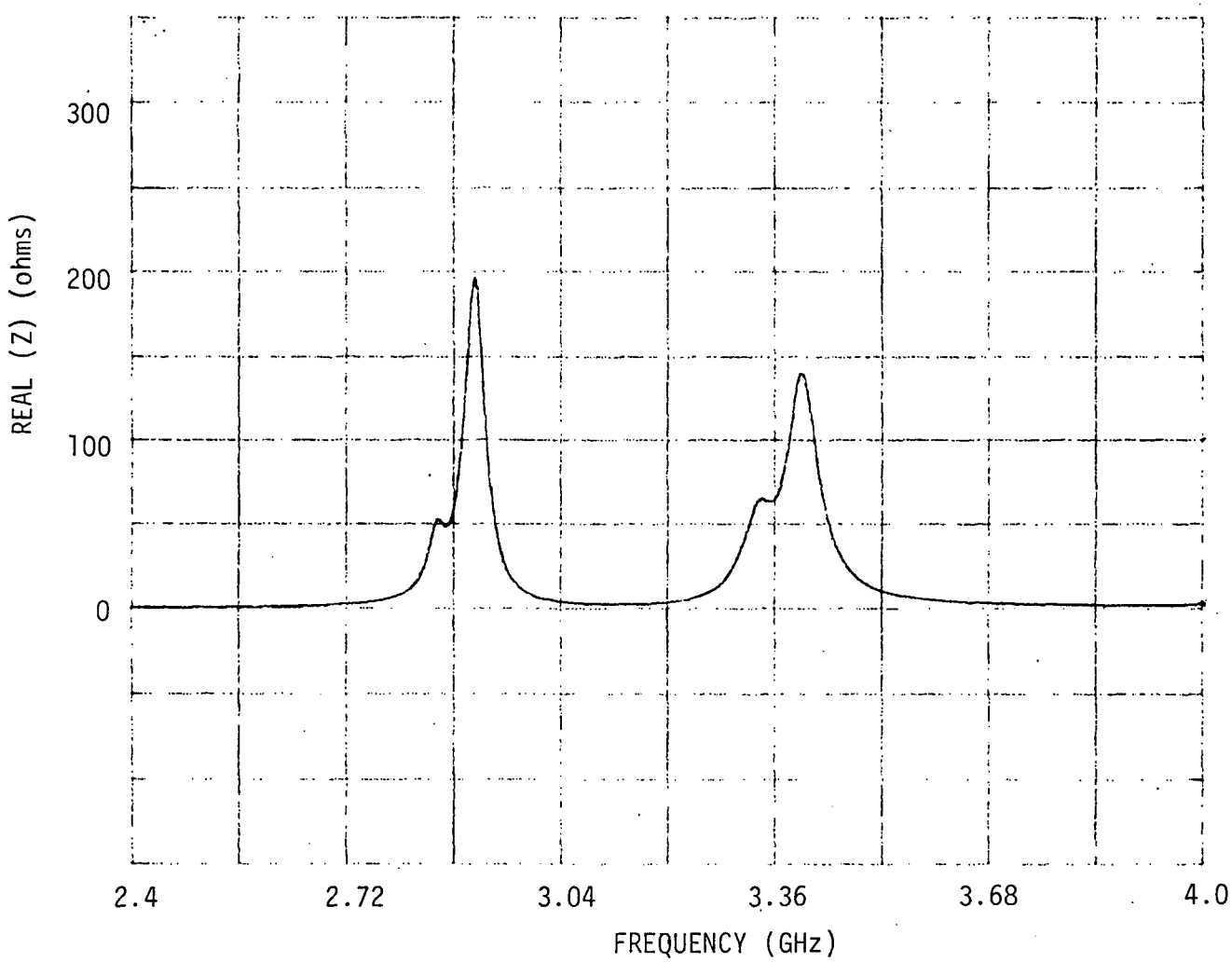

Fig. 3.83 Real part of input impedance verses frequency of the third mode for a loaded 2.96 by 2.96 cm square patch with a feed location of (.45, 1.05 cm), load insets of d = .35 cm, and stub lengths of s_1 = 14.0 cm and s_2 = 14.13 cm.

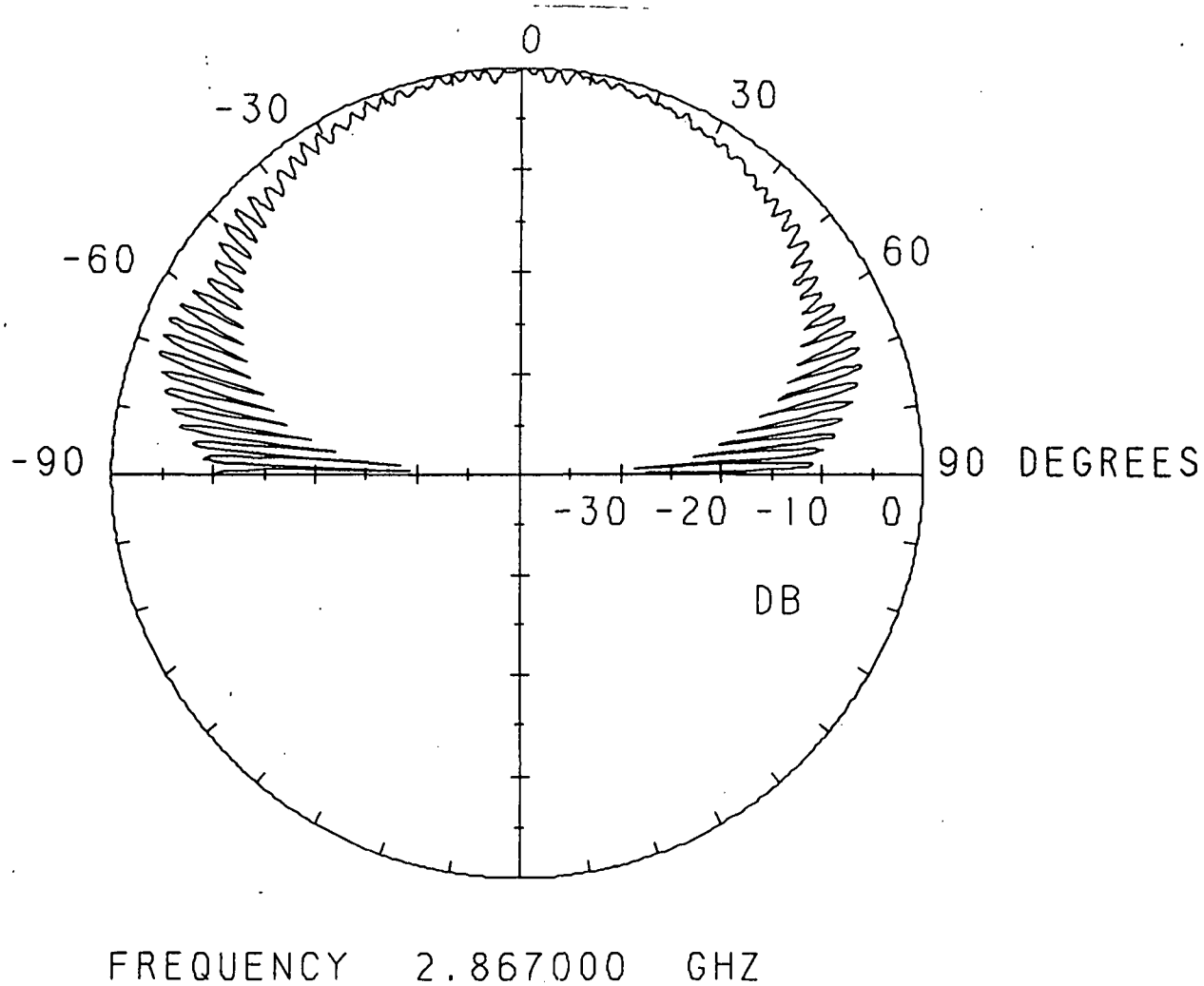

Fig. 3.84 Spinning linear pattern for the lower cp band of the third mode for a loaded 2.96 by 2.96 cm square patch with a feed location of (.45, 1.05 cm), load insets of d = .35 cm, and stub lengths of s_1 = 14.0 cm and s_2 = 14.13 cm.

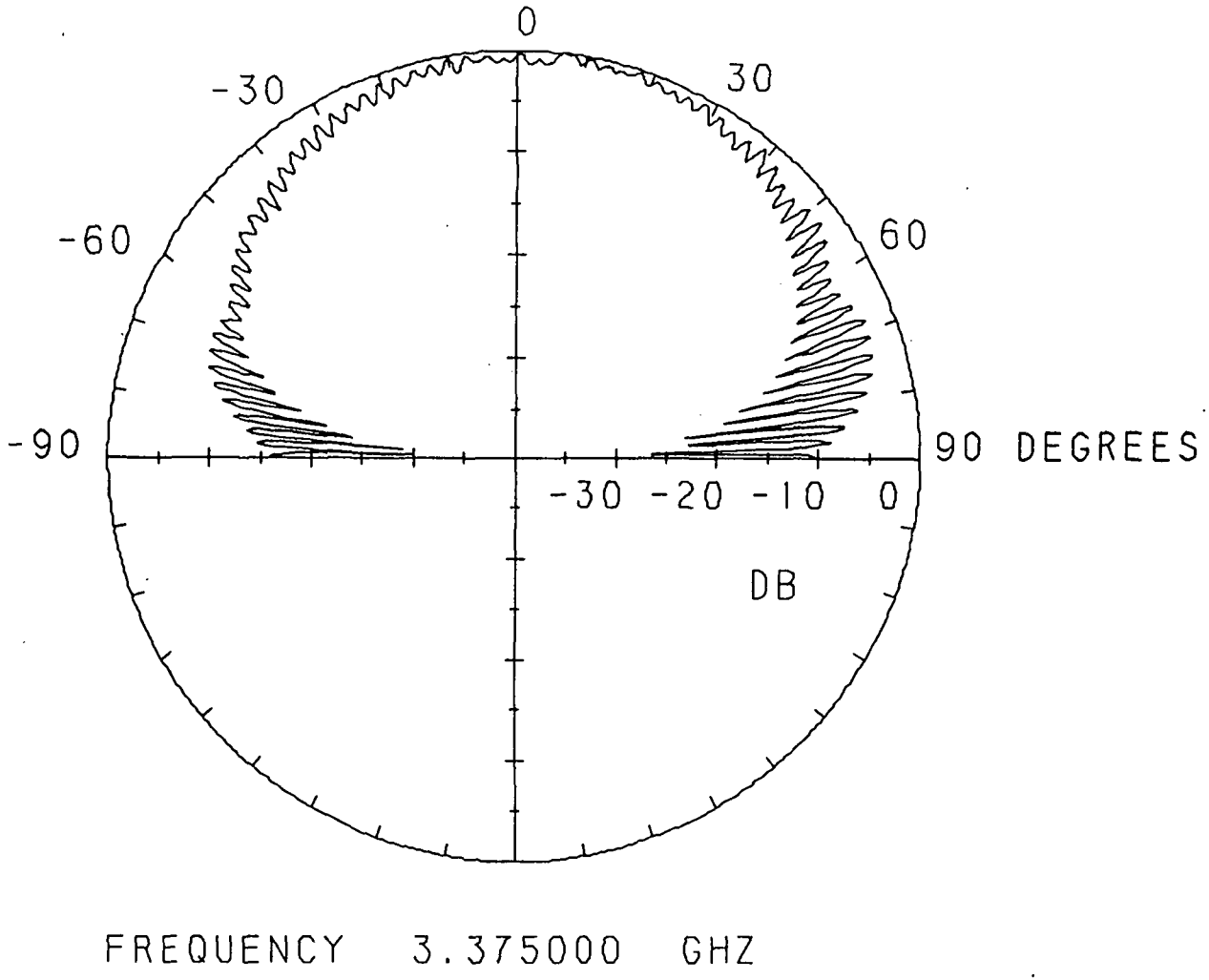

Fig. 3.85 Spinning linear pattern for the upper cp band of the third mode for a loaded 2.96 by 2.96 cm square patch with a feed location of (.45, 1.05 cm), load insets of d = .35 cm, and stub lengths of s_1 = 14.0 cm and s_2 = 14.13 cm.

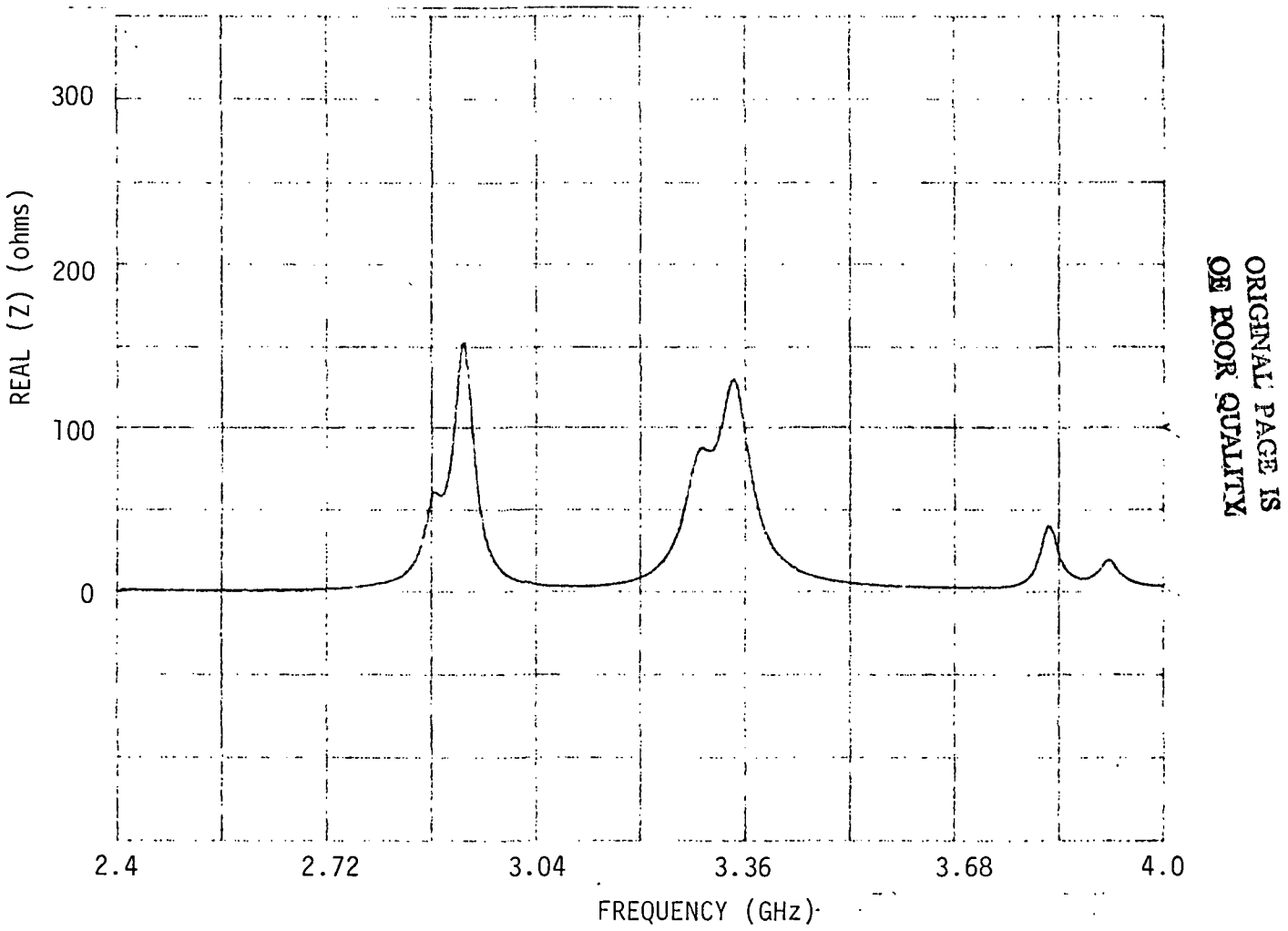

Fig. 3.86 Real part of input impedance verses frequency of the fourth mode for a loaded 2.96 by 2.96 cm square patch with a feed location of (.45, 1.05 cm), load insets of d = .35 cm, and stub lengths of s_1 = 18.8 cm and s_2 = 19.13 cm.

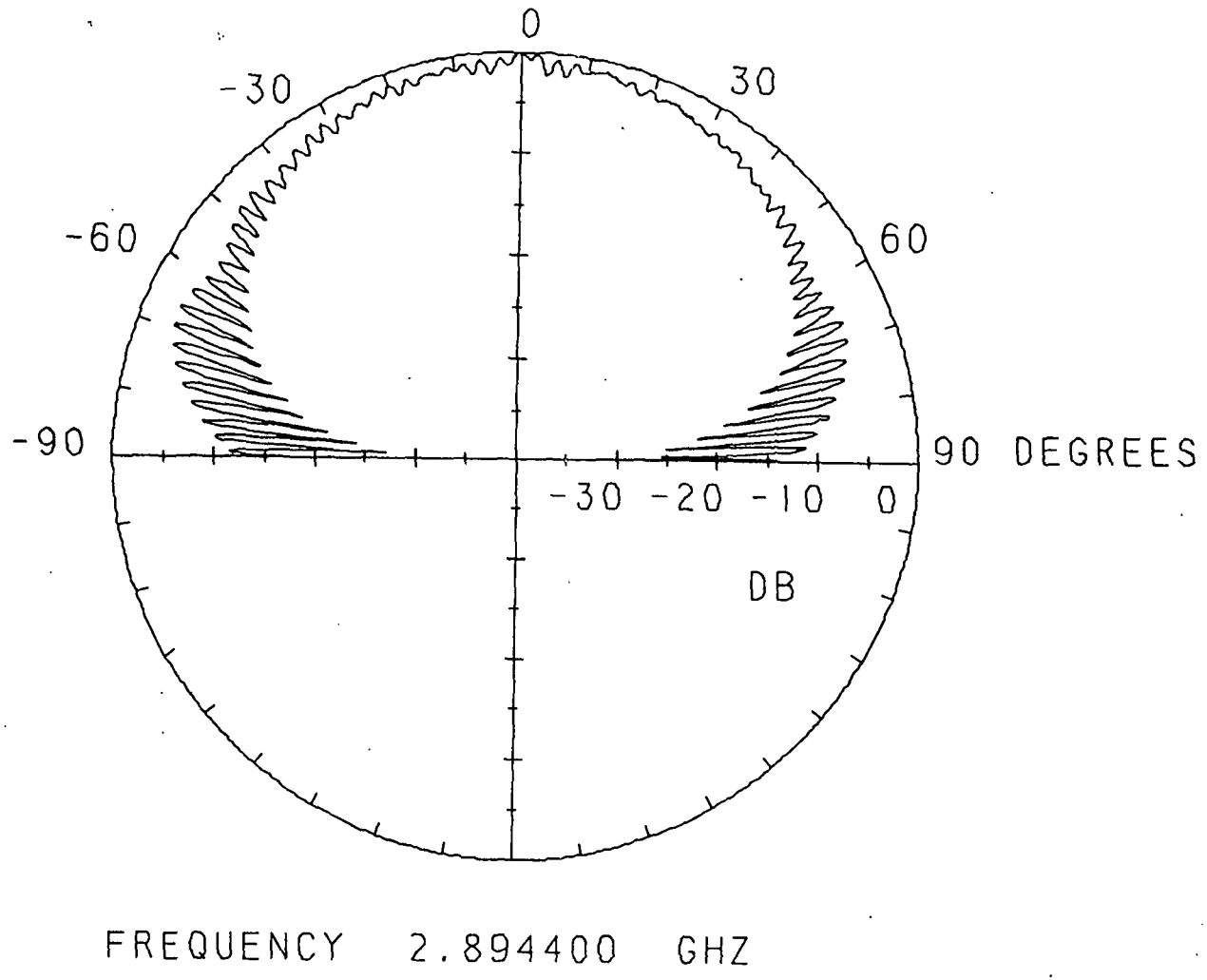

Fig. 3.87 Spinning linear pattern for the lower cp band of the fourth mode for a loaded 2.96 by 2.96 cm square patch with a feed location of (.45, 1.05 cm), load insets of d = .35 cm, and stub lengths of s_1 = 18.8 cm and s_2 = 19.13 cm.

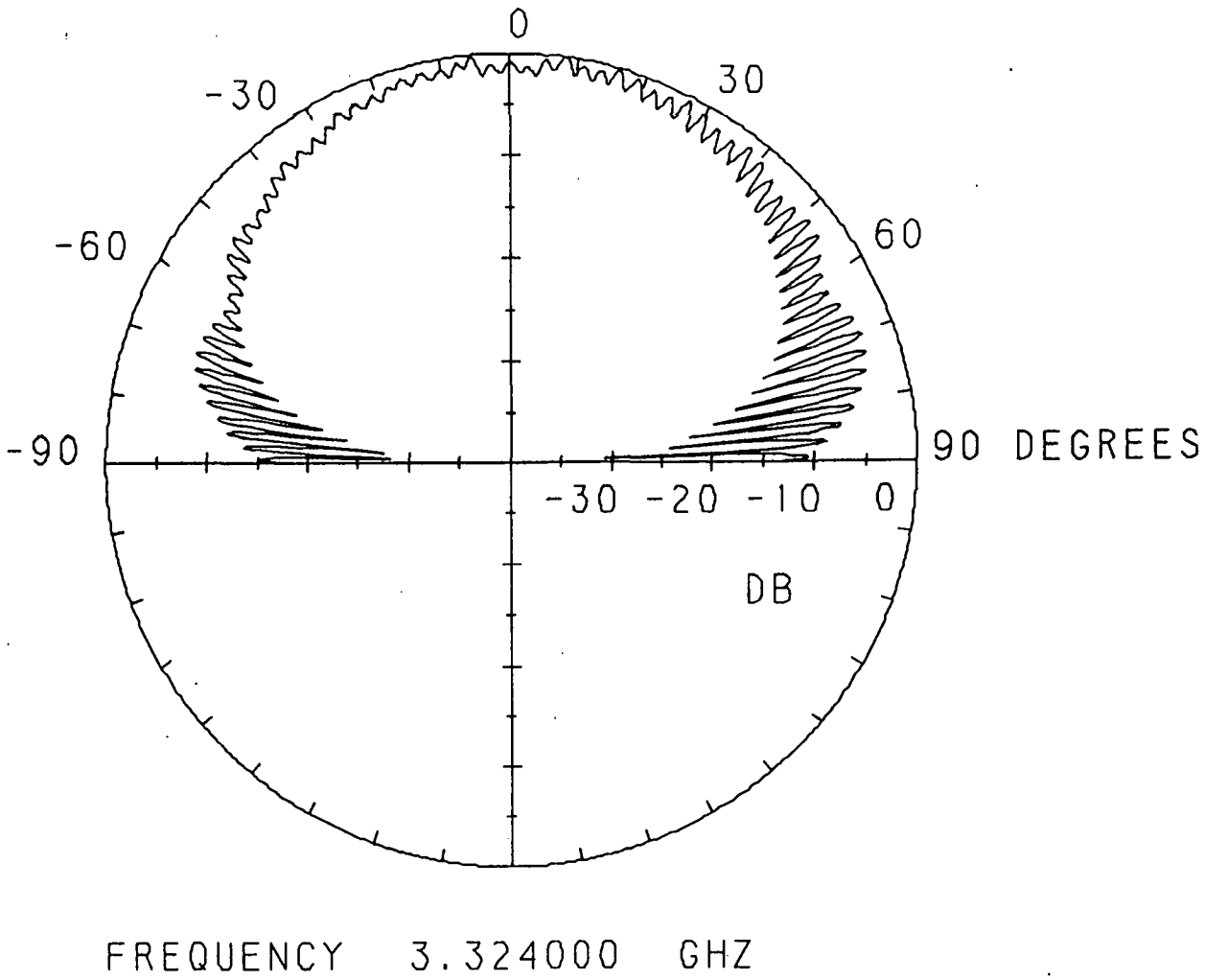

Fig. 3.88 Spinning linear pattern for the upper cp band of the fourth mode for a loaded 2.96 by 2.96 cm square patch with a feed location of (.45, 1.05 cm), load insets of d = .35 cm, and stub lengths of s_1 = 18.8 cm and s_2 = 19.13 cm.

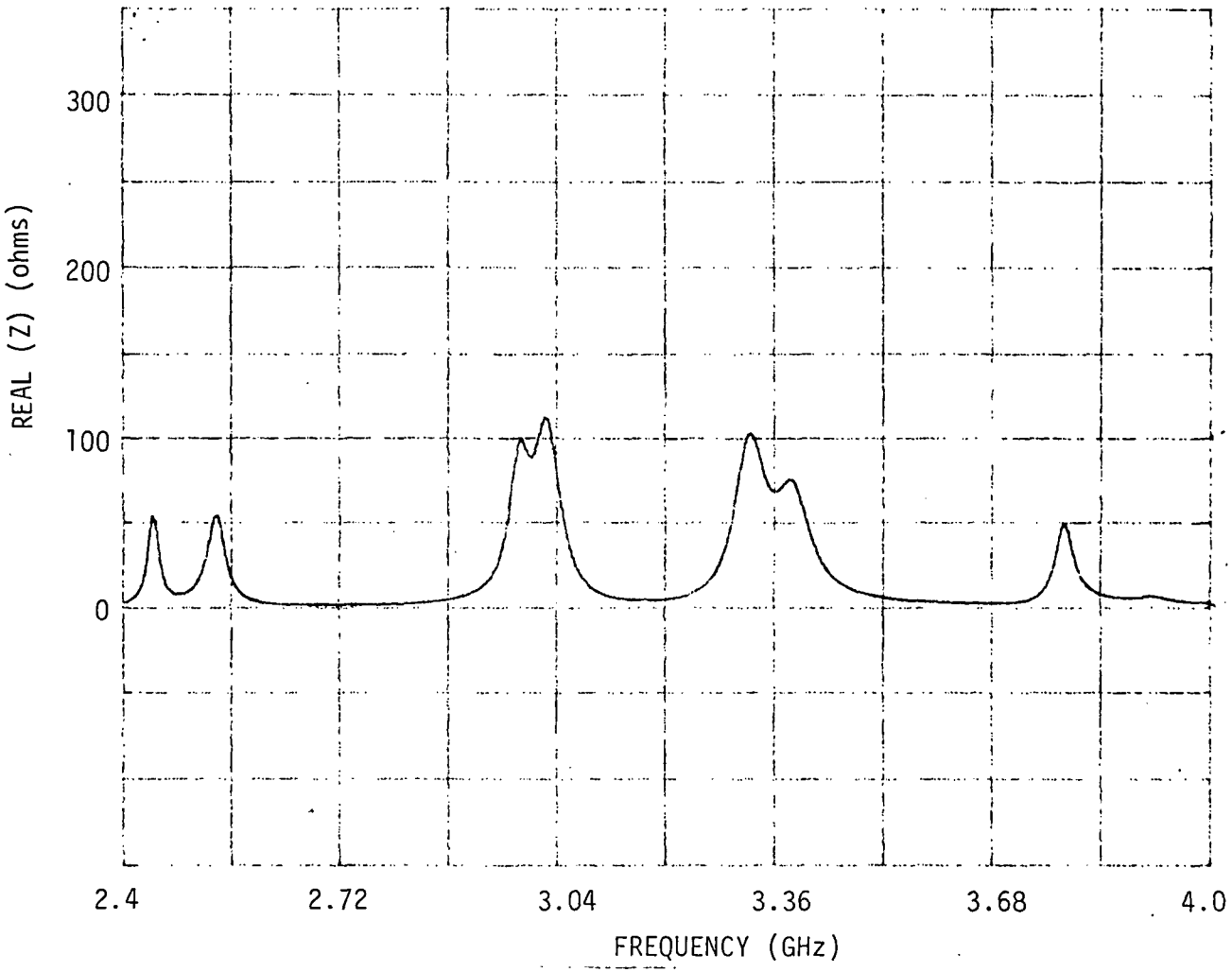

Fig. 3.89 Real part of input impedance verses frequency of the fifth mode for a loaded 2.96 by 2.96 cm square patch with a feed location of (.45, 1.05 cm), load insets of d = .35 cm, and stub lengths of s_1 = 22.6 cm and s_2 = 23.23 cm.

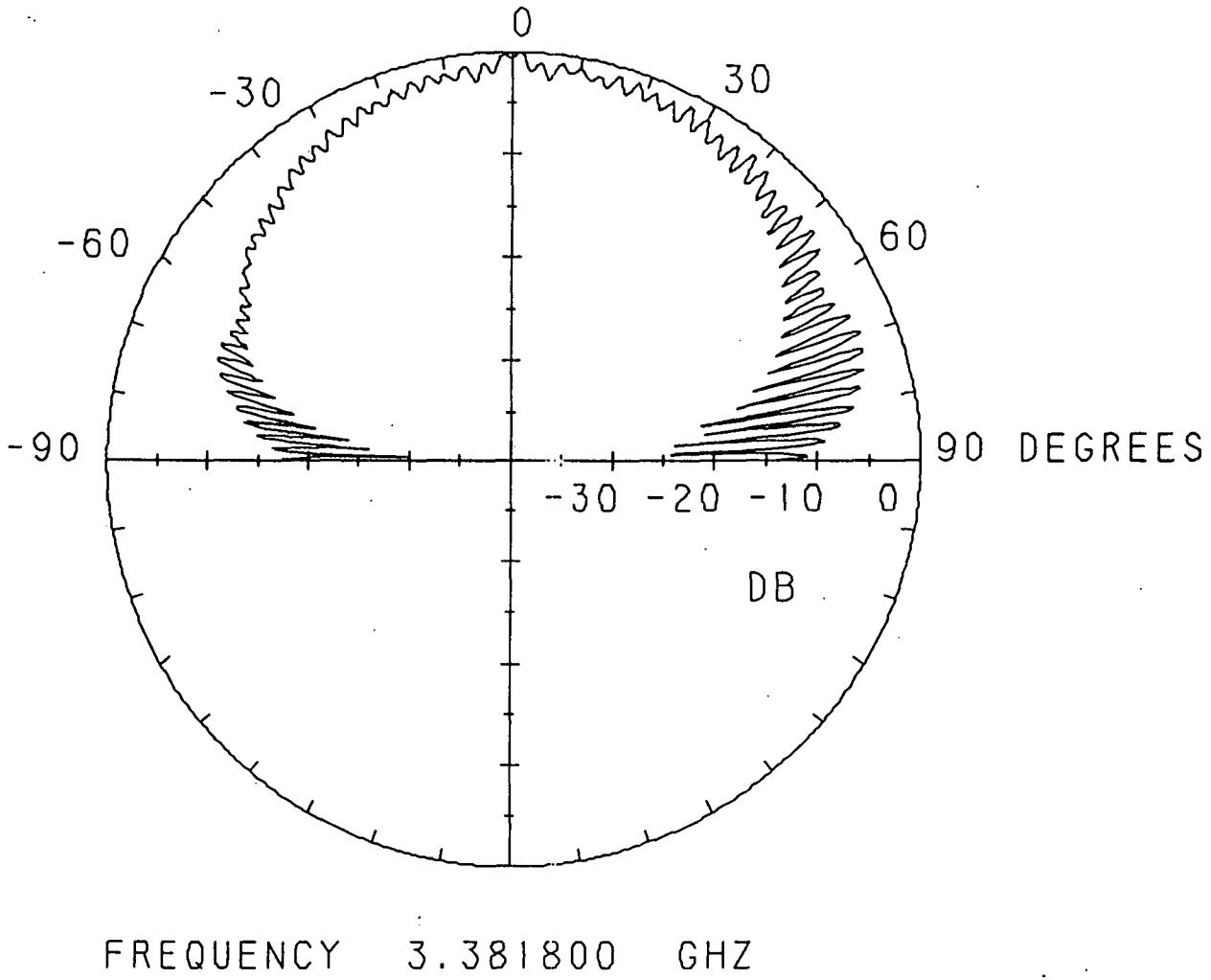

Fig. 3.90 Spinning linear pattern for the lower cp band of the fifth mode for a loaded 2.96 by 2.96 cm square patch with a feed location of (.45, 1.05 cm), load insets of d = .35 cm, and stub lengths of s_1 = 22.6 cm and s_2 = 23.23 cm.

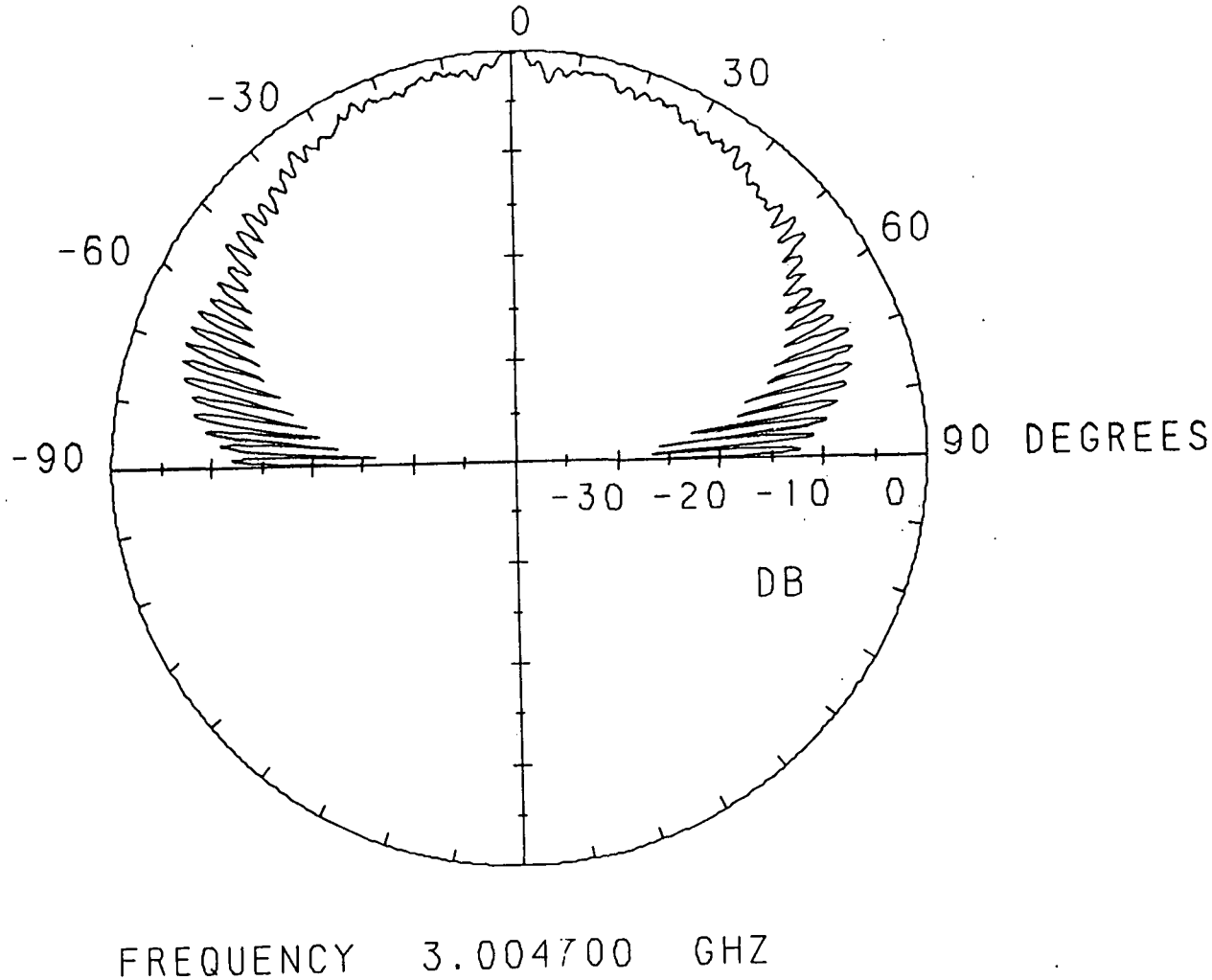

Fig. 3.91 Spinning linear pattern for the upper cp band of the fifth mode for a loaded 2.96 by 2.96 cm square patch with a feed location of (.45, 1.05 cm), load insets of d = .35 cm, and stub lengths of s_1 = 22.6 cm and s_2 = 23.23 cm.

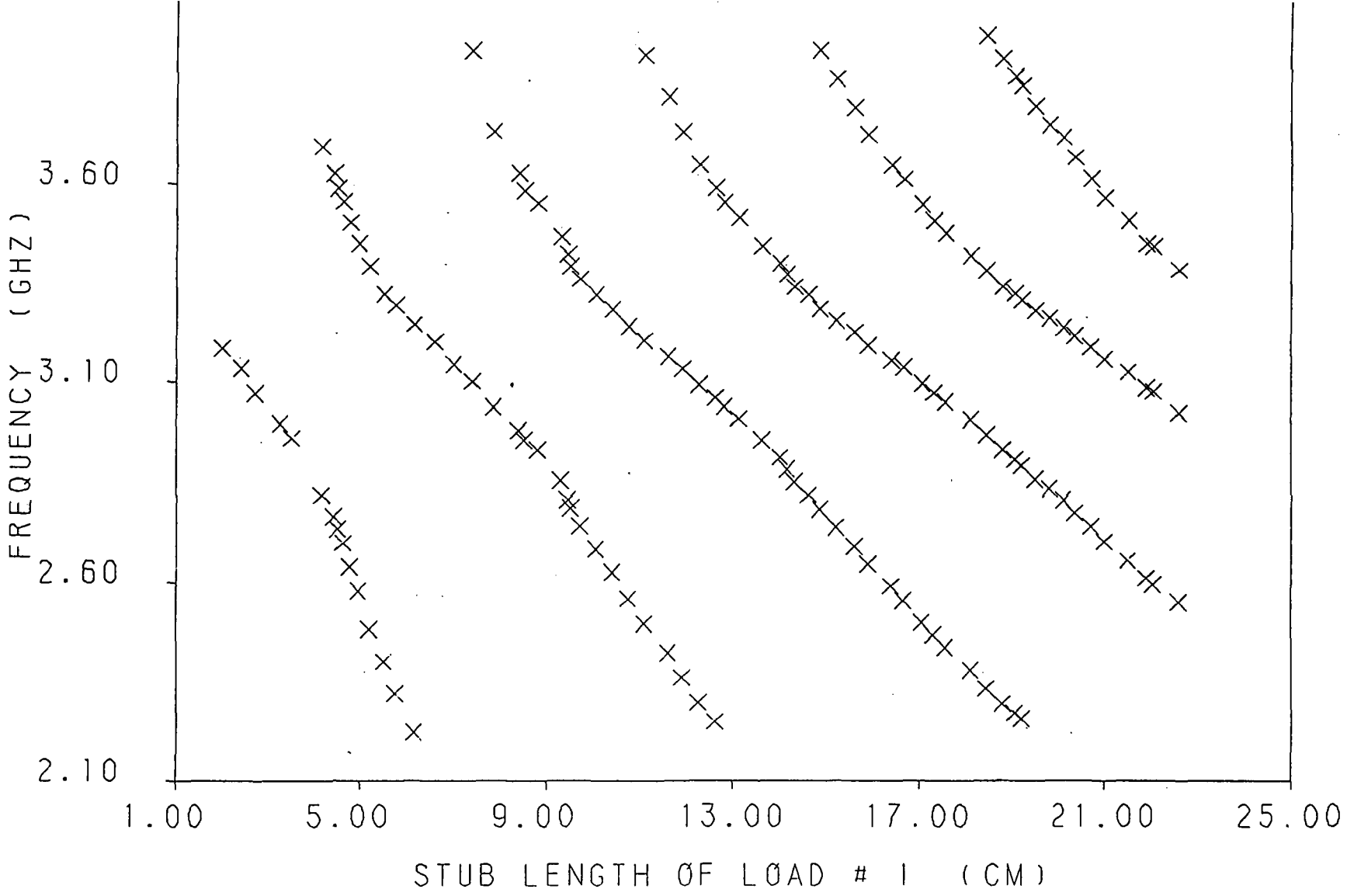

Fig. 3.92 Frequency of upper linearly polarized band (the x-polarized band) verses the short circuit stub length of load #1 for a loaded 2.96 by 2.96 cm square patch with a feed location of (1.05, .45 cm), and load insets of d = .35 cm .

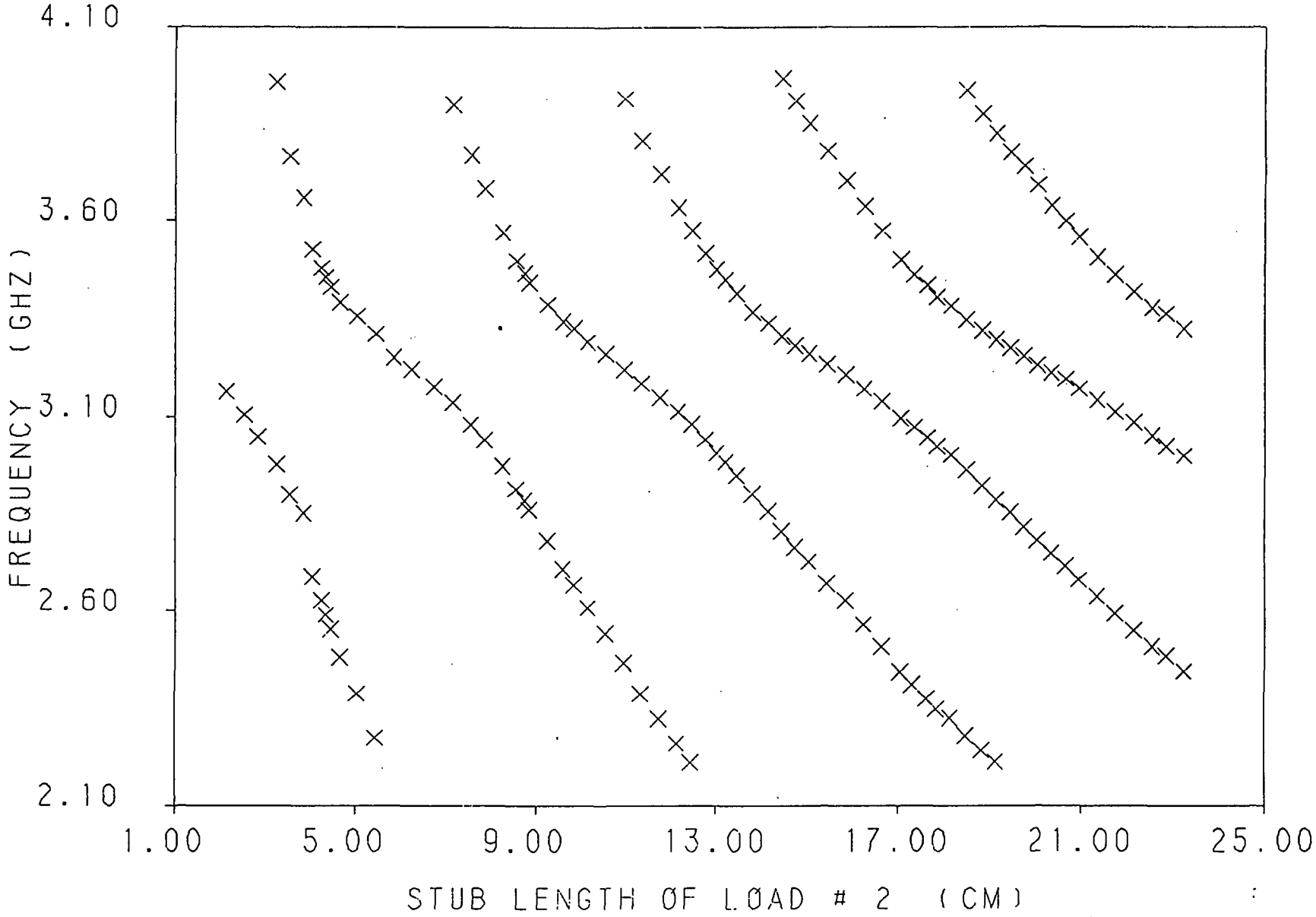

Fig. 3.93 Frequency of lower linearly polarized band (the *y*-polarized band) verses the short circuit stub length of load #2 for a loaded 2.96 by 2.96 cm square patch with a feed location of (1.05, .45 cm), and load insets of d = .35 cm .

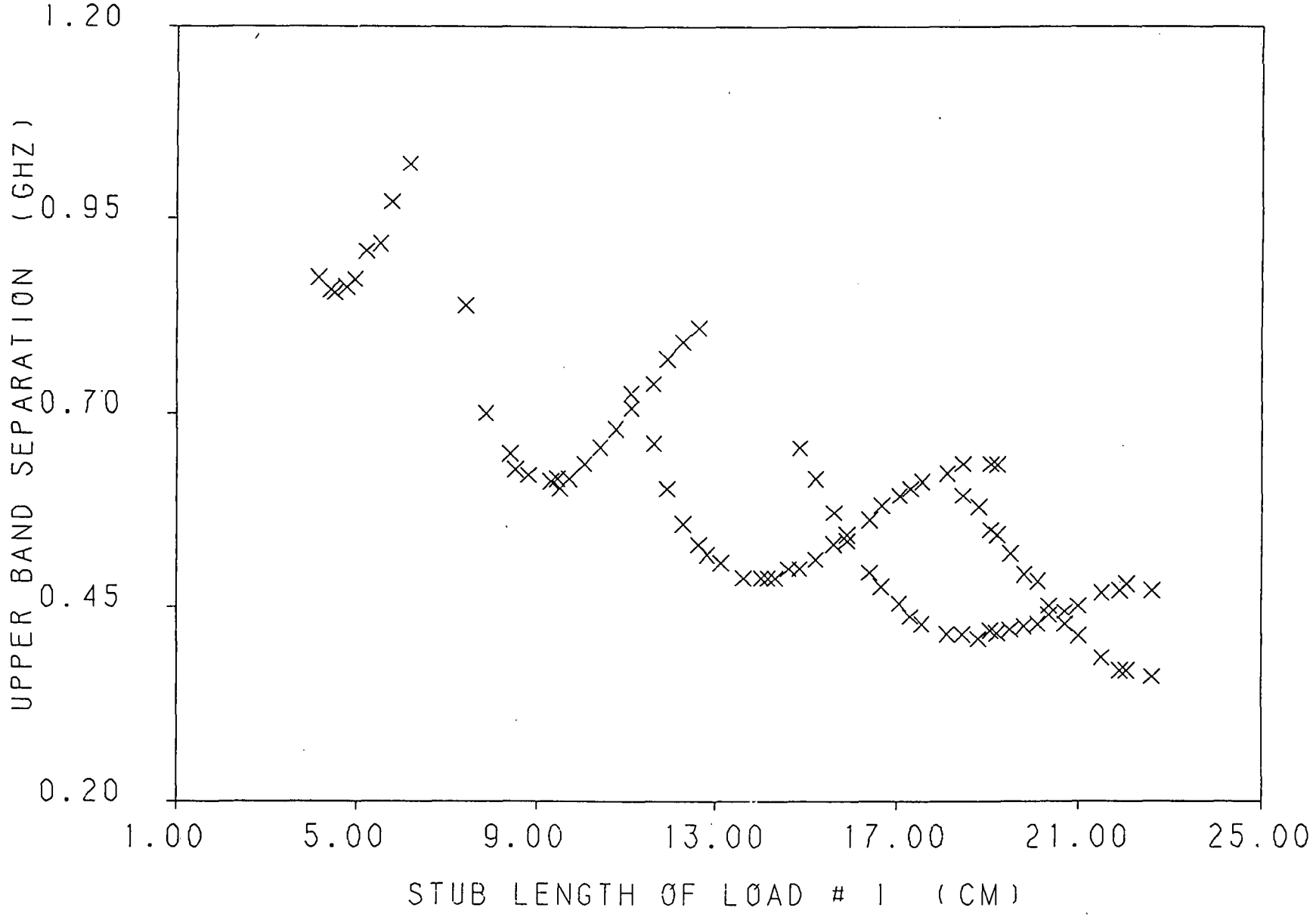

Fig. 3.94 Upper frequency band (the x-polarized band) separation verses the short circuit stub length of load #1 for a loaded 2.96 by 2.96 cm square patch with a feed location of (1.05, .45 cm), and load insets of d = .35 cm .

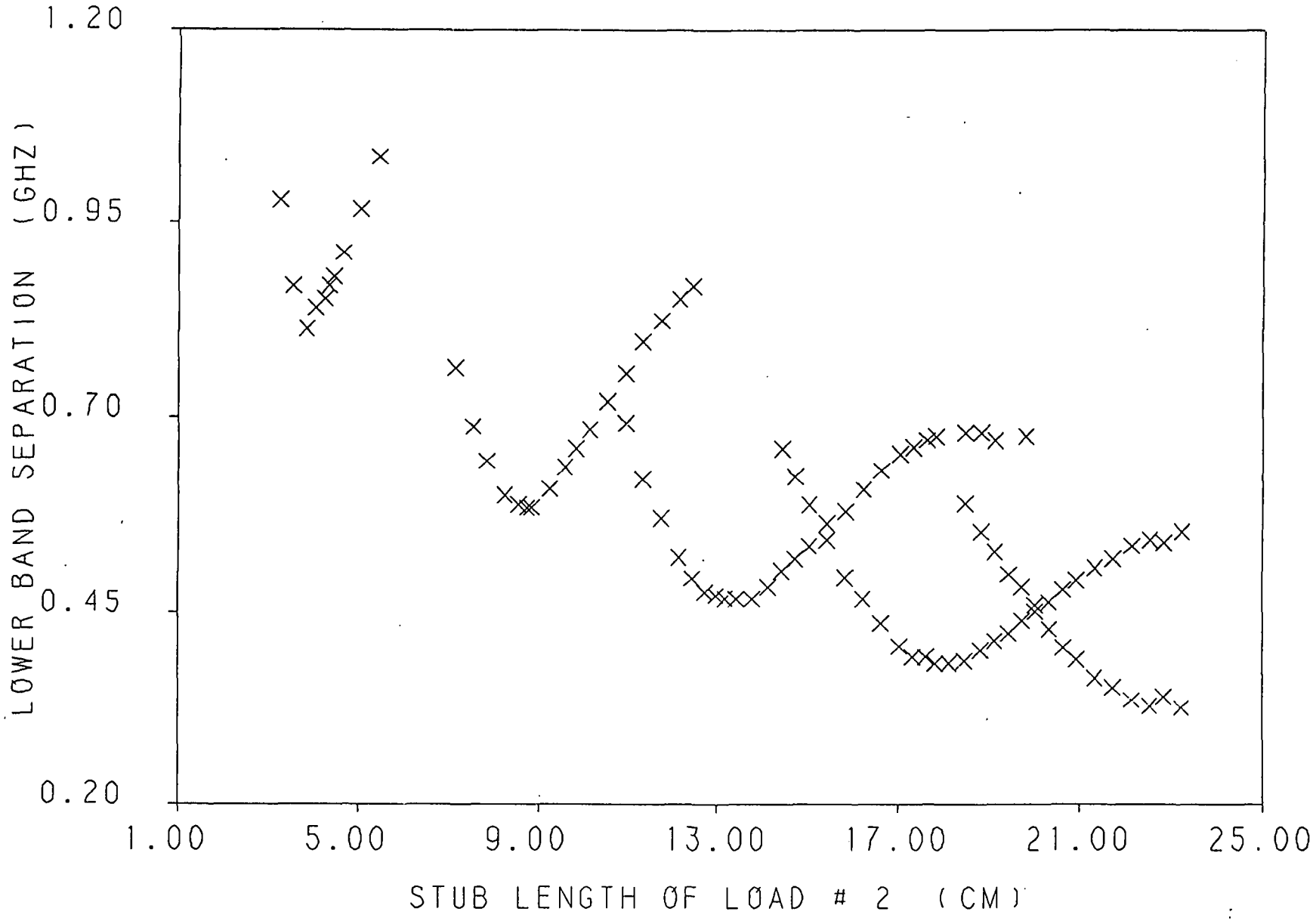

Fig. 3.95 Lower frequency band (the *y*-polarized band) separation verses the short circuit stub length of load #2 for a loaded 2.96 by 2.96 cm square patch with a feed location of (1.05, .45 cm), and load insets of d = .35 cm .

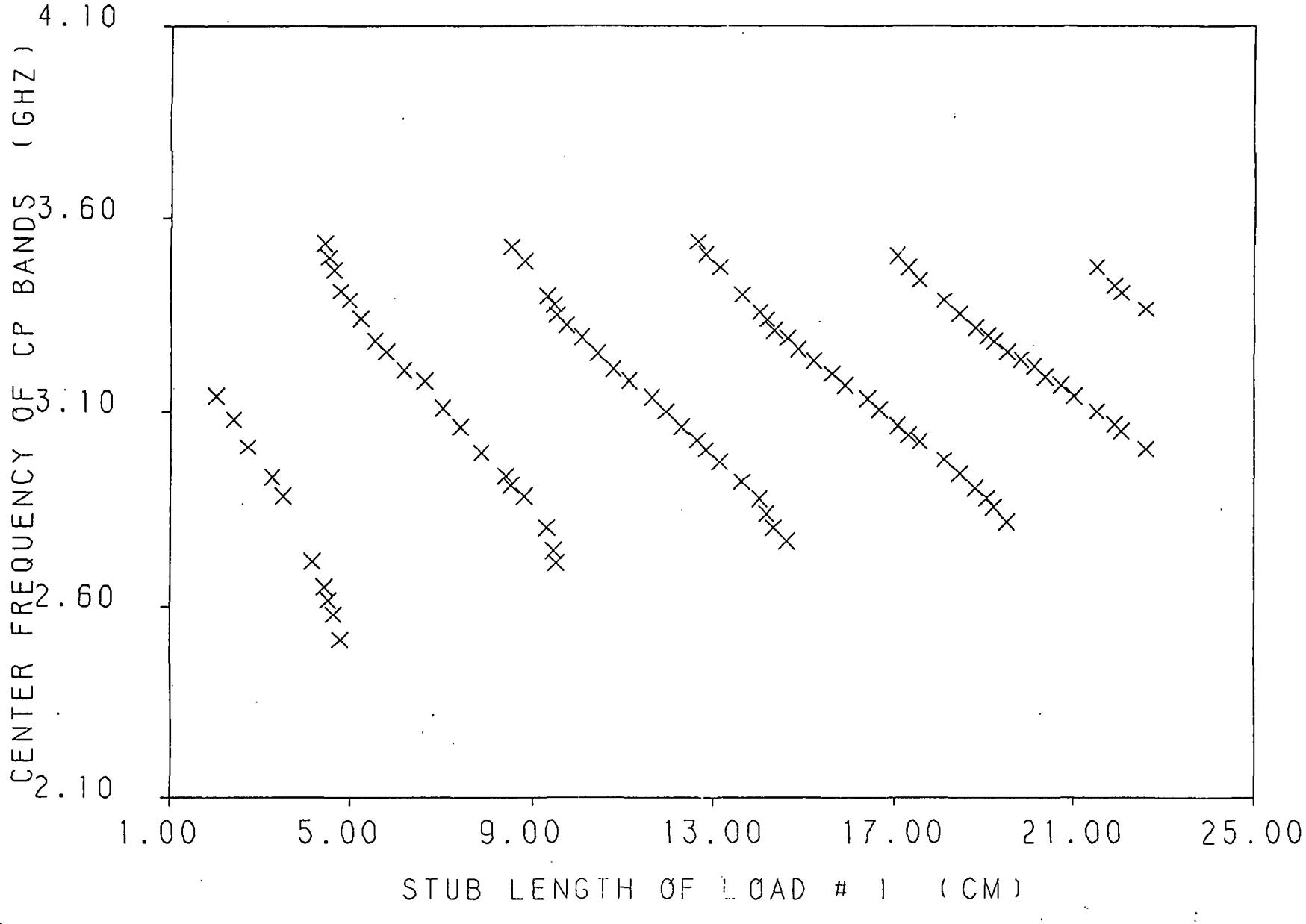

Fig. 3.96 Center frequency of cp bands verses the short circuit stub length of load # 1 for a loaded 2.96 by 2.96 cm square patch with a feed location of (1.05, .45 cm), and load insets of d = .35 cm .

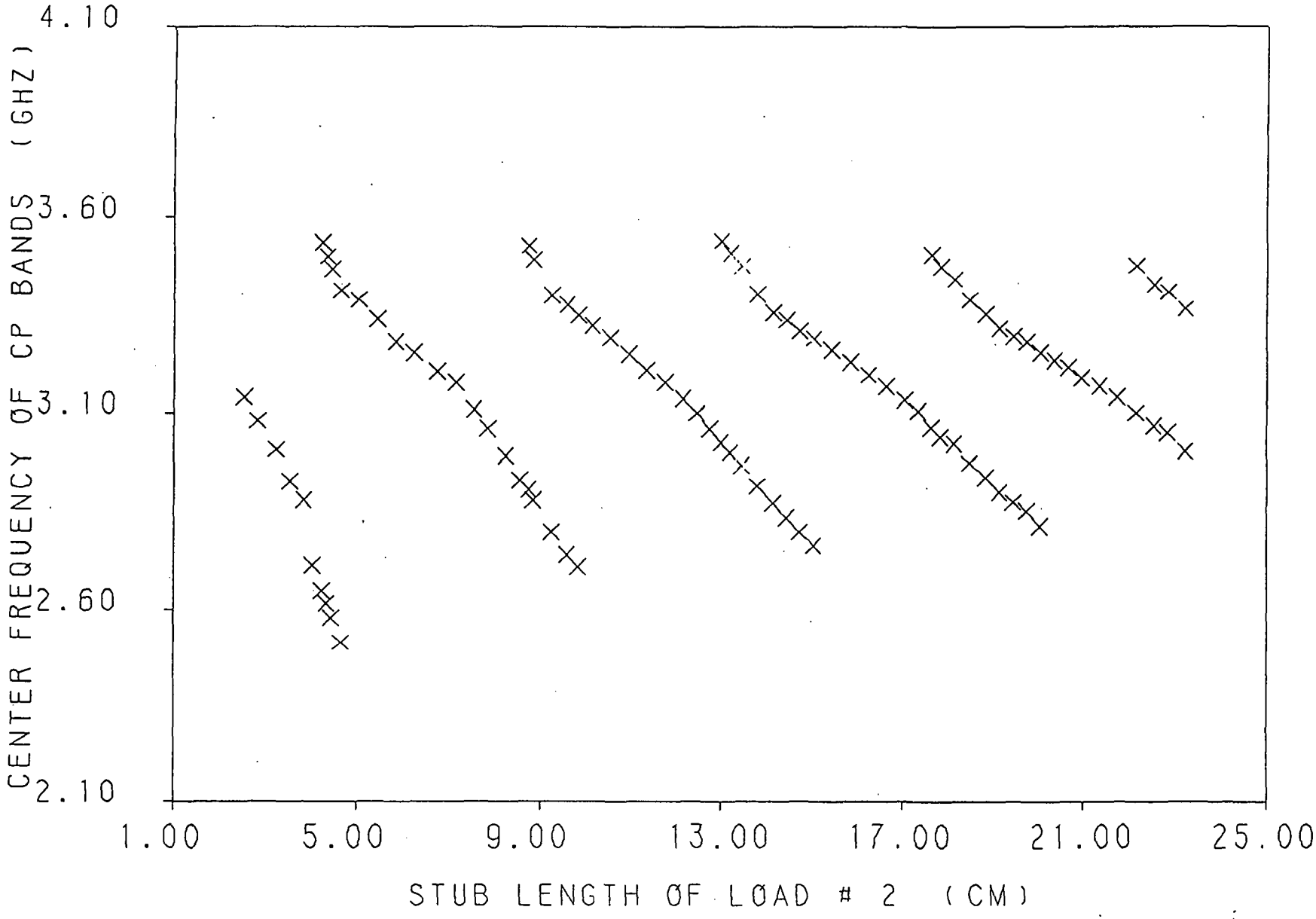

Fig. 3.97 Center frequency of cp bands verses the short circuit stub length of load # 2 for a loaded 2.96 by 2.96 cm square patch with a feed location of (1.05, .45 cm), and load insets of d = .35 cm .

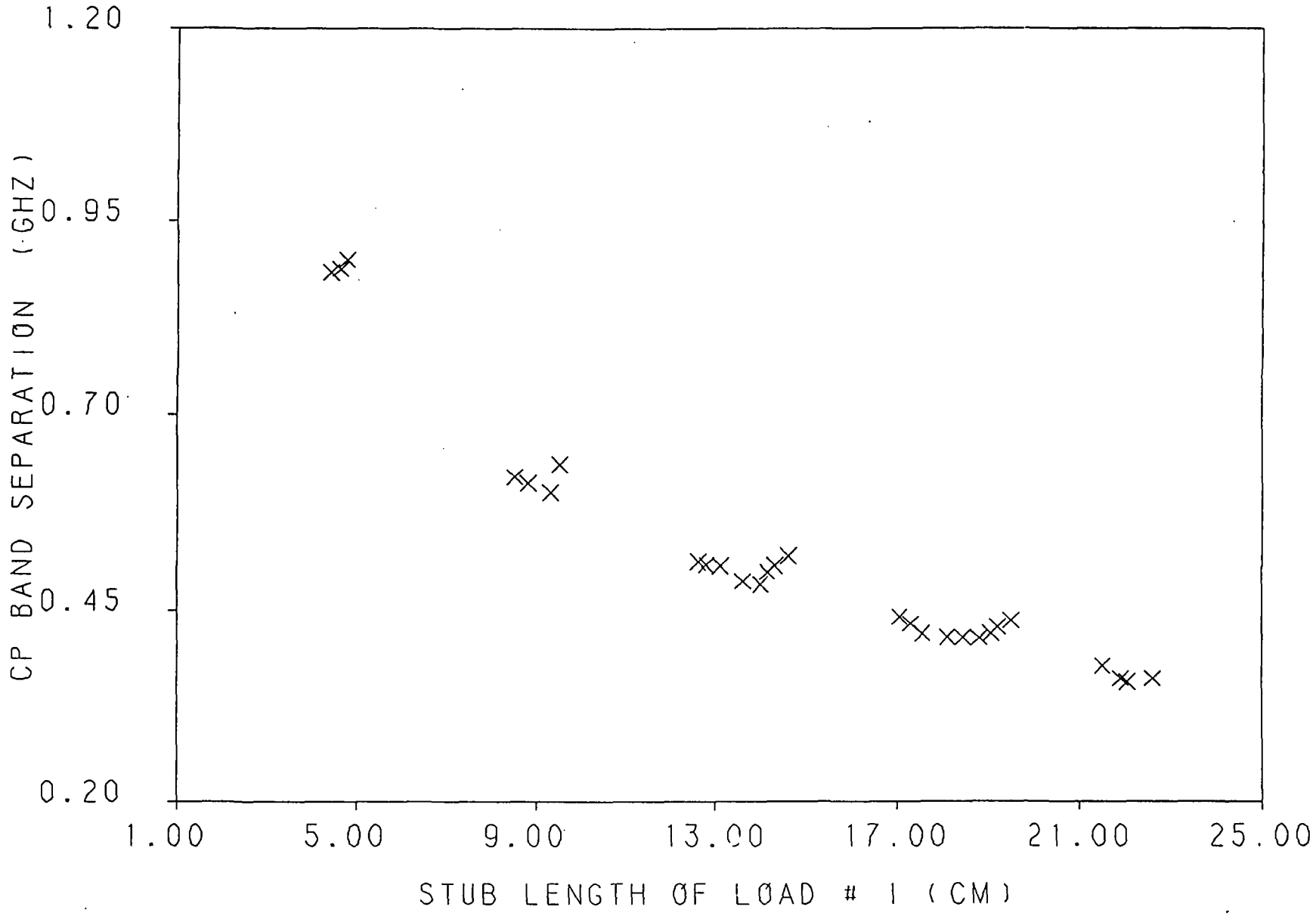

Fig. 3.98 Cp band separation verses the short circuit stub length of load # 1 for a loaded 2.96 by 2.96 cm square patch with a feed location of (1.05, .45 cm), and load insets of d = .35 cm .

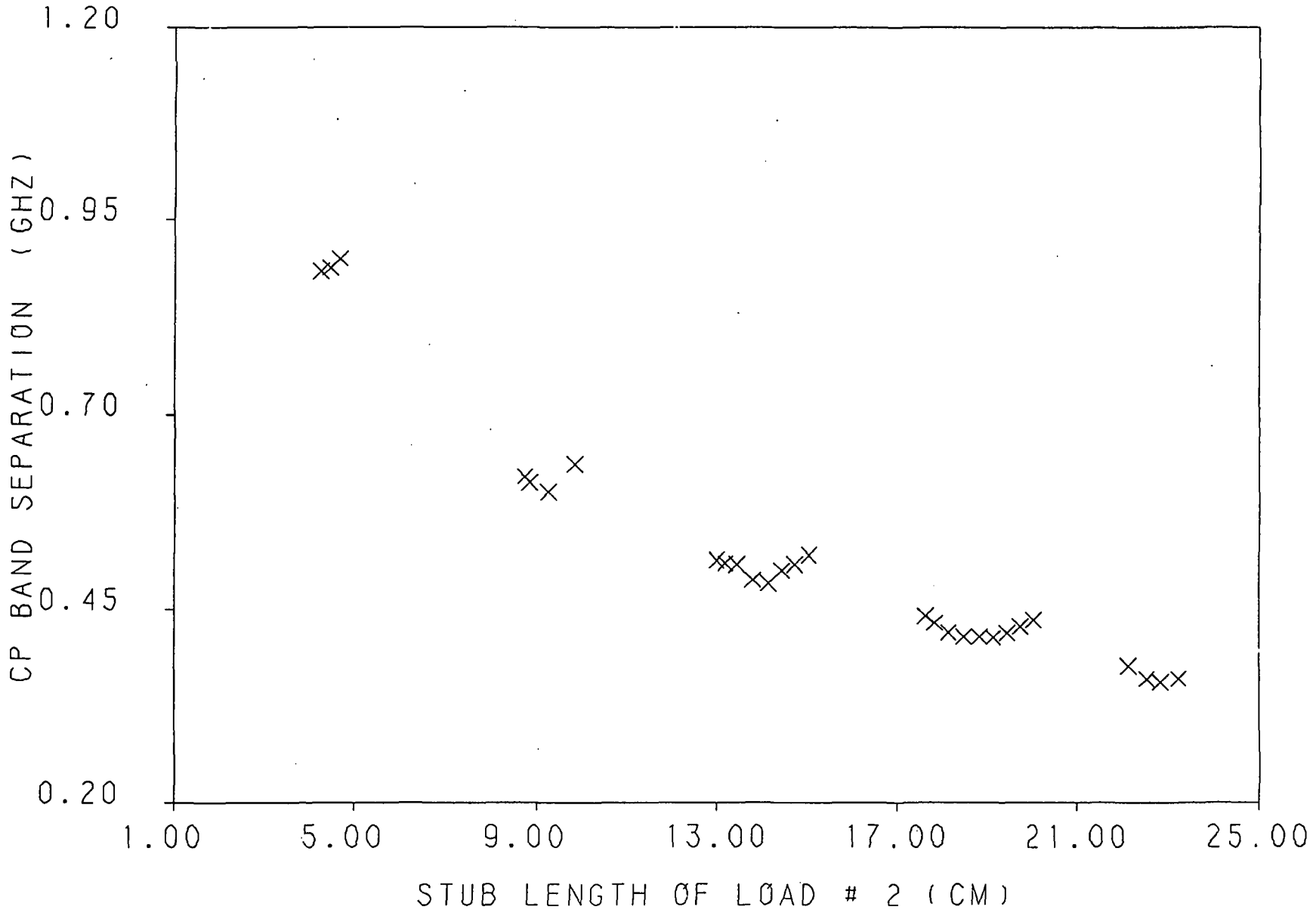

Fig. 3.99 Cp band separation verses the short circuit stub length of load # 2 for a loaded 2.96 by 2.96 cm square patch with a feed location of (1.05, .45 cm), and load insets of d = .35 cm .

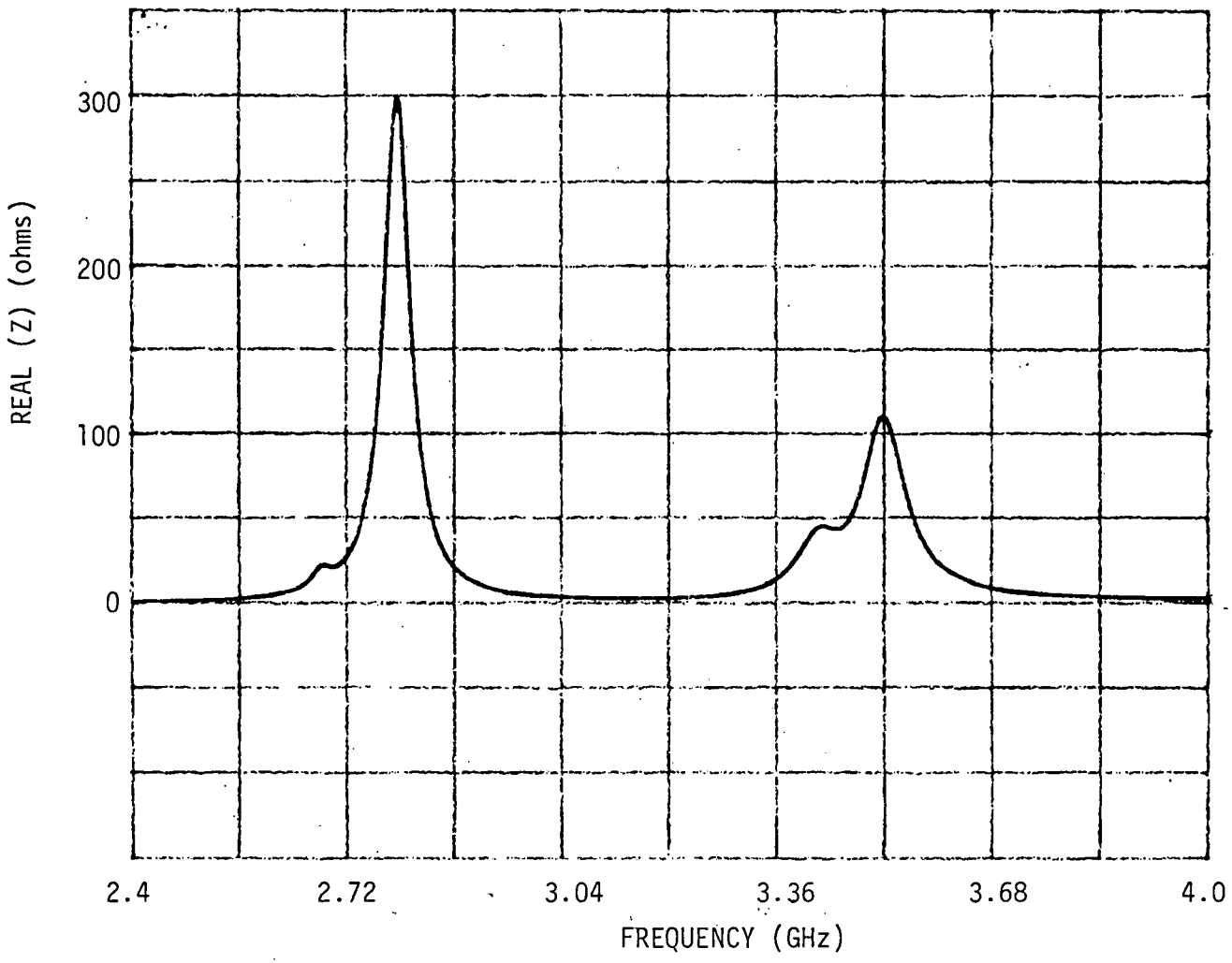

Fig. 3.100 Real part of input impedance verses frequency of the first mode for a loaded 2.96 by 2.96 cm square patch with a feed location of (.45, .85 cm), load insets of d = .60 cm, and stub lengths of s_1 = 4.4 cm and s_2 = 4.33 cm.

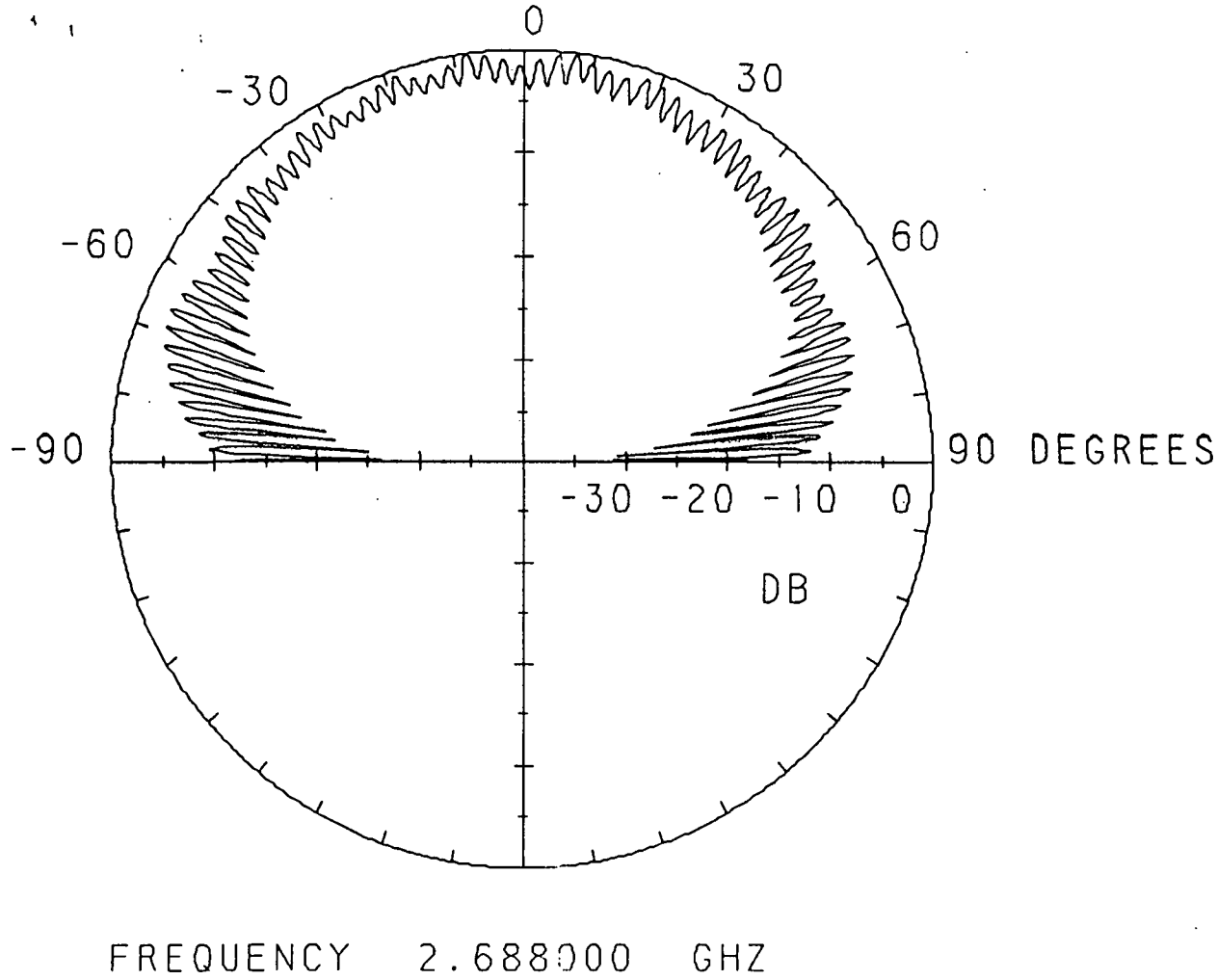

Fig. 3.101 Spinning linear pattern for the lower cp band of the first mode for a loaded 2.96 by 2.96 cm square patch with a feed location of (.45, .85 cm), load insets of d = .60 cm, and stub lengths of s_1 = 4.4 cm and s_2 = 4.33 cm.

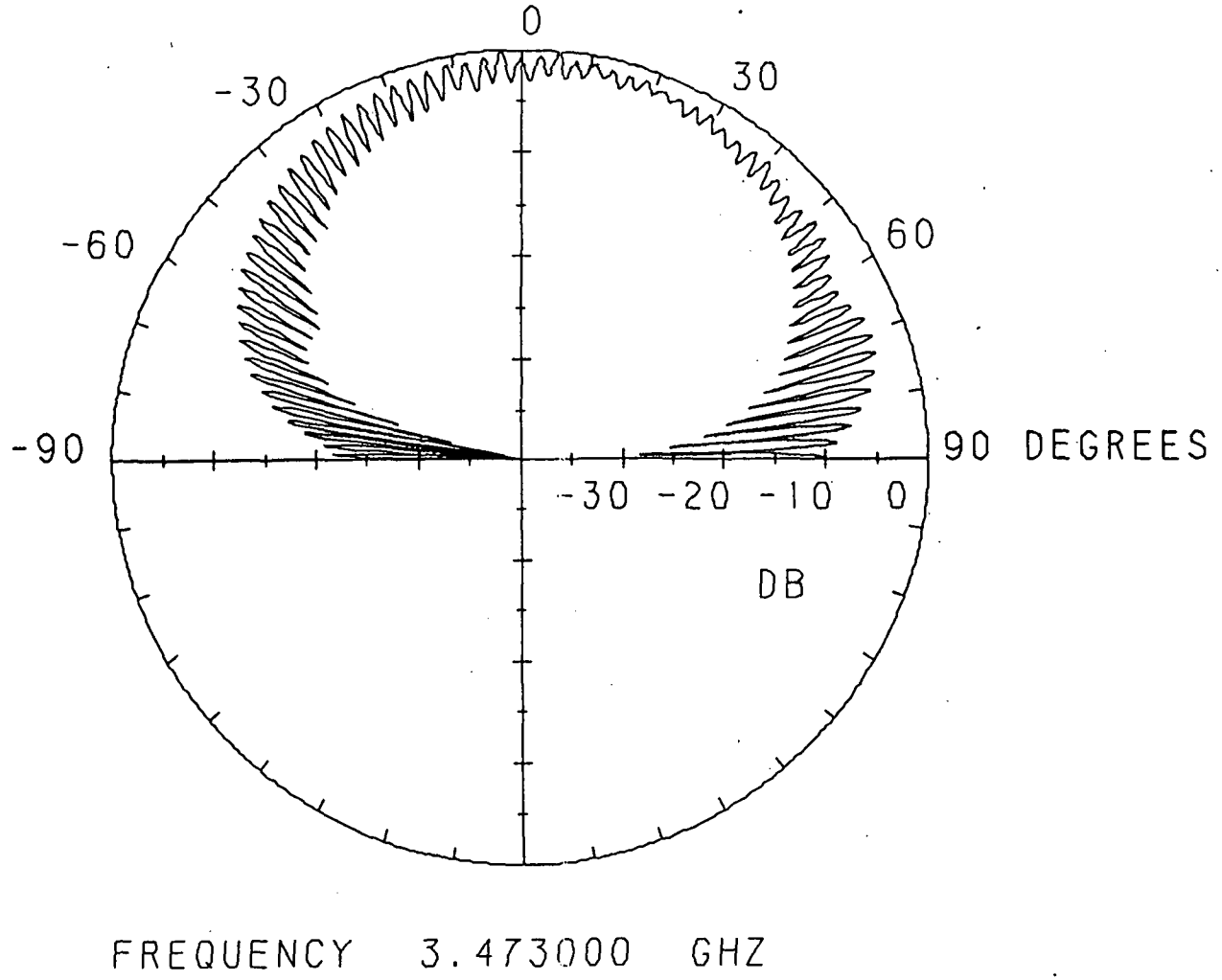

Fig. 3.102 Spinning linear pattern for the upper cp band of the first mode for a loaded 2.96 by 2.96 cm square patch with a feed location of (.45, .85 cm), load insets of d = .60 cm, and stub lengths of s_1 = 4.4 cm and s_2 = 4.33 cm.

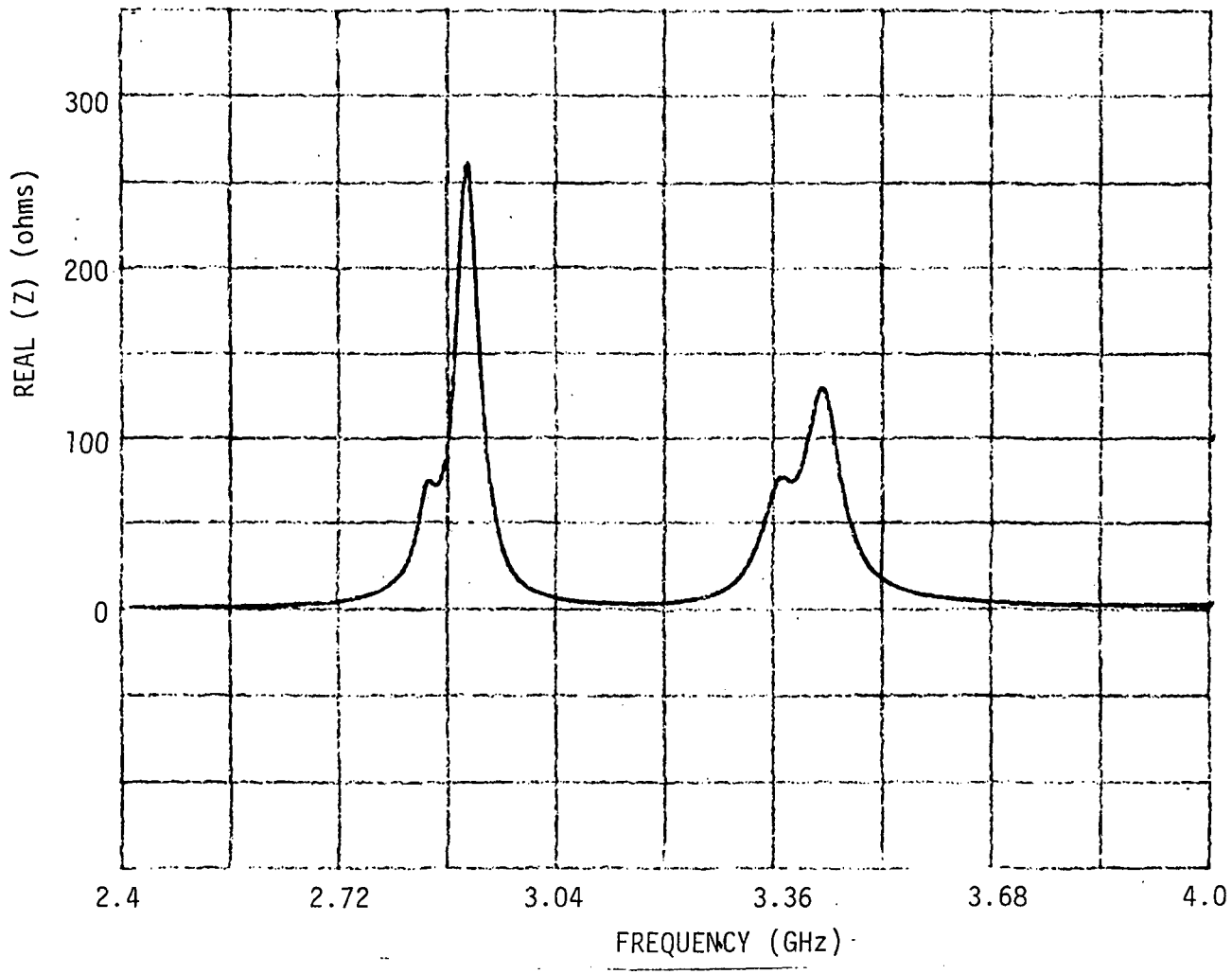

Fig. 3.103 Real part of input impedance verses frequency of the second mode for a loaded 2.96 by 2.96 cm square patch with a feed location of (.45, .85 cm), load insets of d = .60 cm, and stub lengths of s_1 = 9.1 cm and s_2 = 9.08 cm.

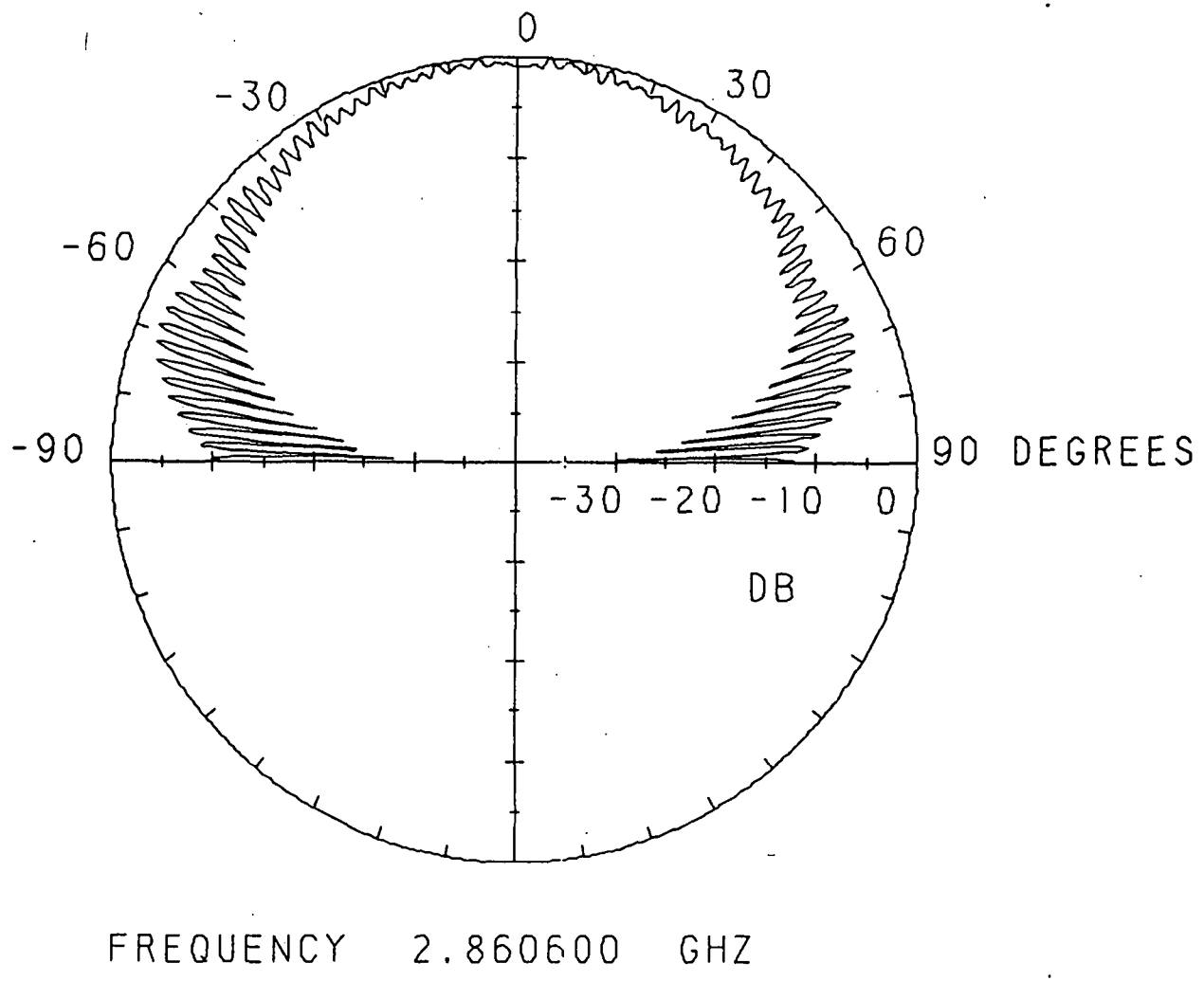

Fig. 3.104 Spinning linear pattern for the lower cp band of the second mode for a loaded 2.96 by 2.96 cm square patch with a feed location of (.45, .85 cm), load insets of d = .60 cm, and stub lengths of s_1 = 9.1 cm and s_2 = 9.08 cm.

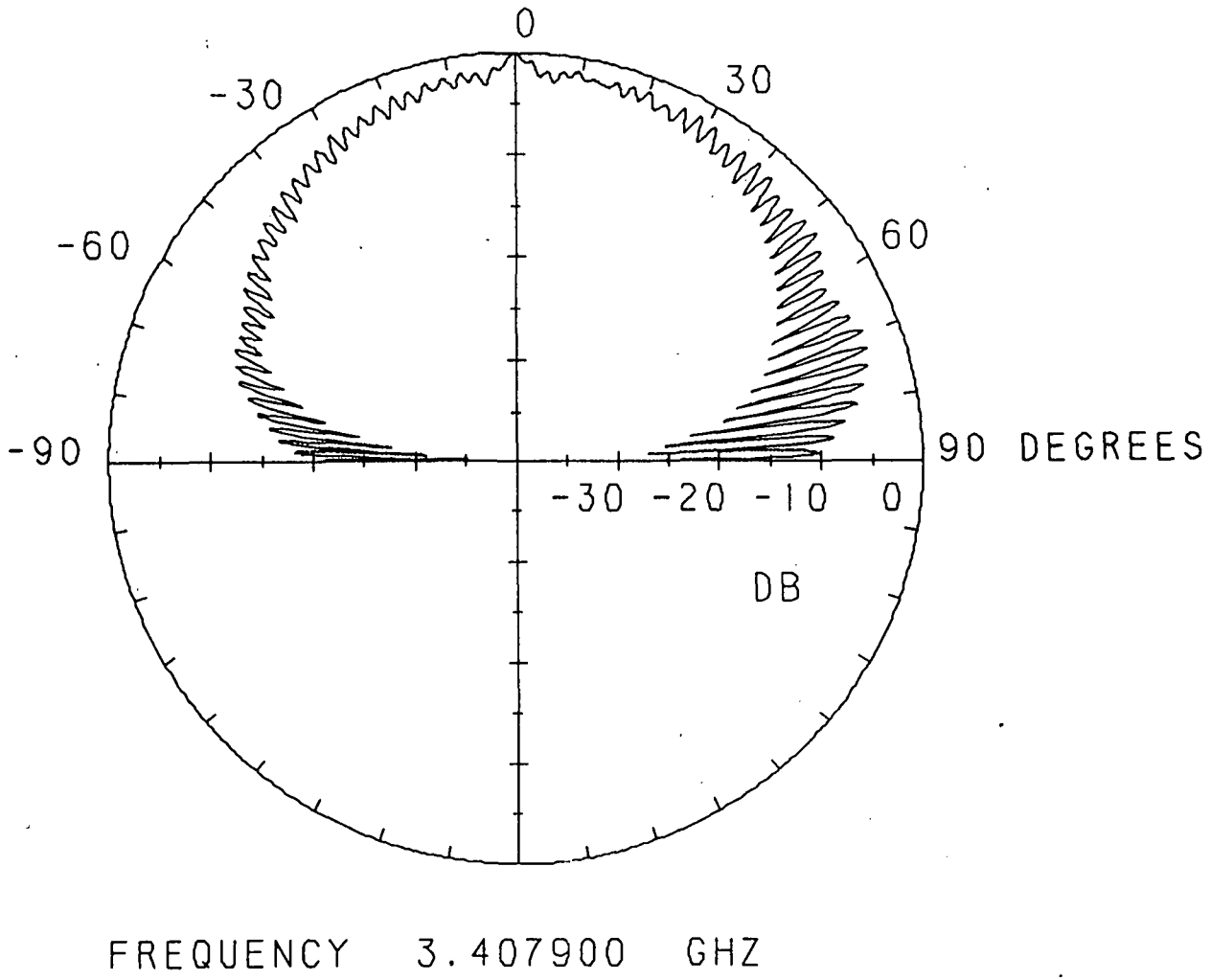

Fig. 3.105 Spinning linear pattern for the upper cp band of the second mode for a loaded 2.96 by 2.96 cm square patch with a feed location of (.45, .85 cm), load insets of d = .60 cm, and stub lengths of s_1 = 9.1 cm and s_2 = 9.08 cm.

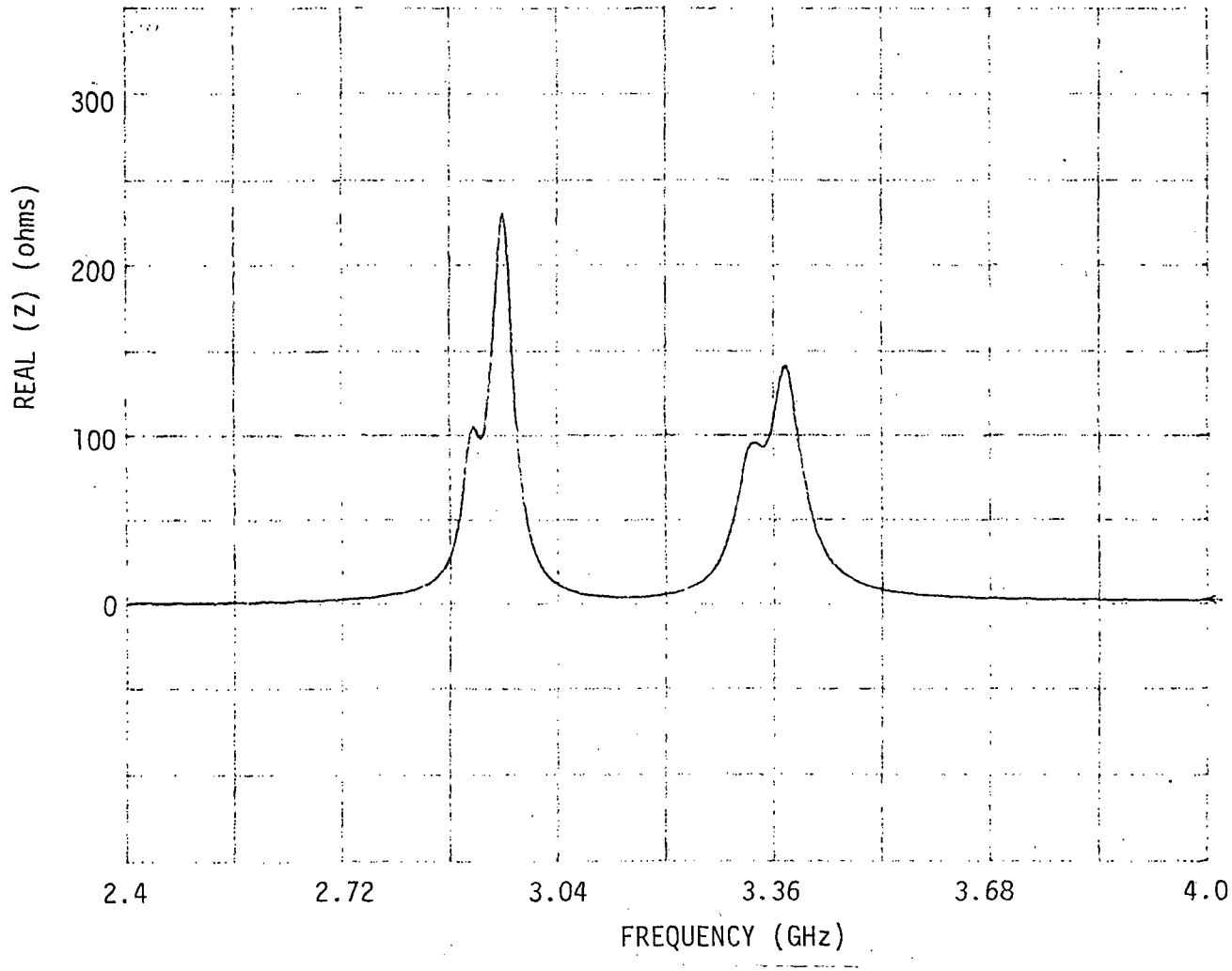

Fig. 3.106 Real part of input impedance verses frequency of the third mode for a loaded 2.96 by 2.96 cm square patch with a feed location of (.45, .85 cm), load insets of d = .60 cm, and stub lengths of s_1 = 13.7 cm and s_2 = 13.93 cm.

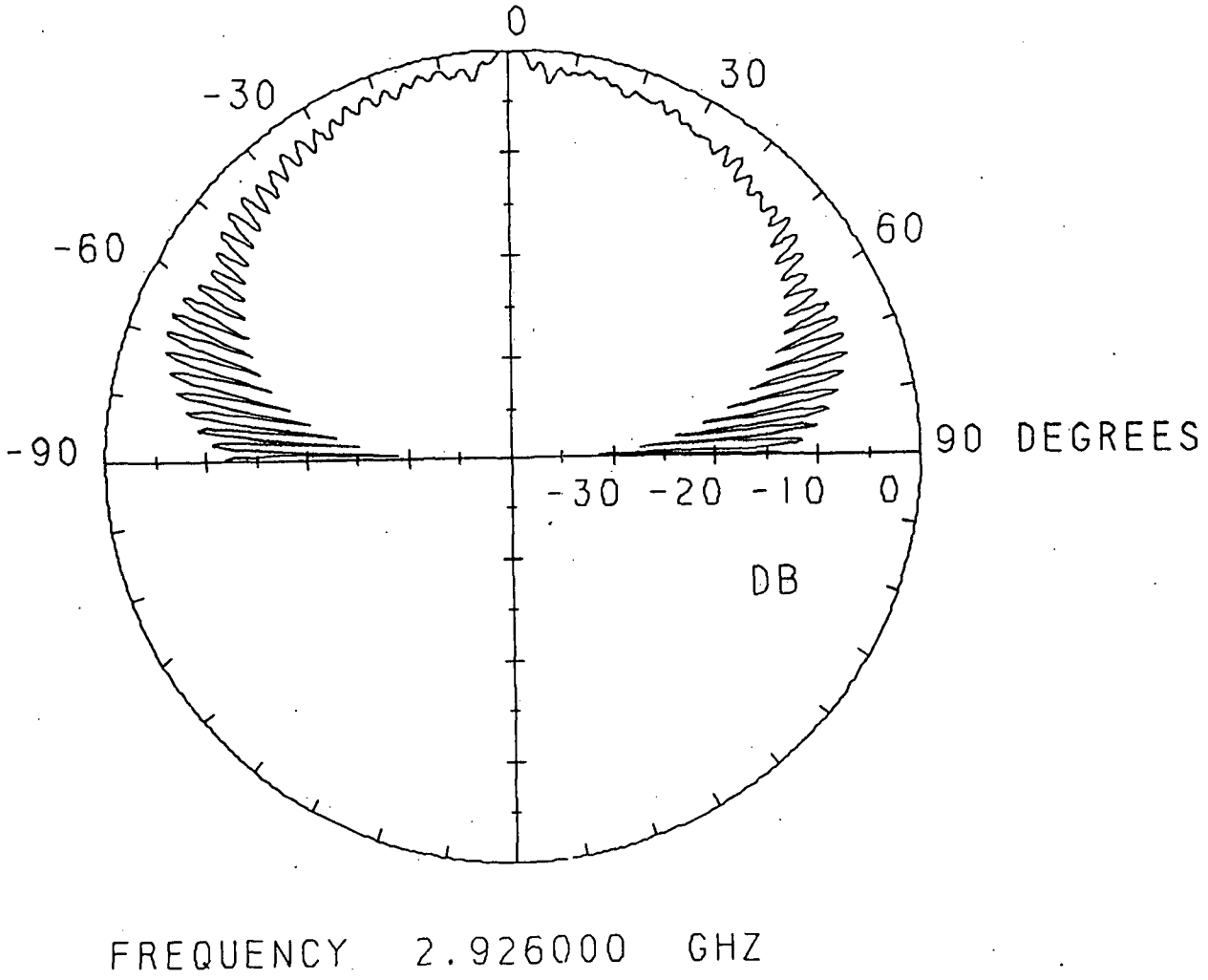

Fig. 3.107 Spinning linear pattern for the lower cp band of the third mode for a loaded 2.96 by 2.96 cm square patch with a feed location of (.45, .85 cm), load insets of d = .60 cm, and stub lengths of s_1 = 13.7 cm and s_2 = 13.93 cm.

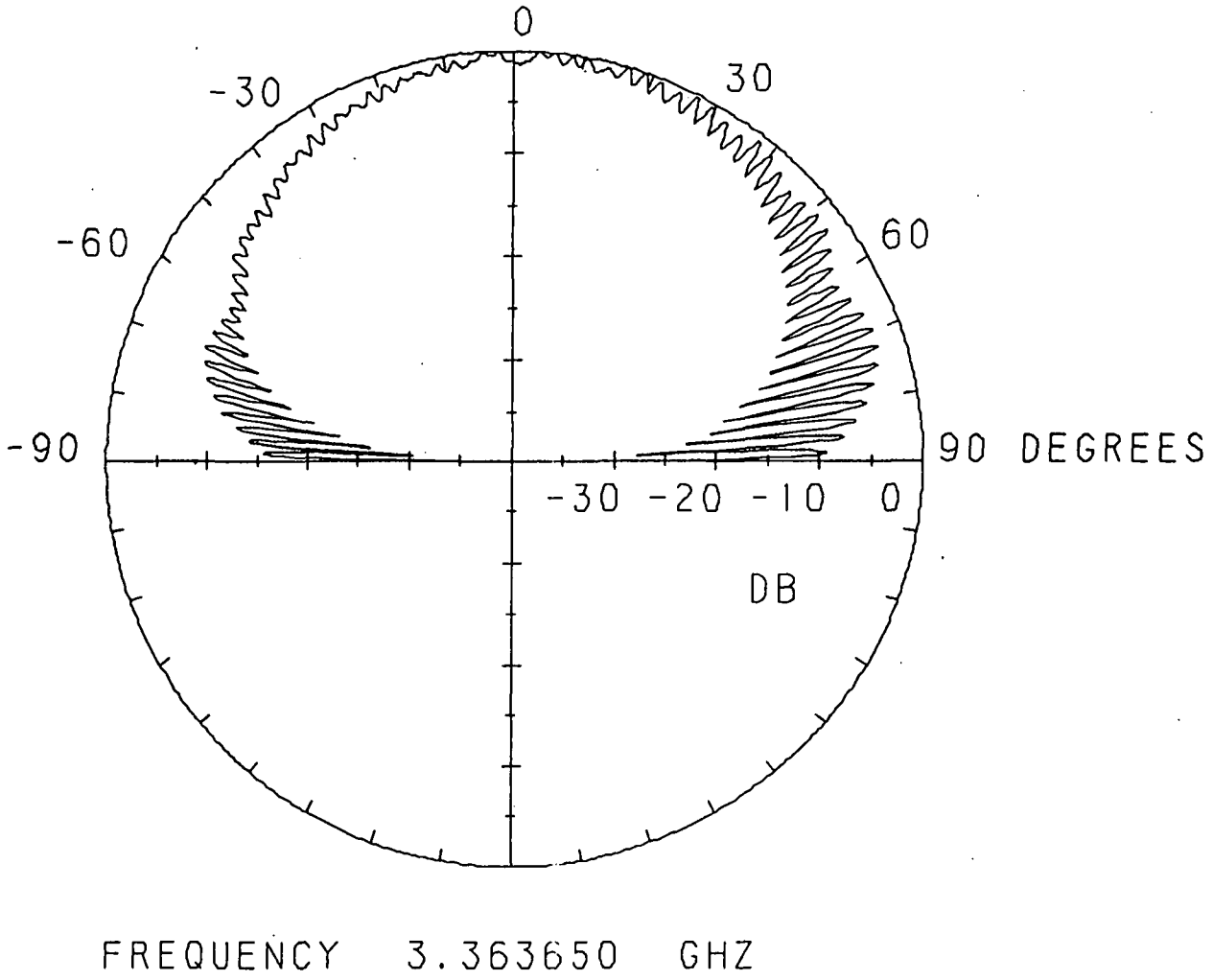

Fig. 3.108 Spinning linear pattern for the upper cp band of the third mode for a loaded 2.96 by 2.96 cm square patch with a feed location of (.45, .85 cm), load insets of d = .60 cm, and stub lengths of s_1 = 13.7 cm and s_2 = 13.93 cm.

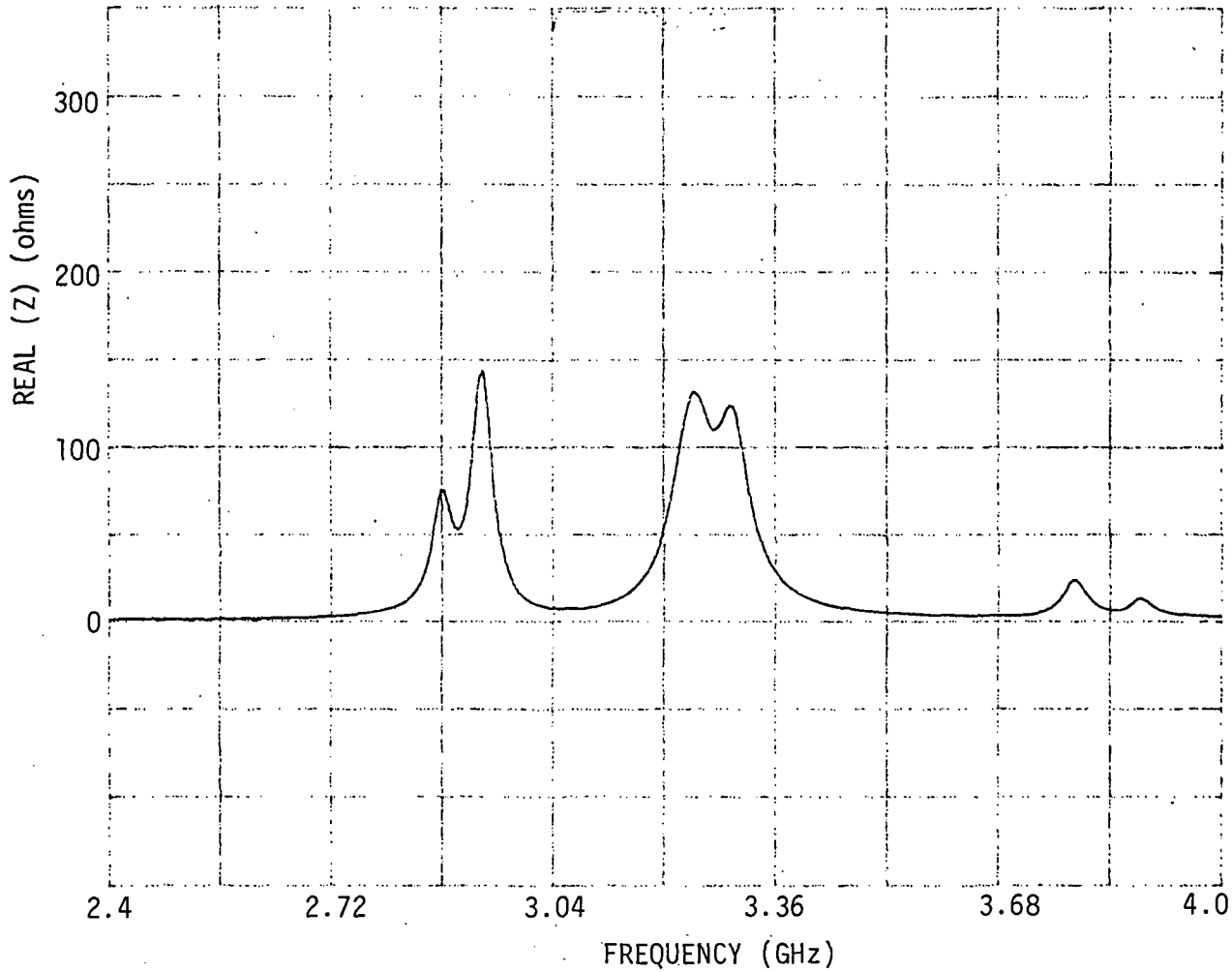

Fig. 3.109 Real part of input impedance verses frequency of the fourth mode for a loaded 2.96 by 2.96 cm square patch with a feed location of (.45, .85 cm), load insets of d = .60 cm, and stub lengths of s_1 = 18.9 cm and s_2 = 19.43 cm.

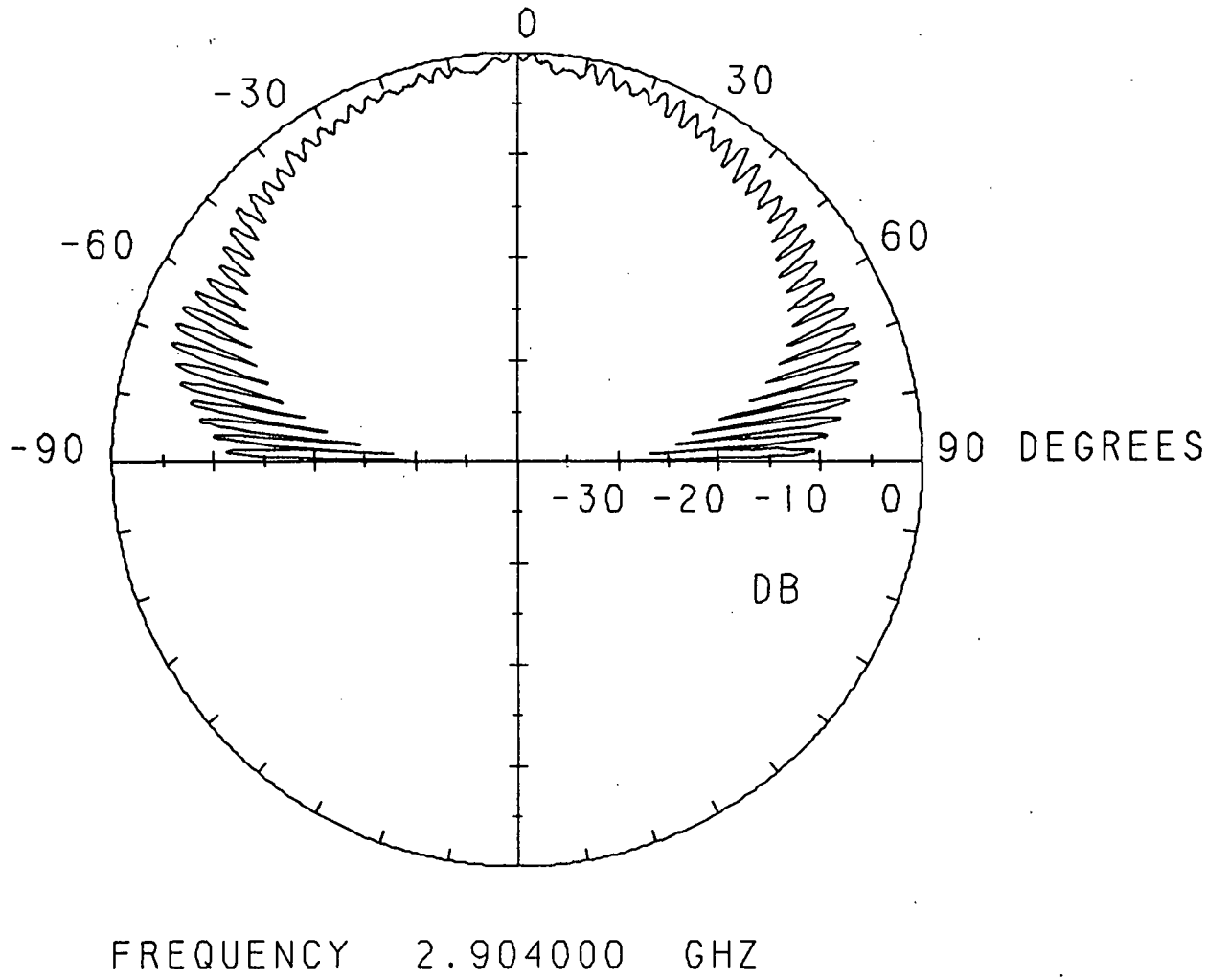

Fig. 3.110 Spinning linear pattern for the lower cp band of the fourth mode for a loaded 2.96 by 2.96 cm square patch with a feed location of (.45, .85 cm), load insets of d = .60 cm, and stub lengths of s_1 = 18.9 cm and s_2 = 19.43 cm.

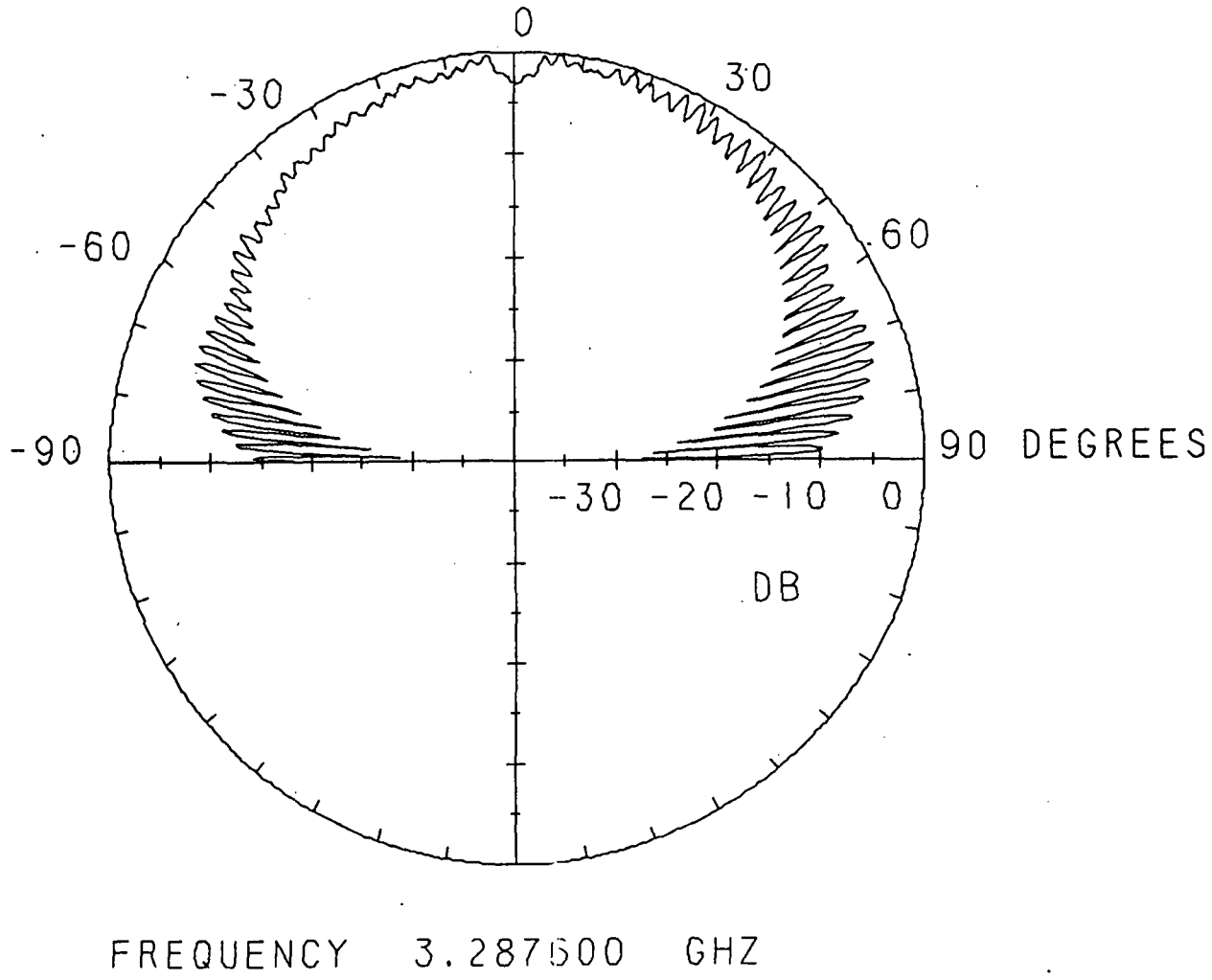

Fig. 3.111 Spinning linear pattern for the upper cp band of the fourth mode for a loaded 2.96 by 2.96 cm square patch with a feed location of (.45, .85 cm), load insets of d = .60 cm, and stub lengths of s_1 = 18.9 cm and s_2 = 19.43 cm.

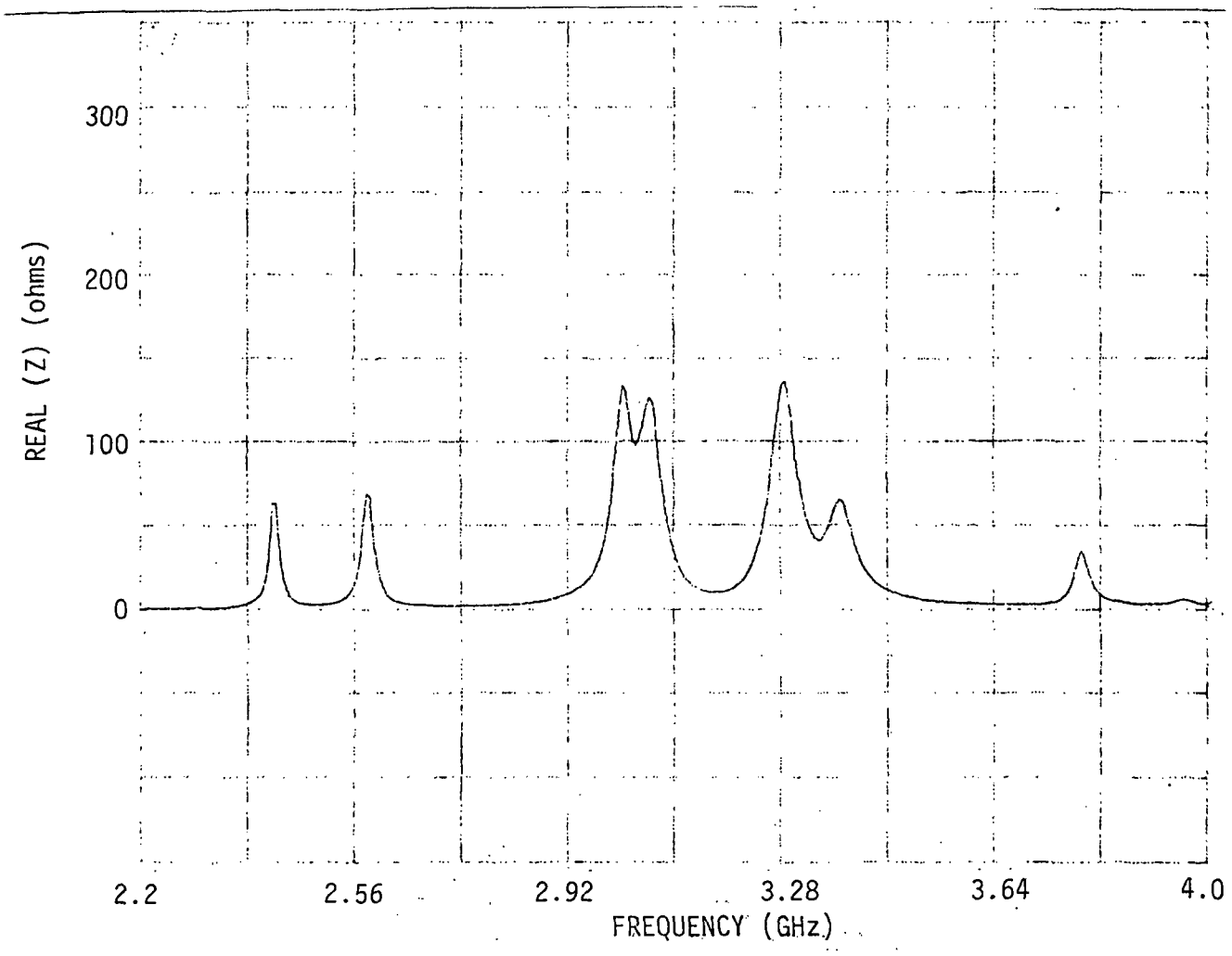

Fig. 3.112 Real part of input impedance verses frequency of the fifth mode for a loaded 2.96 by 2.96 cm square patch with a feed location of (.45, .85 cm), load insets of d = .60 cm, and stub lengths of s_1 = 22.3 cm and s_2 = 23.38 cm.

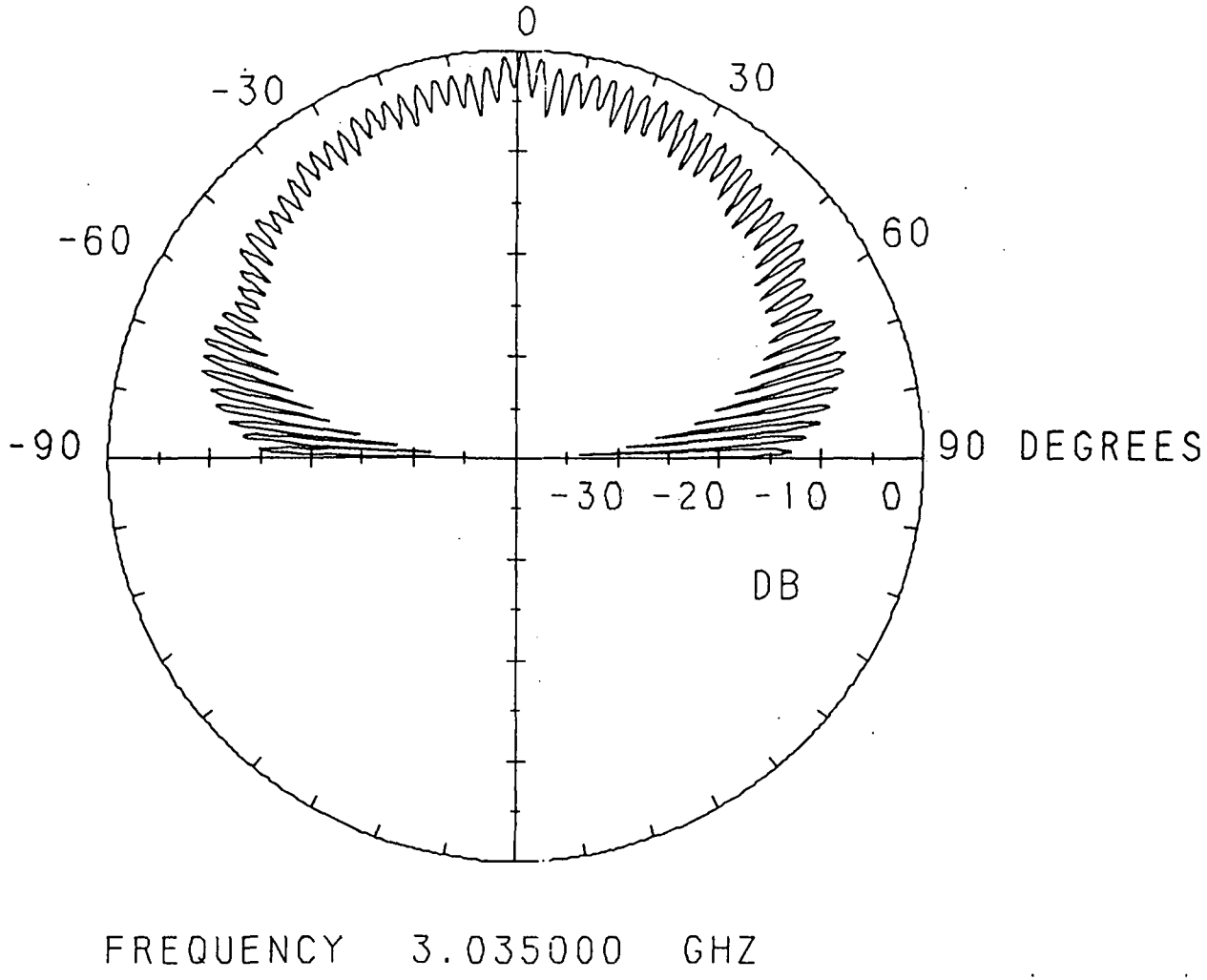

Fig. 3.113 Spinning linear pattern for the lower cp band of the fifth mode for a loaded 2.96 by 2.96 cm square patch with a feed location of (.45, .85 cm), load insets of d = .60 cm, and stub lengths of s_1 = 22.3 cm and s_2 = 23.38 cm.

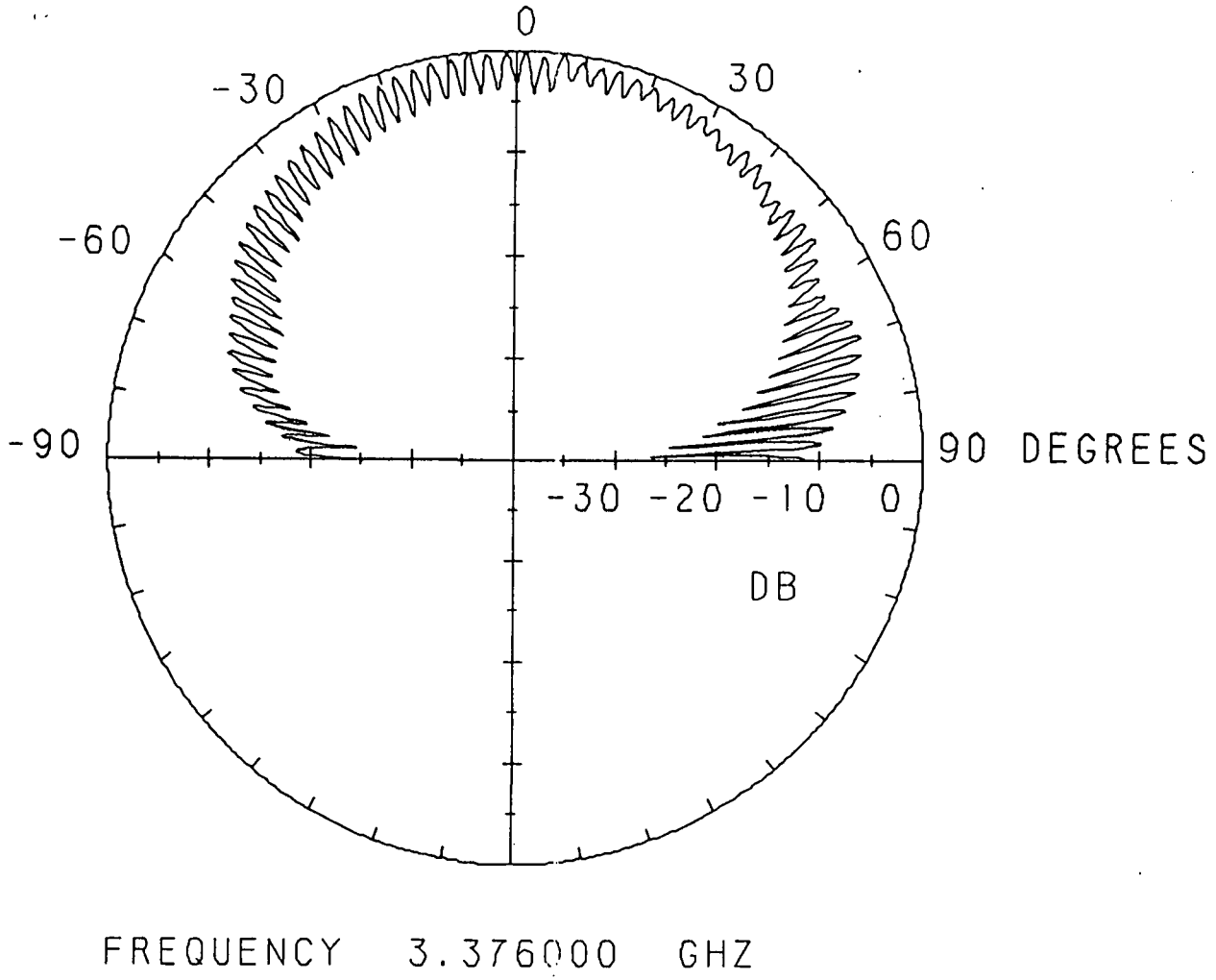

Fig. 3.114 Spinning linear pattern for the upper cp band of the fifth mode for a loaded 2.96 by 2.96 cm square patch with a feed location of (.45, .85 cm), load insets of d = .60 cm, and stub lengths of s_1 = 22.3 cm and s_2 = 23.38 cm.

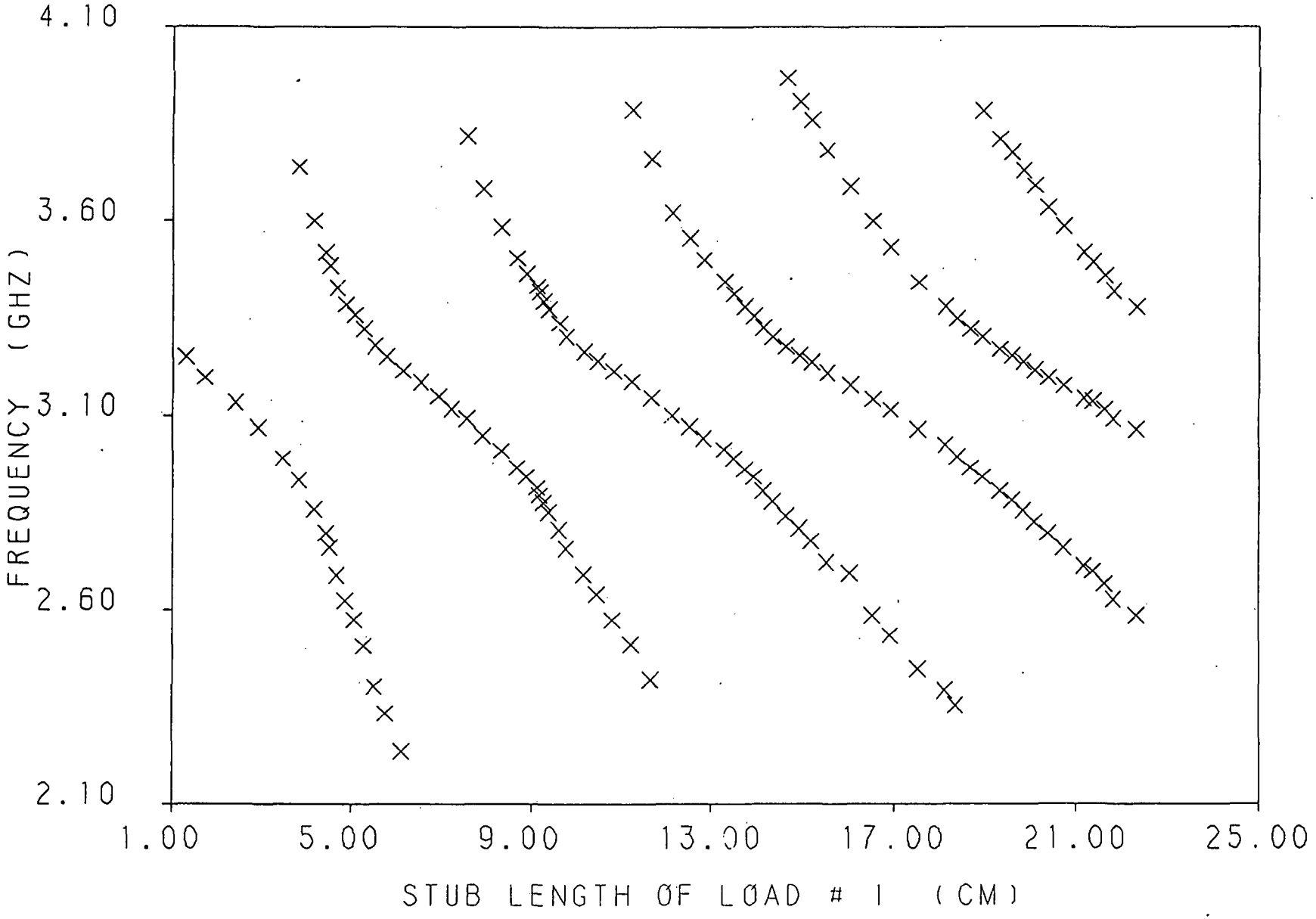

Fig. 3.115 Frequency of upper linearly polarized band (the x-polarized band) verses the short circuit stub length of load #1 for a loaded 2.96 by 2.96 cm square patch with a feed location of (.85, .45 cm), and load insets of d = .60 cm .

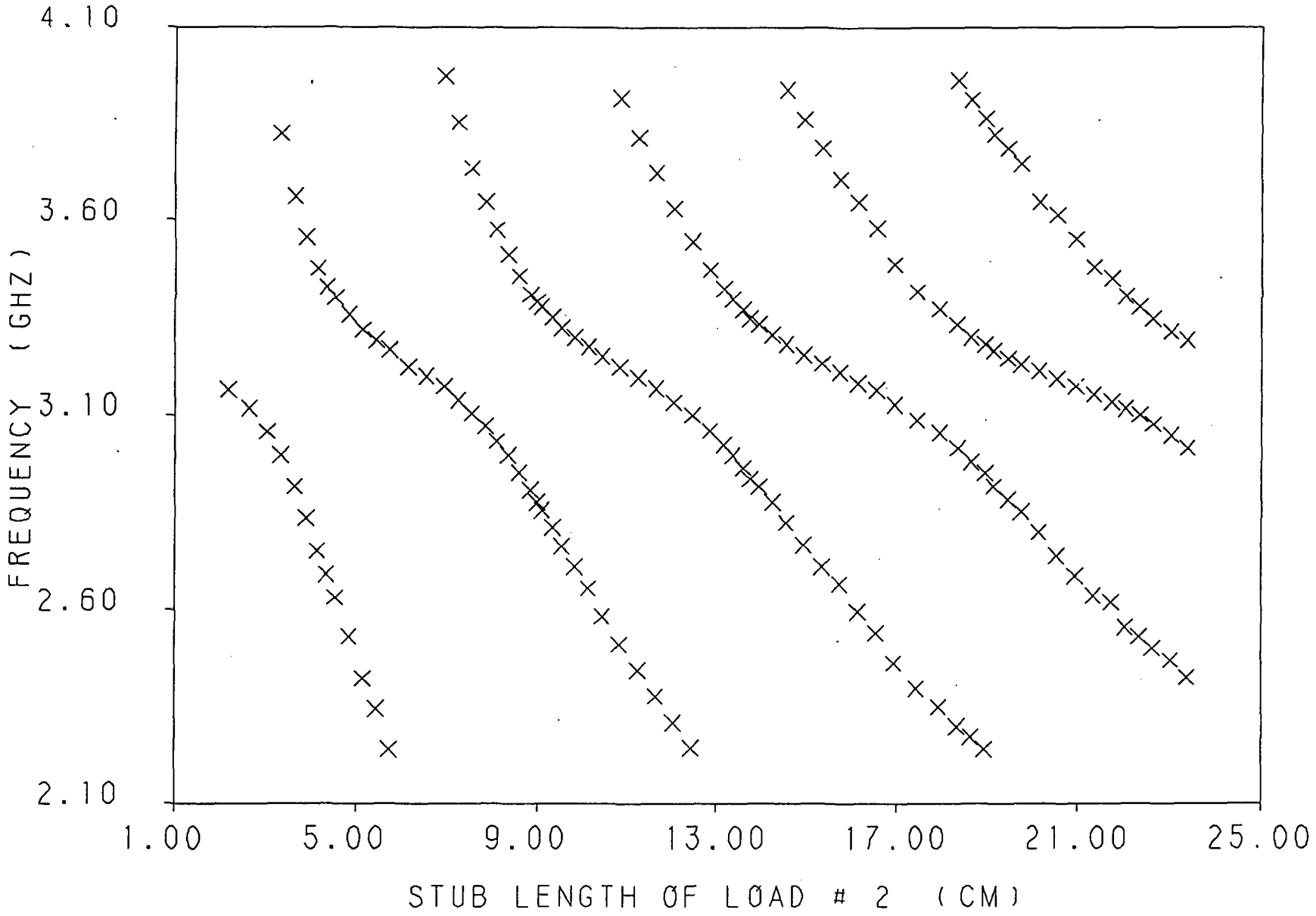

Fig. 3.116 Frequency of lower linearly polarized band (the *y*-polarized band) verses the short circuit stub length of load #2 for a loaded 2.96 by 2.96 cm square patch with a feed location of (.85, .45 cm), and load insets of d = .60 cm .

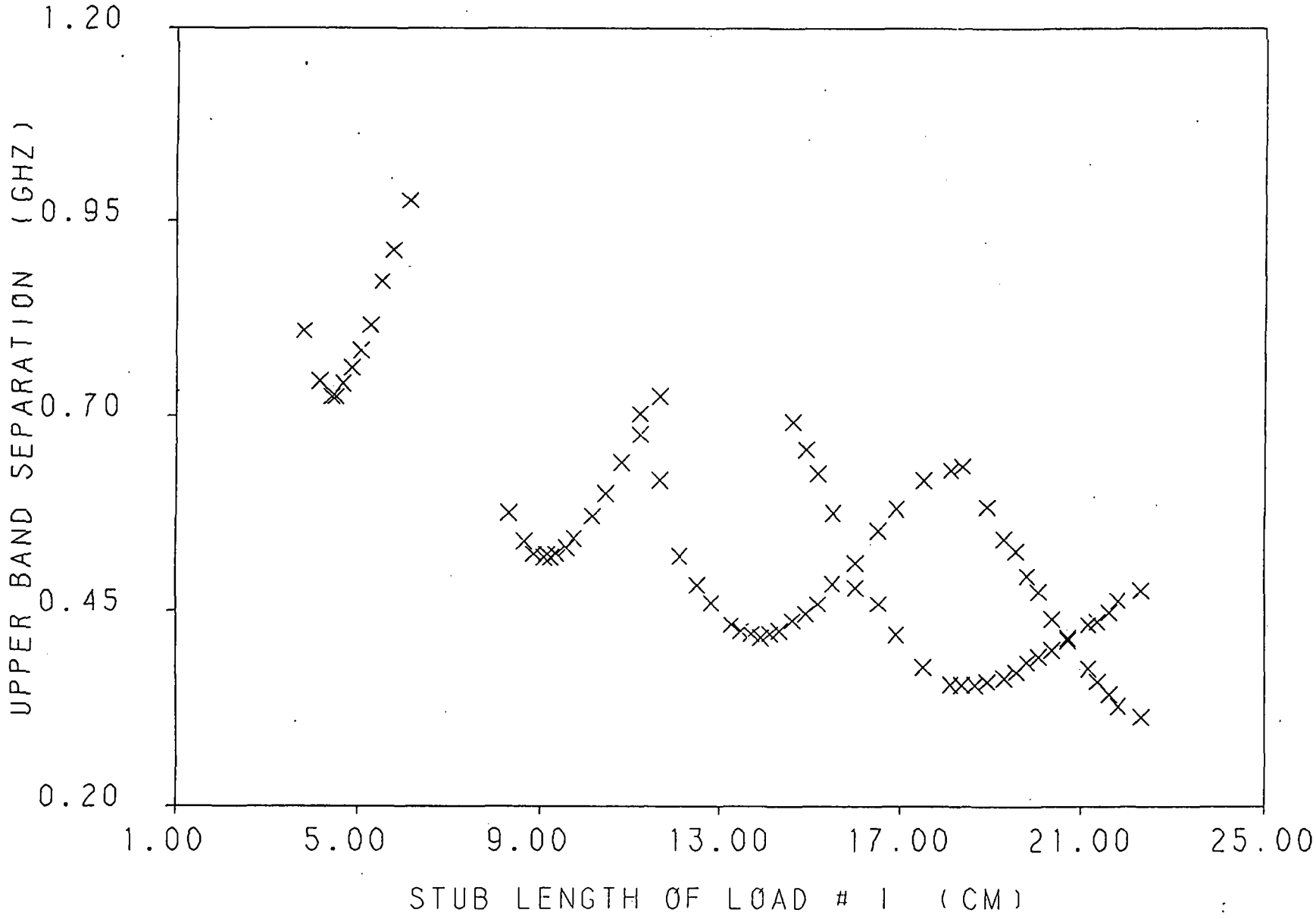

Fig. 3.117 Upper frequency band (the x-polarized band) separation verses the short circuit stub length of load #1 for a loaded 2.96 by 2.96 cm square patch with a feed location of (.85, .45 cm), and load insets of d = .60 cm .

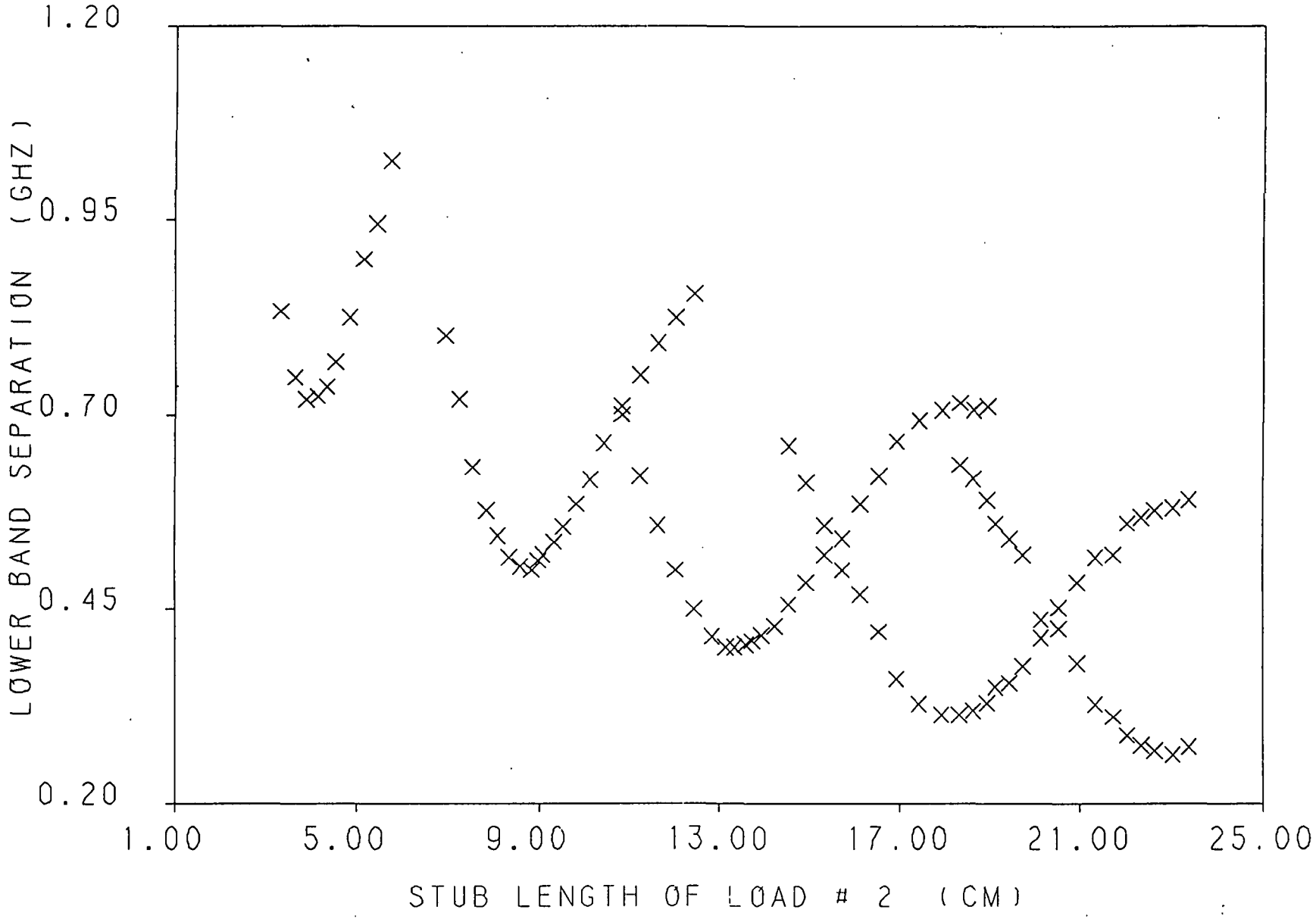

Fig. 3.118 Lower frequency band (the *y*-polarized band) separation verses the short circuit stub length of load #2 for a loaded 2.96 by 2.96 cm square patch with a feed location of (.85, .45 cm), and load insets of d = .60 cm .

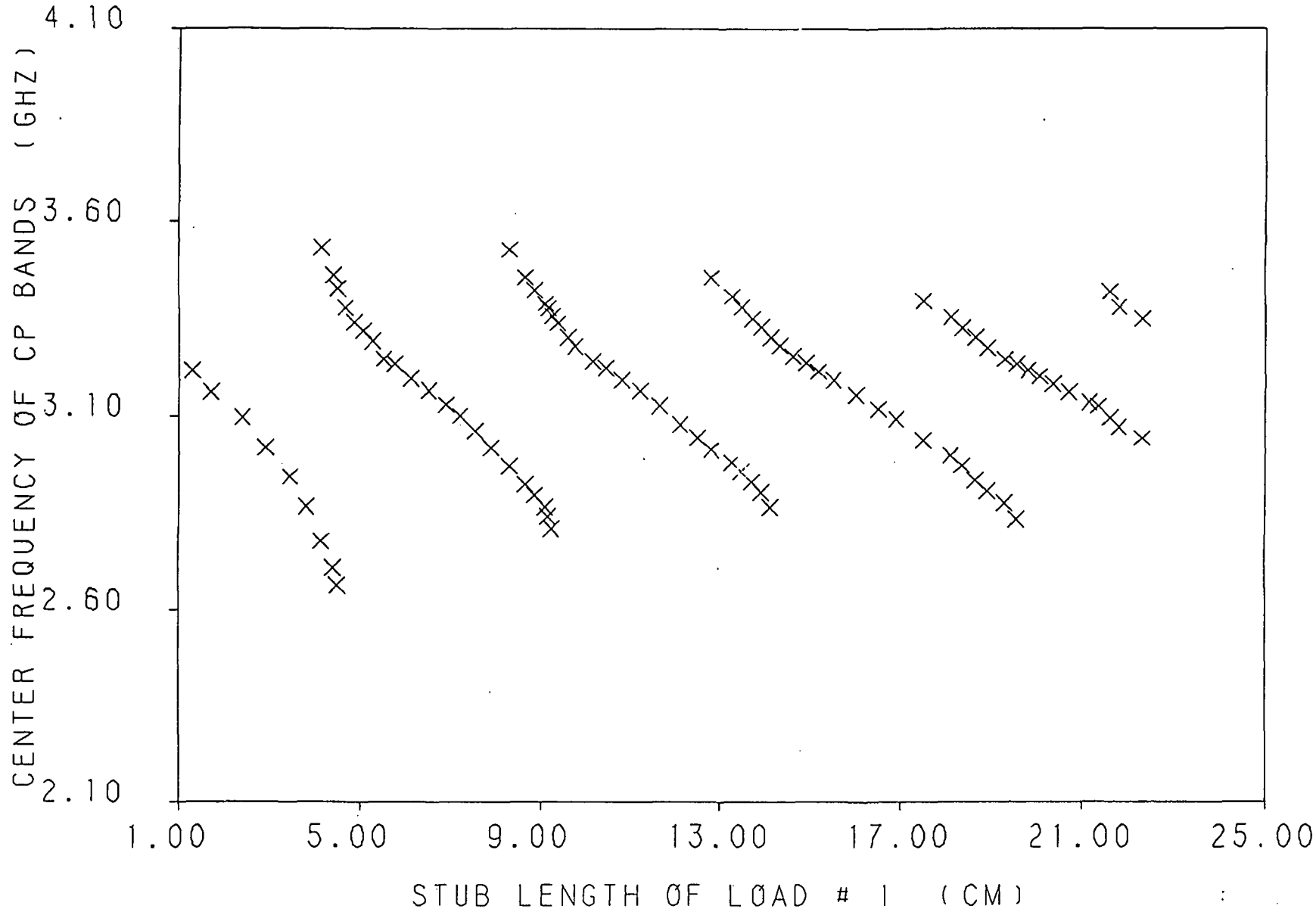

Fig. 3.119 Center frequency of cp bands verses the short circuit stub length of load # 1 for a loaded 2.96 by 2.96 cm square patch with a feed location of (.85, .45 cm), and load insets of d = .60 cm .

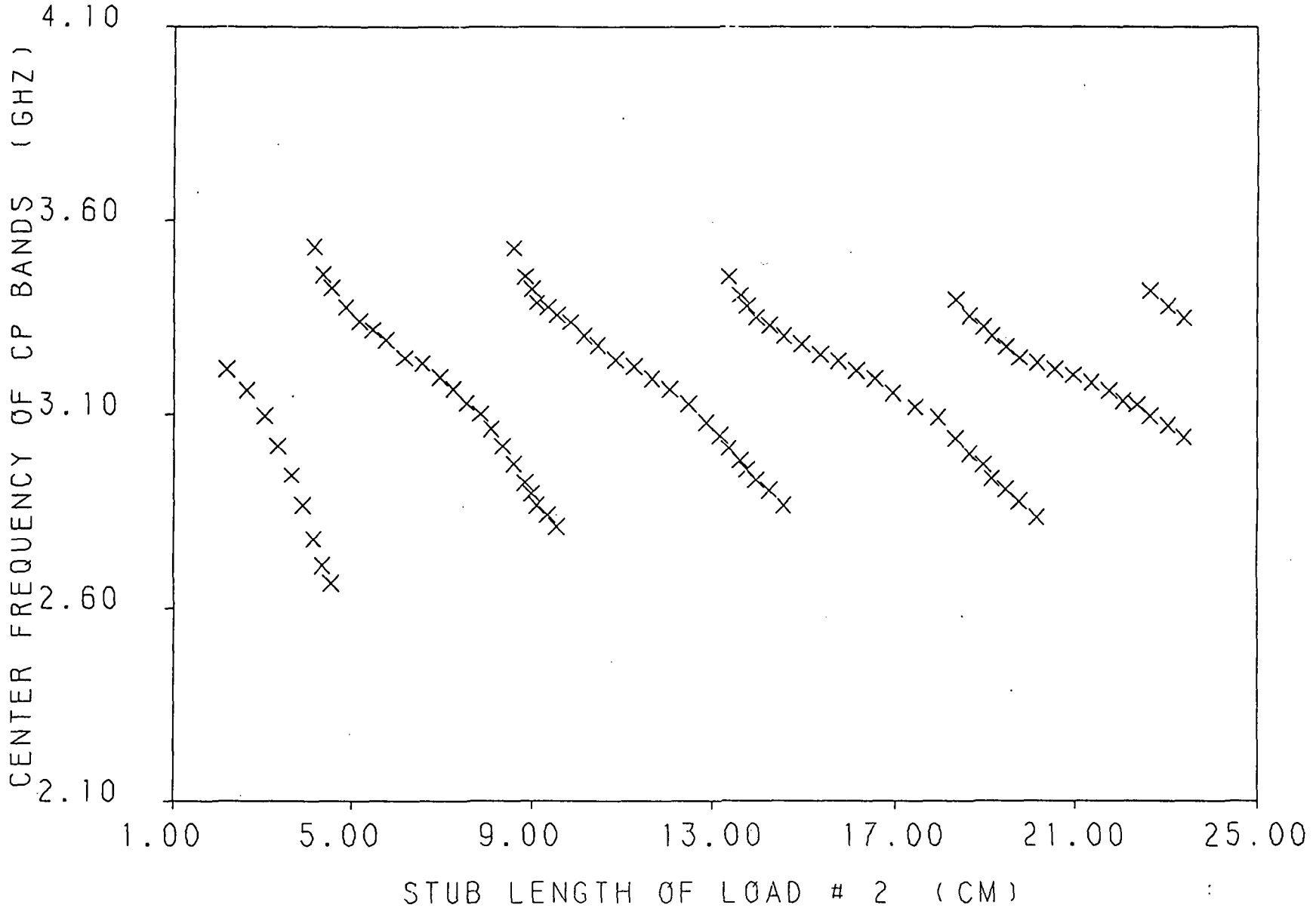

Fig. 3.120 Center frequency of cp bands verses the short circuit stub length of load # 2 for a loaded 2.96 by 2.96 cm square patch with a feed location of (.85, .45 cm), and load insets of d = .60 cm .

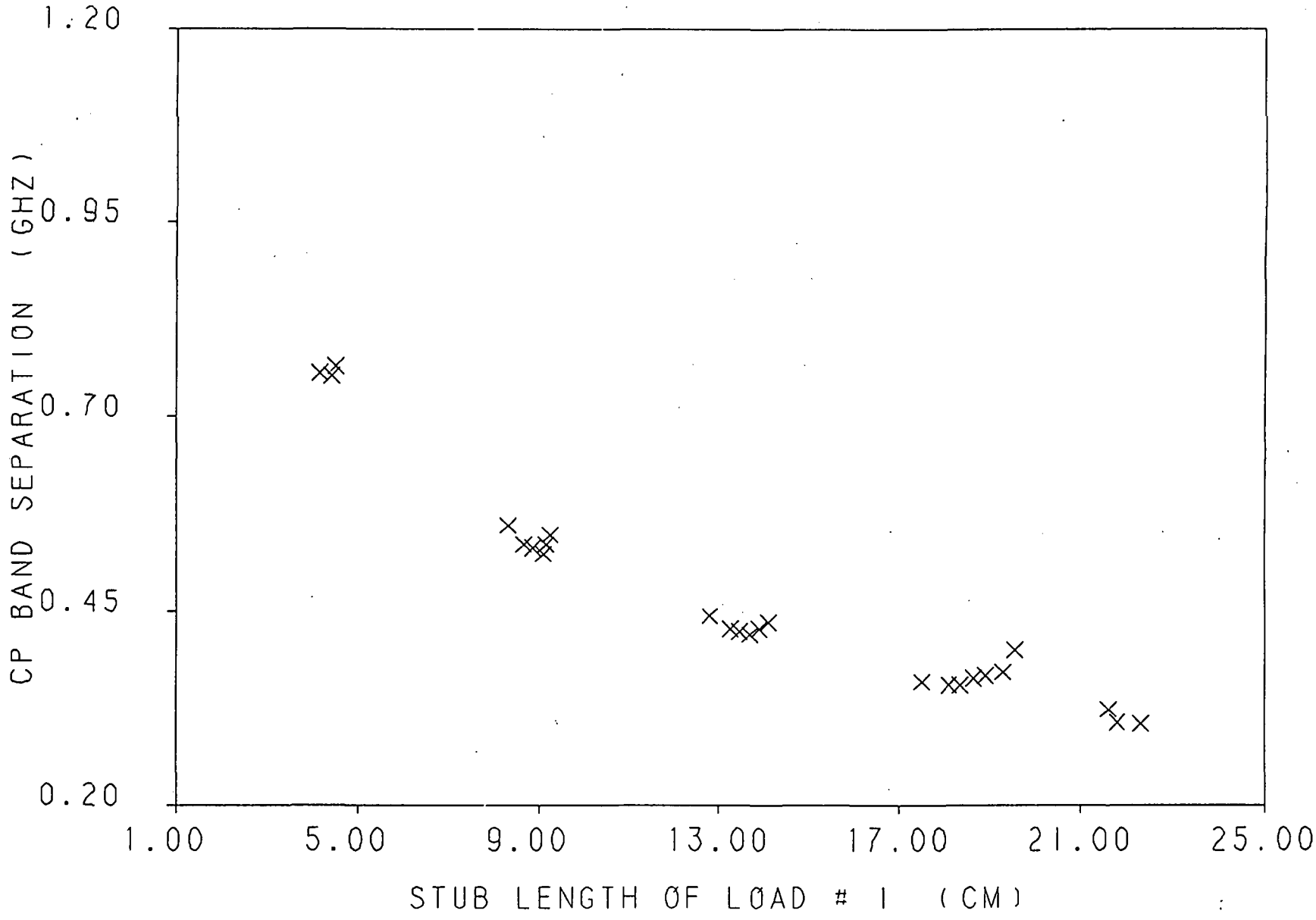

Fig. 3.121 Cp band separation verses the short circuit stub length of load # 1 for a loaded 2.96 by 2.96 cm square patch with a feed location of (.85, .45 cm), and load insets of d = .60 cm .

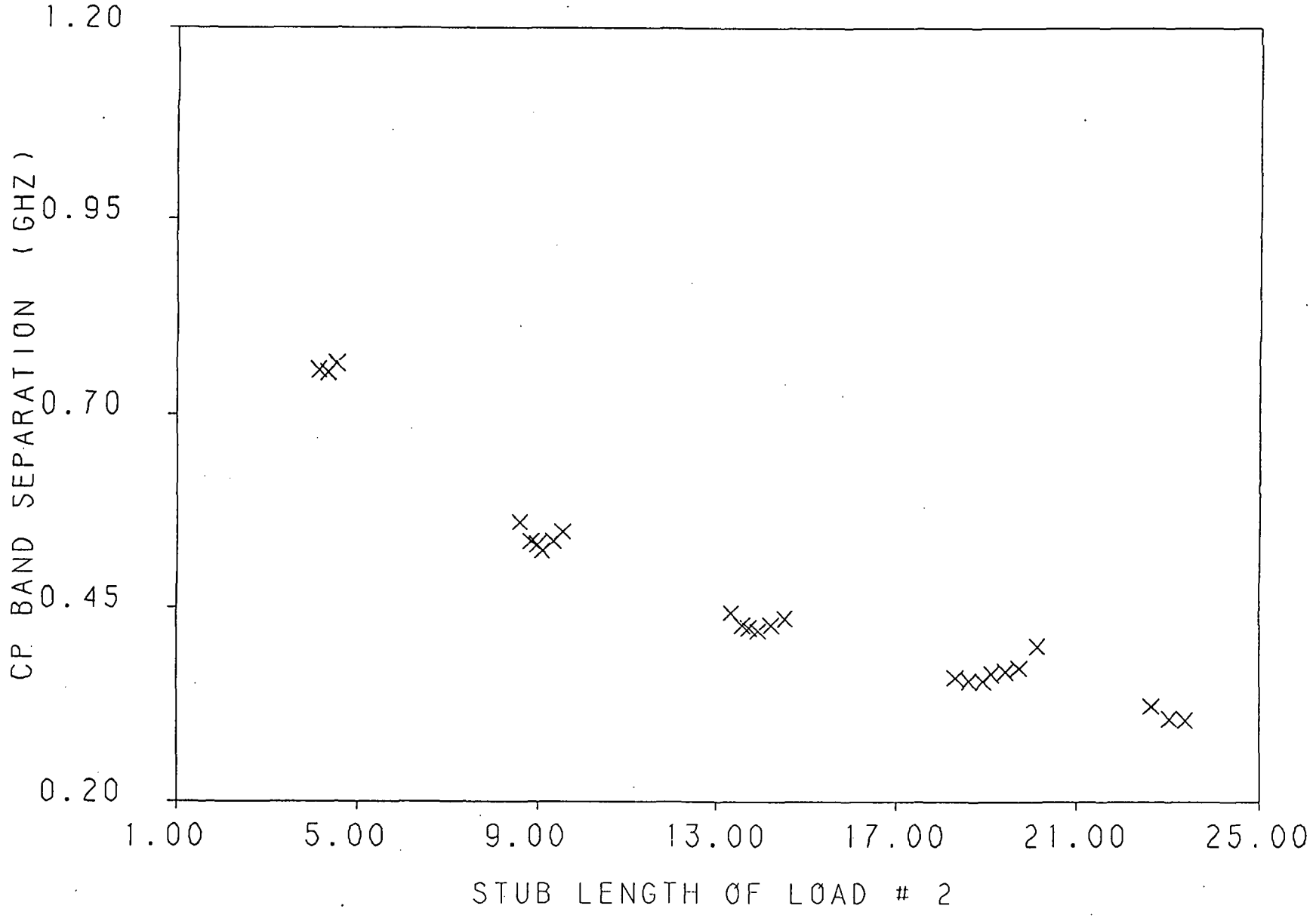

Fig. 3.122 Cp band separation verses the short circuit stub length of load # 2 for a loaded 2.96 by 2.96 cm square patch with a feed location of (.85, .45 cm), and load insets of d = .60 cm .

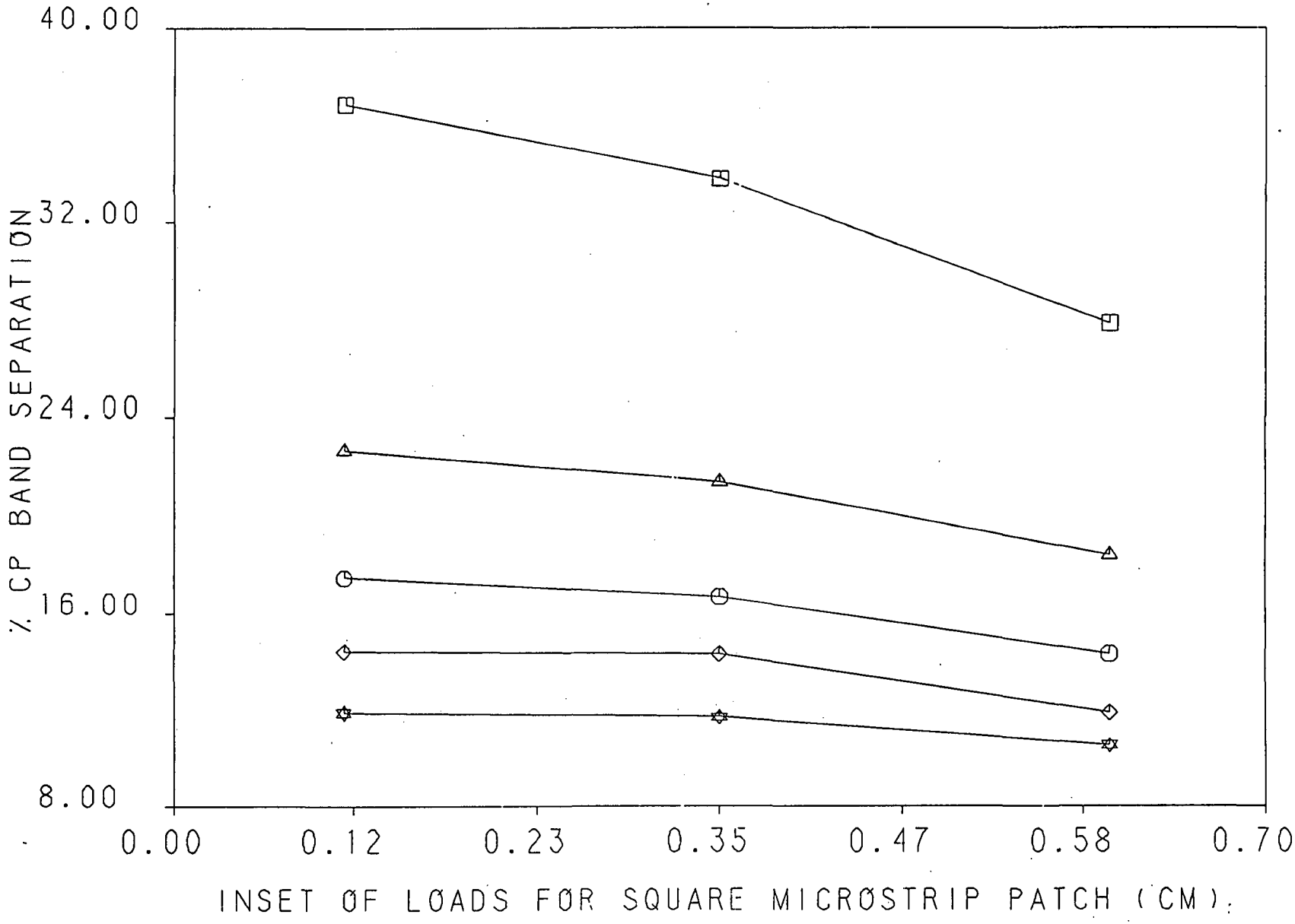

Fig. 3.123 Percentage cp band separation for modes 1 through 5 verses the inset , d, of the loads for a loaded 2.96 by 2.96 cm square patch.

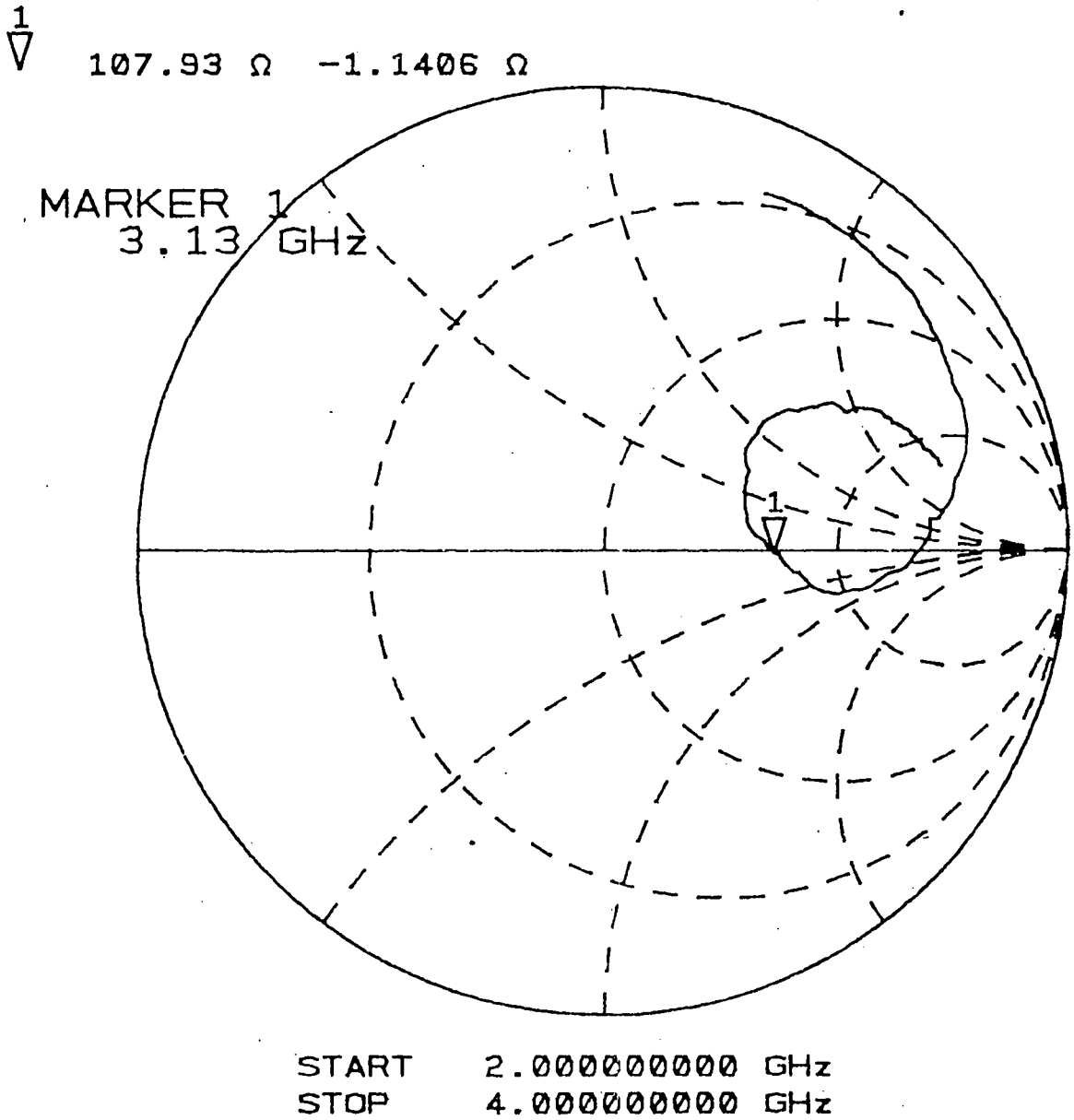

Fig. 3.124 Measured impedance at one port with 50 ohm load on other port.

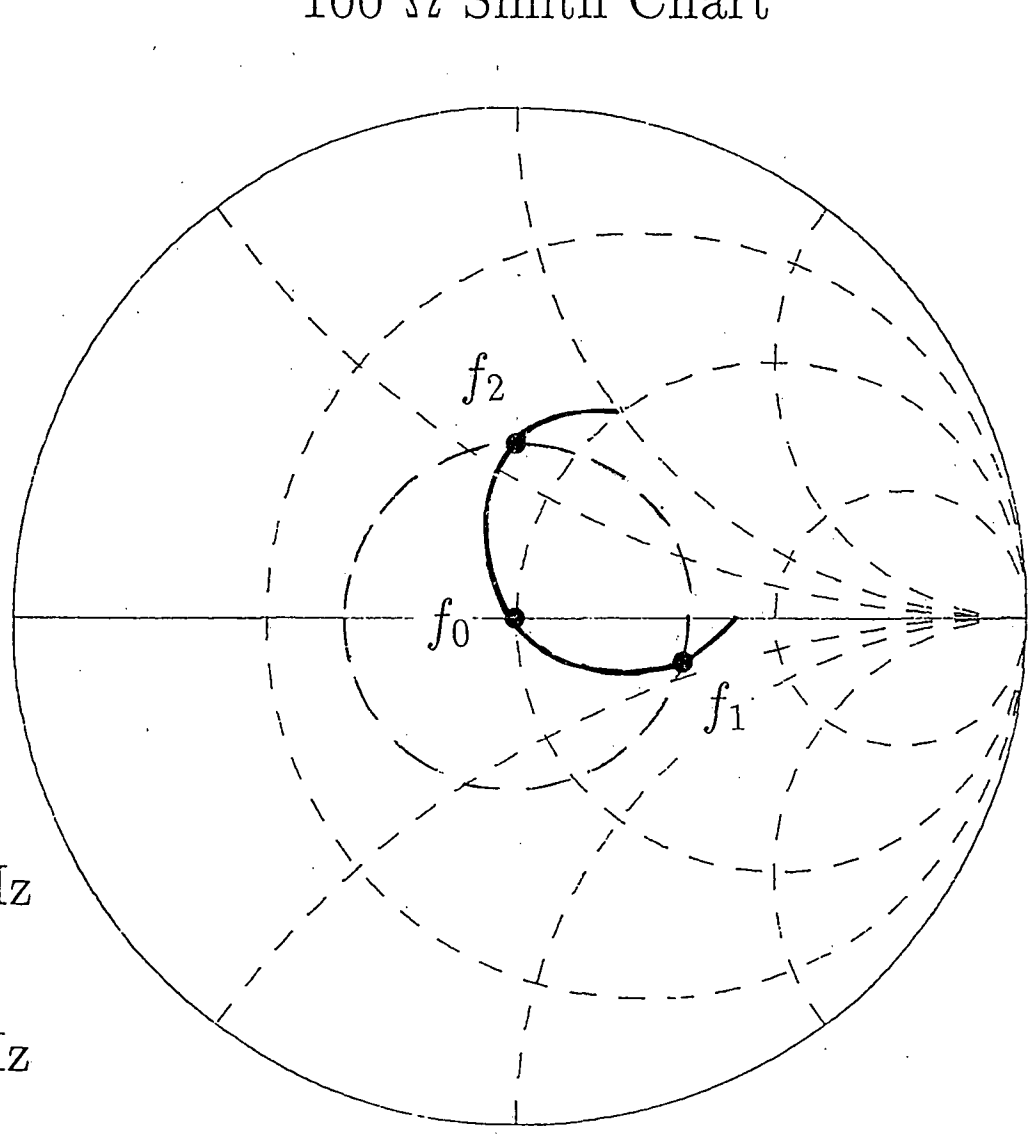

Fig. 3.125 Impedance locus on 100 ohm Smith Chart.

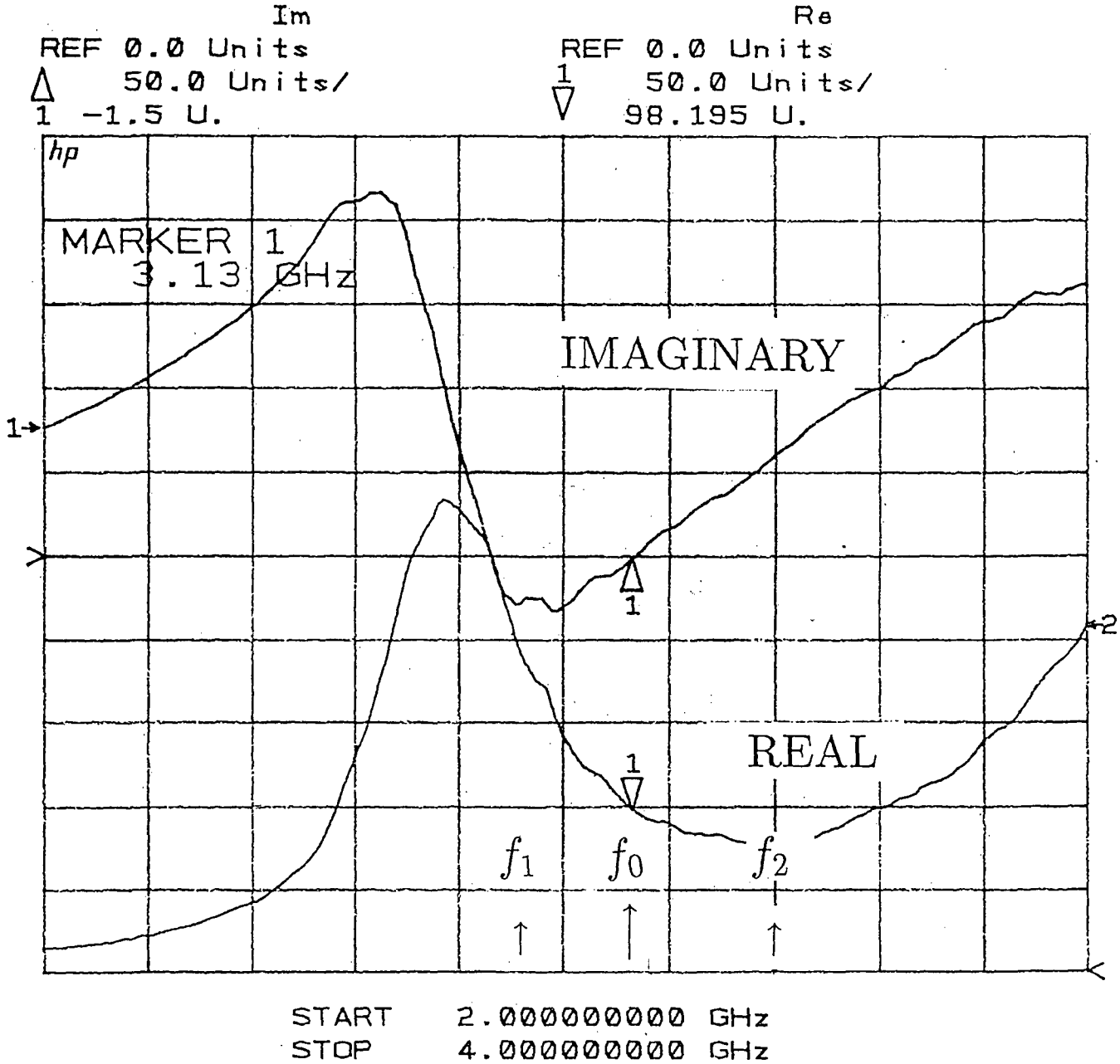

Ω

Fig. 3.126 Real and imaginary part of impedance.

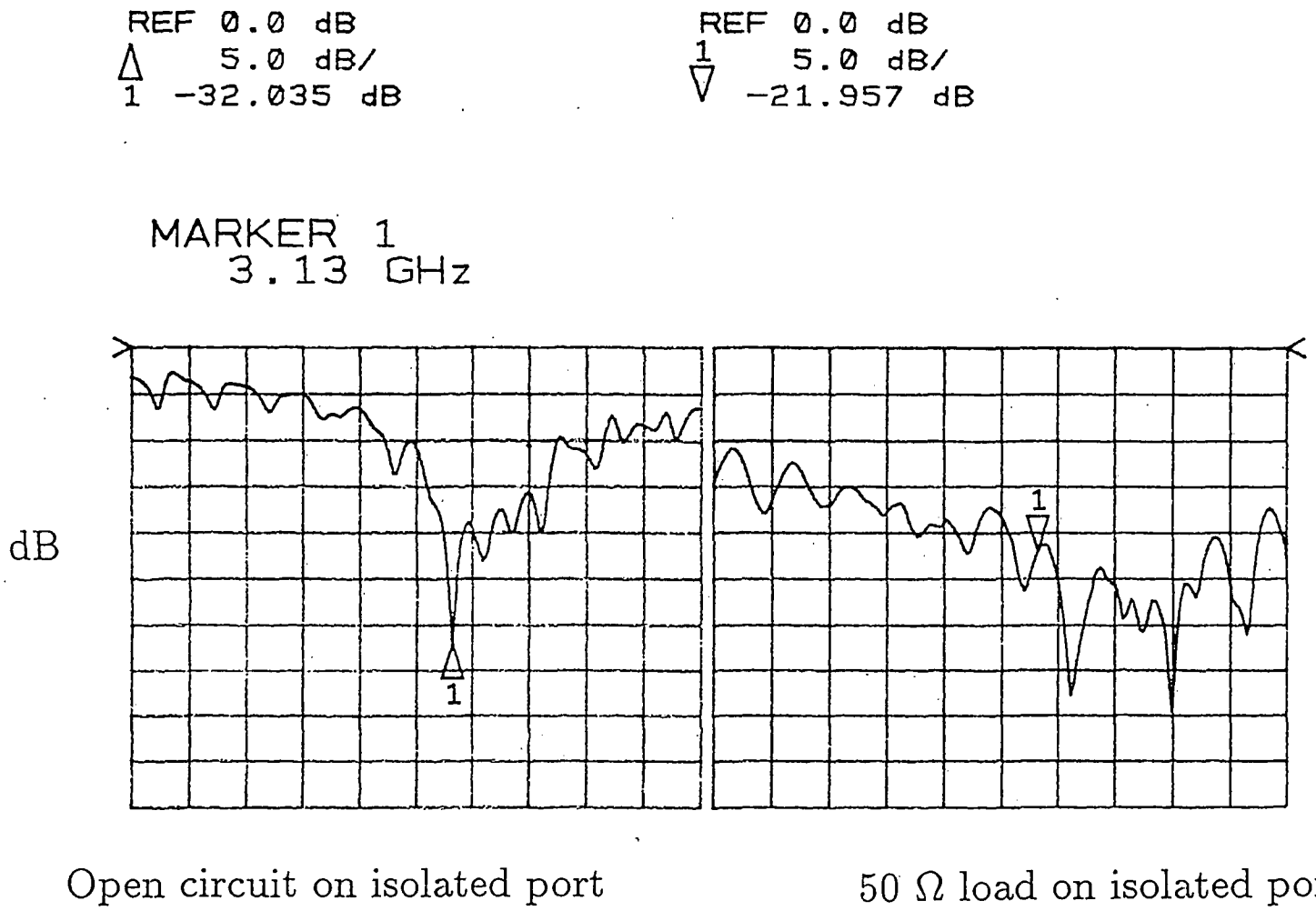

Open circuit on isolated port

50 Ω load on isolated port

Fig. 3.127 Reflection coefficient at hybrid.

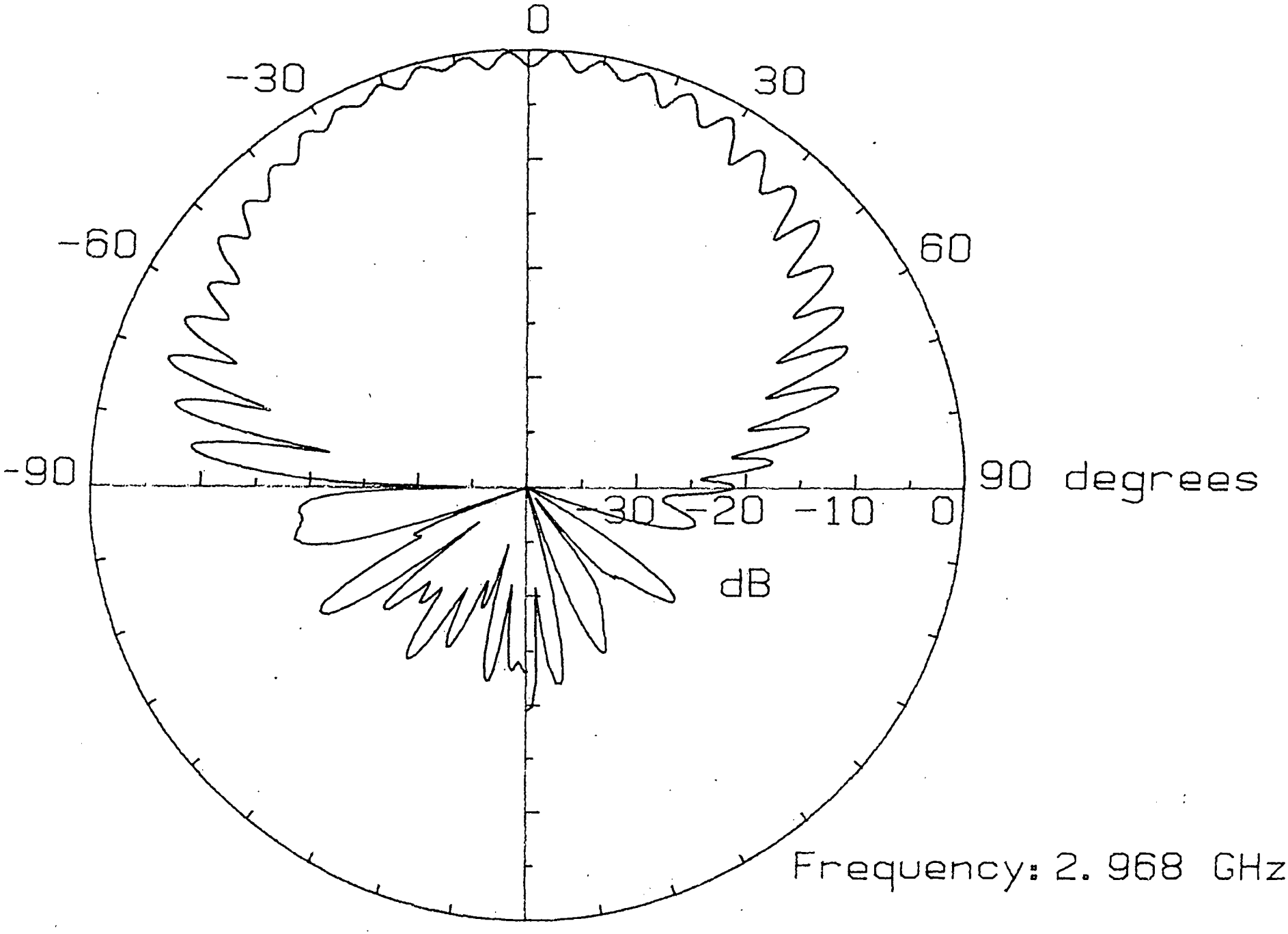

Fig. 3.128 Spinning linear radiation pattern 6% below resonant frequency at 2.968 GHz.

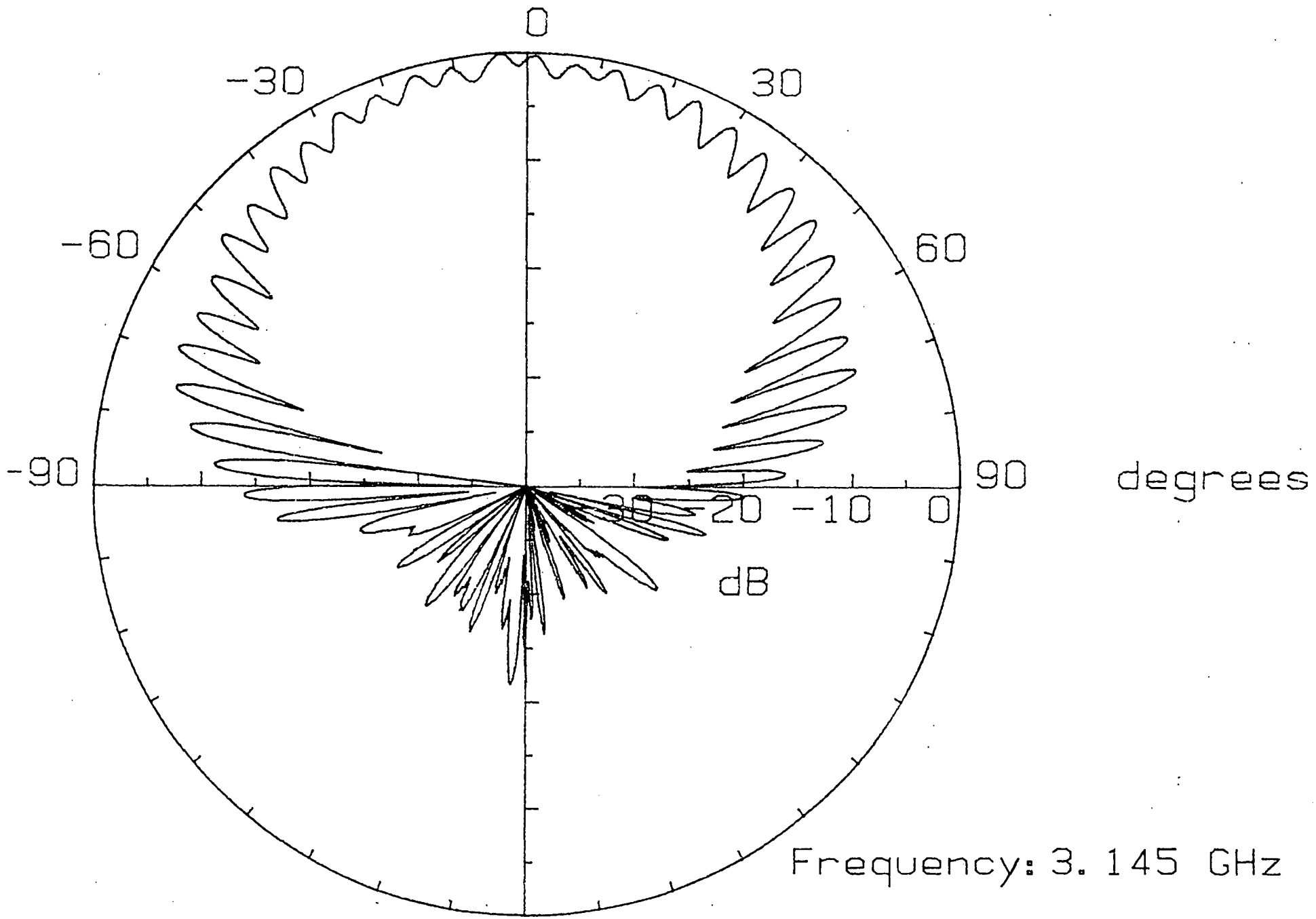

Fig. 3.129 Spinning linear radiation pattern at resonant frequency of 3.145 GHz.

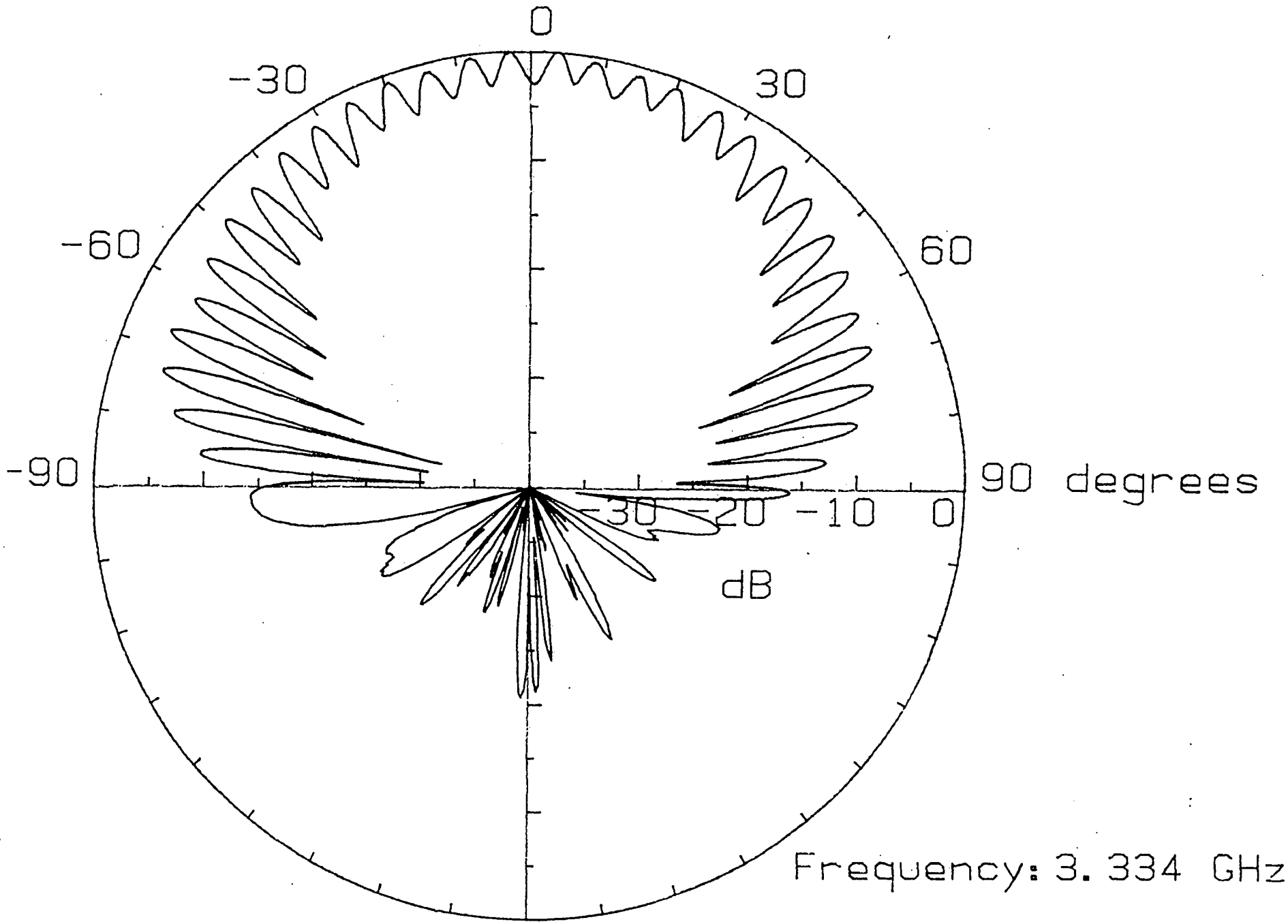

Fig. 3.130 Spinning linear radiation pattern 6% above resonant frequency at 3.334 GHz.

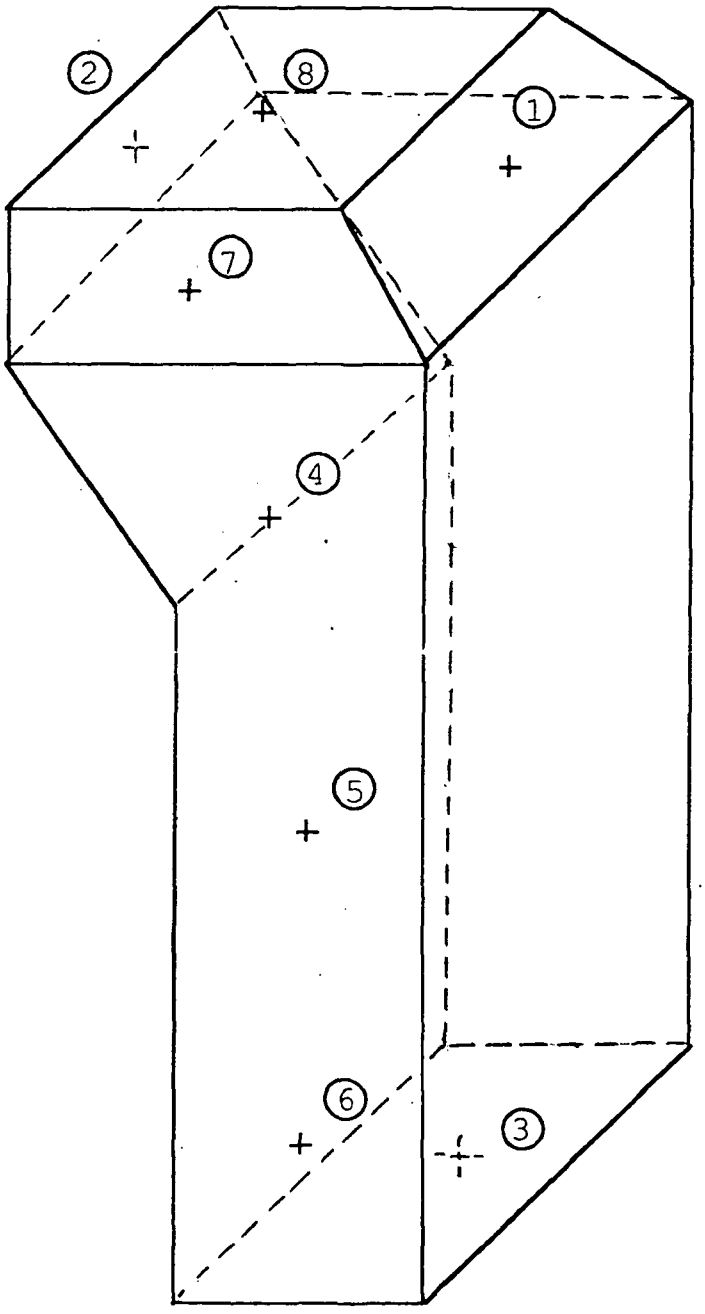

Fig. 4.1 Three dimensional view of the backpack model.

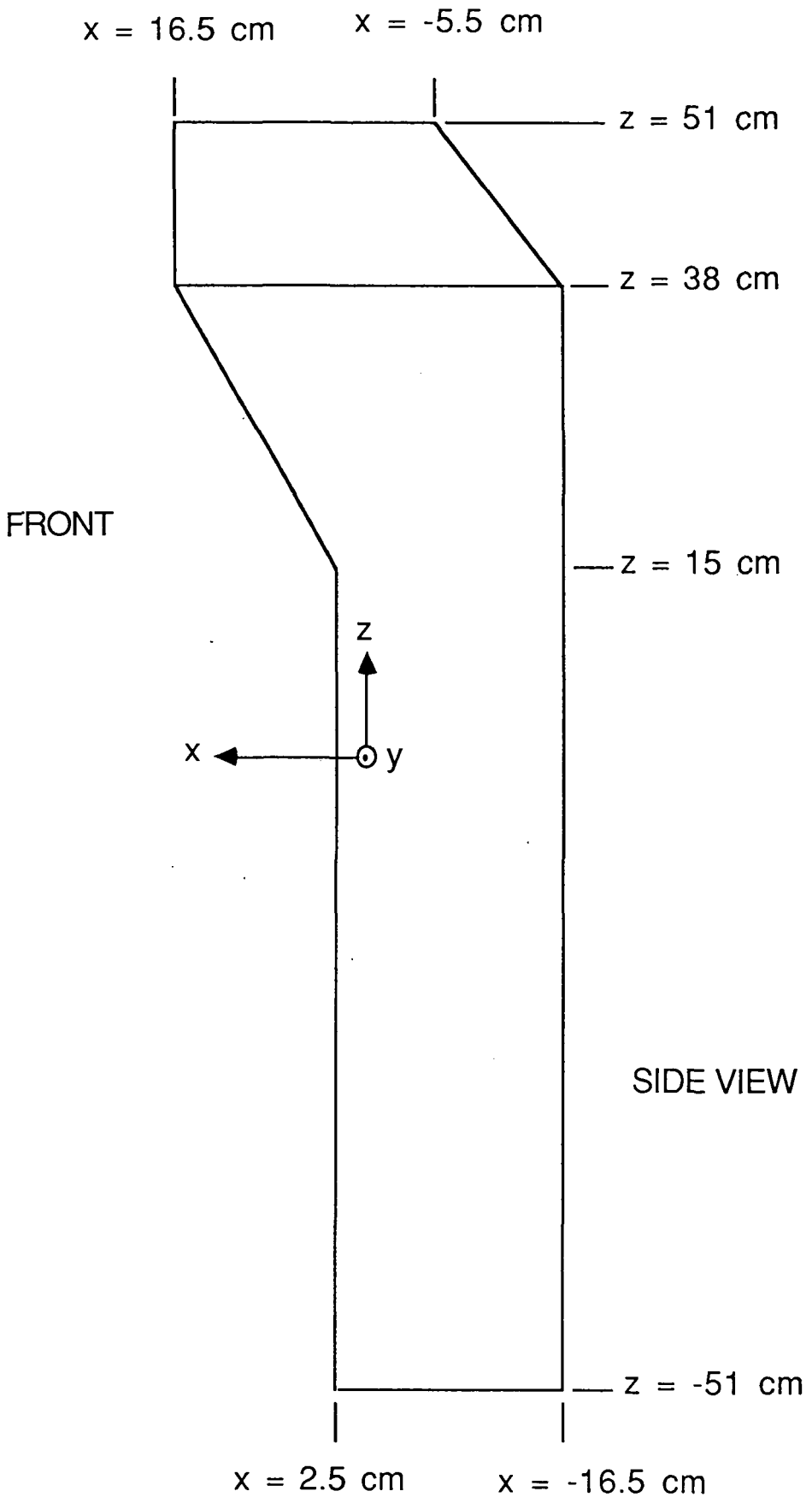

Fig. 4.2 Side view detail of the backpack model.

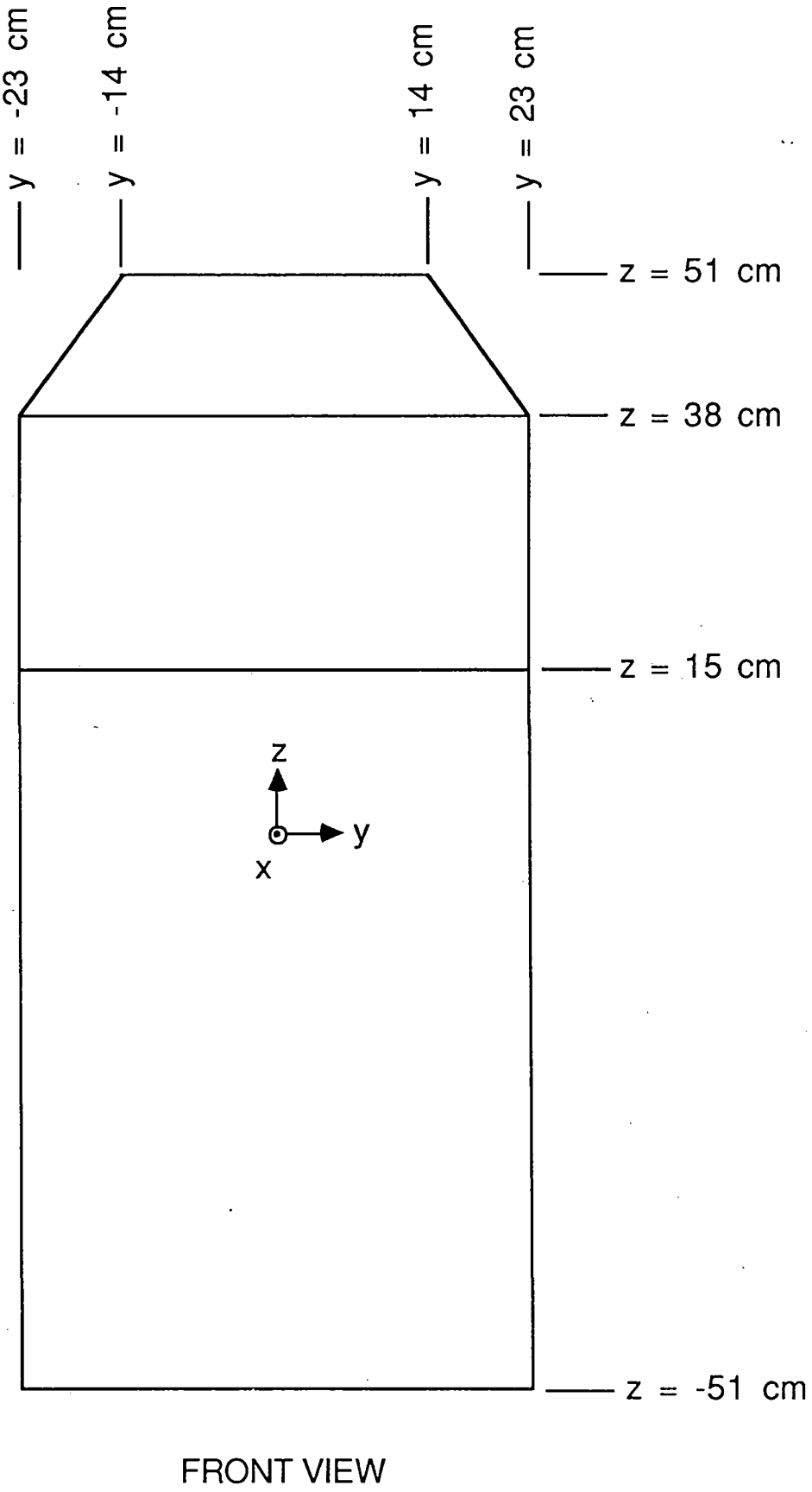

Fig. 4.3 Front view detail of the backpack model.

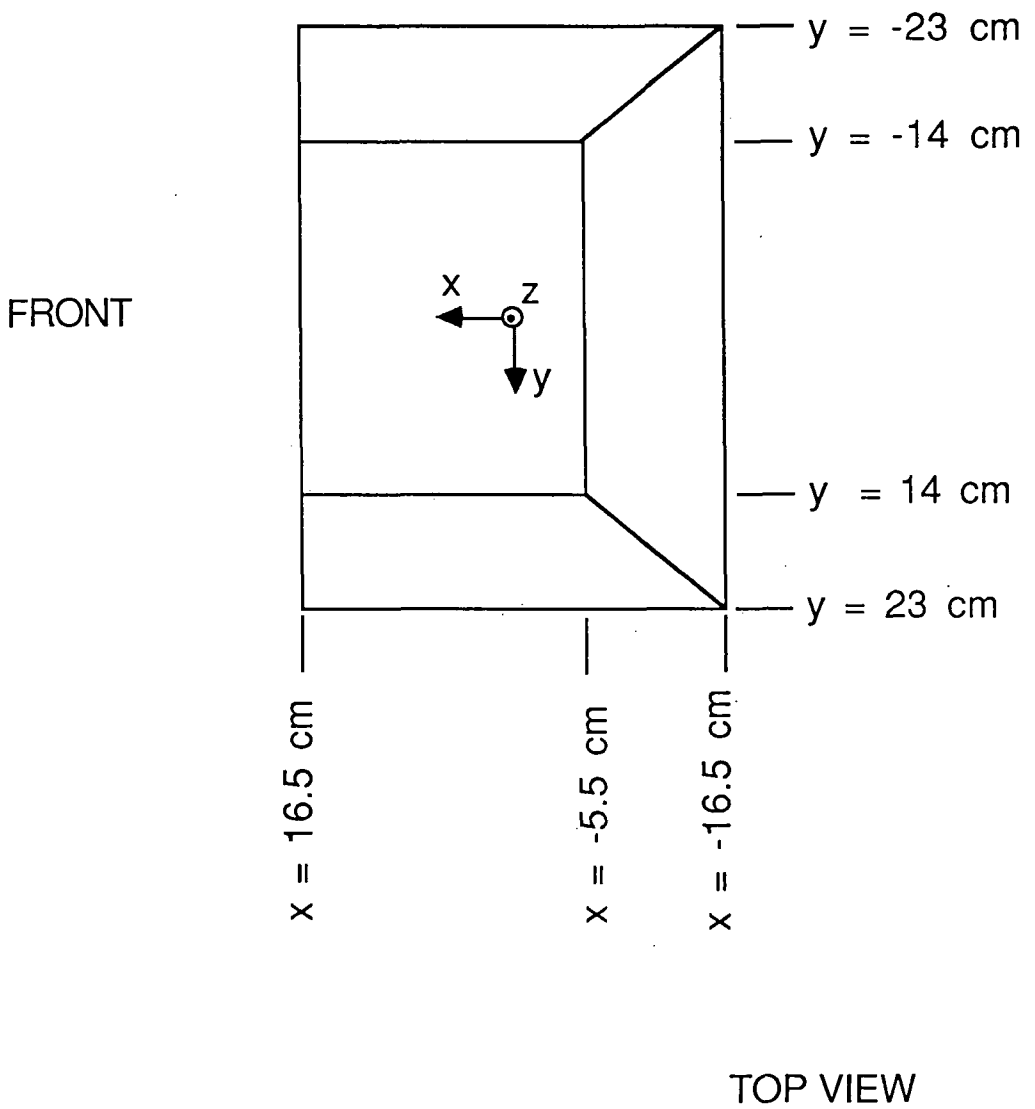

Fig. 4.4 Top view detail of the backpack model.

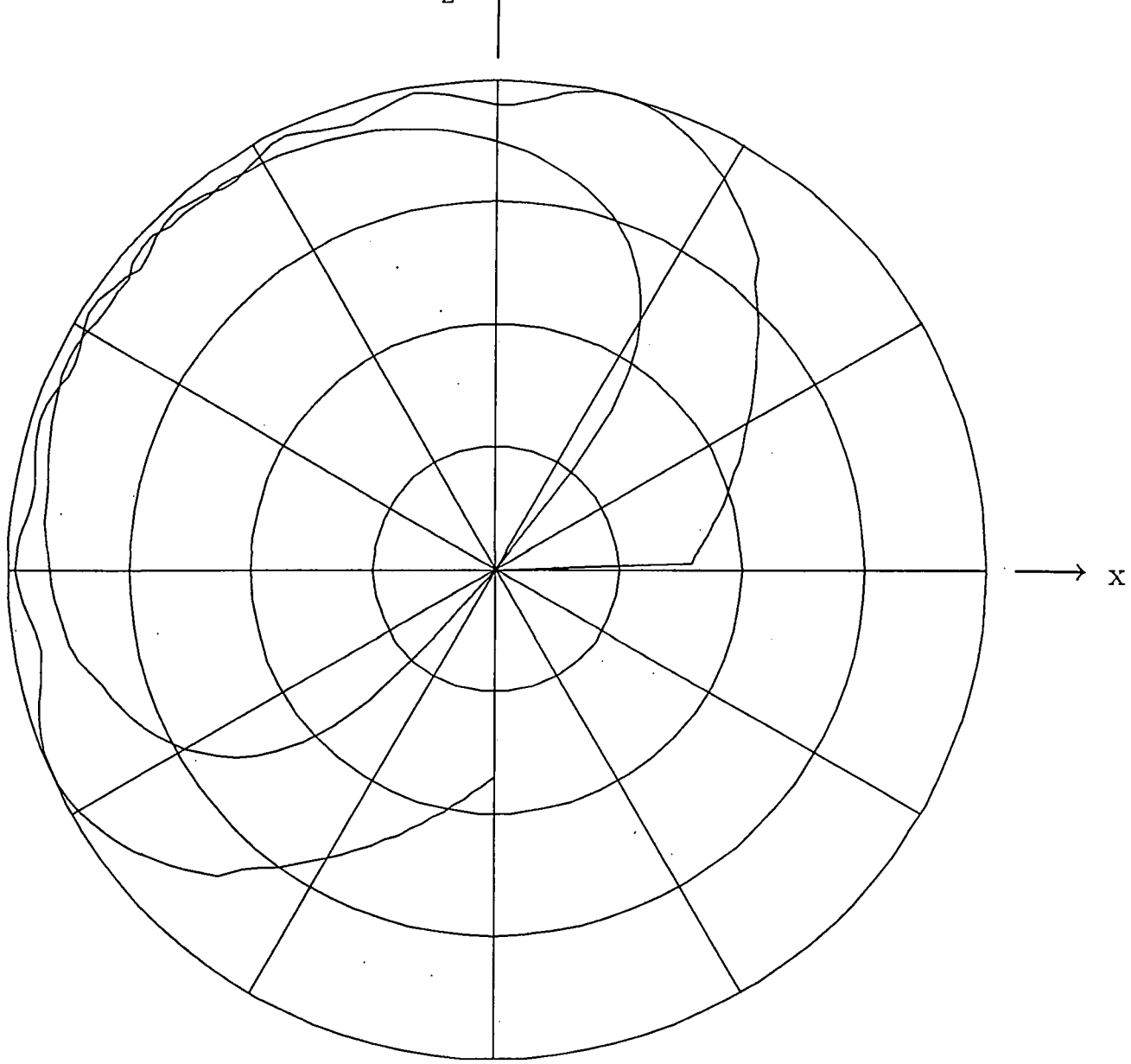

Fig. 4.5 Normalized far field radiation pattern of antenna at position 1 on backpack - 10 dB/division (ϕ = 0°).

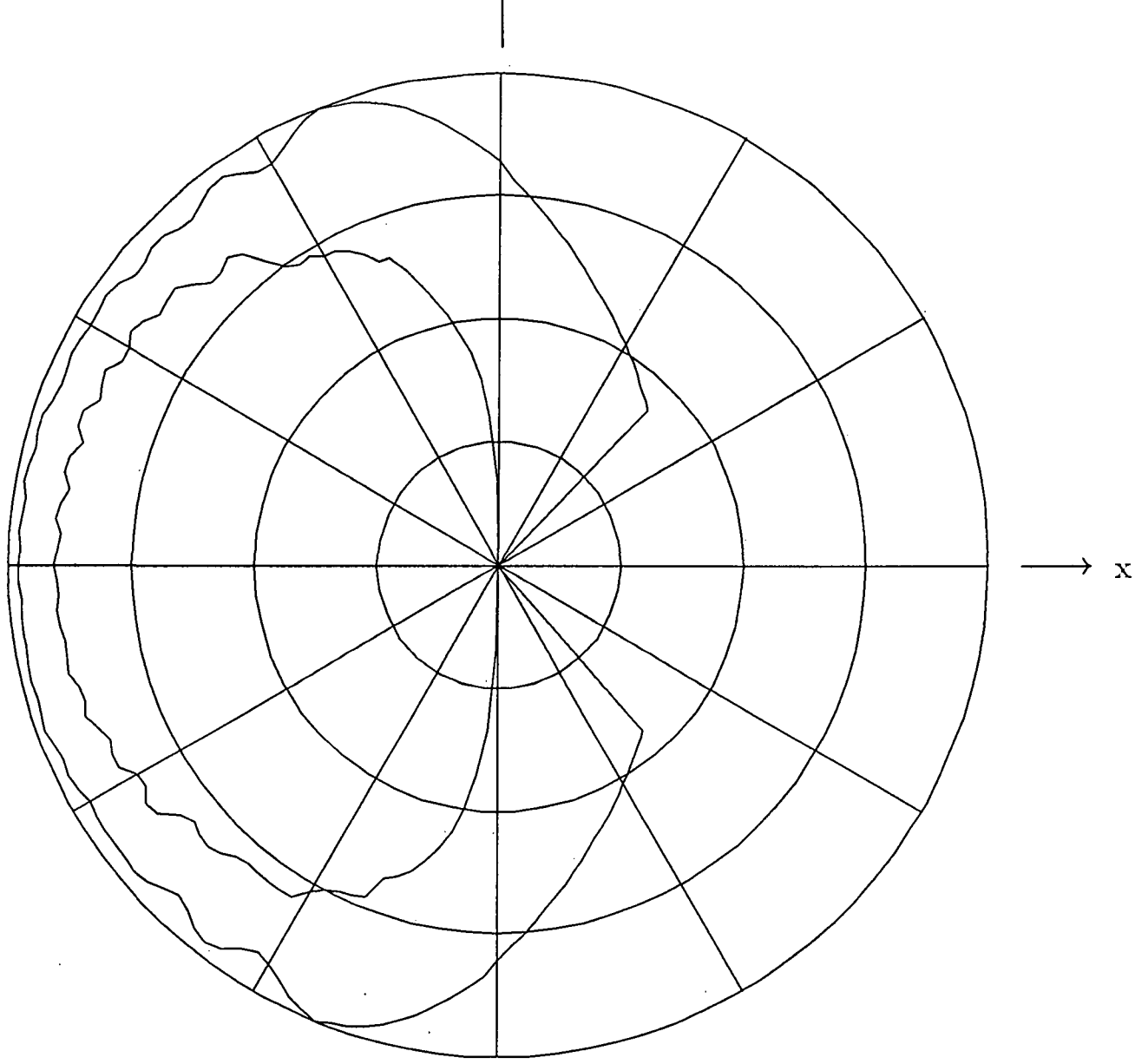

Fig. 4.6 Normalized far field radiation pattern of antenna at position 1 on backpack - 10 dB/division (Θ = 90°).

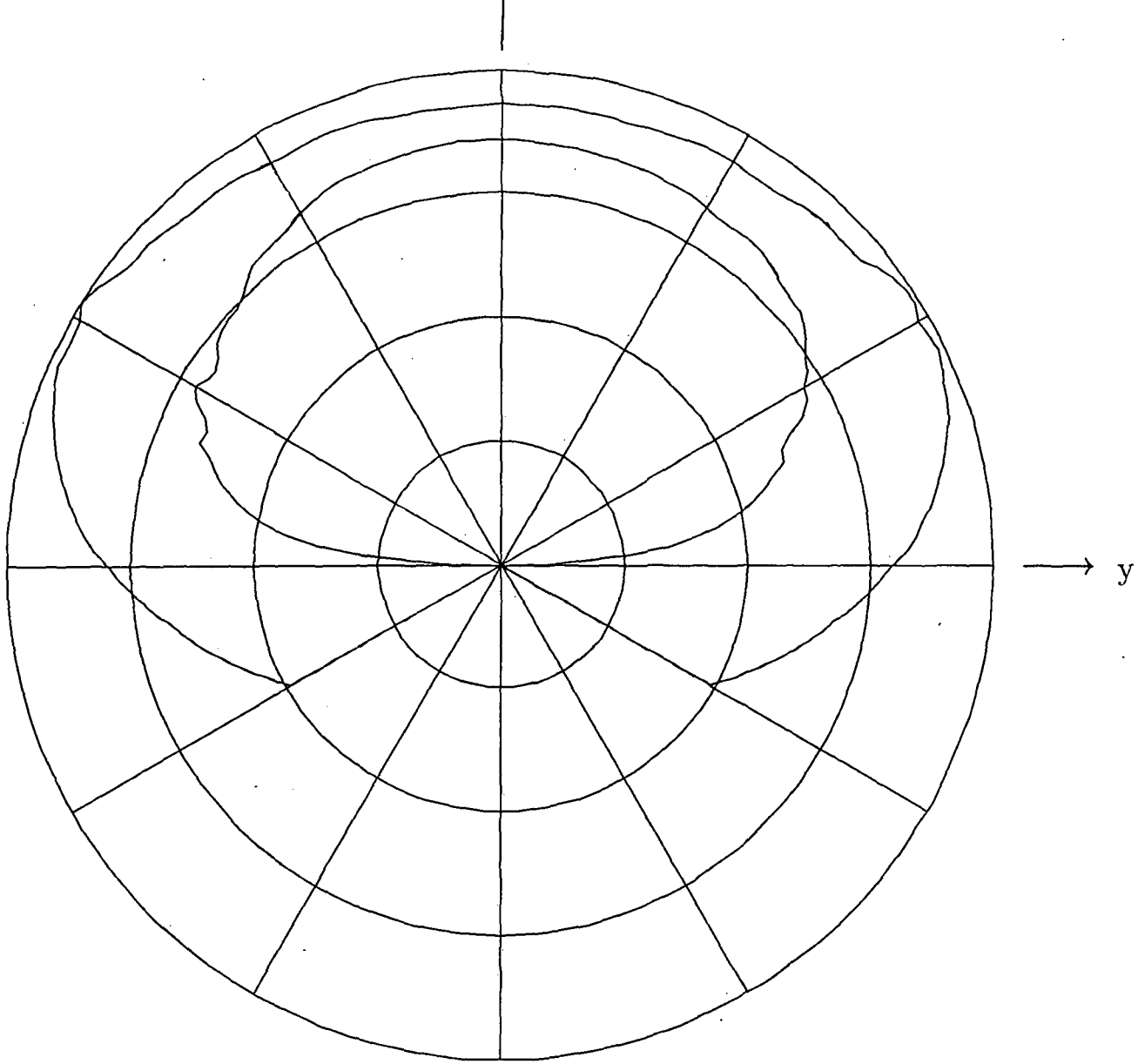

Fig. 4.7 Normalized far field radiation pattern of antenna at position 1 on backpack - 10 dB/division (ϕ = 90°).

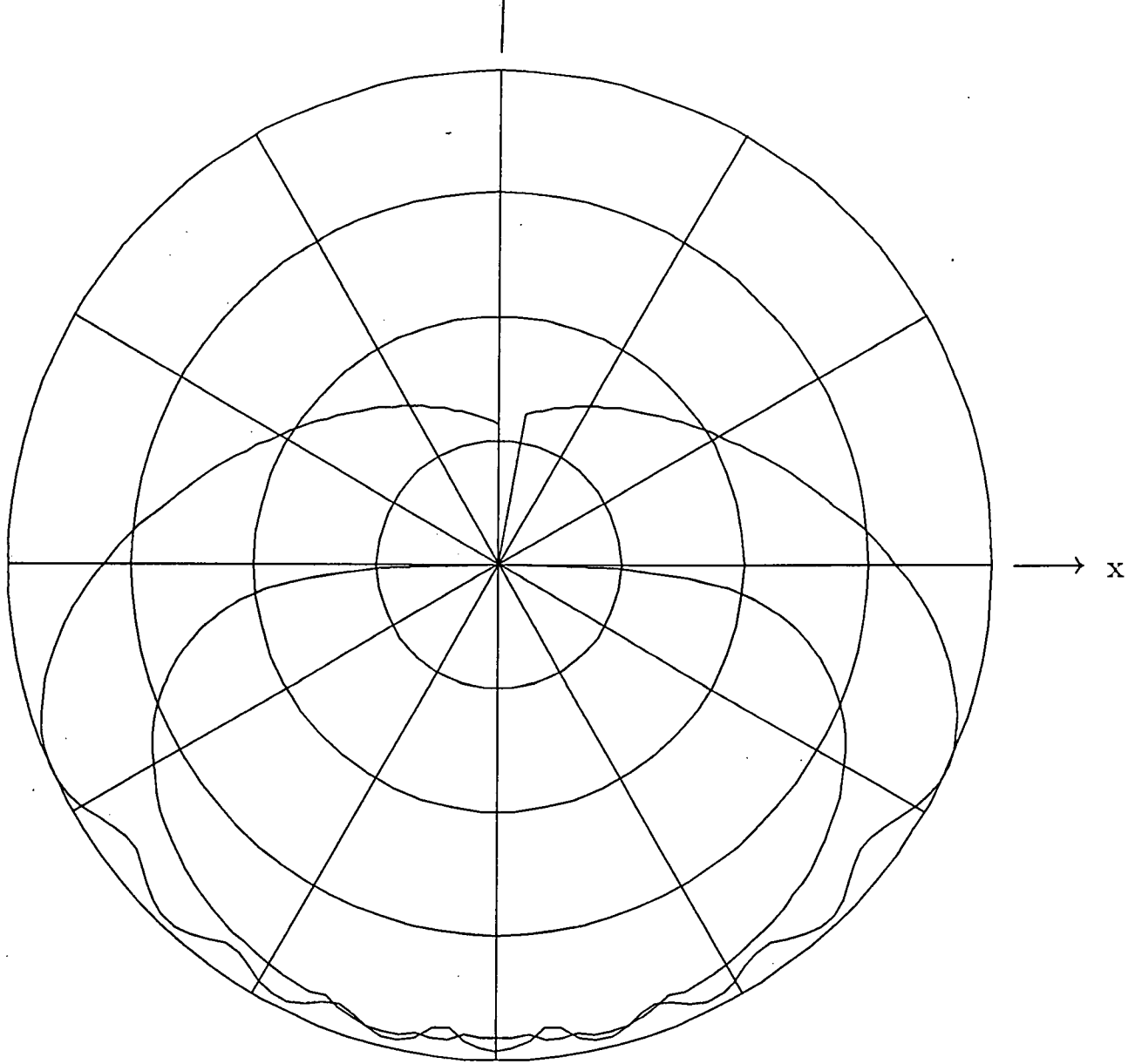

Fig. 4.8 Normalized far field radiation pattern of antenna at position 3 on backpack - 10 dB/division (ϕ = 0°).

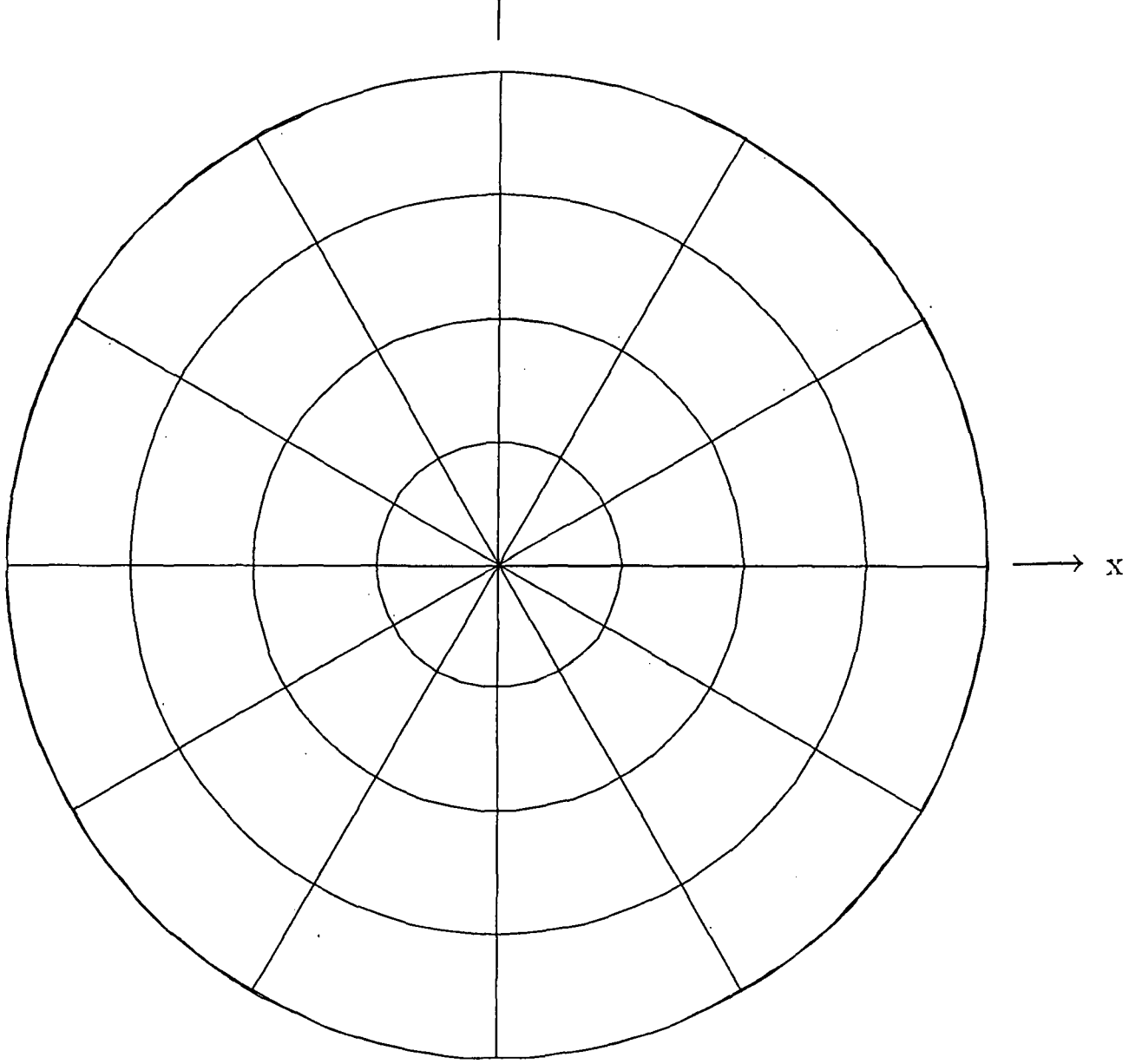

Fig. 4.9 Normalized far field radiation pattern of antenna at position 3 on backpack - 10 dB/division (Θ = 90°).

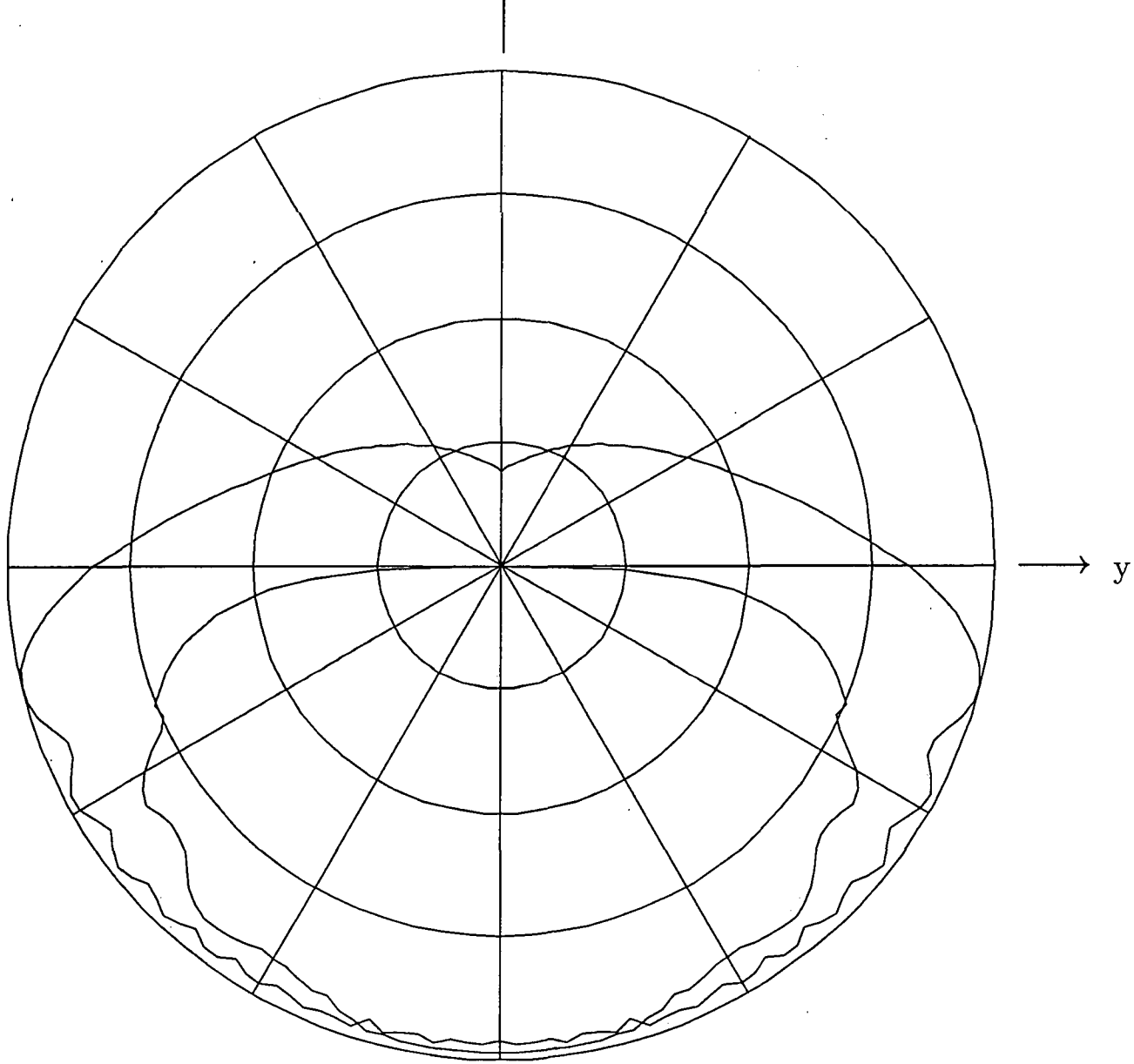

Fig. 4.10 Normalized far field radiation pattern of antenna at position 3 on backpack - 10 dB/division (ϕ = 90°).

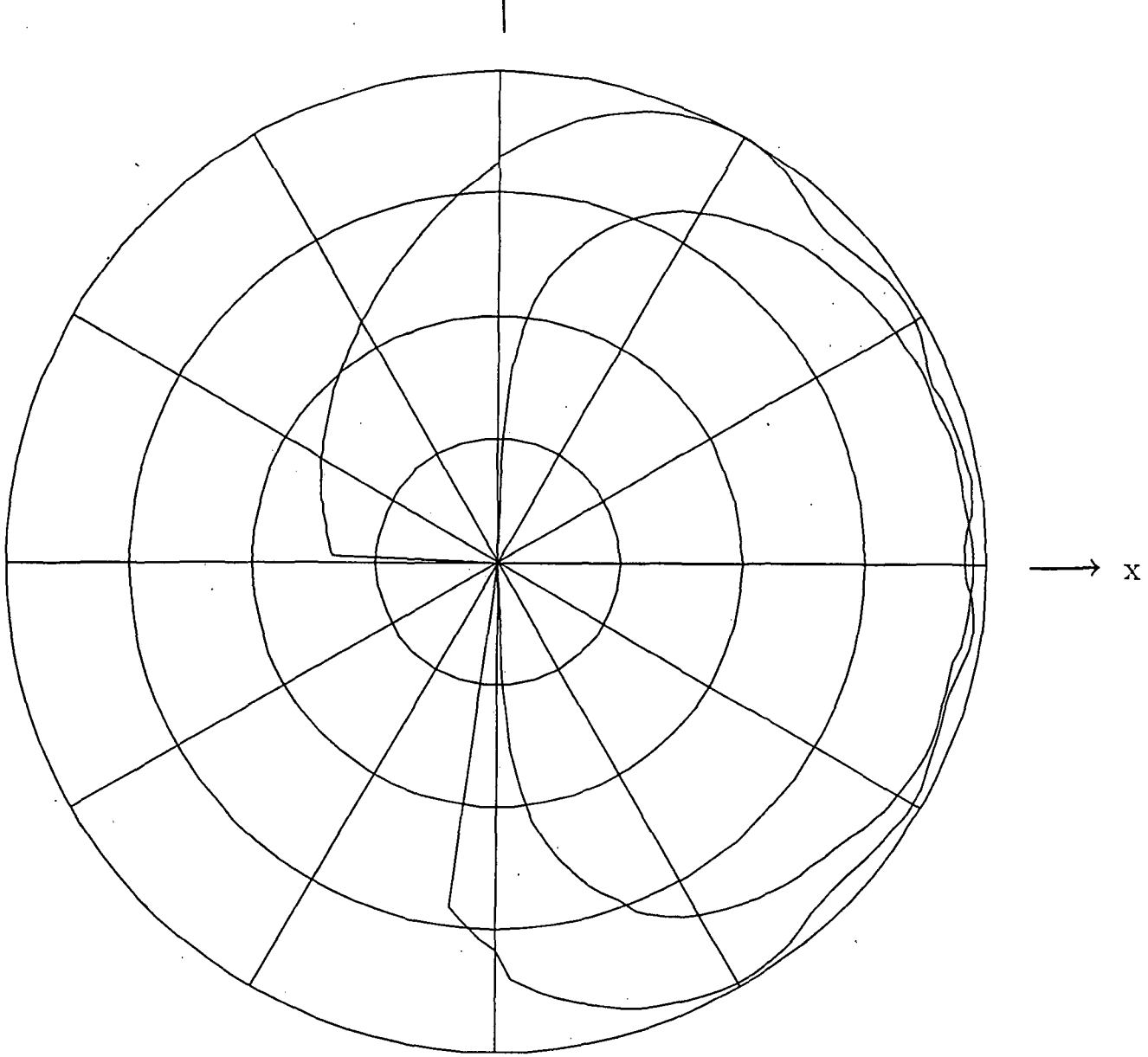

Fig. 4.11 Normalized far field radiation pattern of antenna at position 2 on backpack - 10 dB/division (ϕ = 0^{o}).

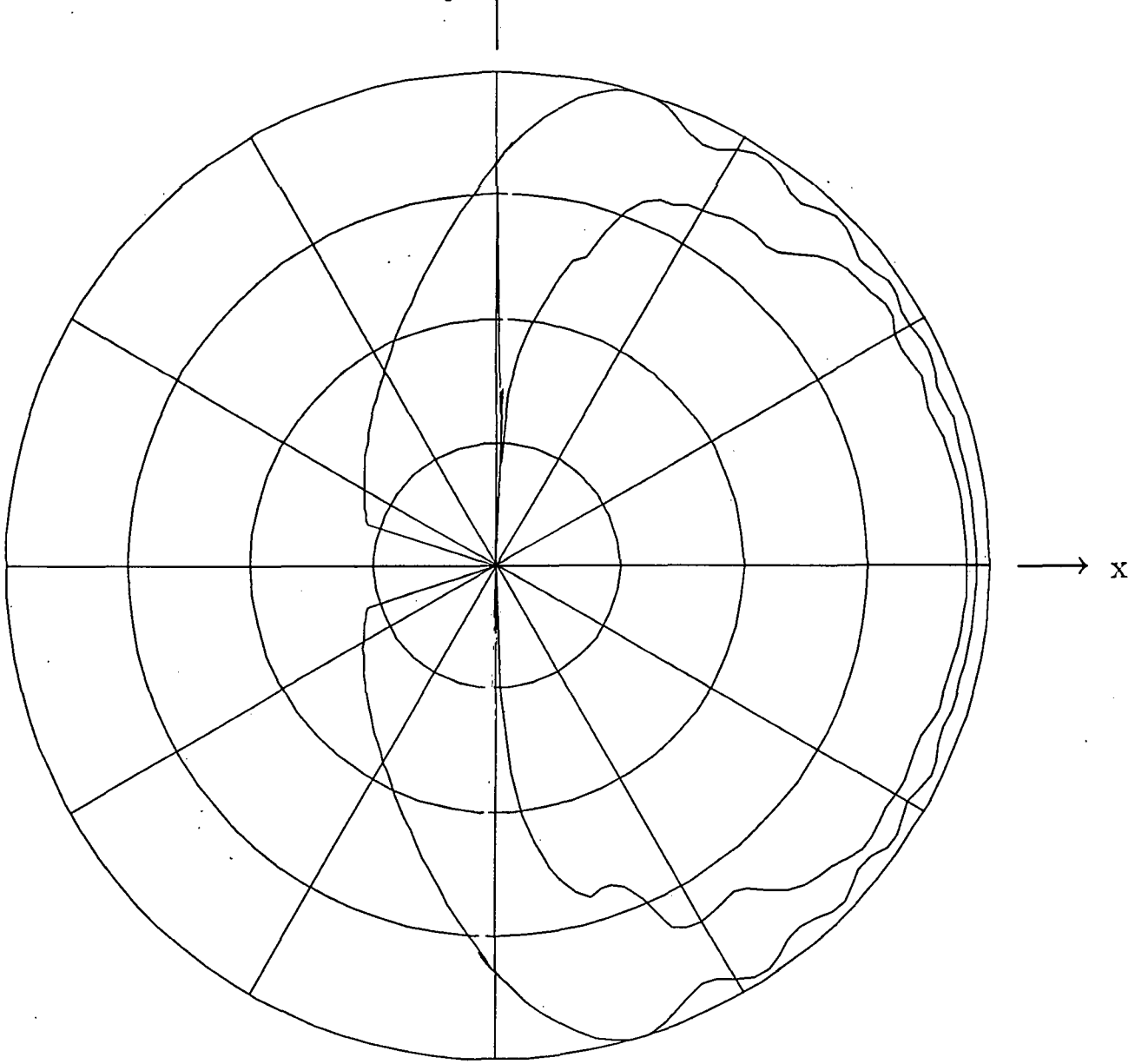

Fig. 4.12 Normalized far field radiation pattern of antenna at position 2 on backpack - 10 dB/division (Θ = 90°).

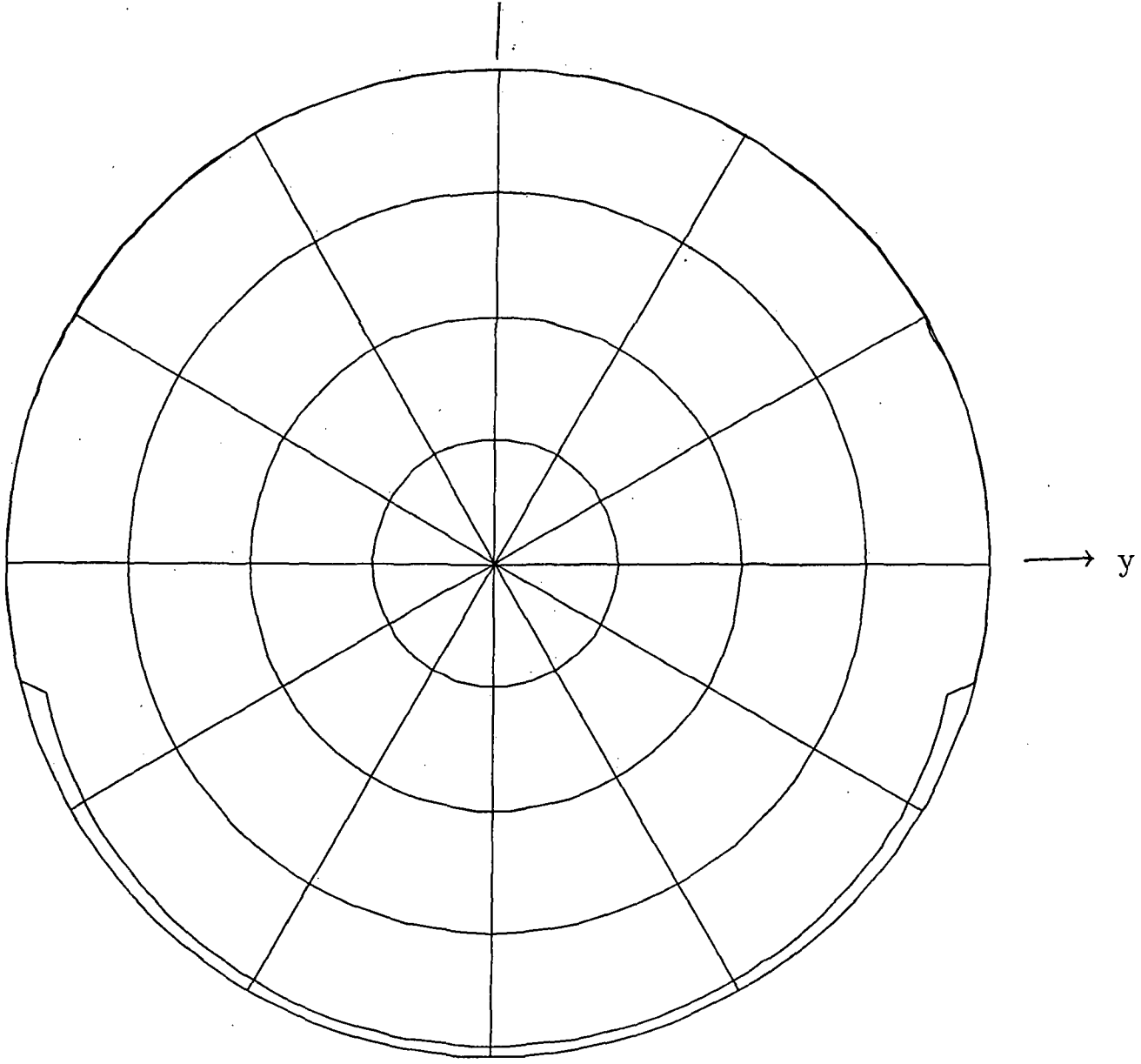

Fig. 4.13 Normalized far field radiation pattern of antenna at position 2 on backpack - 10 dB/division (ϕ = 90°).

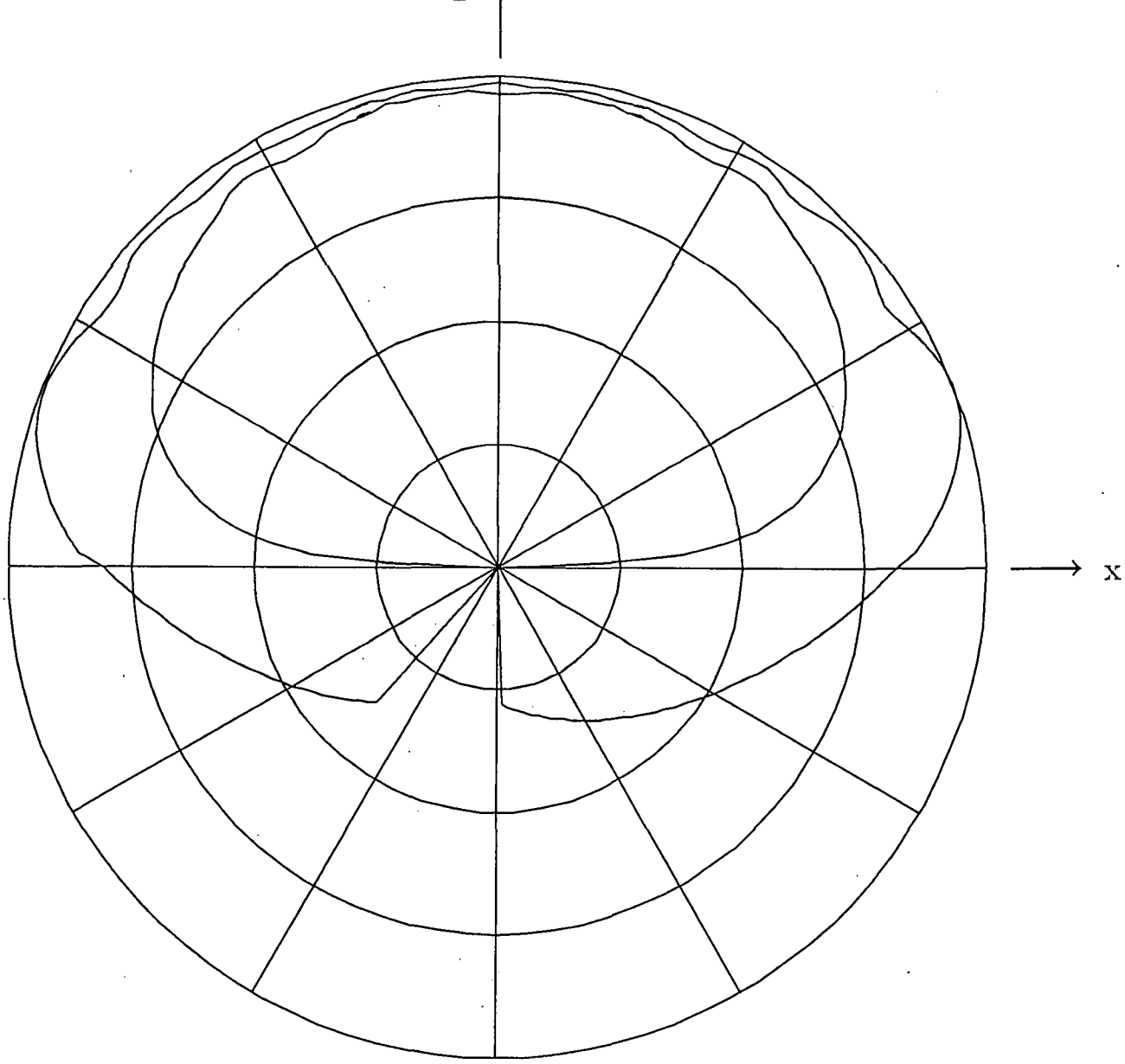

Fig. 4.14 Normalized far field radiation pattern of antenna at position 8 on backpack - 10 dB/division (ϕ = 0°).

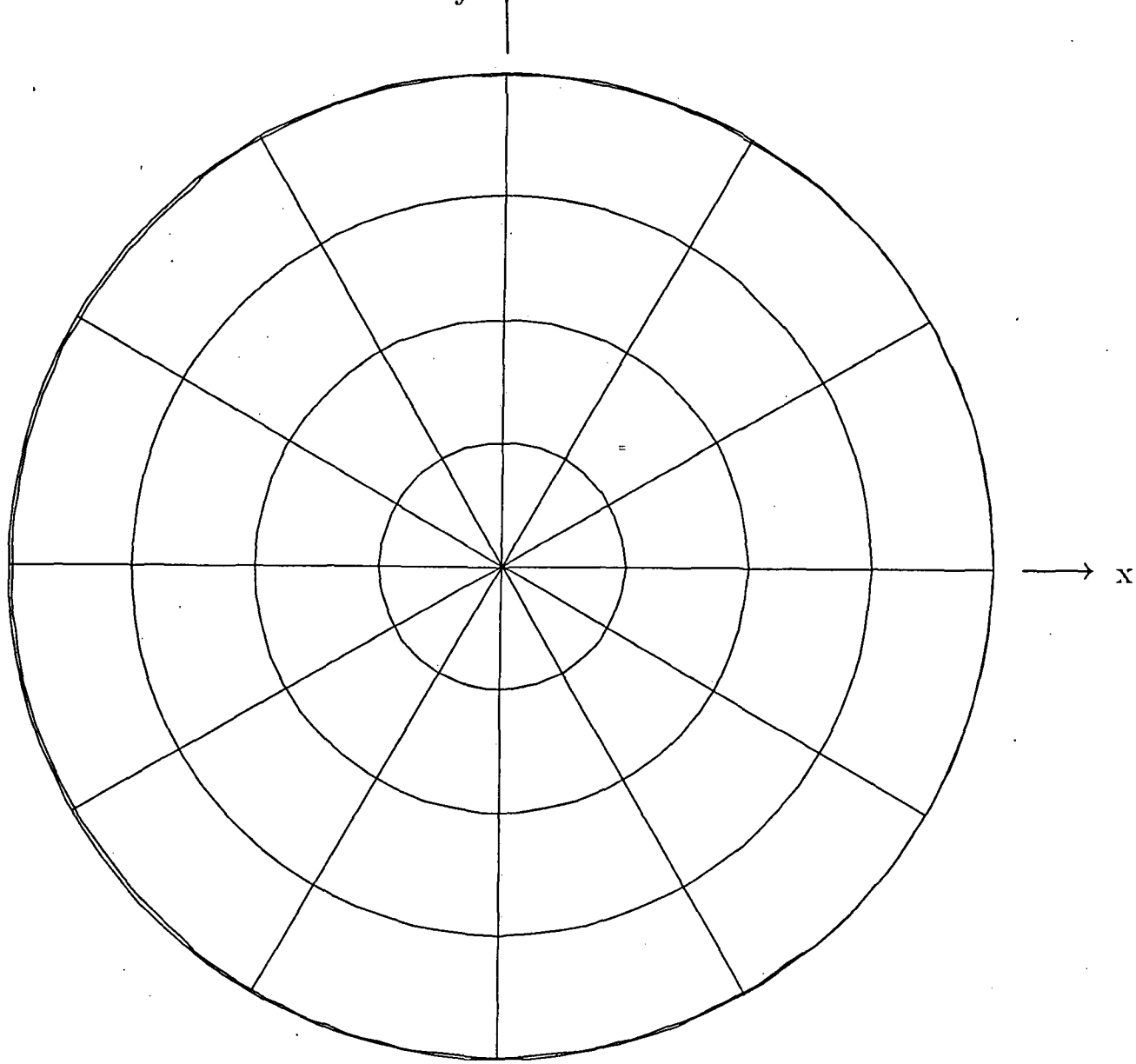

Fig. 4.15 Normalized far field radiation pattern of antenna at position 8 on backpack - 10 dB/division (Θ = 90°).

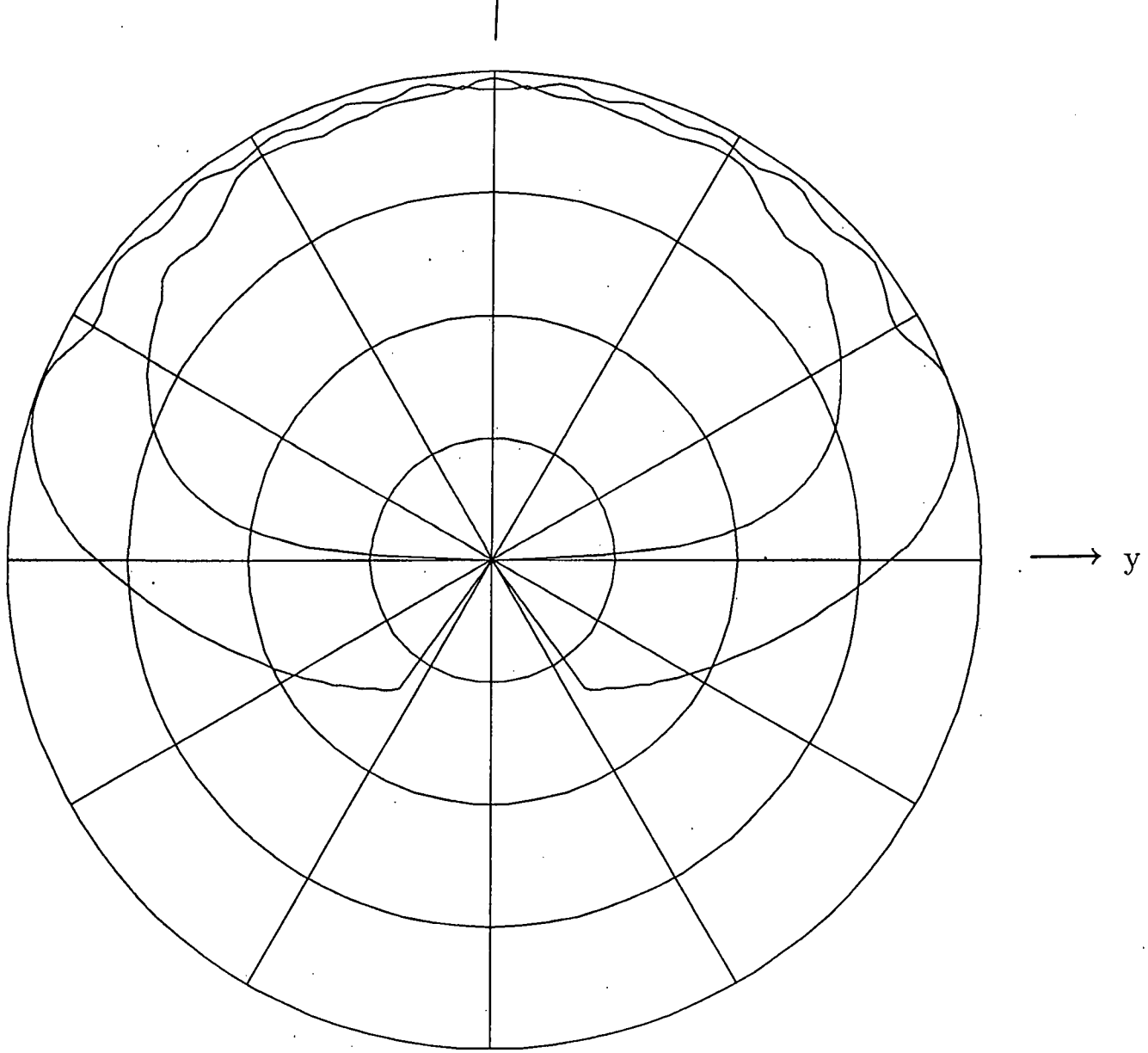

Fig. 4.16 Normalized far field radiation pattern of antenna at position 8 on backpack - 10 dB/division (ϕ = 90°).

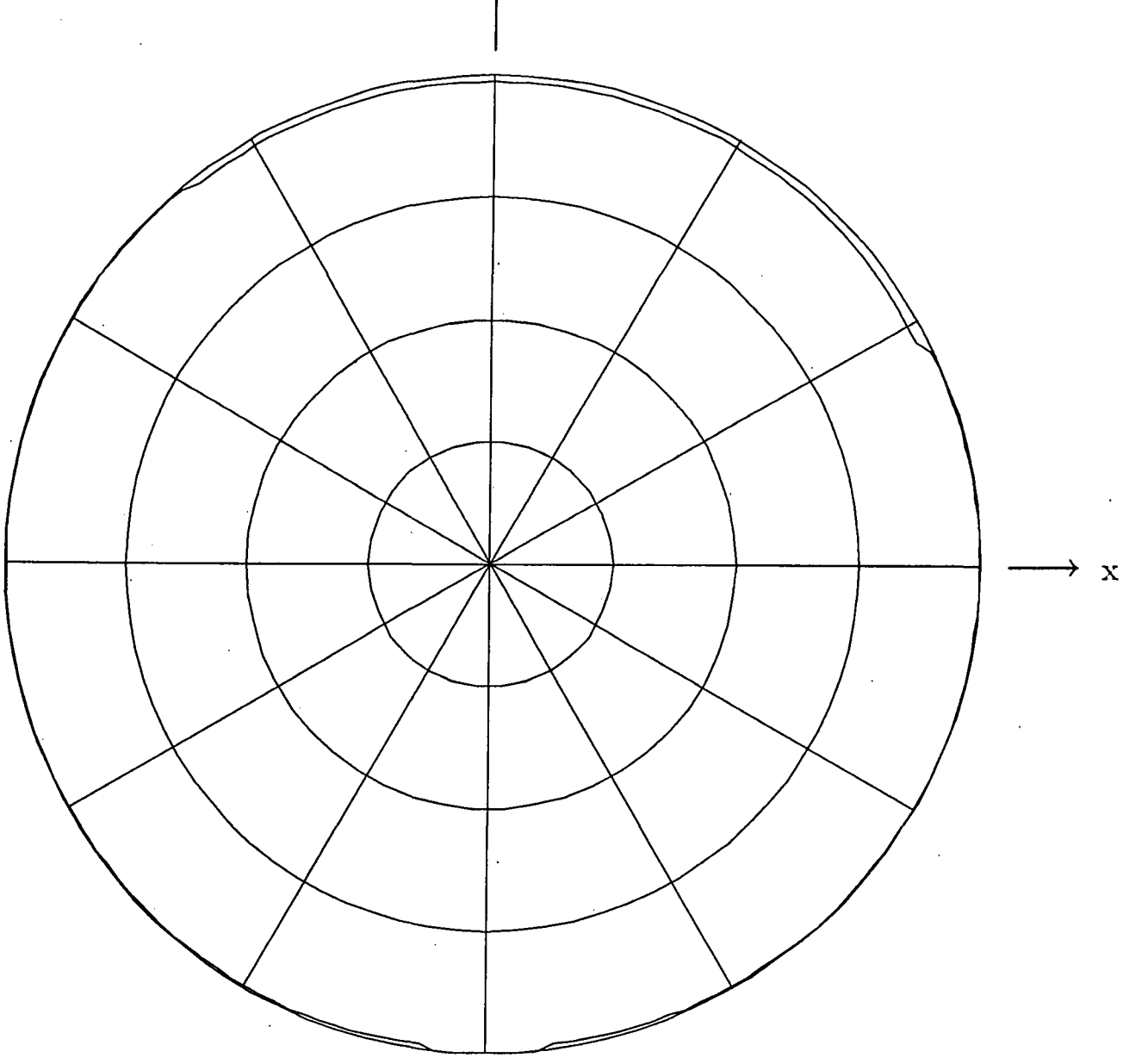

Fig. 4.17 Normalized far field radiation pattern of antenna at position 4 on backpack - 10 dB/division (ϕ = 0°).

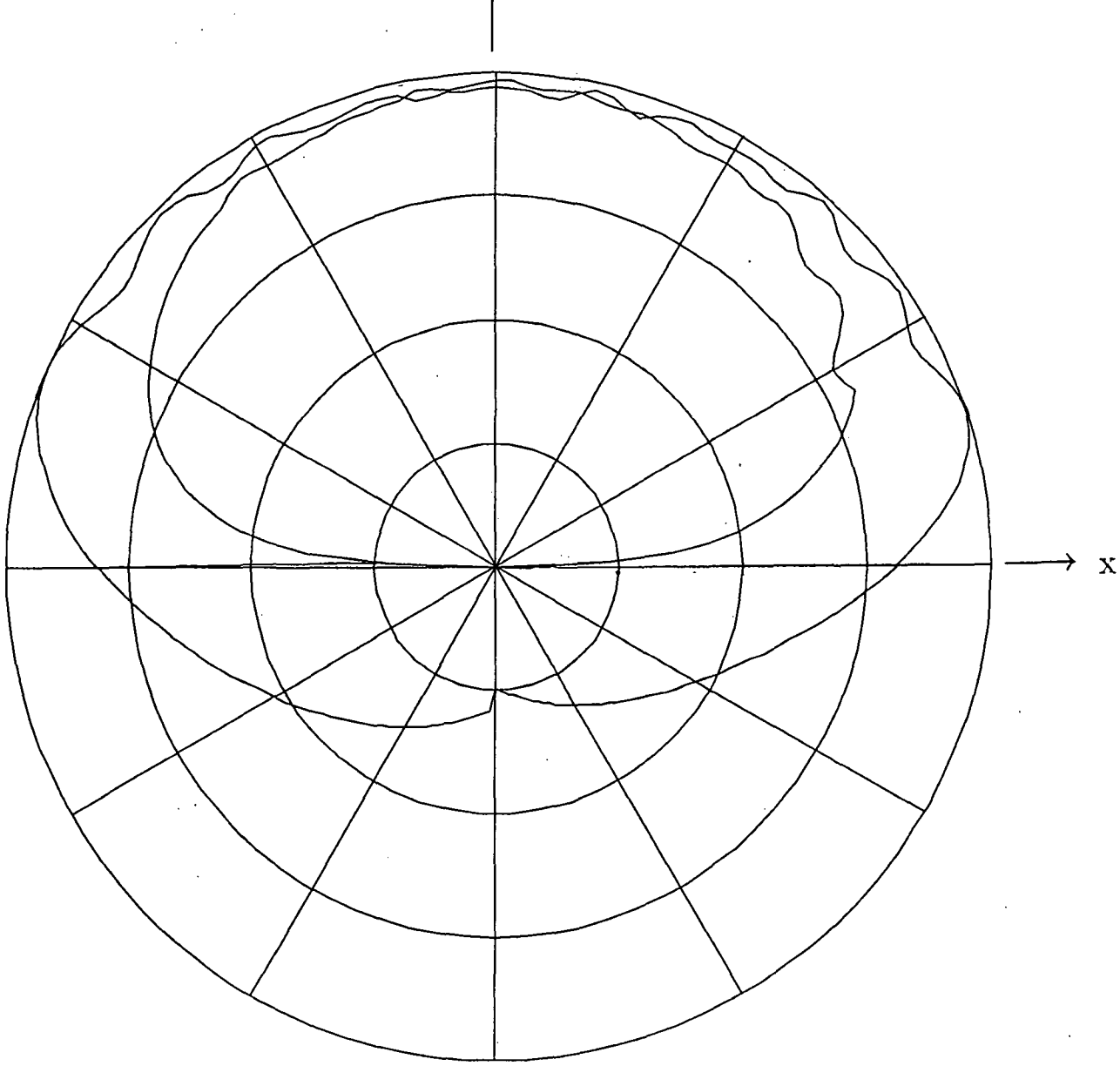

Fig. 4.18 Normalized far field radiation pattern of antenna at position 4 on backpack - 10 dB/division (Θ = 90°).

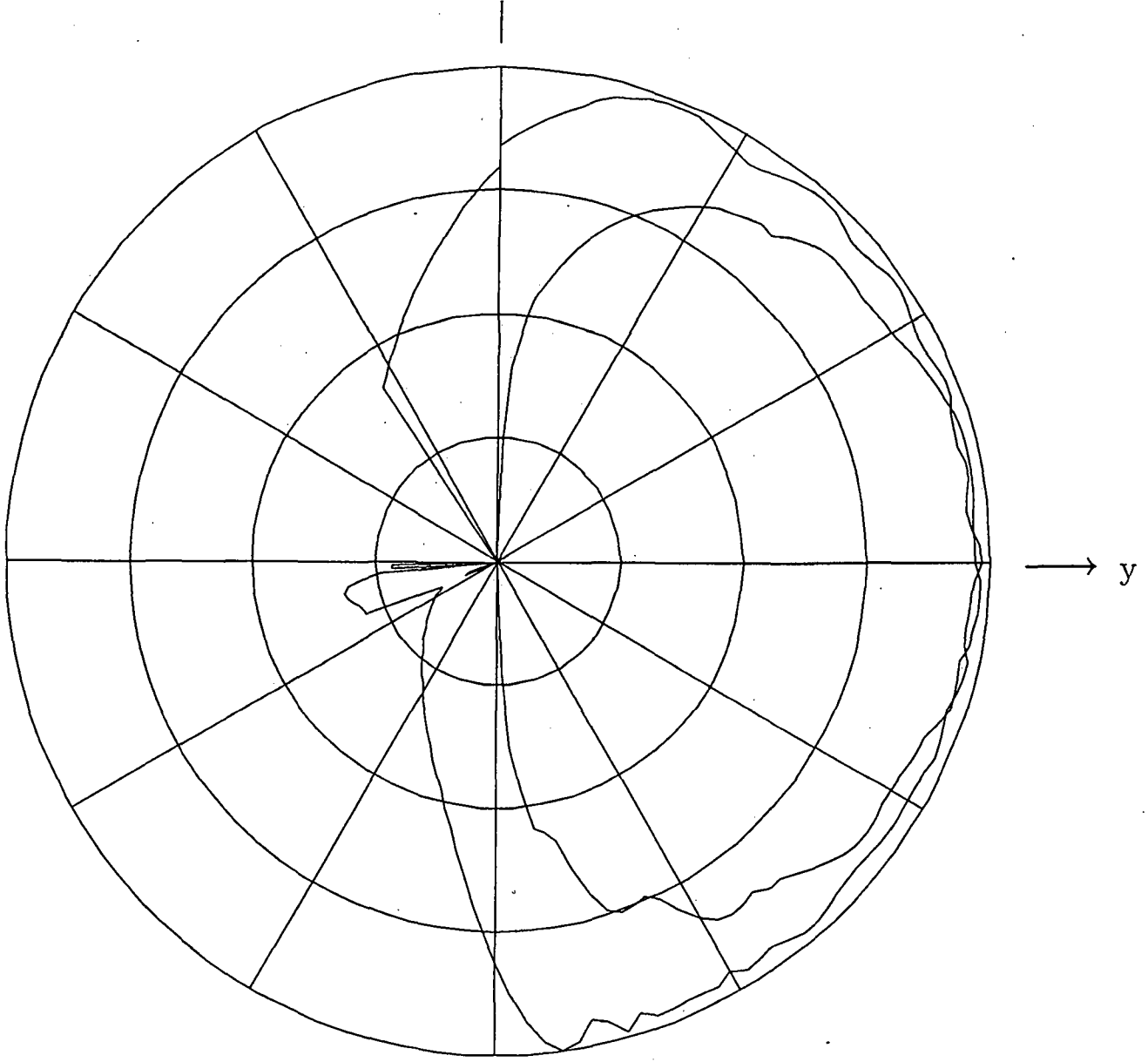

Fig. 4.19 Normalized far field radiation pattern of antenna at position 4 on backpack - 10 dB/division (ϕ = 90°).

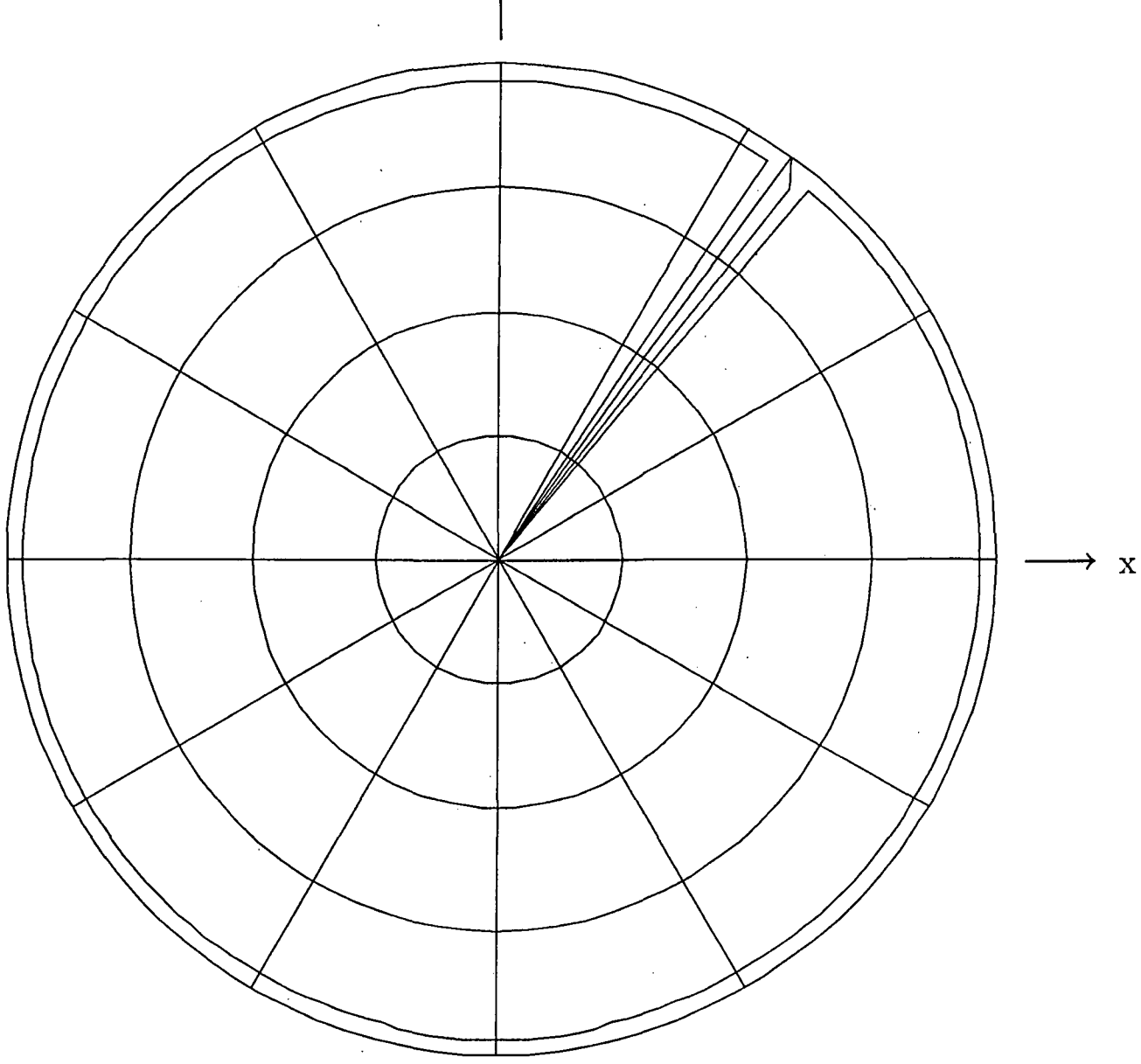

Fig. 4.20 Normalized far field radiation pattern of antenna at position 5 on backpack - 10 dB/division (ϕ = 0°).

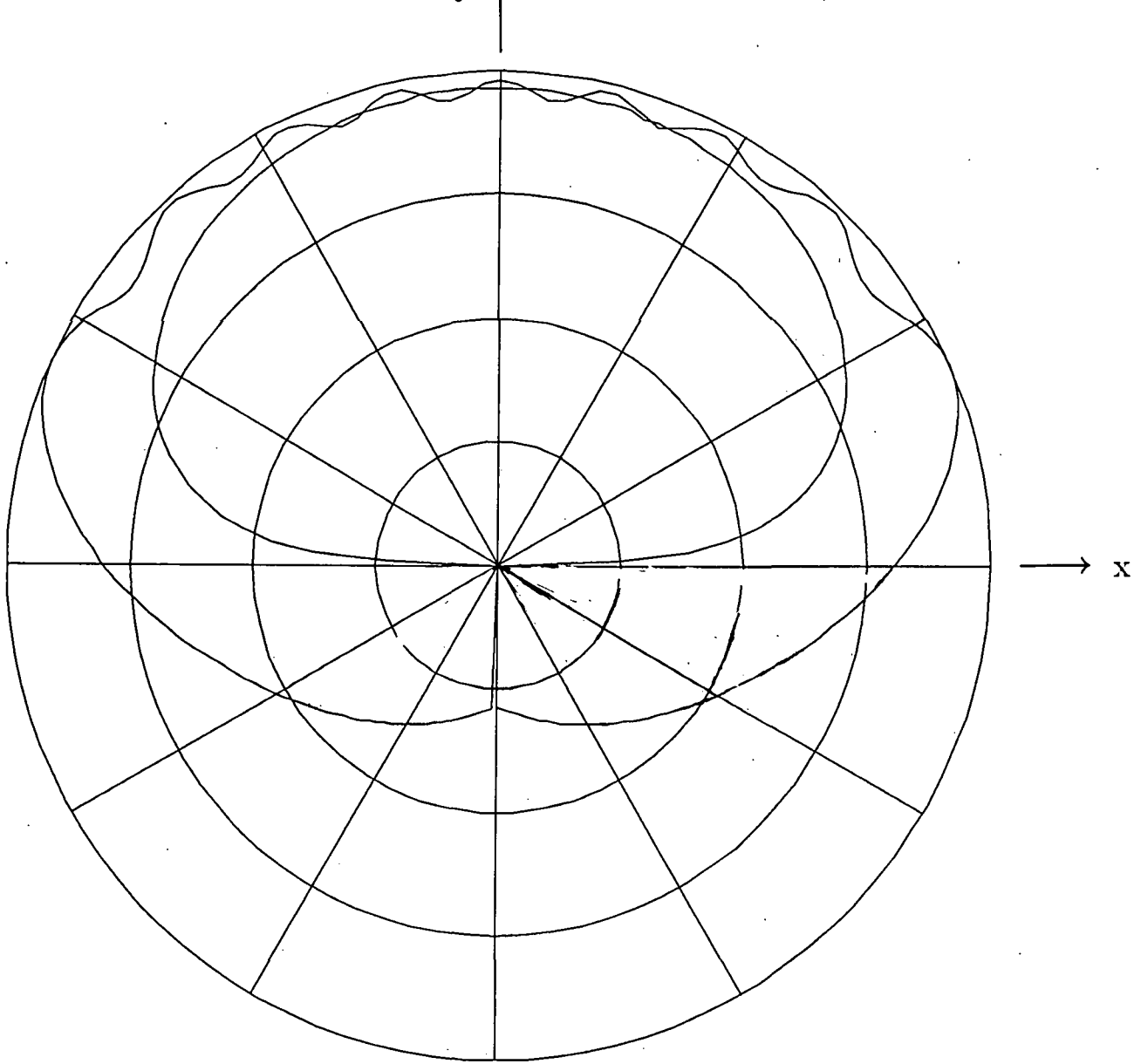

Fig. 4.21 Normalized far field radiation pattern of antenna at position 5 on backpack - 10 dB/division (Θ = 90°).

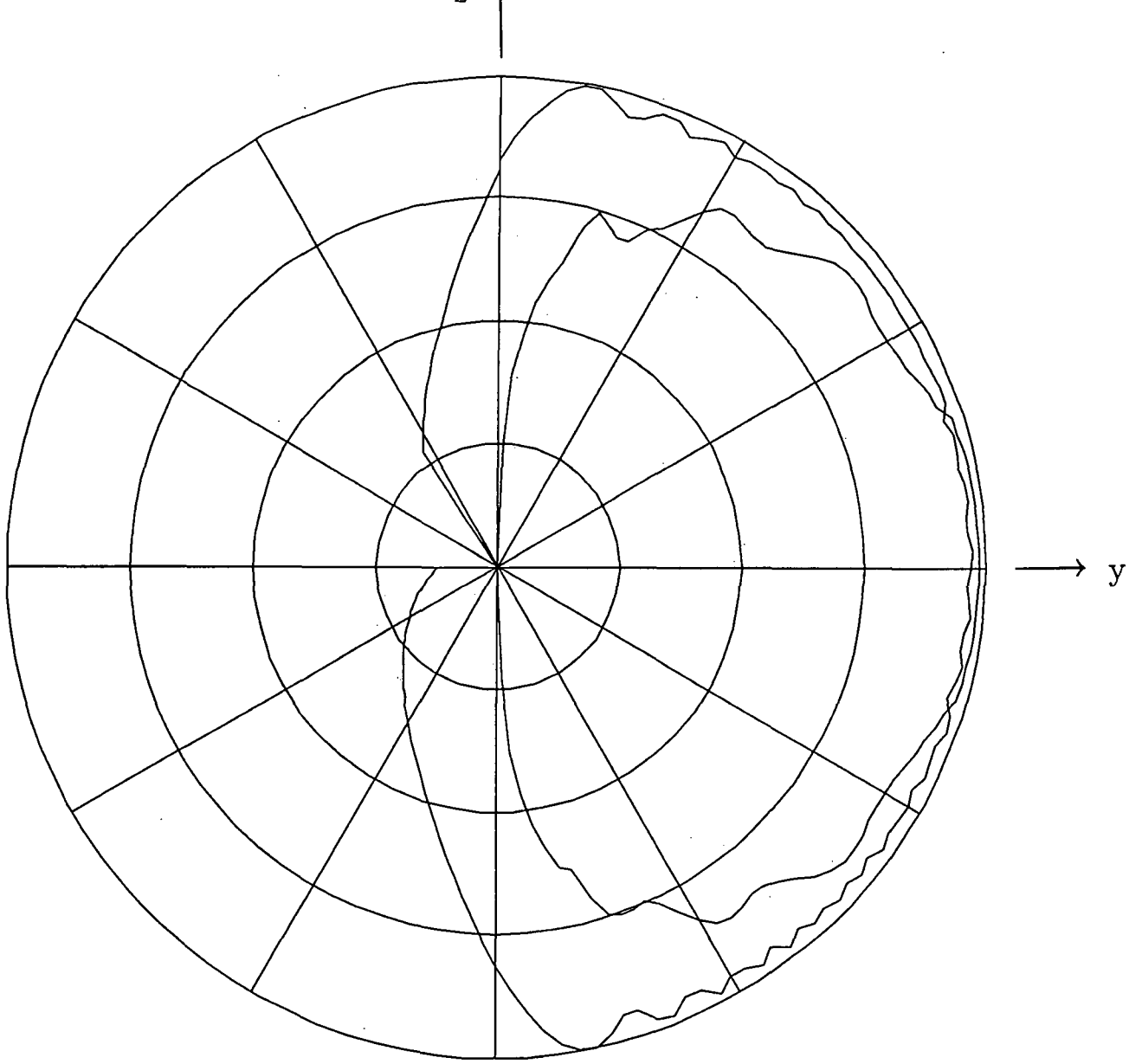

Fig. 4.22 Normalized far field radiation pattern of antenna at position 5 on backpack - 10 dB/division (ϕ = 90°).

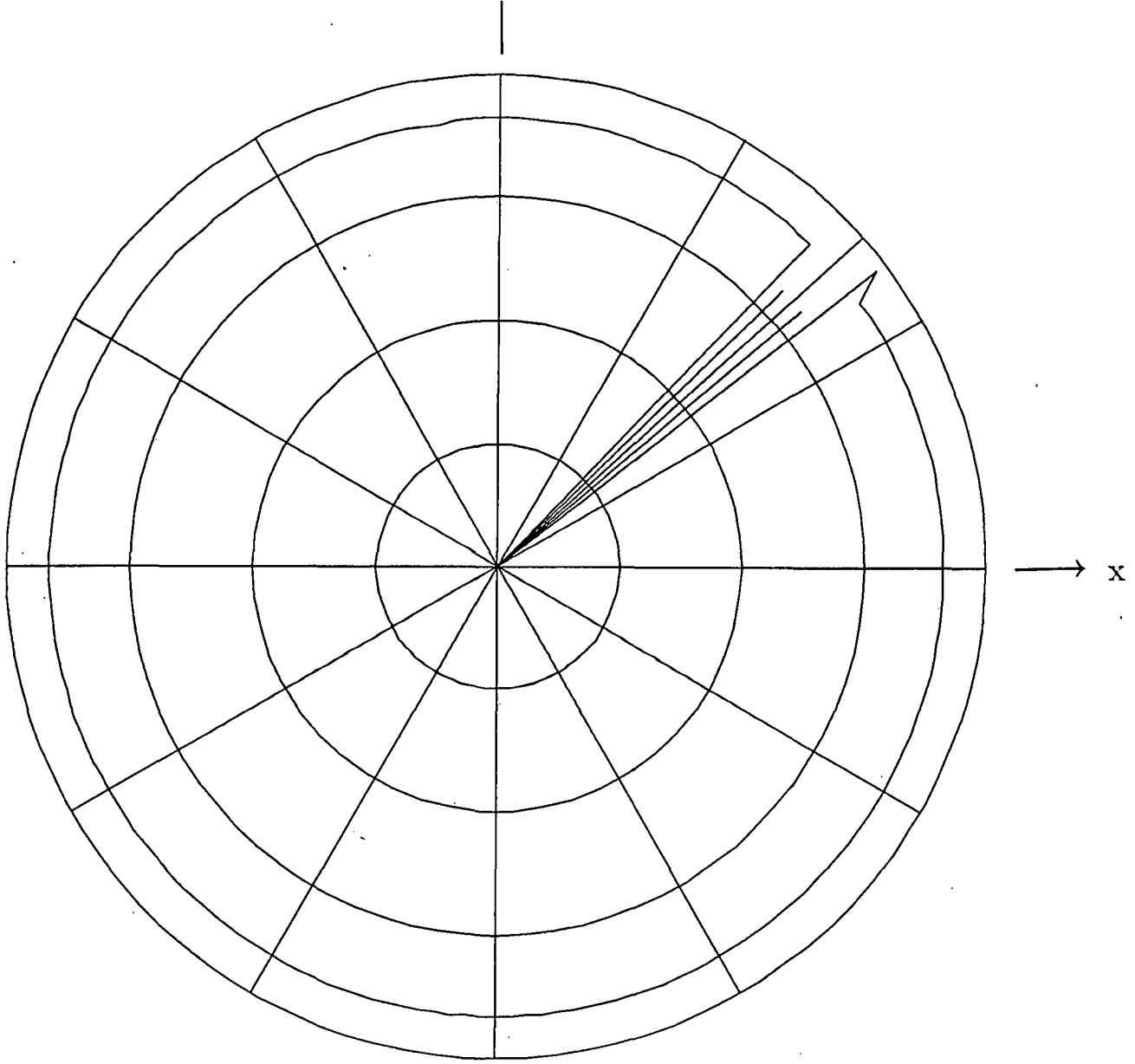

Fig. 4.23 Normalized far field radiation pattern of antenna at position 6 on backpack - 10 dB/division (ϕ = 0°).

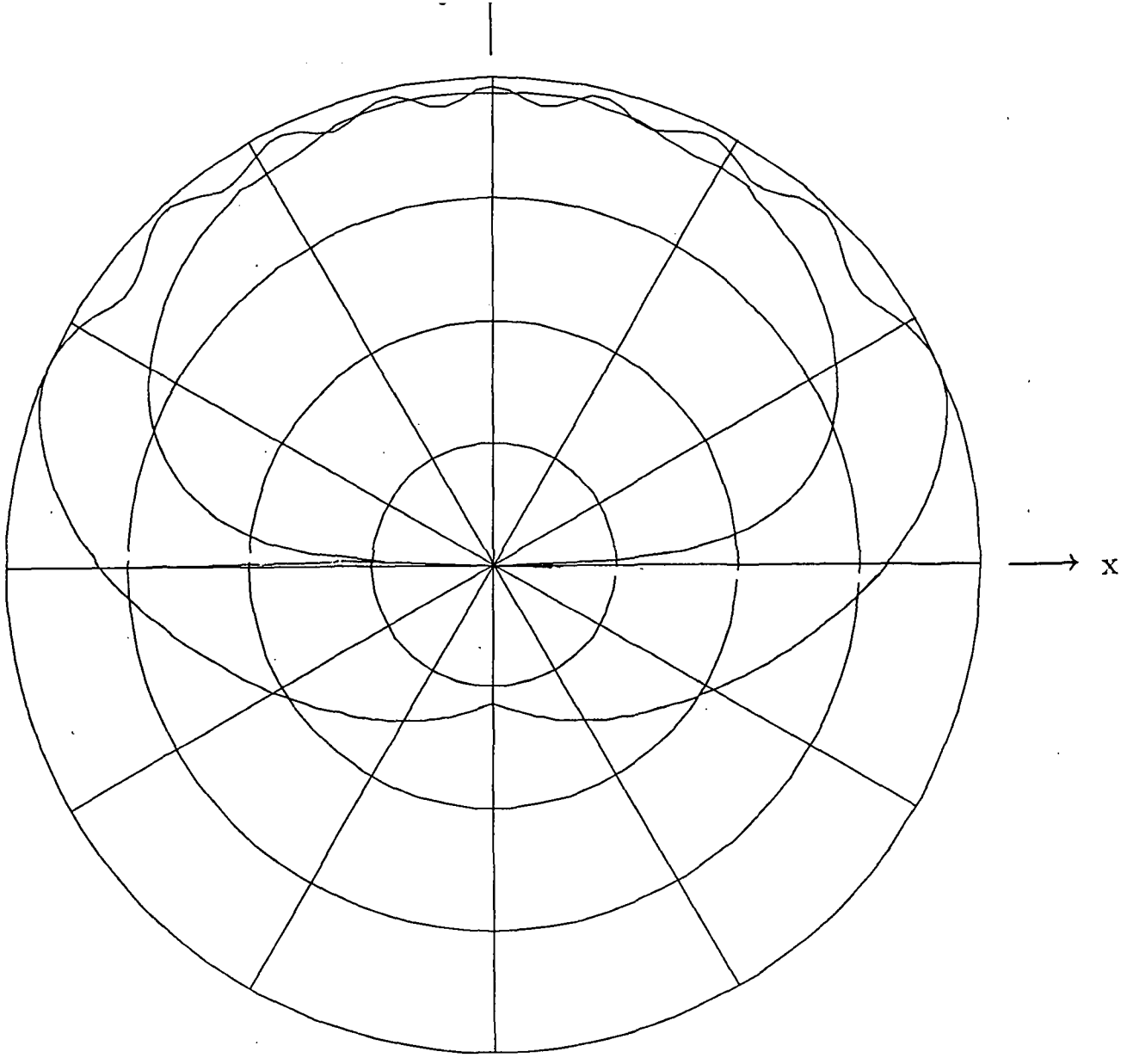

Fig. 4.24 Normalized far field radiation pattern of antenna at position 6 on backpack - 10 dB/division (Θ = 90°).

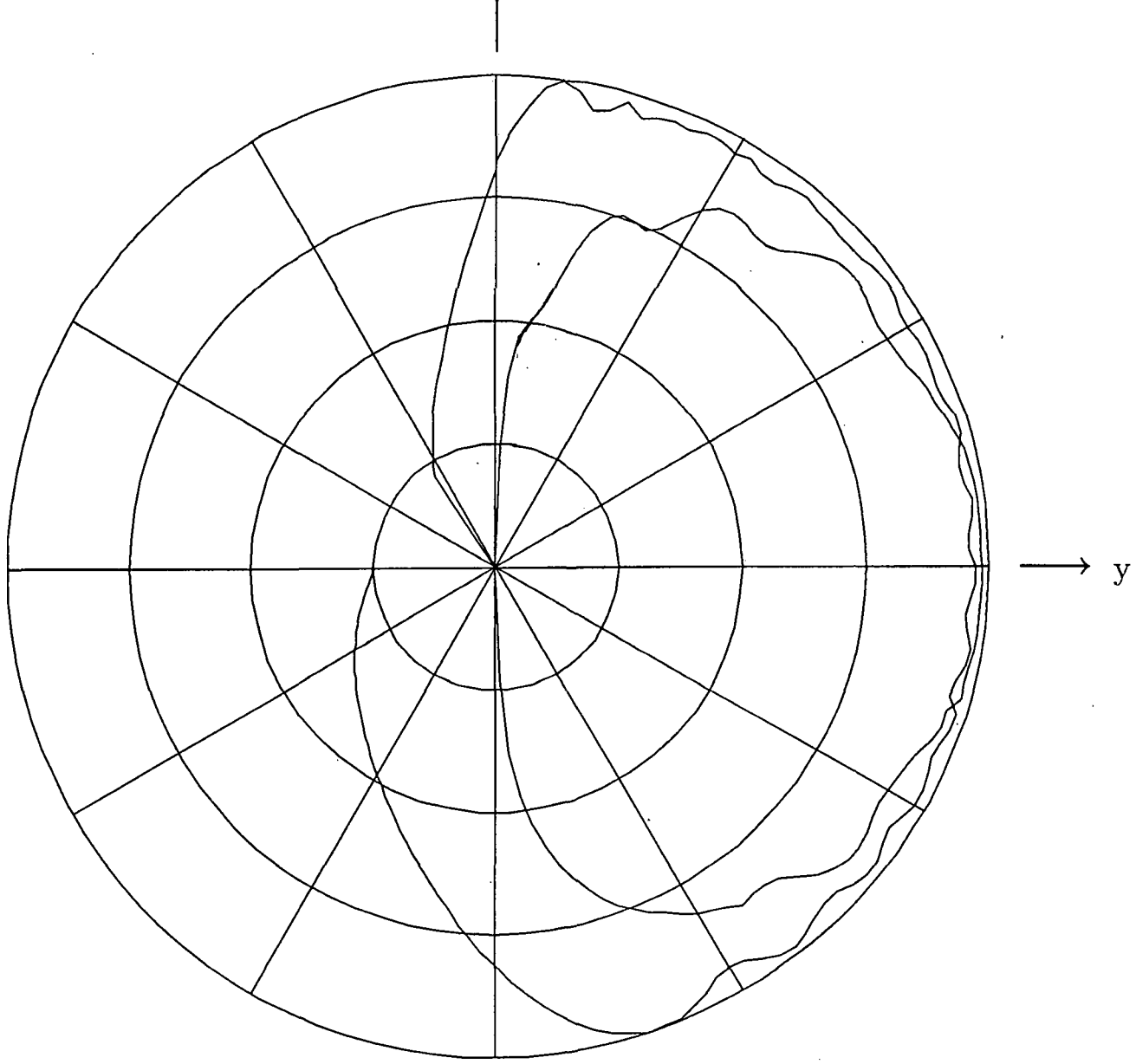

Fig. 4.25 Normalized far field radiation pattern of antenna at position 6 on backpack - 10 dB/division (ϕ = 90°).

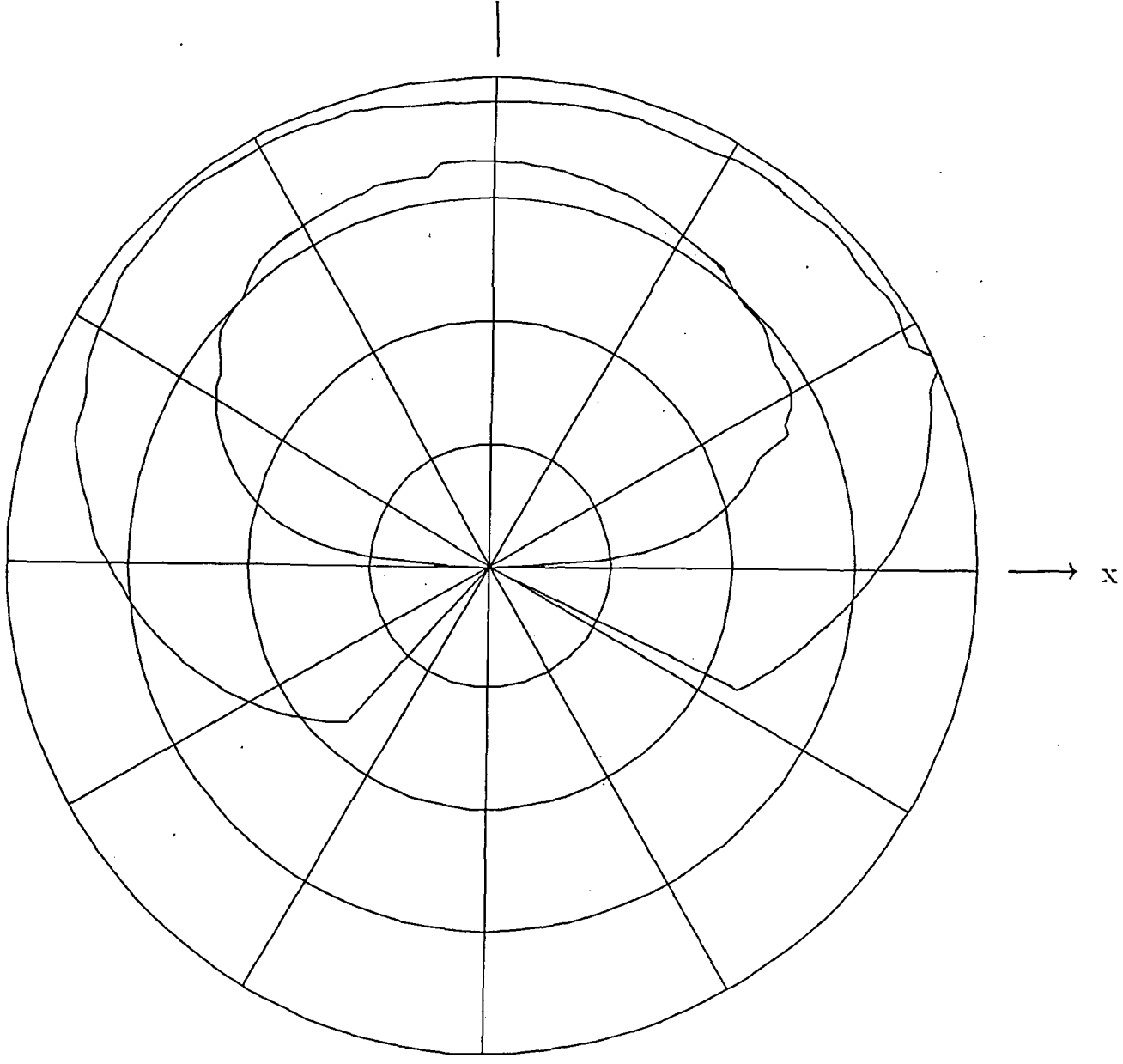

Fig. 4.26 Normalized far field radiation pattern of antenna at position 7 on backpack - 10 dB/division (ϕ = 0°).

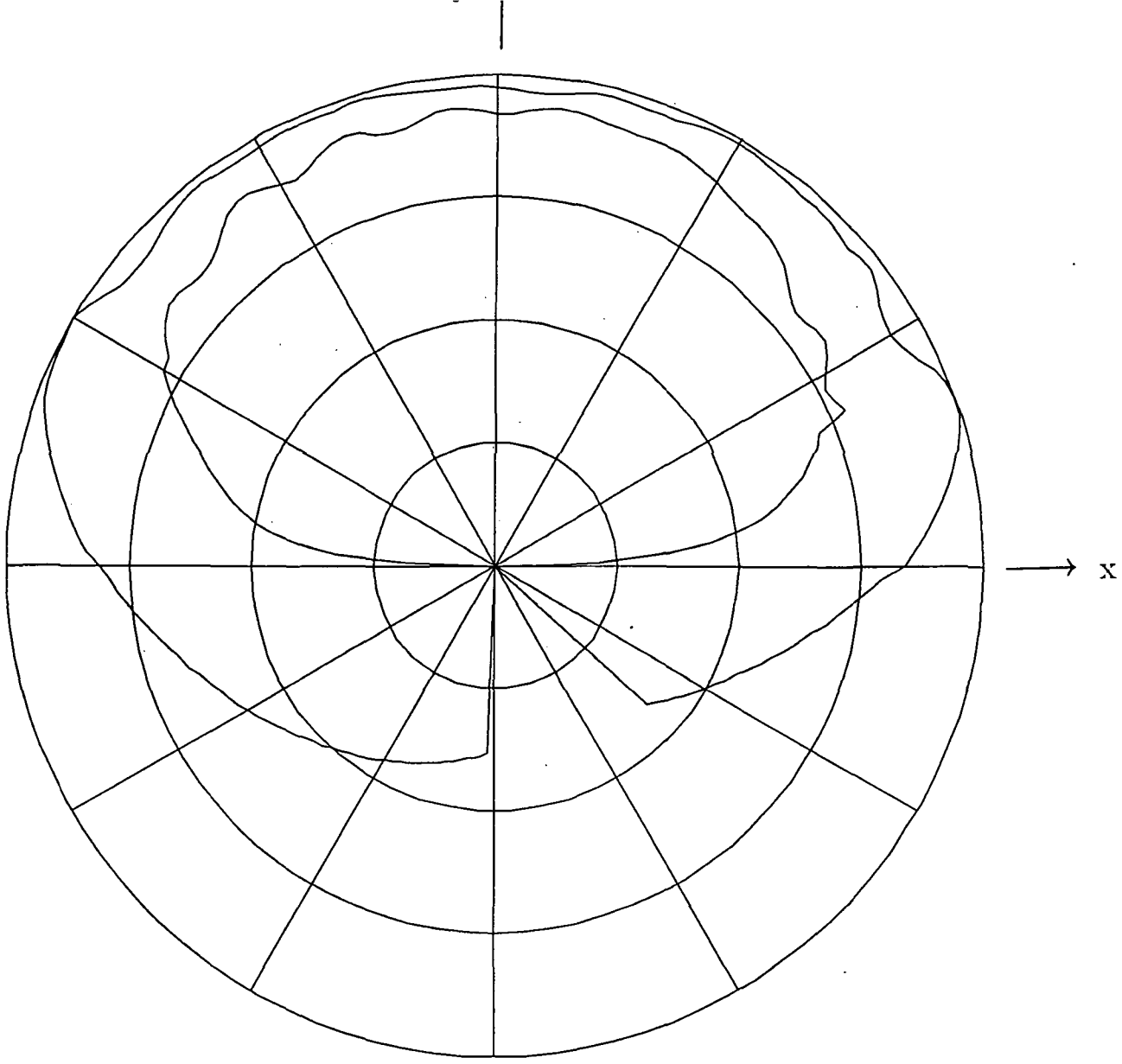

Fig. 4.27 Normalized far field radiation pattern of antenna at position 7 on backpack - 10 dB/division (Θ = 90°).

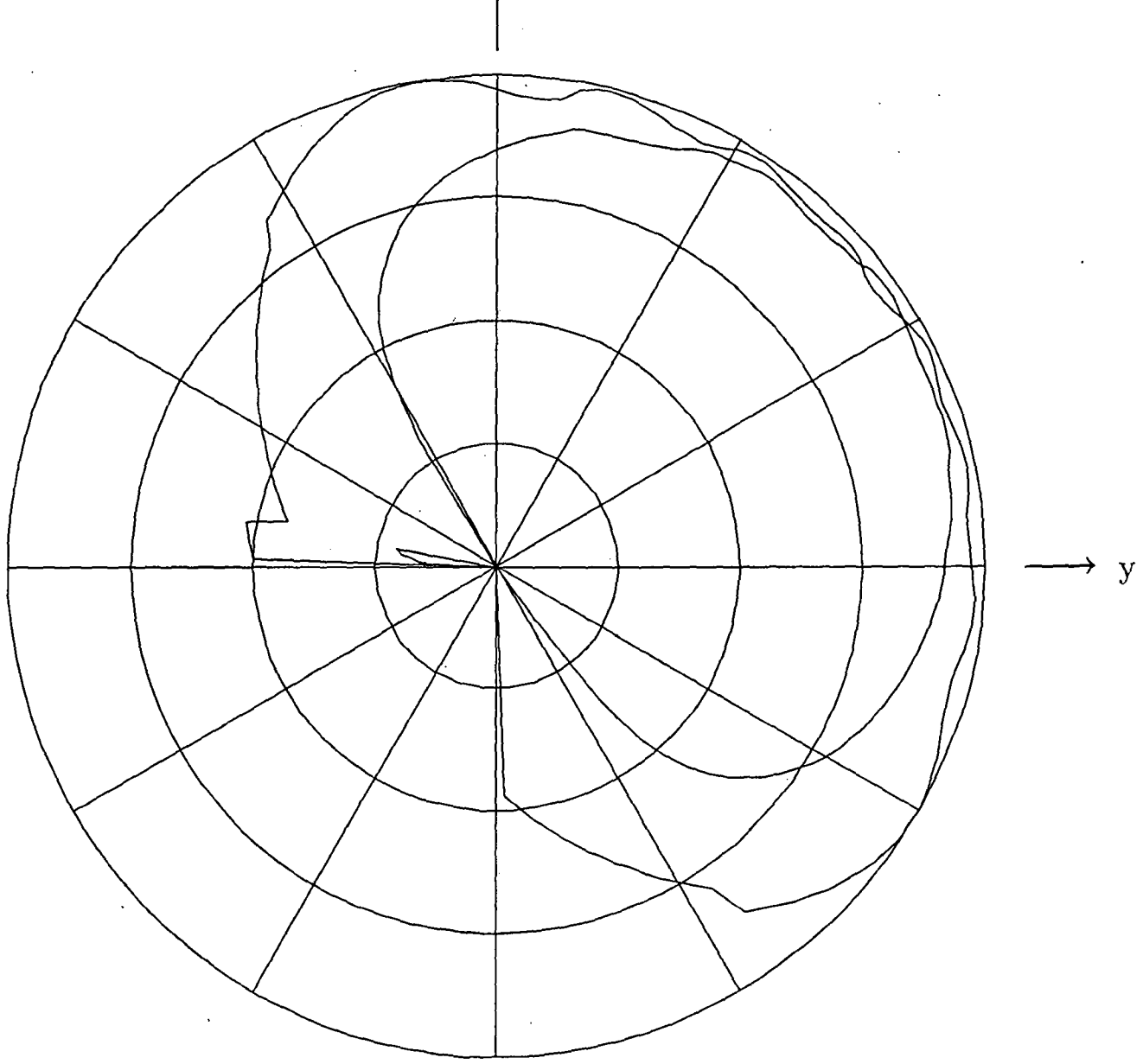

Fig. 4.28 Normalized far field radiation pattern of antenna at position 7 on backpack - 10 dB/division (ϕ = 90°).

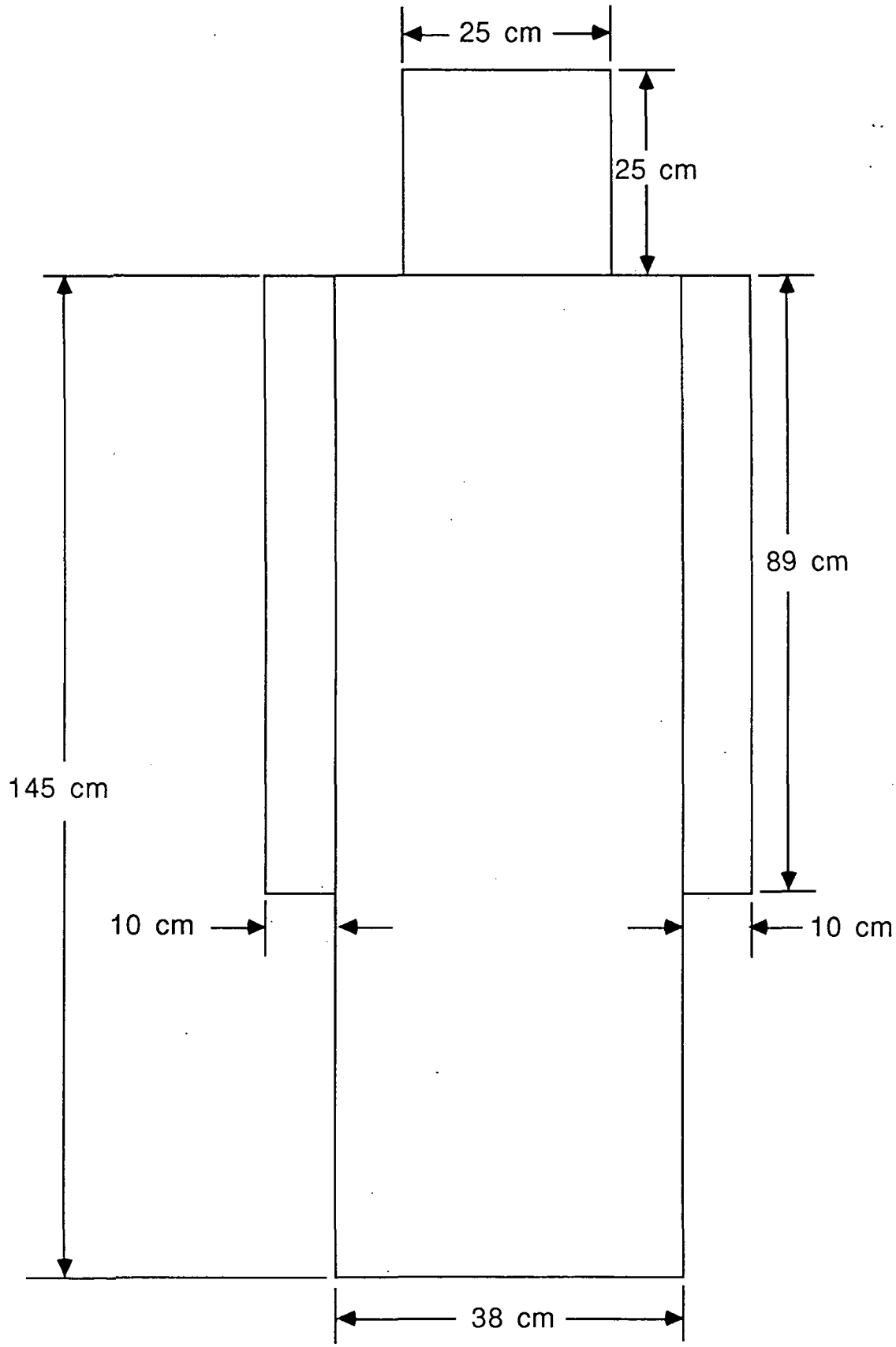

Fig. 4.29 Front view detail of astronaut model.

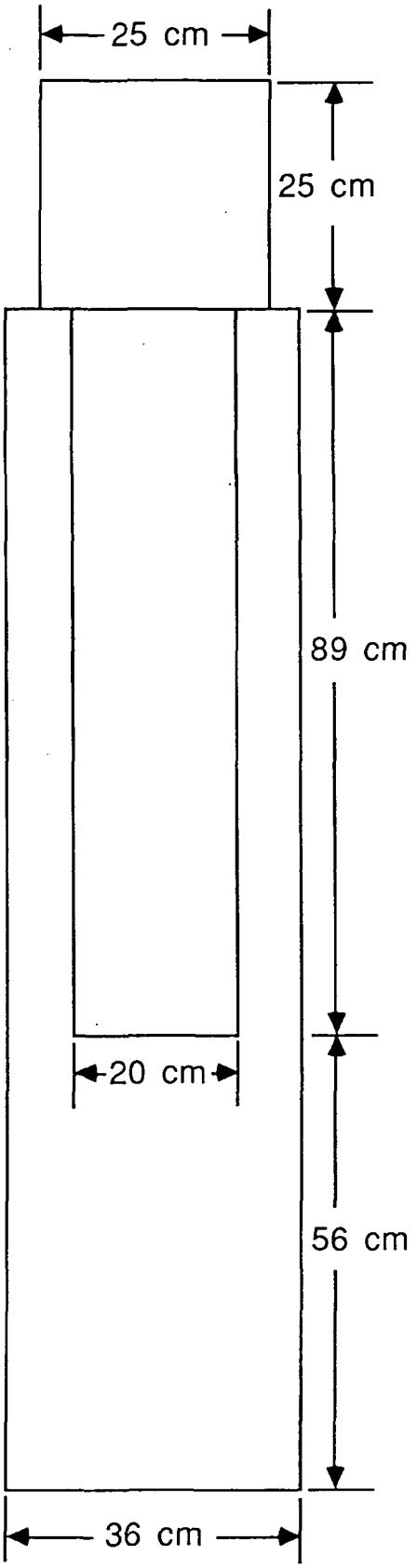

Fig. 4.30 Side view detail of astronaut model.

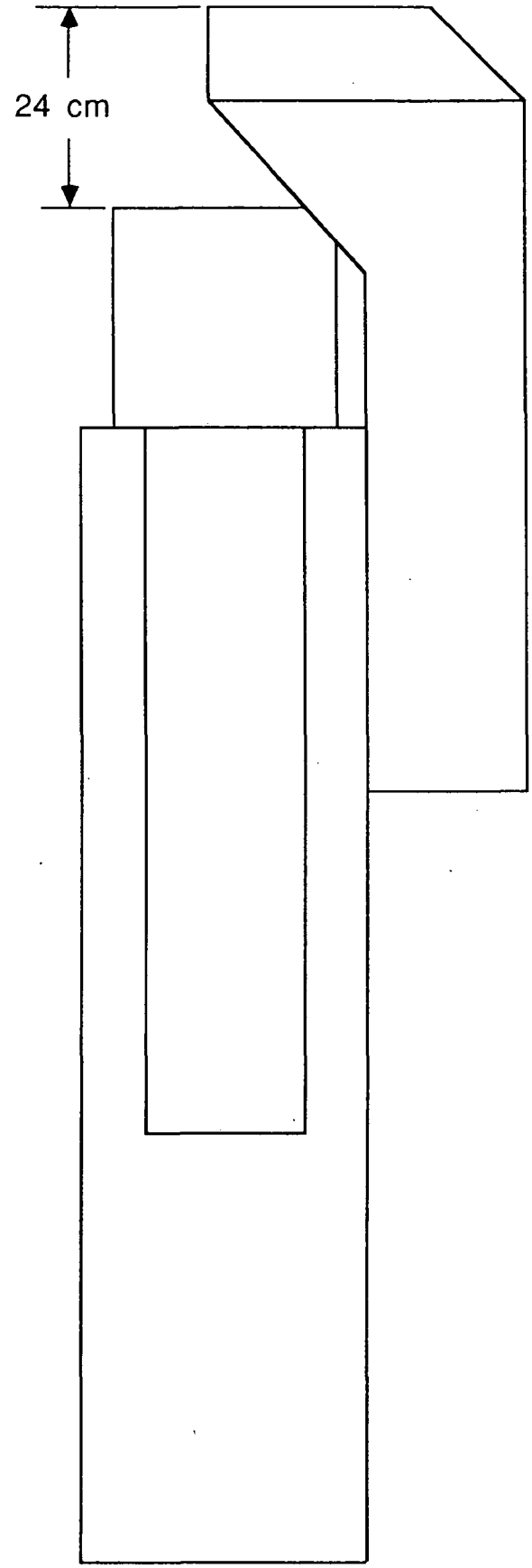

Fig. 4.31 Side view detail of astronaut and backpack models.

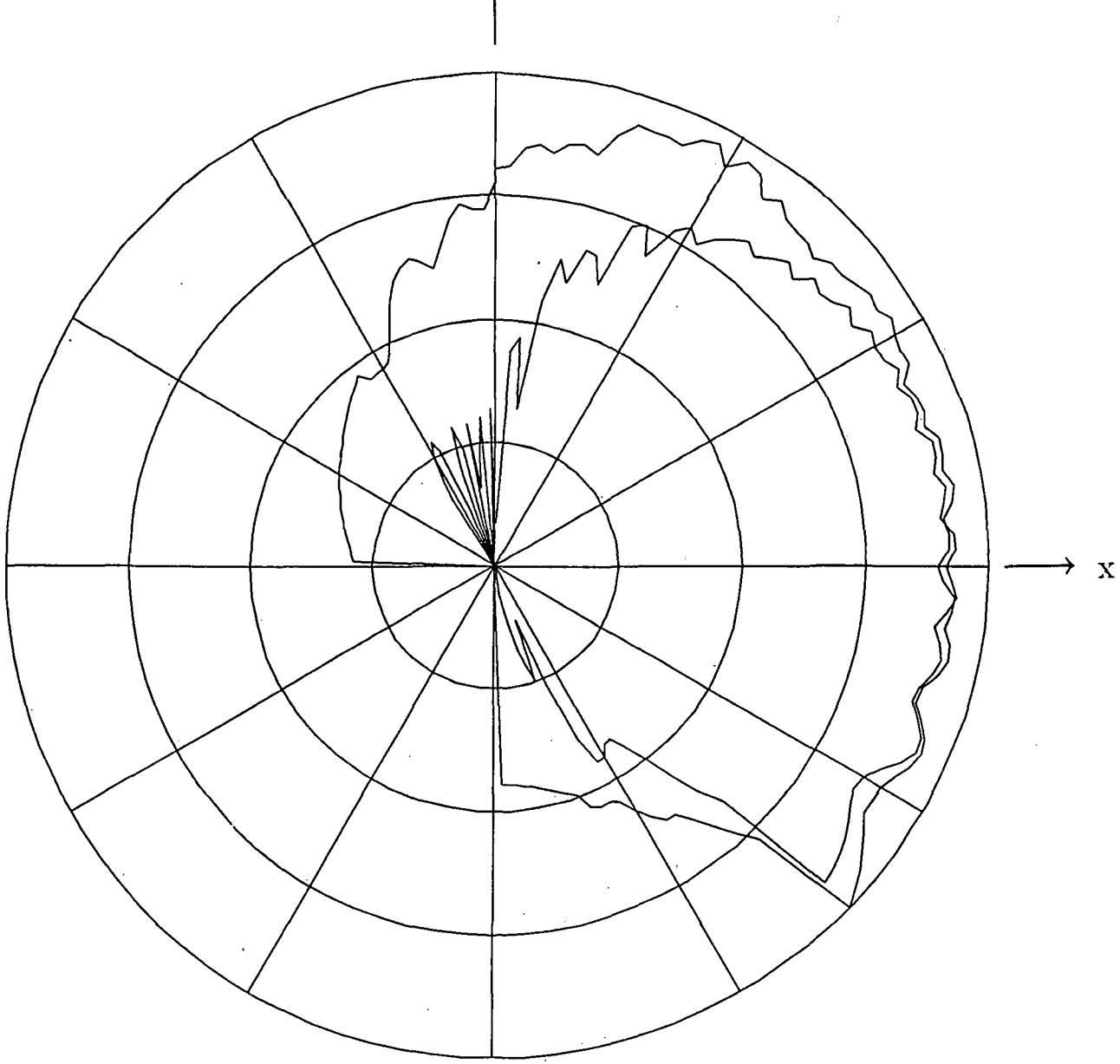

Fig 4.32 Far field radiation pattern of antenna at position 2 on backpack with astronaut ($\phi = 0^o$).

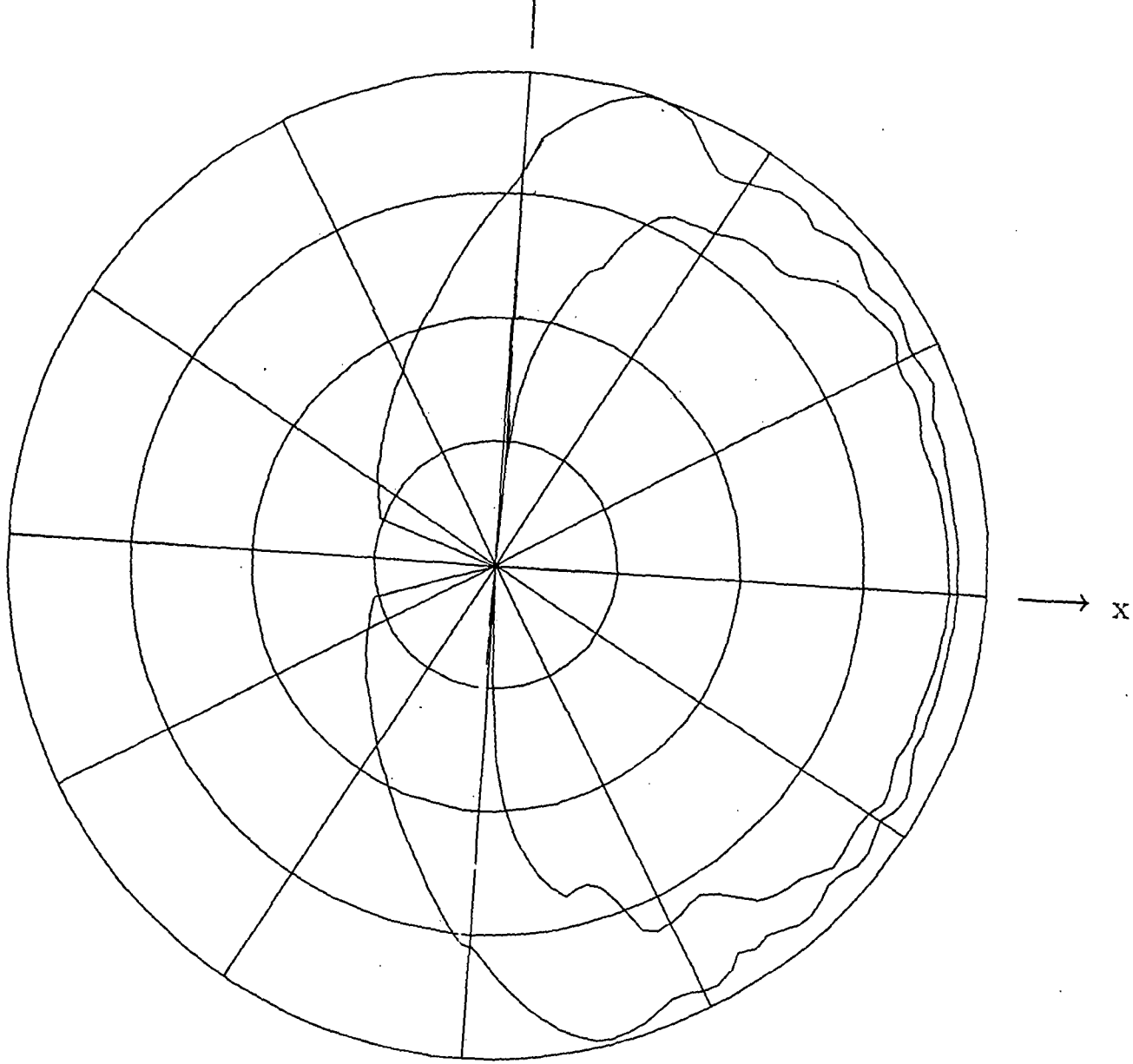

Fig 4.33 Far field radiation pattern of antenna at position 2 on backpack with astronaut (Θ = 90o).

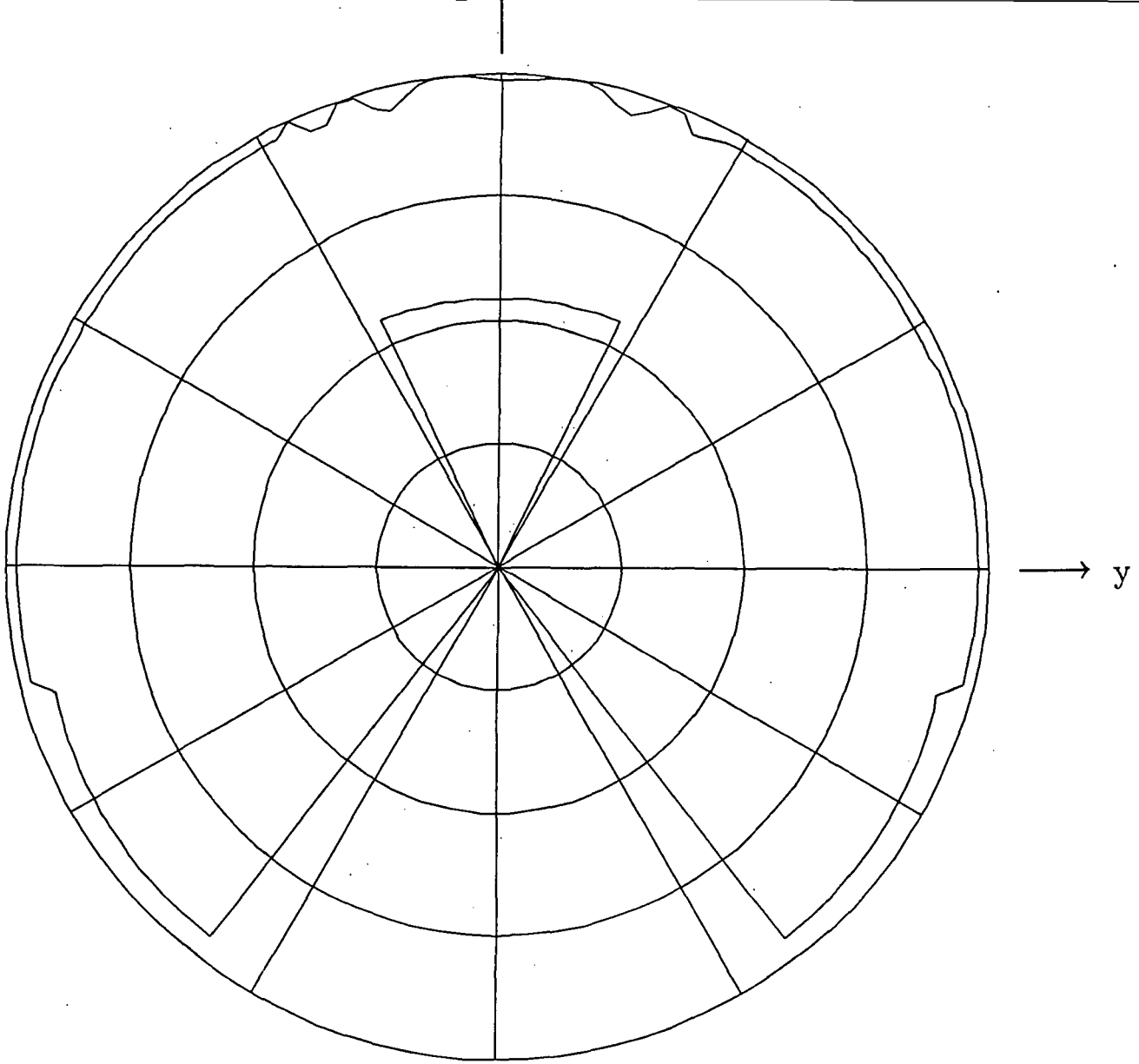

Fig 4.34 Far field radiation pattern of antenna at position 2 on backpack with astronaut ($\phi = 90^{o}$).

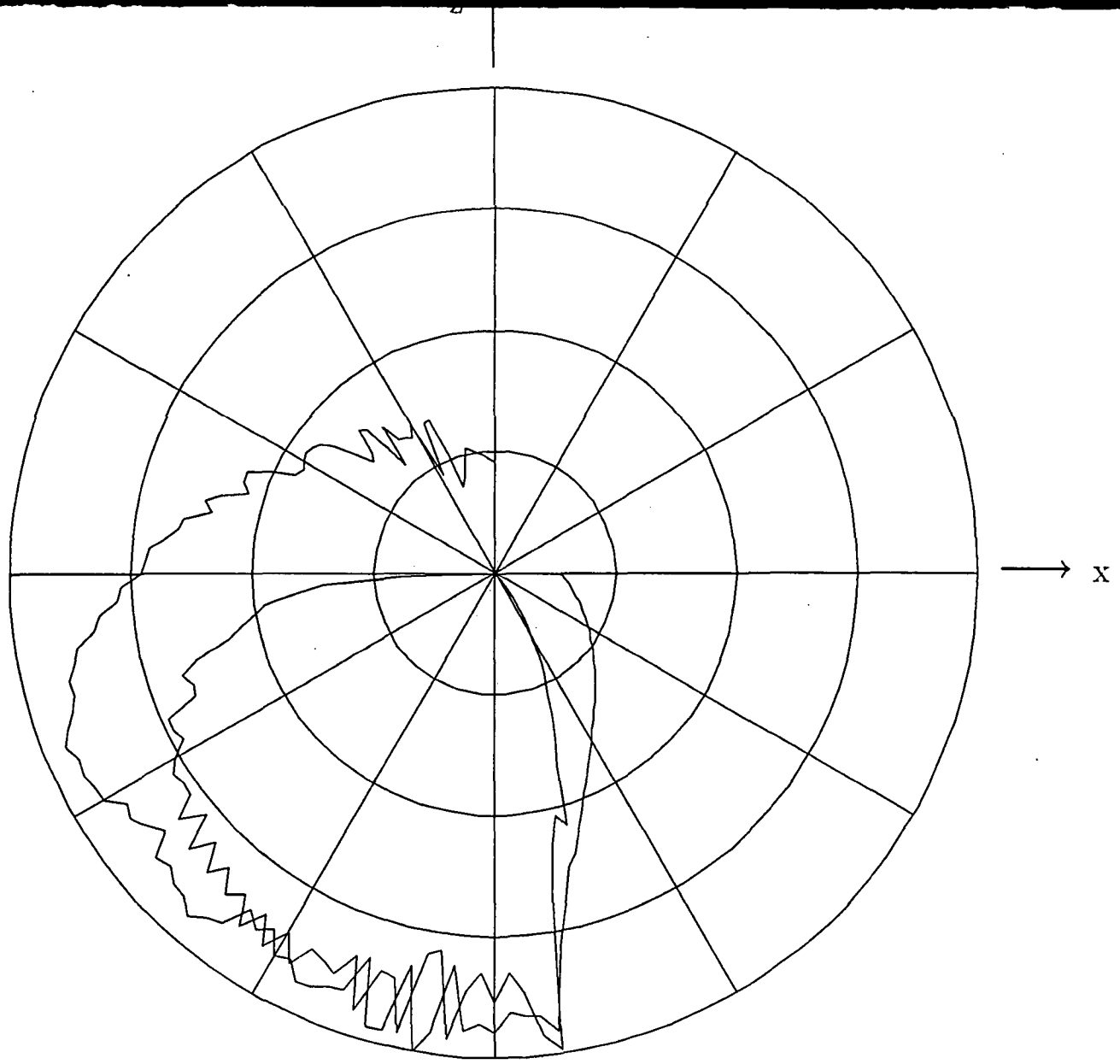

Fig 4.35 Far field radiation pattern of antenna at position 3 on backpack with astronaut (ϕ = 0°).

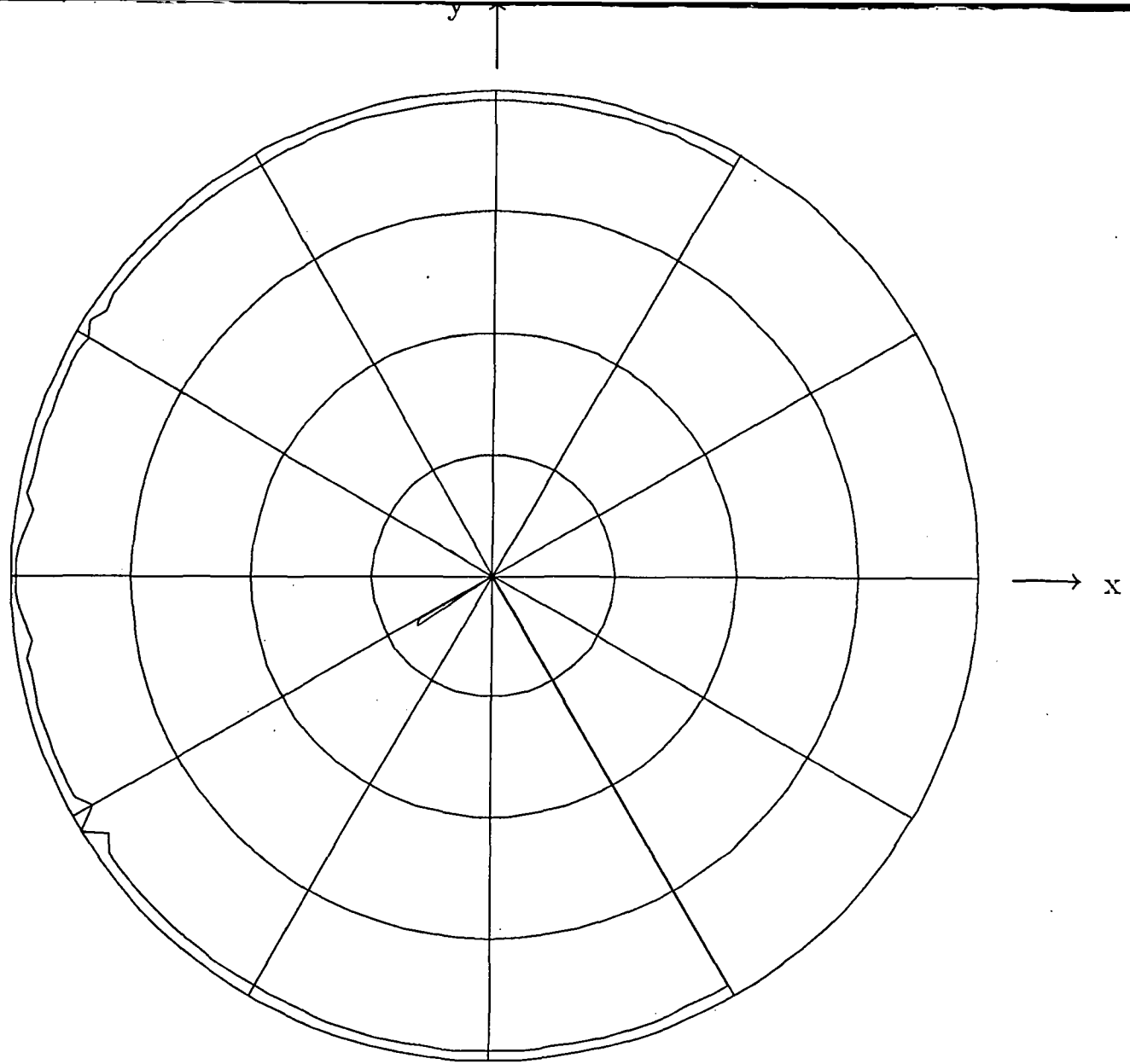

Fig 4.36 Far field radiation pattern of antenna at position 3 on backpack with astronaut ($\Theta = 90^{o}$).

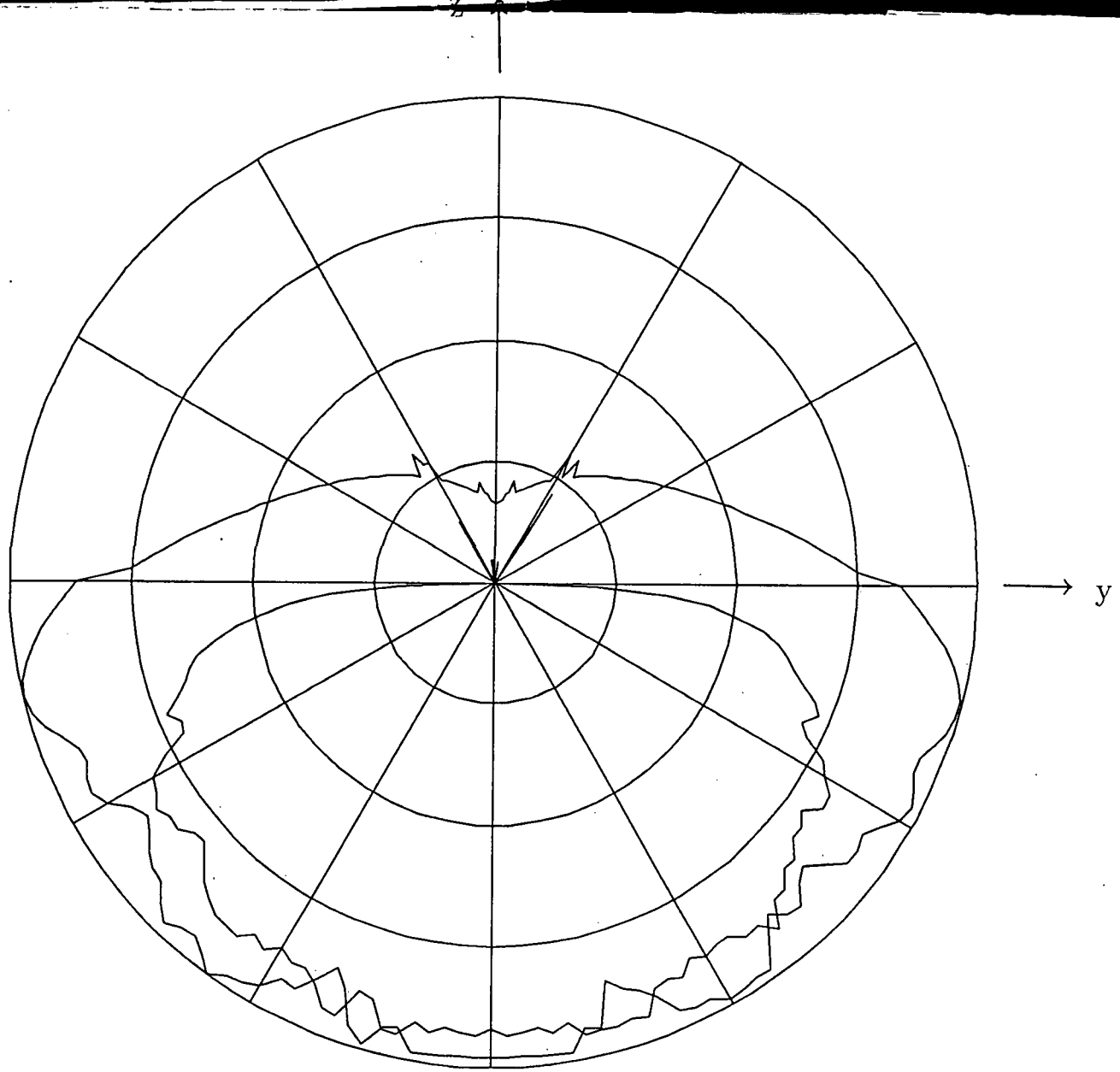

Fig 4.37 Far field radiation pattern of antenna at position 3 on backpack with astronaut ($\phi = 90^{o}$).

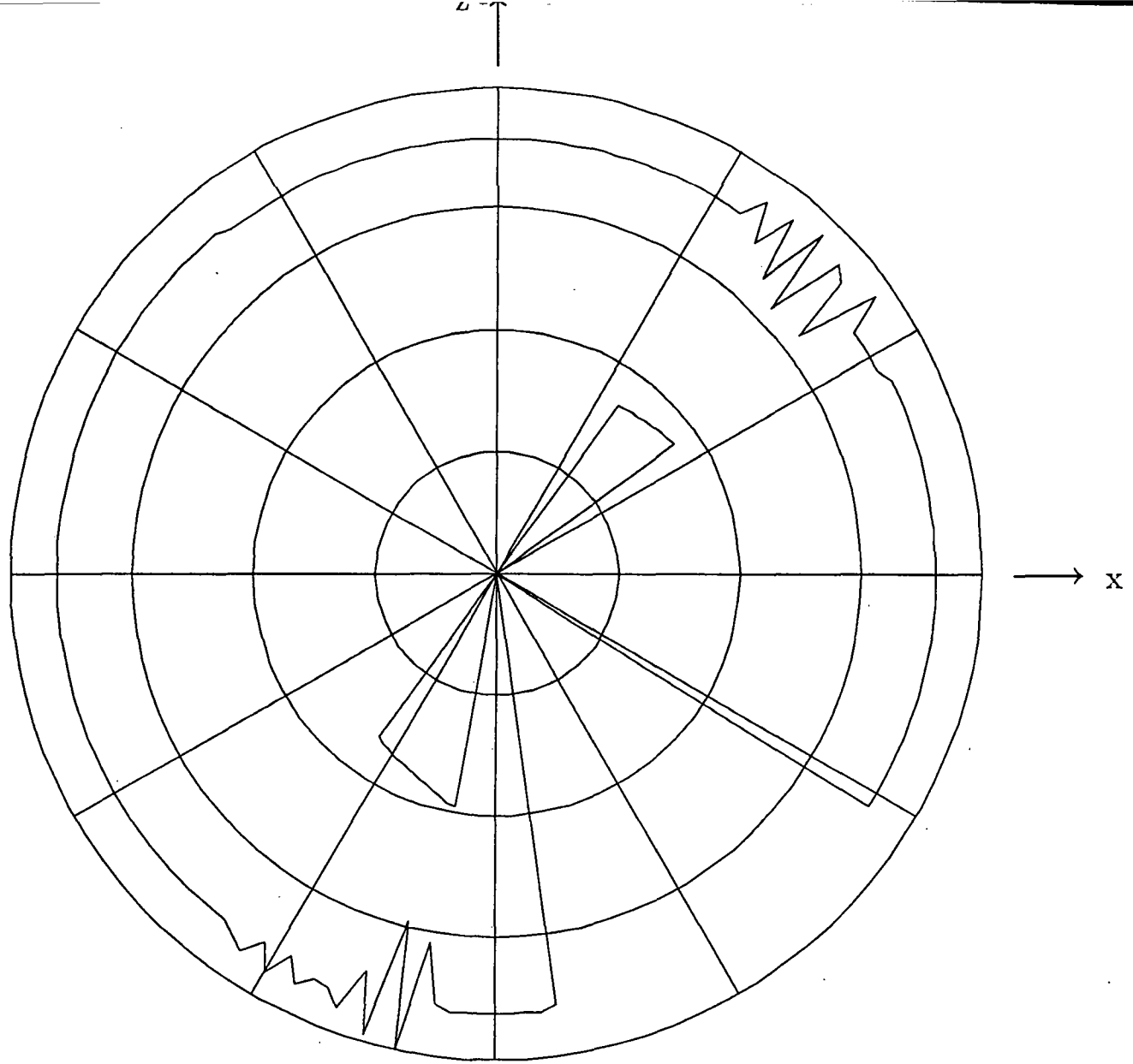

Fig 4.38 Far field radiation pattern of antenna at position 4 on backpack with astronaut ($\phi = 0^o$).

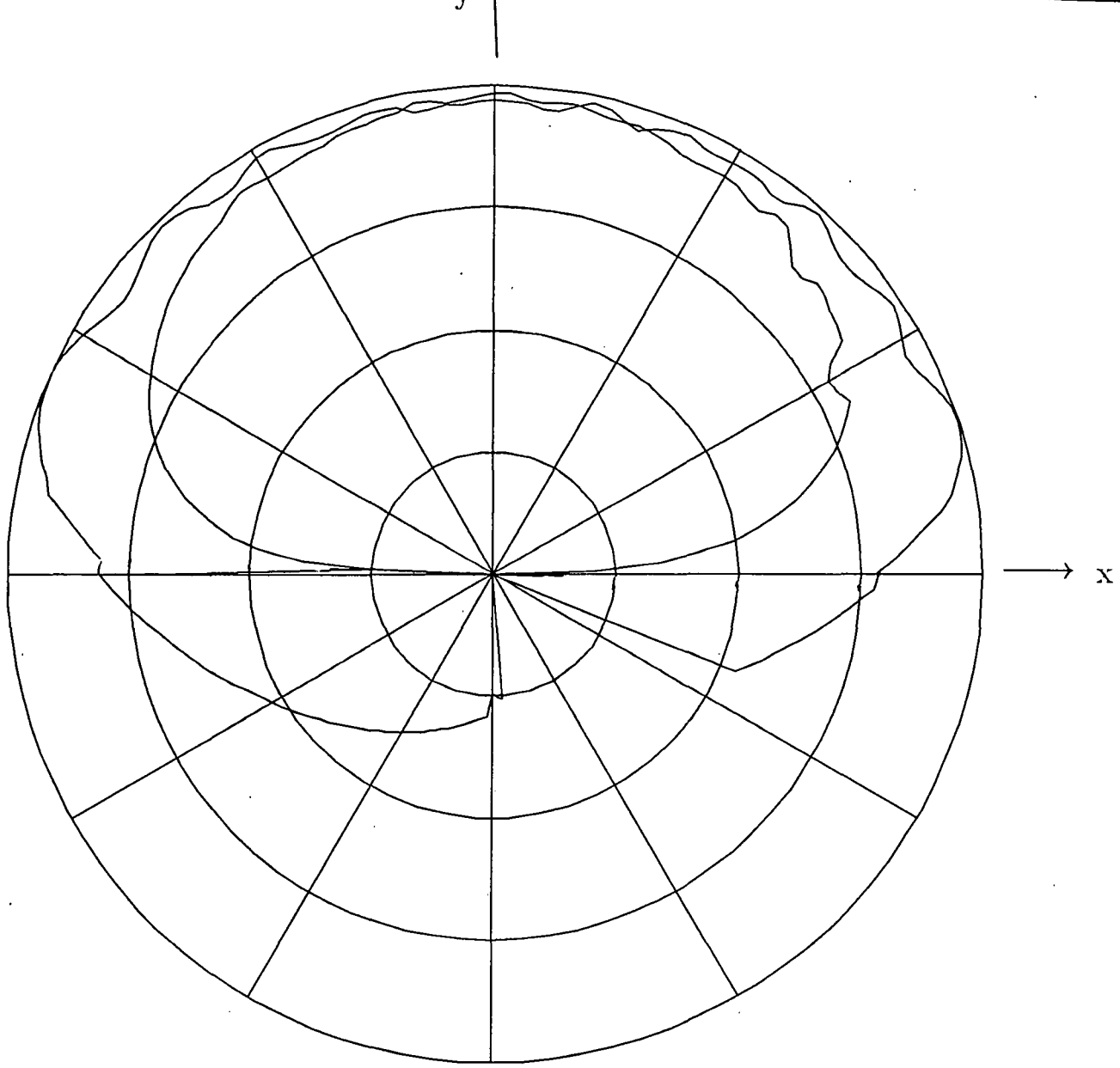

Fig 4.39 Far field radiation pattern of antenna at position 4 on backpack with astronaut ($\Theta = 90^{o}$).

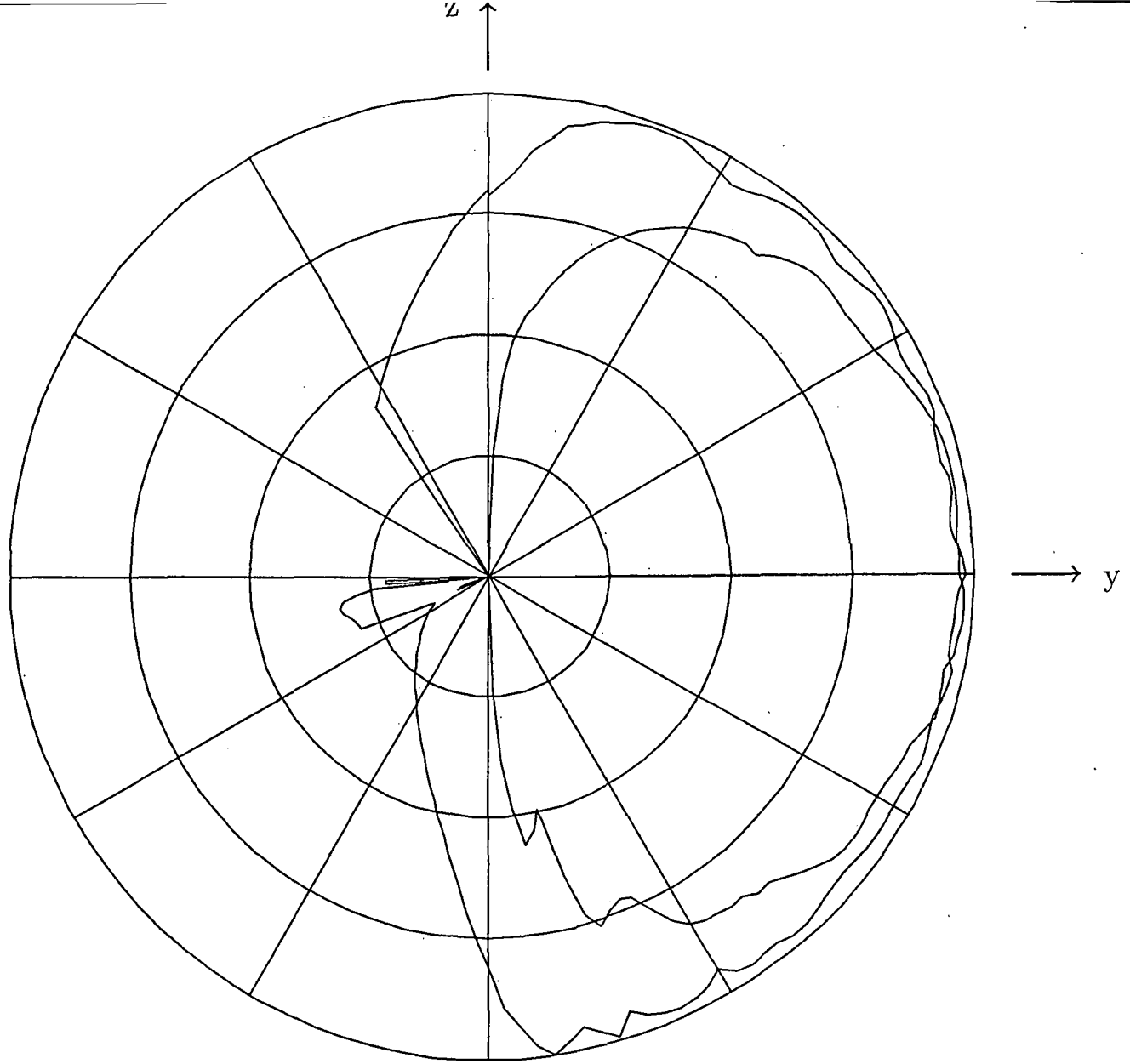

Fig 4.40 Far field radiation pattern of antenna at position 4 on backpack with astronaut (ϕ = 90°).